

Novel concepts of compressed air energy storage and thermo-electric energy storage

THÈSE N° 5525 (2012)

PRÉSENTÉE LE 9 OCTOBRE 2012

À LA FACULTÉ DES SCIENCES ET TECHNIQUES DE L'INGÉNIEUR
LABORATOIRE D'ÉNERGÉTIQUE INDUSTRIELLE
PROGRAMME DOCTORAL EN ENERGIE

ÉCOLE POLYTECHNIQUE FÉDÉRALE DE LAUSANNE

POUR L'OBTENTION DU GRADE DE DOCTEUR ÈS SCIENCES

PAR

Young Min KIM

acceptée sur proposition du jury:

Prof. J. R. Thome, président du jury
Prof. D. Favrat, directeur de thèse
Prof. F. Avellan, rapporteur
Dr J. Hemrle, rapporteur
Prof. E. Sciubba, rapporteur



ÉCOLE POLYTECHNIQUE
FÉDÉRALE DE LAUSANNE

Suisse
2012

Acknowledgements

First of all, I'd like to sincerely thank Prof. Daniel Favrat. I think I was very fortunate and lucky to have met you. I stand where I am now because you allowed me as a PhD student at LENI, despite of my lack of many abilities, and always encouraged my immature ideas. Because of my work in Korea, I was able to come to Switzerland for only short periods every year. Without your faith, support, and guidance, I do not think I would have been able to accomplish this work. You are one of the busiest professors, but you are always cheerful and considerate of others. You love your work and are always professional in everything you do. Watching you made me realize that I wanted to become just like you: you became my role model.

LENI is a very unique research laboratory where various energy systems are studied, and the people there are full of new ideas of fusion technology. I was very lucky to have seen at first hand the various research of MER Dr. François Maréchal and the fuel cell research of MER Dr. Jan Van herle.

I'd like to thank everyone at LENI, Zacharie, Céline, Jonathan, Léda, Emanuele, Matthias, Jean-Baptiste, Johannes, Ramanunni, Thierry, Samuel, Angel, Nicolas and others, for welcoming me wholeheartedly and helping and supporting me. I wish all of you happiness and health.

I'd also like to thank Brigitte, Irene and Suzanne who took great efforts to make sure that I did not feel out of place when I first visited LENI. They showed me such warm hospitality and more than filled up my administrative tasks when I was away in Korea. For that, I am very grateful.

I'd also like to thank Dr. Park Jung-Eung, my EPFL senior, who helped me so much when I first came to Switzerland and was unaware about the academic life here.

Last but not the least, a sincere word of appreciation goes to my colleagues and my family in Korea who showed genuine support while I was studying in Switzerland.

연구원에서 새로운 규정을 만들어가면서 외국에서 학위를 할 수 있도록 기회를 만들어 주신 강건용 박사님, 김용진 박사님, 김완두 박사님, 김석준 박사님께 깊은 감사를 드립니다. 많은 배려와 지원을 해주신 전현직 실장님이신 이장희 박사님, 김창기 박사님, 오승묵 박사님께도 진심으로 감사를 드립니다.

학위기간 동안 책상에서 많은 작업을 하던 저에게 항상 웃음을 만들어 주신 우세종 선생님께 감사 드리며, 제가 없는 과견기간 동안 프로젝트와 관련해서 저의 몫까지 담당해 주신 신동길 선임님께 감사를 드립니다. 오랜 연구원 생활 동안 항상 편안하게 마음을 털어놓고 이야기할 수 있었던 조규백 박사님에게 감사를 드리며, 미국에서 새로운 경험을 통해 더욱 성장하시기를 바랍니다. 묵묵히 성실하게 많은 일을 잘 해나고 계시는 김홍석 박사님께도 감사를 드립니다. 많은 격려를 해 주신 정동수 박사님과 따뜻한 말씀을 해 주신 최교남 선생님에게도 깊은 감사를 드립니다.

올해 승진을 하신 이용규 박사님에게 감사를 드리며 앞으로 좋은 일들이 더 많이 있으시길 기원합니다. 건강상의 이유로 힘든 시간을 보내셨던 김창업 박사님의 격려에도 감사를 드리며 건강과 행복을 기원합니다. 학위디펜스와 관련해서 많은 팁을 알려주신 이선엽 박사님에게 감사 드리며, 가장 먼저 성공적인 학위디펜스를 축하해 주신 최 영 박사님에게도 감사를 드립니다. 선배로서 도움을 주지 못했지만 많은 격려를 해 주고 열심히 맡은 역할을 잘 해 나가고 있는 이석환 박사님, 박철웅 박사님, 김용래 박사님, 김태영 박사님에게도 감사를 드립니다.

연구원 입소부터 지금까지 항상 후배들을 지원하고 격려해 주시는 정용일 박사님께도 감사를 드립니다.

제가 자리를 비울 때에도 세 아이들을 잘 키우고 웃음을 잃지 않는 사랑하는 아내와 항상 아빠를 응원하는 효정과 효민이, 우리 가족에게 기쁨이 되고 있는 늦둥이 하성이에게 감사를 드립니다. 항상 아들을 자랑스러워하시고 잘 되도록 기도해 주시는 어머니와 아버지에게 감사를 드리며, 따뜻한 누나와 동생에게도 감사를 드립니다.

Résumé

L'intérêt pour le stockage d'énergie journalier, voire hebdomadaire, est de plus en plus évident en vue de l'équilibrage entre offre et demande, en particulier avec les perspectives d'accroissement des énergies renouvelables à caractère intermittent. Il est également important pour le stockage d'énergie excédentaire de type électricité nucléaire ou thermique. Les technologies entrant en considération pour l'équilibrage des charges de grands systèmes énergétiques, typiquement sur des heures ou des jours de temps de décharge, incluent le pompage-turbinage hydraulique, l'air comprimé (CAES), les batteries sodium-soufre (NaS), les batteries plomb-acide avancées avec microfibres de verre et les batteries d'écoulement. La technologie CAES est prometteuse en raison de ses avantages qui sont une haute fiabilité, une faisabilité prouvée et un faible impact environnemental. Une autre approche récemment proposée est le stockage thermo-électrique à l'aide de cycles thermodynamiques (TEES). Cette thèse se présente comme un guide permettant de comprendre précisément chaque système sur la base d'analyses énergétiques et exergetiques permettant de dégager les paramètres clefs pour améliorer les rendements de chaque système. En complément, de nouveaux concepts sont proposés qui permettent d'éliminer certains inconvénients tout en élargissant la gamme d'application de certains de ces systèmes.

Les systèmes CAES sont normalement utilisés dans des conditions à volume constant avec un réservoir fixe et rigide et des compresseurs et turbines qui peuvent fonctionner dans le cadre d'une gamme de pression déterminée. Les rapports de pression variables qui en découlent peuvent conduire à des réductions de rendement de compression et de conversion en raison de l'éloignement de certains points de fonctionnement par rapport aux conditions nominales. Bien qu'il soit possible d'accroître le volume de stockage pour réduire le domaine de variation des pressions, une telle approche conduit à une densité d'énergie réduite et des coûts d'investissement plus élevés. Ces inconvénients sont en grande partie résolus par un nouveau concept de CAES à pression constante proposé dans cette thèse. Une analyse énergétique et exergetique de ce nouveau système est présentée qui permet de bien comprendre ses caractéristiques en fonction de différentes approches de compression et de détente. Les influences de la caverne de stockage elle-même, de sa hauteur de stockage et du transfert de chaleur entre deux substances (air et eau) sur les performances de ce nouveau

concept CAES sont aussi analysées.

Alors que les systèmes CAES à grande échelle sont très étroitement dépendants de l'adéquation avec des facteurs géologiques locaux pour le stockage de l'air, un système micro-CAES peut être envisagé avec de bonne perspective d'efficacité pour des réseaux d'énergie décentralisés. De tels micro-systèmes, pourraient permettre un stockage d'énergie et la génération d'électricité à partir de différentes sources et incorporer un cycle à air pour le chauffage et le refroidissement. Cette thèse inclut les résultats d'analyses énergétiques et exergétiques de différents types de micro-CAES, ainsi que des idées nouvelles pour obtenir de hautes efficacités de ces systèmes.

Récemment un autre type de stockage de type mécanique, dit stockage thermo-électrique d'énergie (TEES), qui utilisent alternativement des cycles de pompe à chaleur et des cycles moteurs avec stockage d'énergie thermique ont été proposés. Les avantages des systèmes TEES sont de plus hautes densités d'énergie et leur indépendance par rapport aux contraintes géologiques. En particulier, un système TEES avec cycle transcritique au CO₂ est considéré comme prometteur pour du stockage à grande échelle. Cette thèse fait la revue des systèmes TEES actuellement considérés et propose un nouveau concept de TEES à transformations isothermes dans le cadre de cycles transcritiques au CO₂. Il est ainsi démontré que dans le cadre des systèmes TEES à cycles transcritiques au CO₂, l'efficacité de stockage et la densité énergétique peuvent être accrues à l'aide de compressions et détente isothermes.

En complément, de nouveaux cycles transcritiques ou supercritiques au CO₂ utilisant à la fois des sources thermiques à relativement basse (LT) et haute (HT) températures sont proposés, qui permettent de maximiser la puissance motrice du cycle CO₂ avec des sources thermiques HT typiquement adaptées aux réacteurs nucléaires, aux centrales à énergie solaire concentrée ou aux centrales thermiques avec combustion. De plus, les systèmes TEES proposés dans la littérature et basés sur des cycles transcritiques à CO₂ peuvent être combinés avec le nouveau cycle transcritique au CO₂ utilisant des sources à basse et haute températures (LT et HT)

Mots clefs: Stockage d'énergie, stockage d'énergie à air comprimé (CAES), CAES à pression constante, Micro-CAES, Stockage d'énergie thermo-électrique (TEES), cycle transcritique au CO₂, TEES isotherme.

Abstract

The interest in energy storage is currently increasing, especially from the perspectives of matching intermittent sources of renewable energy with customer demand and storing excess nuclear or thermal power during the daily cycle. Technologies to be considered for load leveling for large-scale energy systems, typically in the range of hours to days of discharge time, include pumped-storage hydroelectricity, compressed air energy storage (CAES), sodium sulfur (NaS) batteries, advanced absorbent glass mat lead acid batteries, and flow batteries. CAES is a promising technology because of significant advantages such as its high reliability, economic feasibility, and low environmental impact. Thermo-electric energy storage (TEES), which was recently proposed as a method for large-scale energy storage, is another mechanical storage method based on thermodynamic cycles. This thesis presents a guide to precisely understand each system along with energy and exergy analyses to characterize the key parameters for achieving high efficiency for each of the systems. In addition, some novel concepts for the systems are proposed in order to address some of the current drawbacks and to widen the scope of their applications.

Conventional CAES systems are most commonly operated under constant volume conditions with a fixed, rigid reservoir and compressors and turbines that can operate over an appropriate pressure range. These varying pressure ratios can degrade the efficiencies of compression and power generation owing to deviations from design points. Although it is possible to increase the storage volume to reduce the operating pressure range, doing so results in reduced energy density and high construction costs. Therefore, in order to resolve such problems, a novel constant-pressure CAES system combined with pumped hydro storage is proposed. An energy and exergy analysis of the novel CAES system was performed in order to understand the operating characteristics of the system according to several different compression and expansion processes. The effects of the height of the

storage cavern and heat transfer between two media (air and water) and the cavern on the performance of the novel CAES system were also examined.

Although the large-scale CAES systems are dependent on the right combination of site-dependent geological factors for air storage, a micro-CAES system with man-made air vessels can be a very effective system for distributed power networks, because it provides energy storage, generates electric power using various heat sources, and incorporates an air cycle heating and cooling system. This thesis presents the results of energy and exergy analyses of different types of micro-CAES systems, as well as some innovative ideas for achieving high efficiency of these systems.

Recently, another type of mechanical storage, namely, thermo-electric energy storage (TEES) systems, which use heat pumps and heat engines with thermal storage, have been proposed. The advantages of TEES systems are their higher energy densities and independence from geological formations. In particular, a TEES system with transcritical CO₂ cycles is considered to be a promising method for large-scale energy storage. This thesis reviews current TEES systems and proposes a novel isothermal TEES system with transcritical CO₂ cycles. It is shown that in the case of TEES systems with transcritical CO₂ cycles, the round-trip efficiency and energy density can be increased by isothermal compression/expansion.

In addition, novel transcritical or supercritical CO₂ cycles using both low-temperature (LT) and high-temperature (HT) heat sources are proposed to maximize the power output of the CO₂ power cycle with the given HT heat sources for use in applications such as nuclear power, concentrated solar power, and combustion. Moreover, the previous TEES system with transcritical CO₂ cycles can be combined with the proposed transcritical CO₂ cycle using both LT and HT heat sources.

Key words: Energy storage, Compressed air energy storage (CAES), Constant-pressure CAES, Micro-CAES, Thermo-electric energy storage (TEES), Transcritical CO₂ cycle, Isothermal TEES.

Contents

Résumé.....	i
Abstract.....	iii
1 Introduction.....	1
1.1 Energy storage	1
1.2 Problem of the thesis.....	3
1.3 About this work	5
2 Overview of Compressed Air Energy Storage	9
2.1 Brief history of CAES.....	9
2.2 Understanding of CAES by energy and exergy flow.....	10
2.3 Various types of CAES systems	14
2.3.1 Conventional diabatic CAES system (with fuel)	14
2.3.2 Adiabatic CAES system	17
2.3.3 Isothermal CAES system	20
2.4 Conclusion	23
3 Constant-pressure CAES system combined with pumped hydro storage (PHS)	25
3.1 Variable-pressure CAES.....	26
3.2 Novel constant-pressure (CP-) CAES system combined with PHS	28

3.2.1	Principle of novel constant-pressure CAES system combined with PHS	28
3.2.2	Energy and exergy analyses of the novel CAES system	32
3.2.3	Operating characteristics of the novel CAES system	42
3.2.4	Effect of height of storage cavern on novel CAES system	46
3.2.5	Effect of heat transfer between the two media (air, water) and the cavern	51
3.2.6	Quasi-isothermal process of hydraulic storage by spray water	56
3.3	Application of novel CP-CAES system combined with PHS	59
3.3.1	Small-scale CP-CAES system combined with PHS	59
3.3.2	Large-scale CP-CAES system combined with PHS	60
3.4	Conclusion	63
4	Micro-CAES and air cycle heating and cooling system	65
4.1	Trigeneration micro-CAES systems	65
4.2	Various types of micro-CAES systems	67
4.2.1	System descriptions	67
4.2.2	Energy and exergy analyses	71
4.2.3	Results and discussion	79
4.3	Conclusion	84
5	Isothermal thermo-electric energy storage system with transcritical CO₂ cycles	85
5.1	Thermo-electric energy storage (TEES)	85
5.1.1	Working principle of thermo-electric energy storage	86
5.1.2	Round-trip efficiency of thermo-electric energy storage	88
5.1.3	TEES system with Brayton cycles	91
5.1.4	TEES system with transcritical CO ₂ cycles	93

5.2 Isothermal TEES system with transcritical CO ₂ cycles	96
5.2.1 System description	96
5.2.2 Operating characteristics of isothermal TEES systems with transcritical CO ₂ cycles.....	102
5.2.3 Higher pressure of isothermal TEES systems with transcritical CO ₂ cycles	114
5.2.4 Real cycles of isothermal TEES system with transcritical CO ₂ cycles	118
5.3 Conclusion	126
6 Transcritical or supercritical CO₂ cycles using both low- and high-temperature heat sources	129
6.1 Transcritical or supercritical CO ₂ (T-CO ₂ or S-CO ₂) power cycles	130
6.1.1 Energy and exergy analyses	131
6.1.2 Comparisons between T-CO ₂ Rankine cycle and T-CO ₂ Brayton cycle	136
6.2 Transcritical CO ₂ cycles using both low- and high-temperature heat sources (LH T-CO ₂ cycle).....	140
6.3 Applications of LH T-CO ₂ cycle	148
6.3.1 Nuclear power plant	148
6.3.2 Hybrid system of LH T-CO ₂ cycle combined with TEES	157
6.4 Conclusion	161
7 General conclusions	163
7.1 Conclusionns.....	163
7.2 Future work.....	166
Bibliography	169
Nomenclature	177

List of Figures	183
List of Tables	189
Curriculum Vitae	191

1. Introduction

1.1 Energy storage

The interest in energy storage is currently increasing, especially for matching intermittent sources of renewable energy with customer demand, as well as for storing excess nuclear or thermal power during the daily cycle. According to the Energy Technology Perspectives (ETP) 2010 BLUE scenario for power supply (IEA, 2010), the increased use of renewable energy and nuclear technologies can play an important role in dramatically reducing CO₂ emissions in the power sector. Over the period to 2050, the BLUE scenario achieves almost a 90% reduction (compared to 2007 levels) in the carbon intensity of electricity generation, with renewables accounting for almost half of global production and nuclear for slightly less than one-quarter [1].

There are various energy storage technologies in terms of power quality and discharge time, as shown in Fig. 1.1 [2]. Technologies that meet the need to assure the continuity and quality of power and regulation of its frequency for only seconds or less include flywheels, superconducting magnetic energy storage (SMES), lead acid batteries, lithium ion batteries, flow batteries, and ultracapacitors (supercapacitors). Technologies to be considered for load leveling for large-scale energy systems, typically in the range of hours to days of discharge time, are pumped-storage hydroelectricity, sodium sulfur (NaS) batteries, advanced absorbent glass mat lead acid batteries, and flow batteries. High efficiencies can be achieved by batteries; however, their lifetimes and number of charge cycles are limited. In contrast, mechanical storage systems, e.g., pumped hydro and compressed air, have significant advantages concerning both factors [3] and are based on mature technologies.

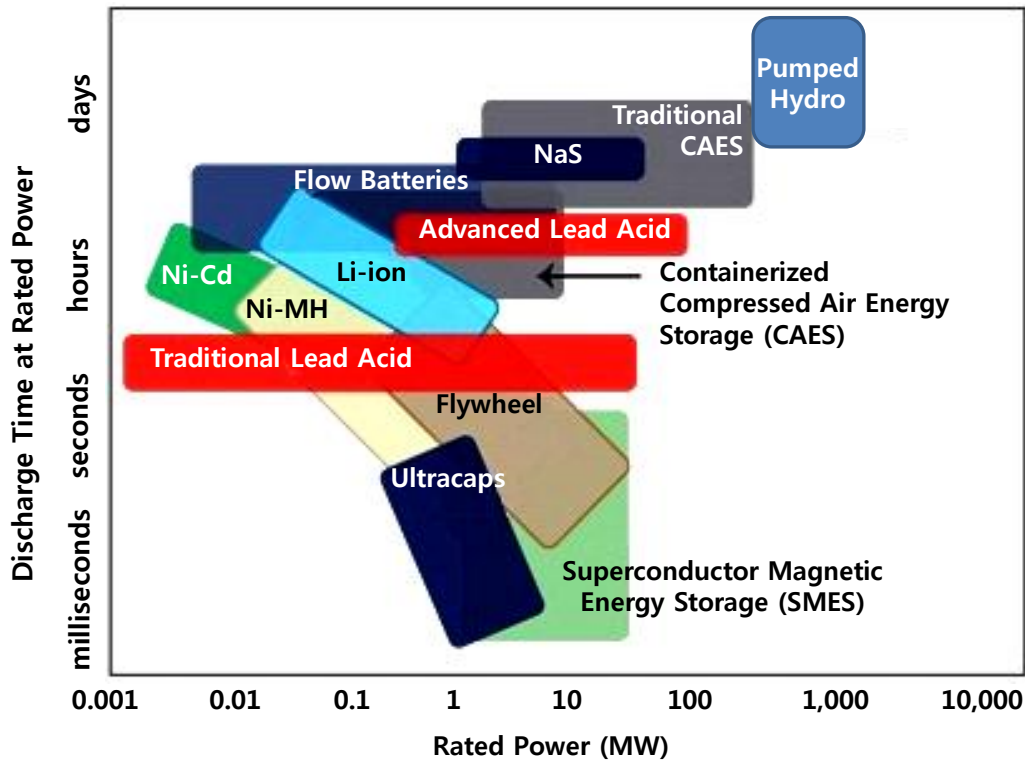


Fig. 1.1: Comparison of various energy storage technologies in terms of power capacity and discharge time (Source: Raytheon Company).

Although pumped hydro is a well-known and widely used method of energy storage, its dependence on specific geographic features and environmental concerns make new developments in this area difficult. A promising method for energy storage and an alternative to pumped hydro storage is compressed air energy storage (CAES), with high reliability and economic feasibility and its low environmental impact [4,5,6]. Although two large-scale CAES plants ever built are still in operation, they have some disadvantages, such as energy loss due to dissipation of heat of compression and use of fossil fuels [7,8,9,10]. Moreover, large-scale CAES is very dependent on appropriate geological formations for air storage, such as salt caverns, aquifers and lined rock caverns.

The first part of this thesis reviews the main drawbacks of the existing CAES systems and presents some innovative concepts for advancing CAES that can address such problems through energy and exergy analyses and thus widen the scope of CAES applications. In

particular, this thesis proposes a multipurpose micro-CAES system combined with air cycle heating and cooling for decentralized energy systems, because it provides energy storage, generates electric power using various heat sources, and incorporates an air cycle heating and cooling system. It also proposes a novel constant-pressure CAES system combined with pumped hydro storage for a high efficiency and energy density of the system.

Recently, thermo-electric energy storage (TEES) systems were proposed as a new method for large-scale energy storage where the electric power is stored using thermal energy storage (TES) by a heat pump and retrieved from TES by a heat engine [11,12]. The advantages of TEES systems are their higher energy density and independence from geological formations. In particular, a TEES system with transcritical CO₂ cycles is considered to be a promising method for large-scale energy storage [11]. The second part of this thesis includes a review of current TEES systems and proposes a novel isothermal TEES system with transcritical CO₂ cycles for high round-trip efficiency and energy density of the system. In addition, some ideas for TEES applications are proposed by analyzing the characteristics of transcritical CO₂ cycles.

1.2 Problem of the thesis

CAES is not a simple energy storage system like batteries, since it involves the process of converting electrical energy into a mechanical form of energy such as heat or pressure and vice versa. All of the processes in a CAES system are accompanied by significant amounts of heat transfer. Since it is very difficult to understand the electrical energy flow in a CAES system by using the first law of thermodynamics, which deals with heat and work equally, we can use exergy flow, which is based on the first and second law of thermodynamics, to better understand the characteristics of CAES systems [13]. These analyses greatly help us to understand the characteristics of each CAES system and to compare different CAES systems. Then, some innovative concepts for CAES systems are presented.

Conventional CAES systems are most commonly operated under constant volume conditions

with a fixed, rigid reservoir and compressors and turbines that can run over an appropriate pressure range [14,15]. These varying pressure ratios can degrade the efficiencies of compression and power generation owing to deviation from design points. Existing CAES plants were designed to throttle the cavern air to a designed pressure despite the throttling loss. Although it is possible to increase the storage volume to reduce the operating pressure range, doing so results in low energy density and high construction costs. Therefore, in order to resolve such problems, a novel constant-pressure CAES system combined with pumped hydro storage is proposed [16,17,18]. This concept can be applied to both small-scale CAES using man-made air vessels and large-scale CAES using salt caverns or lined rock caverns. Especially, in the case of micro-CAES, it is very important to increase the energy density and reduce the volume of the storage tank at a feasible cost because of the high cost and space required for the storage tank.

Micro-CAES with subsurface or aboveground pressure vessels is a more adaptable solution, especially for decentralized energy systems in which excess energy will not be stored in a central system but rather in many small storage units [19]. In a micro-CAES system, it is possible to use the dissipated heat of compression for heating and to use compressed air for both power generation and cooling. A micro-CAES system combined with air cycle heating and cooling could be a very effective energy system owing to its multipurpose nature [17]. Because the pressure ratio of CAES is much higher than that of conventional air cycle refrigeration to reduce the volume of air storage, multiple-stage compression and expansion is needed to achieve high efficiency for the system. Alternatively, quasi-isothermal compression and expansion by liquid injection can be used for a high efficiency micro-CAES system combined with air cycle heating and cooling [17].

A thermo-electric energy storage (TEES) system, recently proposed as a new method for large-scale energy storage, is also another method of electrical energy storage based on thermodynamic cycles. In a TEES system with a good thermal-matching, the exergy losses occurring in the turbomachinery have a greater impact on round-trip efficiency than the exergy losses in the heat exchangers [11]. For a given efficiency of the compressor/expander, the maximum round-trip efficiency decreases rapidly with an increase in the back work ratio, defined as the ratio of ideal compression work to ideal expansion work for the discharging

mode. This means that it is very important to minimize the back work ratio of the reference thermodynamic cycle to optimize the TEES system.

In the case of TEES systems with Brayton cycles using general gas, a very large temperature difference between the hot storage and the cold storage is needed to reduce the back work ratio. Furthermore, highly efficient compressors and expanders are needed to achieve a reasonable round-trip efficiency level. However, in the case of TEES systems with transcritical CO₂ cycles, even if the temperature difference between the hot storage and the cold storage is much lower than in systems with Brayton cycles, their round-trip efficiency is higher than that for Brayton cycle systems because of the reduced back work ratio, assuming the same efficiency of the compressor/expander. Moreover, a TEES system with transcritical CO₂ cycles has the advantage of using water for inexpensive thermal storage. According to the results of the first optimization of the system based on pinch analysis, a realistic round-trip efficiency of 0.6 was obtained for the base case TEES configuration by assuming isentropic efficiencies of expansion and compression similar to those of commercially available turbomachinery and by considering a minimum temperature difference for heat transfer [11].

This thesis reviews current TEES systems and proposes a novel isothermal TEES system with transcritical CO₂ cycles for a higher round-trip efficiency of the system. The isothermal TEES system with transcritical CO₂ cycles can maximize the expansion work by isothermal expansion with effective heat transfer directly with the hot storage tank, resulting in a higher round-trip efficiency because of a lower back work ratio than for an isentropic system. Hot water from the hot storage tank is used by a water pump/turbine to compress/expand the supercritical CO₂ as the liquid piston, and a portion of the water is sprayed with a circulation pump to cool/heat the supercritical CO₂.

1.3 About this work

CAES and TEES are promising alternative methods of electrical energy storage for load leveling. Both are based on energy conversion processes characterized by well-known

thermodynamic cycles. However, since they are different from conventional power cycles, it is very important to precisely understand each system and the key parameters for achieving high efficiency of the system. Then, it is possible to put together some novel combinations with other energy systems in order to widen the scope of their applications and realize a big synergistic effect.

Chapter 2 reviews existing CAES systems and the advantages of new concepts such as adiabatic CAES and isothermal CAES by employing energy and exergy analysis. In the case of conventional diabatic CAES plants, the heat of compression needs to be dissipated to prevent deterioration of the cavern and pressure drop of the stored air in the cavern by heat loss and then, during the discharging process, natural gas is used to heat the compressed air. But adiabatic CAES stores the heat of compression and reuses it to heat the compressed air during the discharging process. Isothermal CAES can also minimize the energy loss that occurs during the charging and discharging processes by minimizing the temperature difference of the air with the environment.

In chapter 3, for reducing the air storage volume while maintaining a high efficiency level for a CAES system at a design condition, a novel constant-pressure CAES system combined with pumped hydro storage is proposed. In this study, an energy and exergy analysis was performed in order to study the characteristics of the novel CAES system in comparison with conventional CAES. Furthermore, the daily operation characteristics of the novel CAES system were examined according to several different compression and expansion processes. With a particular focus on large-scale systems, the effects of the height of the storage cavern and heat transfer between the two media (air, water) and the cavern on the performance of the system were also examined.

In chapter 4, this study presents the results of energy and exergy analyses of different types of micro-CAES systems, as well as some innovative ideas for achieving high efficiency for these systems. This study proposes a multi-purpose micro-CAES system for energy storage and air cycle heating and cooling for a building's HVAC system. As mentioned before, the quasi-isothermal compression and expansion by liquid injection can be used for a high-efficiency micro-CAES system combined with air cycle heating and cooling.

Chapter 5 reviews current TEES systems and proposes a novel isothermal TEES system with transcritical CO₂ cycles for a higher round-trip efficiency of the TEES system. Through a simple model of the system, the operating characteristics of an isothermal TEES system with transcritical CO₂ cycles were studied in comparison with the isentropic case. In addition, the actual cycles of the isothermal TEES system with transcritical CO₂ cycles were studied in comparison with the isentropic case by considering a small temperature rise/drop during the isothermal compression/expansion and thermal energy by the internal dissipation of the compressor/expander.

In chapter 6, novel transcritical or supercritical CO₂ cycles using both low- and high-temperature heat sources ('low-temperature' means an intermediate temperature between the highest temperature of heat sources and the lowest temperature of heat sink) are proposed. By utilizing these cycles, it is possible to maximize the power output of the CO₂ power cycle with the given high-temperature heat sources for use in applications such as nuclear power, concentrated solar power, and combustion. Moreover, the proposed CO₂ cycles combined with the thermal energy storage of the waste heat by itself offer the advantage of load leveling over other CO₂ cycles with the given high-temperature heat sources. Energy and exergy analyses of the systems were performed to show the merits of the novel systems in comparison with conventional systems.

2. Overview of Compressed Air Energy Storage

This chapter reviews the CAES systems in existence and the advantages of new concept of CAES concepts such as adiabatic CAES, isothermal CAES by energy and exergy analyses. These analyses greatly help us to understand the characteristics of each CAES system and to compare different CAES systems.

2.1 Brief history of CAES

The idea of storage plants based on compressed air is not new. In 1978, the first CAES plant of 290-MW capacity was built at Huntorf in Germany. In 1991, another 110-MW plant was built in McIntosh, Alabama. Both plants are still in operation [20,21]. However, the existing CAES plants have some disadvantages such as their energy loss due to dissipation of heat of compression, use of fossil fuels, and dependence on geological formations. Therefore, some innovative concepts of CAES have been recently proposed [13].

In the case of conventional diabatic CAES plants, the heat of compression needs to be dissipated to prevent deterioration of the cavern and pressure drop of the stored air in the cavern by heat loss and then, during the discharging process, natural gas is used to heat the compressed air. But adiabatic CAES stores the heat of compression and reuses it to heat the compressed air during the discharging process. The efficiencies of several adiabatic CAES configurations are analyzed with the help of an energy balance [22,23]. Isothermal CAES can

also minimize the energy loss that occurs during the charging and discharging processes by minimizing the temperature difference of the air with the environment [20,24].

2.2 Understanding of CAES system by energy and exergy flow

CAES is not a simple energy storage system, like other batteries. It can be viewed as a hybrid system of an energy storage and a gas turbine power plant. Unlike conventional gas turbines, which consume about two-thirds of their input fuel to compress the air at the time of power generation, CAES precompresses the air, using low-cost electricity from the power grid at off-peak times, and utilizes it with some gas fuel to generate electricity when required [25]. The compressed air is stored in appropriate underground caverns or aboveground air vessels. The schematic of a modern CAES system is presented in Fig. 2.1 [14].

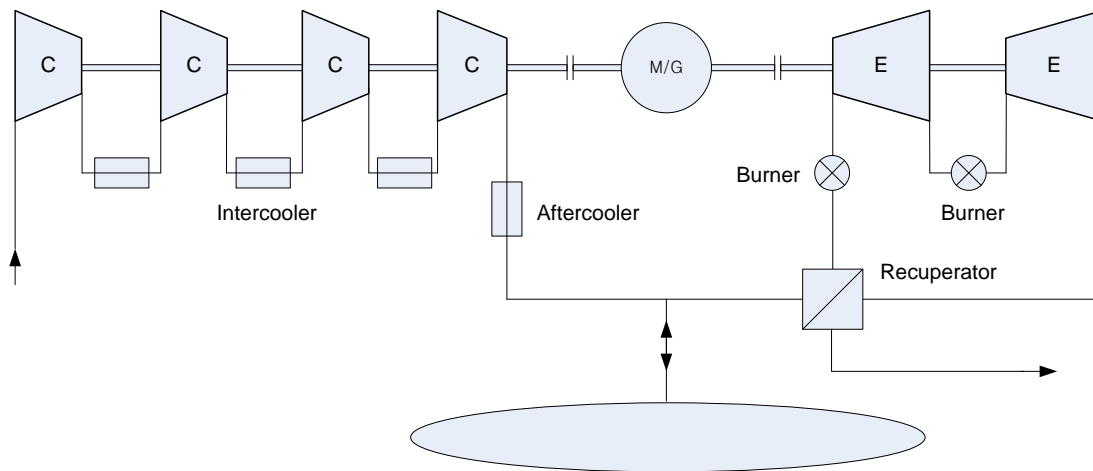


Fig. 2.1: Conventional CAES system: Schematic of the McIntosh plant in Alabama, USA.

Since the CAES system can be considered to be a combination of an energy storage system and a power plant, and all processes are accompanied by a significant amount of heat transfer, understanding the electrical energy flow in the CAES system is very difficult using the first law of thermodynamics, which considers with heat and work at equal level; therefore, we can use exergy flow, which is based on the first and second law of thermodynamics, to better

understand the characteristics of the CAES system. Exergy can be defined as the maximum useful work possible that can be obtained during a process that brings the system into an equilibrium with the environment while interacting solely with this environment [26]. Assuming that potential and kinematic energy effects are negligible and no chemical reaction occurs, the exergy of an air stream can be expressed as [27]

$$\dot{E}_a = \dot{M}_a [h - h_0 - T_0 (s - s_0)] \quad (2.1)$$

where h and s are specific enthalpy and entropy, respectively, and the subscript 0 indicates that the properties are taken at reference temperature and pressure ($T_0=20^\circ\text{C}$, $P_0=1$ bar) as a dead state.

In the case of perfect gas flow,

$$h - h_0 = c_p (T - T_0) \quad (2.2)$$

$$s - s_0 = c_p \ln \frac{T}{T_0} - r \ln \frac{P}{P_0} \quad (2.3)$$

where c_p is isobaric specific heat at average temperature and r is the specific gas constant.

The exergy in Eq. 2.1 can be split into two parts—the mechanical part and the thermal part—as follows [26]:

$$\dot{E}_a = \dot{E}_{a(M)} + \dot{E}_{a(T)} \quad (2.4)$$

$$\dot{E}_{a(M)} = \dot{M}_a r T \ln \frac{P}{P_0} \quad (2.5)$$

$$\dot{E}_{a(T)} = \dot{M}_a c_p \left(T - T_0 - T_0 \ln \frac{T}{T_0} \right). \quad (2.6)$$

Fig. 2.2 shows the energy and exergy flow of the simplified CAES system. The processes of the CAES system are compression (1-2), cooling (2-3), charging or discharging (3-4), heating (4-5), expansion (5-6), and recuperation (6-7). Although the compression work varies according to various compression processes, e.g., isothermal, adiabatic compression, and two-, three-, and four-stage compression with intercooling, the compressed air is cooled and stored at the same environmental temperature (T_0) and storage pressure (P_s). This means

that only the mechanical exergy of the compressed air is stored in the air storage, and the thermal exergy of the compressed air is dissipated by the cooler or can be stored in a thermal energy storage and reused during the discharging process.

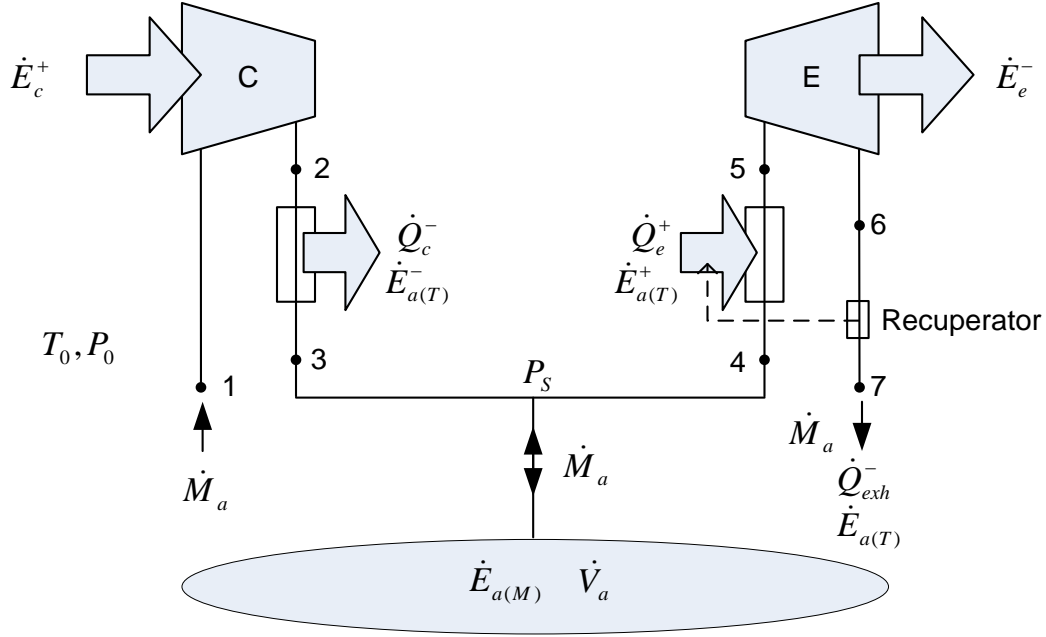


Fig. 2.2: Energy and exergy flow of simplified CAES system.

The isentropic efficiencies of the compressor and expander, $\eta_{c,s}$ and $\eta_{e,s}$, respectively, are expressed as

$$\eta_{c,s} = \frac{W_{c,s}^+}{W_c^+} = \frac{h_{\text{out},s} - h_{\text{in}}}{h_{\text{out}} - h_{\text{in}}} \quad (2.7)$$

$$\eta_{e,s} = \frac{W_e^-}{W_{e,s}^-} = \frac{h_{\text{in}} - h_{\text{out}}}{h_{\text{in}} - h_{\text{out},s}} \quad (2.8)$$

where the subscript s denotes an isentropic compression/expansion process.

The efficiencies of motor and generator, η_m and η_g , are expressed as

$$\eta_m = \frac{W_c^+}{E_c^+} \quad (2.9)$$

$$\eta_g = \frac{E_e^-}{W_e^-} \quad (2.10)$$

In order to study the energy and exergy analyses of different types of CAES systems, we adopted the following assumptions and elements of inlet data. Although these assumptions are far from real conditions, these simplifications help greatly help us to understand the characteristics of each CAES system and compare different CAES systems briefly.

- (a) Each compression and expansion is assumed to occur at a steady state with a steady flow, constant-pressure air storage, have negligible potential and kinematic energy effects, and exhibit no chemical reaction.
- (b) For simplicity, the pressure drop in all heat exchangers is neglected.
- (c) Air pressure in the storage cavern (or vessel) is assumed to remain constant at 5 MPa by adoption of constant-pressure air storage [16,17]. The designed pressure ratios of the compressor and expander are 50, with isentropic (adiabatic) efficiencies of 85%. Although the air storage pressure must be optimized by energy density, efficiency, and cost of the system, 5 MPa of air storage pressure, as a general value of air releasing pressure for CAES gas turbine [14,15], is adopted.
- (d) The efficiencies of the motor and generator are assumed to be 95%.

For multistage compression, each stage was assumed to consist of an adiabatic compression process, and each stage had the same pressure ratio; the compressed air was cooled to the ambient temperature by intercooling. Moreover, the total compression work and heat rejection are the sums of individual values of these quantities at all stages. For the discharging process, the recuperator can be used for recovering the heat of the expanded hot gas.

2.3 Various types of CAES systems

2.3.1 Conventional diabatic CAES system (with fuel)

In the case of conventional CAES plants such as the one shown in Fig. 2.1, in order to increase the overall efficiency of the system, it is customary to perform multistage compression with intercooling and multistage expansion with reheating, and for the discharging process, the compressed air is generally heated using gas fuel. Fig. 2.3 shows the energy and exergy flow of the diabatic CAES system for the production of 1-kWh output.

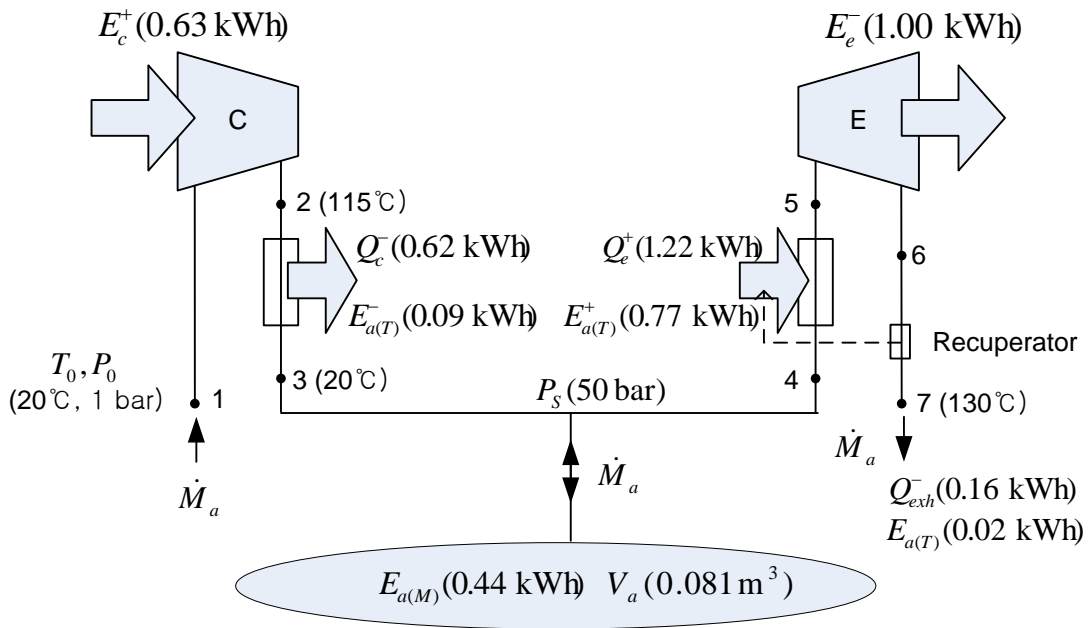


Fig. 2.3: Energy and exergy flow of the conventional CAES system.

The CAES system in Fig. 2.3 is based on the McIntosh plant, which has four-stage compression with intercooling and an exhaust gas temperature of 130°C. The heat input is 1.22 kWh to produce 1 kWh electric output, and the inlet temperatures of high pressure (HP) turbine with the inlet pressure of 50 bar and low pressure (LP) turbine with the inlet pressure of 15 bar are 537°C and 871°C, respectively. The electric power is 2.26 times higher than the

exergy of the compressed air by the thermal exergy added by using fuel. The thermal exergy of 0.77 kWh in Figure 2.3 is not a chemical exergy but a total thermal exergy added in form of heat during the multistage expansion with reheating. In general, the energy efficiency of the CAES system can be calculated by adding the heat input by fuel, Q , to the electric input as follows [15,25,28].

$$\eta_{ee} \equiv \frac{E_{out}}{E_{in} + Q} \quad (2.11)$$

where E_{in} is the electric input and E_{out} is the electric output.

But, this value may not be considered a useful measure of electrical storage efficiency, because the heat input is not equivalent to the electric input. Rather, it may be seen as a mixed efficiency of the electrical storage efficiency and thermal efficiency of a power plant. Therefore, the net electrical storage efficiency of a CAES system can be calculated by adding the amount of electric energy generated by natural gas (or other fuels) to the electric input of the CAES system as follows [15,25,28]:

$$\eta_{se} \equiv \frac{E_{out}}{E_{in} + Q\eta_p} \quad (2.12)$$

where $Q\eta_p$ is the electric energy that would be produced if the amount of fuel consumed by the CAES system were burned in another power station (Q is the lower caloric value of the fuel and η_p is the thermal efficiency of the conventional power plant).

If the standard thermal efficiency of the power plant $\eta_p = 0.4$ [29] is assumed, the net electrical storage efficiency of the CAES system shown in Fig. 2.3 is 89%. However, if the thermal efficiency of a conventional power plant, $\eta_p = 0.5$, is used, the net electrical storage efficiency of the CAES system is 81%. Therefore, the net electrical efficiency of the CAES system, defined in Eq. 2.12, depends significantly on the value of the adopted η_p . Further, when the heat is obtained from waste heat or solar power, the net electrical storage efficiency of a CAES system becomes more ambiguous. Fig. 2.4 shows a new configuration of diabatic CAES system, one that uses a conventional gas turbine and the exhaust heat from the gas turbine to heat the compressed air before the expander, as a CAES bottoming cycle [30].

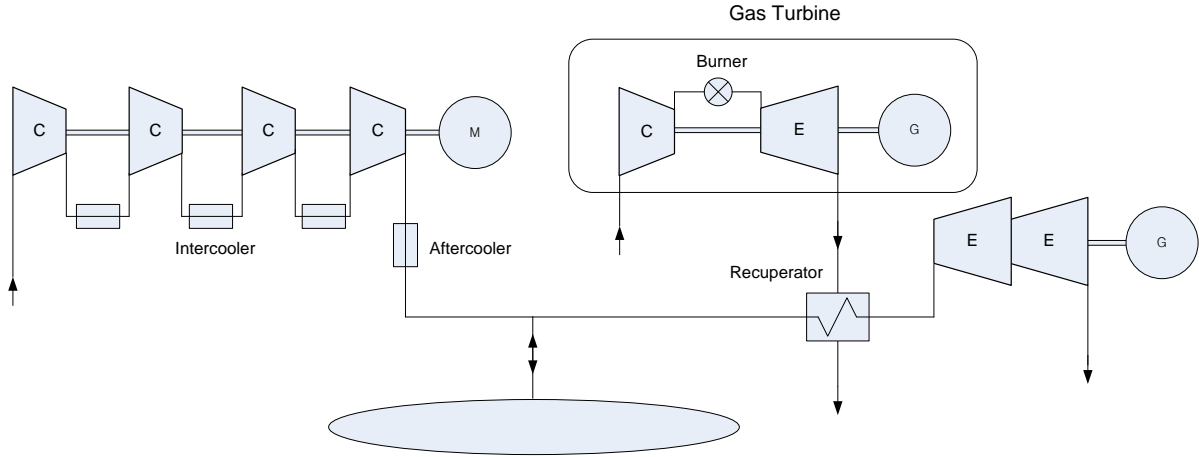


Fig. 2.4: Configuration of CAES system as a bottoming cycle.

Therefore, in this paper, a new expression for the electrical storage efficiency of the CAES system, based on the exergy analysis, has been proposed. It is given as

$$\eta_{se} \equiv \frac{E_{out}}{E_{in} + E_{a(T)}} \quad (2.13)$$

where $E_{a(T)}$ is the thermal exergy of compressed air added by heat sources.

The new electrical storage efficiency, defined in Eq. 2.13, of the CAES system in Fig. 2.3 is 71%. Unlike the conventional gas turbine system, in the case of the CAES system, there is a very little exergy loss of exhaust gas. This advantage can compensate for the exergy loss of heat of compression. Although the heat of compression is dissipated in existing CAES plants, it is possible for this dissipated heat to be used for residential heating through cogeneration, which can contribute to improved energy efficiency. Moreover, although existing CAES plants use fossil fuel, waste heat and several other types of renewable energies such as solar, biomass, and biogas can be used as heat sources in the CAES system. SolarCAT Inc. has developed an energy storage technology using compressed air energy storage and concentrating solar power (CSP) design concepts. The company's design replaces the CAES facility's expander train with multiple expanders integrated with parabolic dish solar collectors, which reflect and concentrate incident sunlight onto their focal receivers to heat the compressed air fed to the collectors from storage [20].

2.3.2 Adiabatic CAES system

One of the drawbacks of existing CAES systems is the use of fuel. Adiabatic CAES uses no fuel to heat the compressed air for the expansion process, representing an emission-free, pure storage technology with high storage efficiency [20]. The basic idea of the adiabatic CAES concept is the use of heat storage as the central element of the plant, as shown in Fig. 2.5 [14,20,31]. This implies that the heat needed to heat the compressed air for the expansion process is recovered from the compression and stored in a thermal energy storage (TES) unit to eliminate the need for a combustor [25].

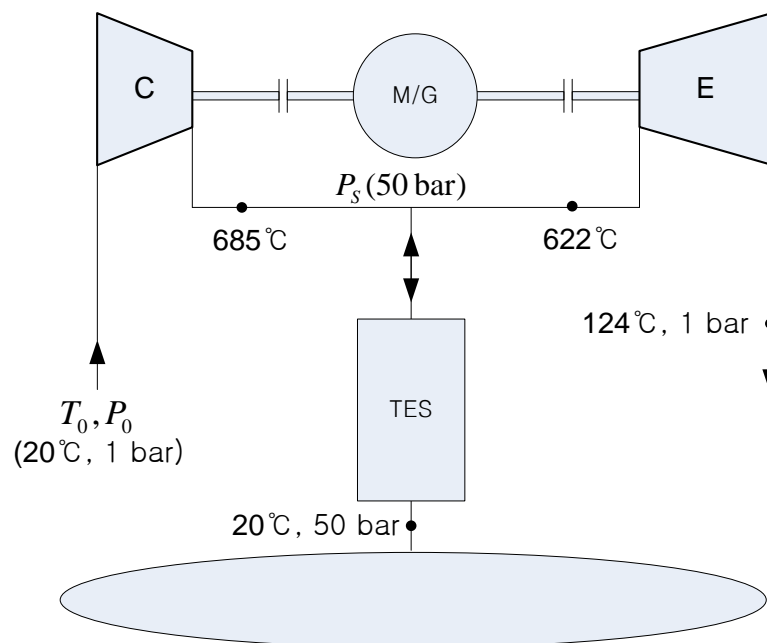


Fig. 2.5: Diagram of an adiabatic CAES system in single-stage configuration.

Fig. 2.6 shows the energy and exergy flow of the adiabatic CAES system in single-stage configuration for the production of 1 kWh output.

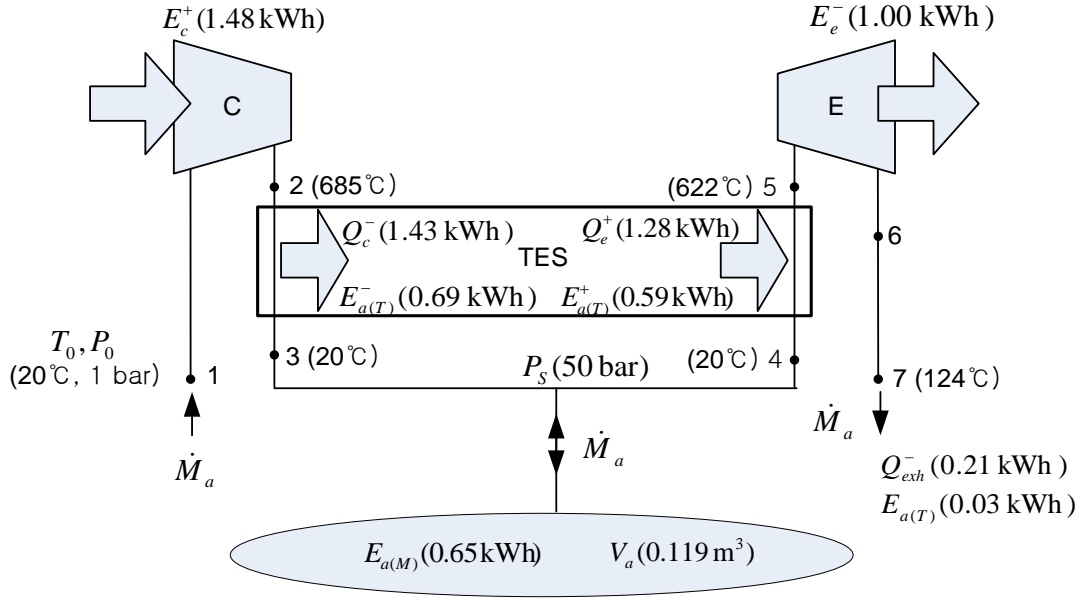


Fig. 2.6: Energy and exergy flow of the adiabatic CAES system in single-stage configuration.

If the air is compressed up to 50 bar adiabatically, the outlet air temperature of compressor is about 685 °C (isentropic efficiency 85%). The thermal exergy of the compressed air $\dot{E}_{a(T)}$ is roughly equivalent to the mechanical exergy of the compressed air $\dot{E}_{a(M)}$. During the charging process, the heat is extracted from the compressed air and stored. When the grid demands electric power, the compressed air is heated using the thermal energy storage up to 622 °C and expanded through an air turbine. It was assumed that the efficiency of TES (the ratio of heat input to the compressed air to the heat output from the compressed air) is 90%. Then, the electrical storage efficiency of the adiabatic CAES system without any external thermal input is 68%. The adiabatic CAES can be considered a combination of CAES and TES, because a substantial portion of the exergy is stored in the form of thermal energy.

Adiabatic CAES technology was evaluated previously in the European Advanced-Adiabatic CAES project [31]. The resulting conceptual designs of the four main plant components (compressor, heat storage, cavern, and air turbine) helped to identify some key technical risks, particularly for the adiabatic compression and the heat storage device. The outlet temperature of the compressor is maintained above 600 °C, and the corresponding compression heat is stored in the TES consisting of an arrangement of solid materials, typically ceramic bricks or natural stones [20,31].

Another configuration of adiabatic CAES is shown in Fig. 2.7, using cold and hot oil as the TES [22,23]. During the charging process, the oil is flowing from a cold tank to a hot tank to intercool the compressed air. Inversely, during discharging process, the oil is flowing from the hot tank to the cold tank to heat the compressed air for power production. The design is based on using standard, industry-proven equipment components. Fig. 2.8 shows the energy and exergy flow of the adiabatic CAES system in two-stage configuration for the production of 1 kWh output. If the air is compressed up to 50 bar in two stages, the outlet air temperature of the compressor is about 275 °C (isentropic efficiency 85%). The thermal exergy of the compressed air, $\dot{E}_{a(T)}$, is less than half of the mechanical exergy of the compressed air, $\dot{E}_{a(M)}$. During the charge period, the heat is extracted from the compressed air and stored by the flowing oil. When the grid demands electric power, the compressed air is heated using thermal energy storage up to 250 °C and expanded through an air turbine. The efficiency of TES is assumed to be 90%, as in the previous adiabatic CAES system in single-stage configuration. Then, the electrical storage efficiency of the adiabatic CAES system without any external thermal input is 67%. This adiabatic CAES configuration needs bigger air storage than does the prior one, because its TES exergy storage is much smaller than the prior one, due to the lower temperature of TES.

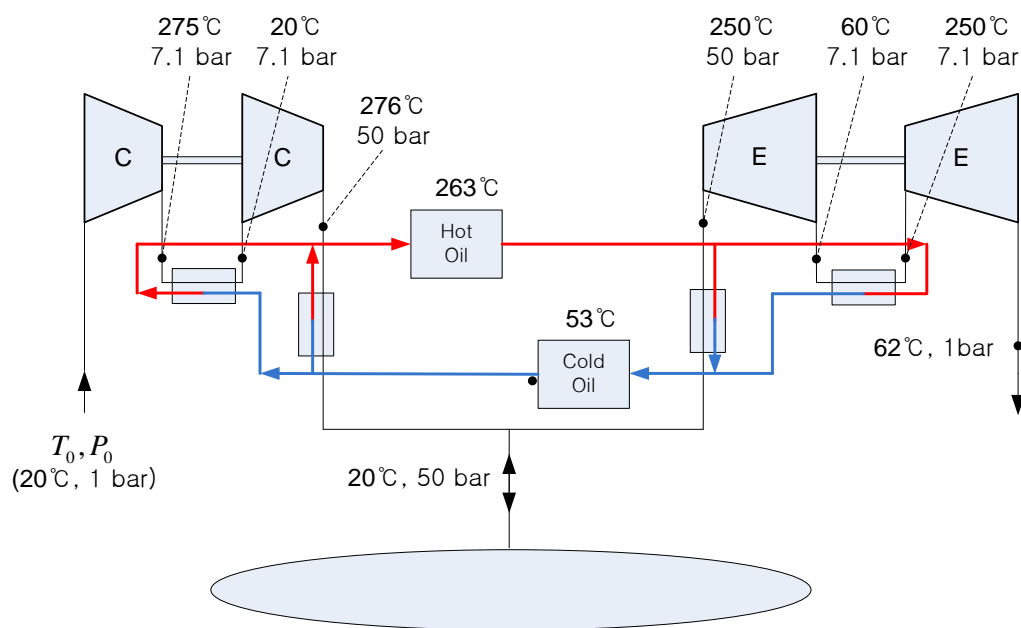


Fig. 2.7: Diagram of an adiabatic CAES system in two-stage configuration.

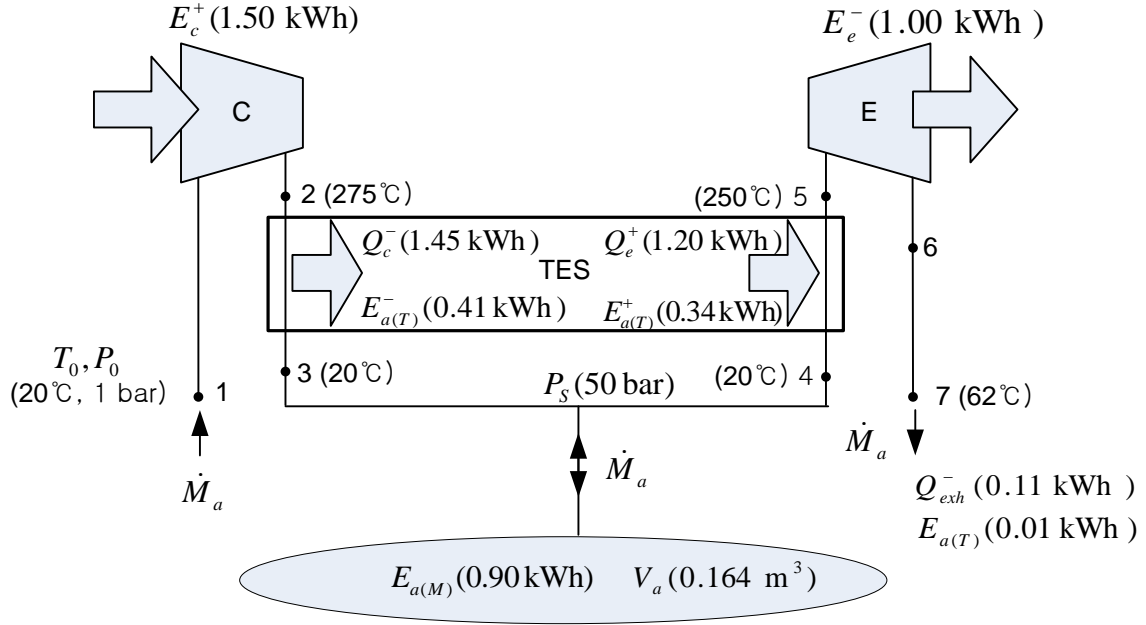


Fig. 2.8: Energy and exergy flow of the adiabatic CAES system in two-stage configuration.

2.3.3 Isothermal CAES system

Isothermal CAES is an alternative CAES system which eliminates the need for fuel and high temperature thermal energy storage. Isothermal CAES can minimize the compression work and maximize the expansion work done through isothermal compression/expansion by means of effective heat transfer with the vessel's surroundings, which involves slow gas pressure change by liquid piston [20,24]. The CAES systems of SustainX Inc. and Enairys Powertech Ltd. use hydraulic pumps to isothermally compress air at rates that allow the high-pressure air to exchange heat with its surroundings, as shown in Fig. 2.9. During isothermal expansion, the gas is able to do more work by absorbing heat from its surroundings. The expanding air in the isothermal CAES system drives a hydraulic motor, which in turn drives an electric generator. The use of hydraulic pumps and motors enables a variable ratio of compression and expansion of air, heat transfer with the surroundings, and a high level of thermal and overall system efficiency [20,24]. But, this type of isothermal CAES has size limitations imposed by technological reasons due to its big size of the liquid piston for the isothermal compression and expansion processes.

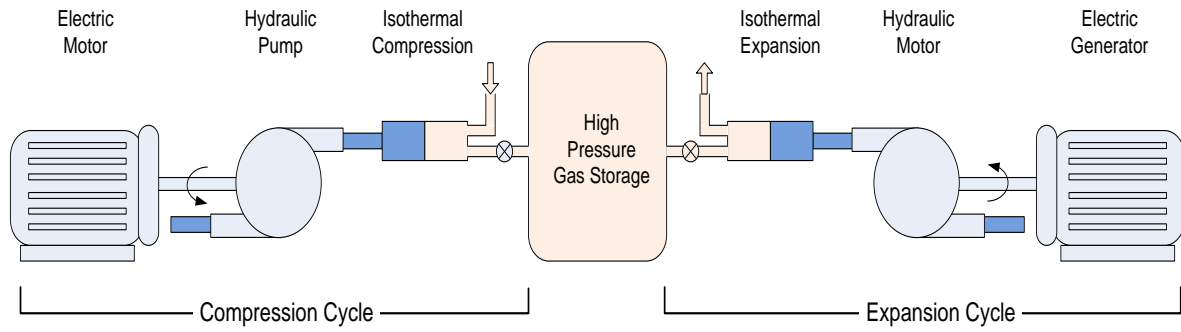


Fig. 2.9: Function diagram of an isothermal CAES system (Source: SustainX Inc.).

Fig. 2.10 shows the energy and exergy flow of the isothermal CAES system for the production of 1 kWh output. The air is compressed up to 50 bar isothermally and stored; then, the compressed air is expanded isothermally. The ideal isothermal compression and expansion work, $W_{c,t}^+$ and $W_{e,t}^-$, respectively, can be obtained as follows:

$$W_{c,t}^+ = M_a (q_{c,t}^- + \Delta h) = M_a (-T_c \Delta s + \Delta h) \quad (2.14)$$

$$W_{e,t}^- = M_a (q_{e,t}^+ - \Delta h) = M_a (T_e \Delta s - \Delta h) \quad (2.15)$$

where the working fluid is assumed to be real gas then Δh is very small but not equal to zero.

The isothermal efficiencies of compression and expansion, $\eta_{c,t}$ and $\eta_{e,t}$, respectively, are expressed as

$$\eta_{c,t} = \frac{W_{c,t}^+}{W_c^+} \quad (2.16)$$

$$\eta_{e,t} = \frac{W_e^-}{W_{e,t}^-} \quad (2.17)$$

where W_c^+ and W_e^- are the actual compression work and expansion work considering a loss of mechanical work by internal dissipation and a small temperature deviations from isothermal process.

It was assumed that the isothermal efficiencies of compression and expansion are 90%, considering the high efficiency of the hydraulic pump/motor and the effective heat transfer with its surroundings; the isentropic efficiencies of hydraulic water pump/motor are

92%~94% [24] and it was reported that the temperature deviation during the expansion (or compression) process from 1 bar to 200 bar is less than 12 °C by water injection, which means that the work by integrating the pressure-volume curve is 96% of isothermal work (Source: SustainX Inc.).

Although there is much heat transfer between the system and its surroundings for the compression and expansion processes, the thermal exergy of the air $\dot{E}_{a(T)}$ is nearly equal to zero, because the temperature change of the air is very small. Although the isothermal CAES system requires about twice the volume of air storage in comparison with the conventional (diabatic) and adiabatic CAES systems, because no thermal exergy is added to the compressed air for the discharging process, the use of high pressure (from 1 bar to 200 bar) reduces the storage volume required. The electrical storage efficiency of the isothermal CAES system without external thermal input is 73%.

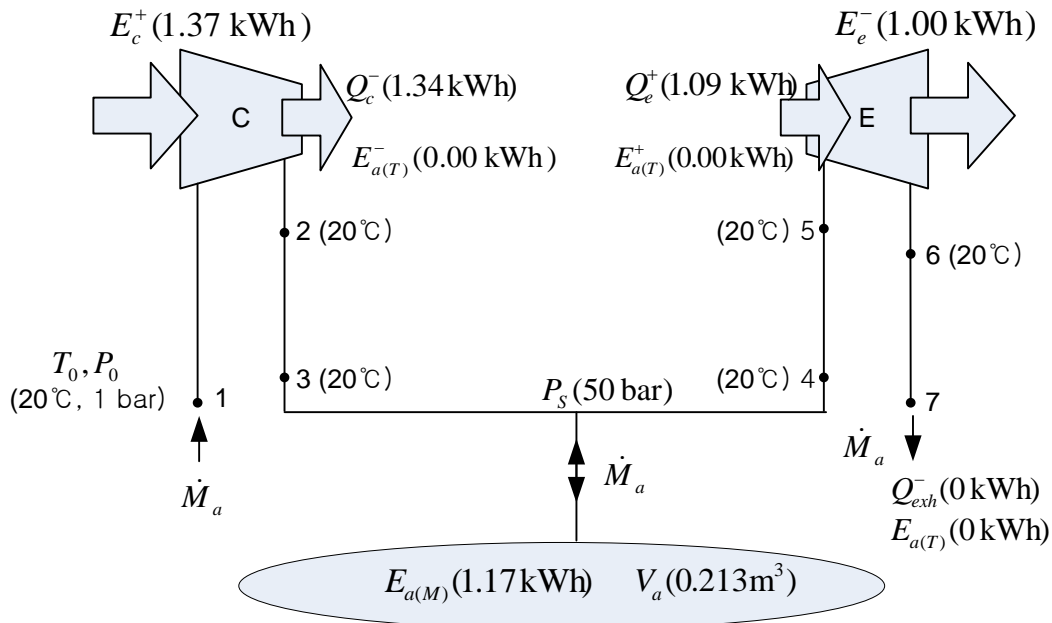


Fig. 2.10: Energy and exergy flow of the isothermal CAES system.

2.4 Conclusion

Energy and exergy analysis was used to provide an understanding of the current CAES methods and the advantages of new concepts of CAES systems such as adiabatic CAES or isothermal CAES. Although existing CAES plants use natural gas as fuel, waste heat and renewable energies such as solar, biomass, and biogas can be used as heat sources for the CAES system. Adiabatic CAES traps the heat of compression and reuses it for expansion; hence, it can be considered a combination of CAES and thermal energy storage (TES), because a substantial portion of the exergy is stored in the form of thermal energy. Isothermal CAES can minimize the compression work and maximize the expansion work done through isothermal compression/expansion with effective heat transfer with the system's surroundings and without the use of fuel or high temperature thermal storage. The existing CAES systems have a few drawbacks, but these can be addressed by employing some new CAES concepts. Compressed air energy storage can be combined with power generation using various heat sources and thermal energy storage.

3. Constant-pressure CAES system combined with pumped hydro storage (PHS)

Although the required storage volume of CAES has to be minimized in order to reduce the construction cost and optimize utilization of the given space, the operating pressure range in the cavern must be limited in order to reduce the deterioration in efficiency of the CAES system at off-design conditions. In an attempt to minimize the storage volume while maintaining a high efficiency of the CAES system at a design condition, a water-compensated CAES system, using a water head supplied by an aboveground reservoir, was proposed to keep the storage cavern at a constant pressure throughout operation [14,15,29]. However, this system requires a very deep air storage cavern in order to produce the required pressure difference by means of the water column, which increases the construction cost. Therefore, for the purpose of addressing the current problems of CAES systems, a novel constant-pressure CAES system combined with pumped hydro storage is proposed [16,17,18]. The concept can be applied to both large-scale CAES utilizing lined rock caverns or salt caverns and small-scale CAES using man-made air vessels or ground-level pipelines because it does not depend on the depth of the cavern.

In this study, an energy and exergy analysis of the system is performed in order to study the characteristics of the novel CAES in comparison with conventional CAES. And the daily operation characteristics of the novel CAES system according to several different compression and expansion processes are examined. With particular focus on large-scale systems, the effects of the height of the storage cavern and heat transfer between the two media (air, water) and the cavern on the performance of the system are also examined.

3.1 Variable-pressure CAES system

Conventional CAES systems are most commonly operated under constant volume conditions, with a fixed, rigid reservoir operating over an appropriate pressure range [14,15]. In general, both charging and discharging of a high-pressure vessel are unsteady-state processes, where the pressure ratios are changing. These varying conditions can result in low efficiencies of compression and expansion, owing to deviation from design points. Although it is possible to design a system that allows the hp turbine inlet pressure to vary with the cavern pressure (reducing output), most efforts have focused on keeping the inlet pressure of the hp turbine constant by throttling the upstream air to a fixed pressure because of the increase in turbine efficiency that results from constant inlet pressure operation [14,15]. The Huntorf CAES plant is designed to throttle the cavern air to a pressure of 46 bar at the hp turbine inlet (with caverns operating between 48 to 66 bar) and the McIntosh system similarly throttles the incoming air to 45 bar (operating between 45 and 74 bar) [14,15]. Recently, a CAES system of Electric Power Research Institute Inc. with aboveground storage has been designed to throttle the incoming air to 55 bar (operating between 55 and 103 bar) [30] in order to reduce the cost of vessels or pipeline air storage systems, despite the big throttling loss.

The characteristics of some existing CAES plants with varying air storage pressures are presented in Table 3.1.

Table 3.1: Characteristics of some existing CAES plants with varying pressure of air storage
(*CP-P* : Constant Pressure *P* Storage)

Site	Capacity (MW)	P_{S1} (bar)	P_{S2} (bar)	P_{S2}/P_{S1}	Throttling Loss	$CP - P_{S1}$ Volume	$CP - P_{S2}$ Volume
Huntorf	290	48	66	1.38	4.1%	38%	27%
McIntosh	110	45	74	1.64	6.6%	65%	39%
EPRI	15	55	103	1.87	7.9%	87%	47%

The pressure of the cavern (or vessel) varies over the operating range of the storage pressure (from P_{S2} to P_{S1}). The energy losses resulting from the throttling process are calculated based on exergy analysis, and presented in Table 3.1.

The specific exergy of an air stream can be expressed as

$$k = h - h_0 - T_0(s - s_0) \quad (3.1)$$

where k , h , and s are the specific exergy, enthalpy, and entropy, respectively, and the subscript 0 indicates that the properties are taken at reference temperature and pressure (T_0, P_0) as a dead state.

The exergy destruction rate \dot{L}_t and total exergy destruction L_t resulting from the throttling process for one cycle (from P_{S2} to P_{S1}) can be defined as follows:

$$\dot{L}_t \equiv \frac{k(t) - k_{PS1}}{k(t)} \quad (3.2)$$

$$L_t \equiv \frac{\int_0^t \dot{M}_a k(t) dt - \int_0^t \dot{M}_a k_{PS1} dt}{\int_0^t \dot{M}_a k(t) dt} \quad (3.3)$$

$$\dot{M}_a = -\frac{dM_s}{dt} = \frac{V_s}{rT} \frac{dP_s}{dt} \quad (3.4)$$

where $k(t)$ is the specific exergy of a mass flow at time t from Eq. 3.1; k_{PS1} , the specific exergy of regulated pressure P_{S1} of air; M_s , the mass of air in storage volume; V_s , the air storage volume; and P_s , the pressure of air in storage volume.

Fig. 3.1 shows the pressure variation in the storage cavern and the exergy destruction rate for the one cycle of discharging process in the case of Huntorf CAES plant. In practice, even during the compression process, the varying pressure ratio can result in low compression efficiency as a result of the deviation from the design point. The use of a constant-pressure compensated cavern may reduce the required storage volume significantly. In Table 3.1, the $CP - P_{S1}$ and $CP - P_{S2}$ volumes are the percentages of volume ratio with the application of constant-pressure P_{S1} and P_{S2} in the cavern using a compensating water column, respectively.

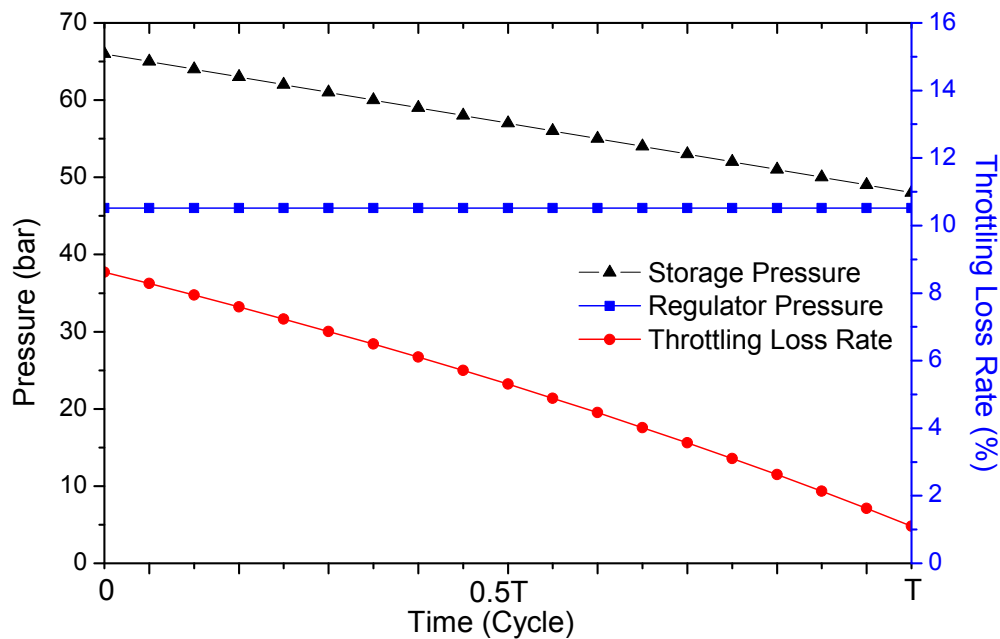


Fig. 3.1: Pressure variation in the storage cavern and throttling loss rate for discharging process in the case of Huntorf CAES plant.

3.2 Novel constant-pressure CAES system combined with PHS

3.2.1 Principle of constant-pressure CAES system combined with PHS

In order to minimize the air storage volume while maintaining a high efficiency of CAES system at a design condition, a constant-pressure CAES system with a compensating water column is proposed, as shown in Fig. 3.2, where water from a surface reservoir displaces compressed air [14,15]. The use of a constant-pressure compensated cavern requires the smallest cavern among all the designs. It was estimated that for a configuration similar to the Huntorf design (with a storage pressure of 60 bar), a constant pressure cavern could deliver the same output with only 23% of the storage volume required for a constant volume configuration with variable inlet pressure (with caverns operating between 48 to 66 bar) [32].

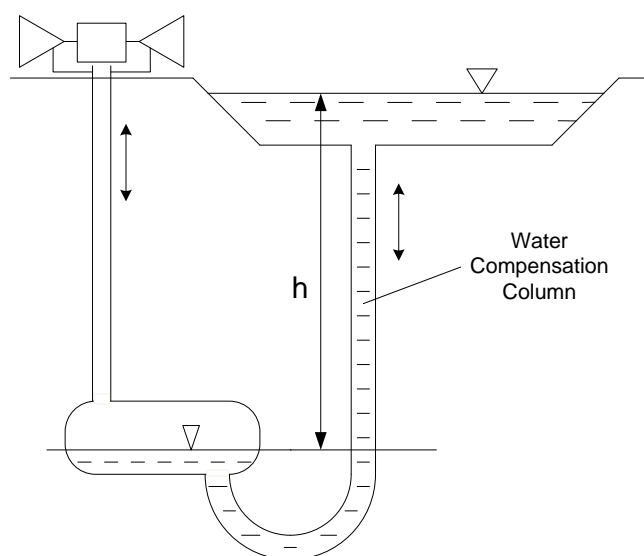


Fig. 3.2: Constant-pressure CAES system with compensating water column.

However, the constant pressure system requires a very deep air storage cavern in order to produce the required pressure difference by means of a water column, which results in increased construction costs. In order to use an air storage cavern with a shallow depth, the CAES that provides constant air pressure by using a hydraulic pump instead of elevation difference of the water column has previously been proposed [29], as shown in Fig. 3.3. However, one disadvantage of such a system is that the hydraulic pump consumes approximately 15% of the generated power.

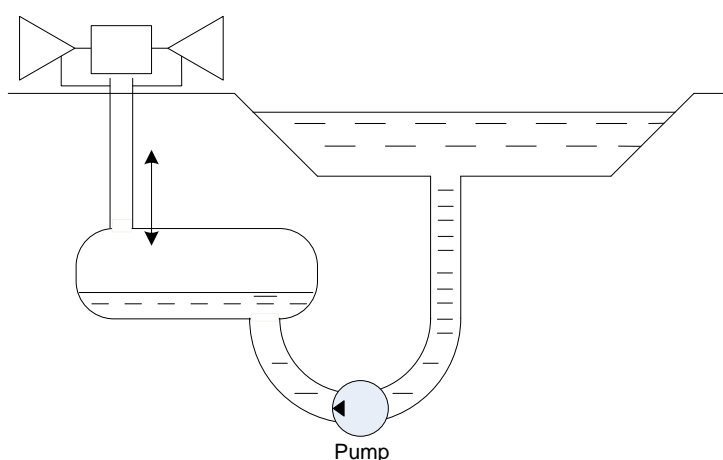


Fig. 3.3. Constant-pressure CAES system with water pump.

Therefore, for the purpose of addressing the current problems of CAES system, a novel constant-pressure (CP-) CAES system combined with pumped hydro storage (PHS) is proposed [16,18]. The system combines constant-pressure air storage and hydraulic energy storage, as shown in Fig. 3.4, and consists of at least two compressed air storage tanks that are connected by a connection pipe attached to their lower portions; each of these have separate spaces for air and water storage [16,18]. Thus, when compressed air of a desired pressure is injected into one of the storage tanks (left) connected to a compressor using off-peak power, the storage water is forcibly transferred into the other sealed air storage tank (right) by a water pump installed on the connection pipe using off-peak power; thus, the pressure in the storage tank (left) is maintained at a constant value. The sealed air tank (right) serves as an accumulator for storing hydraulic energy due to the compression of sealed air.

Furthermore, when the compressed air in the storage tank connected to a turbine is discharged during periods of high demand, the hydraulic pump (or separate hydraulic turbine) on the connection pipe serves as a hydraulic turbine (or motor) and supplies the storage water into the storage tank storing the compressed air (left) to maintain a constant pressure in the storage tank (left). At that time, electricity is generated by using the hydraulic energy stored in the accumulator through the water turbine (or hydraulic motor). Therefore, the sealed air tank is used to maintain a constant pressure in the air storage tank of the CAES system and also serves as hydraulic energy storage, which is one of the most efficient methods for storing energy.

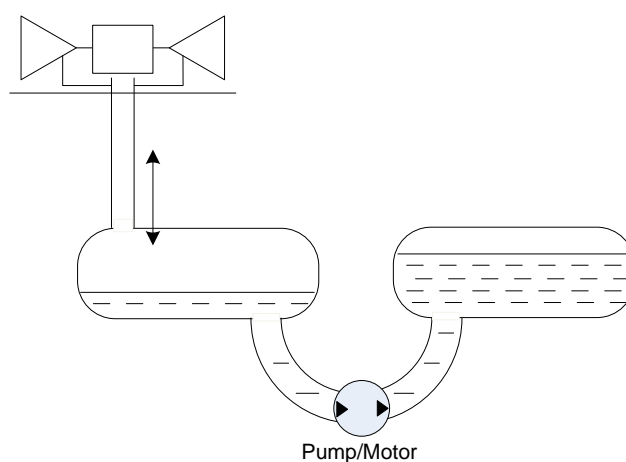


Fig. 3.4: Constant-pressure CAES combined with pumped hydro storage.

The novel constant-pressure CAES system to be analyzed is shown in Fig. 3.5 and has two tanks of the same volume (V_1). At the start of charging of the air storage tank with compressed air of the desired pressure (P_s) from the compressor, the air storage tank (left) is completely filled with water, and the other sealed tank (right) is filled with compressed air of a pressure (P_1) slightly higher than P_s . At the end of the charging process, the volume of compressed air in the sealed tank (right) is V_2 , the pressure of the sealed air is P_2 , and the volume corresponding to the displaced water ($V_1 - V_2$) in the air storage tank (left) is charged with compressed air of the desired pressure (P_s). Discharging of the air storage tank is the reverse of the charging process.

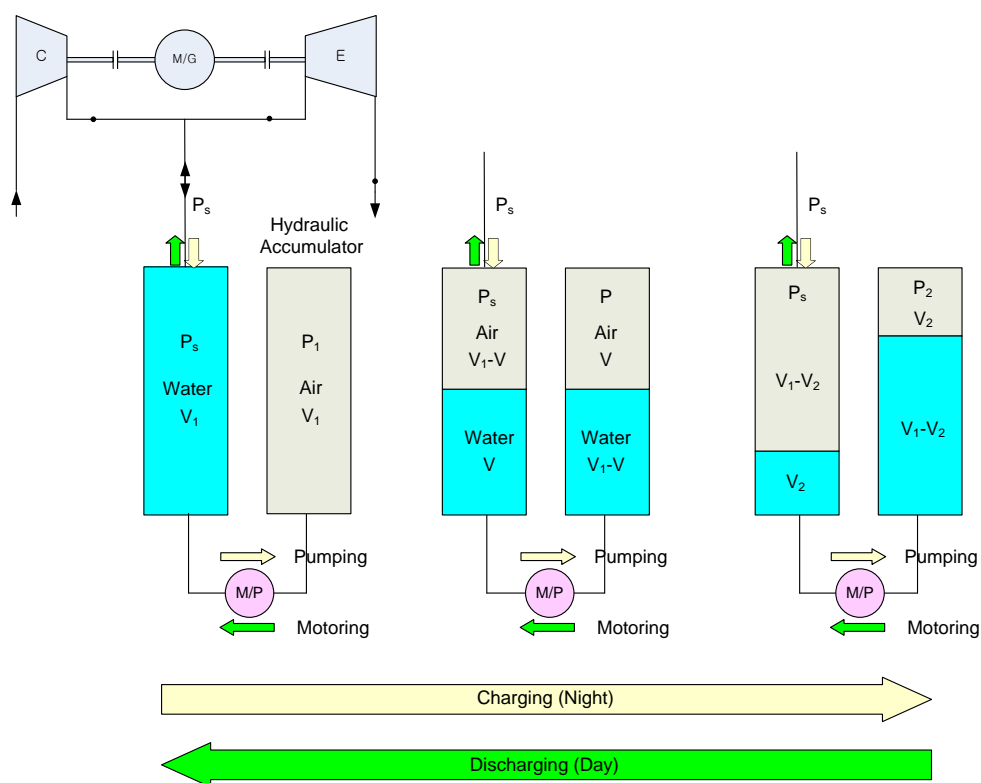


Fig. 3.5: Operation process of constant-pressure CAES combined with pumped hydro storage.

3.2.2 Energy and exergy analyses of the novel CAES system

The following assumptions are made for the analysis of the novel CAES system:

- (a) The gas (air) acts as a perfect gas.
- (b) The hydraulic fluid (water) is incompressible.
- (c) In the gas and liquid flows, negligible potential and kinetic energy effects, absence of phase change, and no chemical reaction were assumed.
- (d) There is no pressure loss in the pipes of gas and liquid flows.

The general exergy balance can be expressed in the rate form as

$$\dot{E}^+ - \dot{E}^- = \dot{L} \quad (3.5)$$

where \dot{E}^+ is the rate of exergy transfer to the system by heat, work, and mass; \dot{E}^- is the rate of exergy transfer from the system; and \dot{L} is the rate of exergy destruction [27].

Exergy transfer to the system by heat, \dot{E}_q^+ , can be defined as:

$$\dot{E}_q^+ \equiv \int (1 - \frac{T_0}{T}) \delta \dot{Q}^+ \quad (3.6)$$

where \dot{Q}^+ is the heat exchange rate received from the thermal source at temperature T .

Exergy transfer from the system by heat, \dot{E}_q^- , can be defined as:

$$\dot{E}_q^- \equiv \int (1 - \frac{T_0}{T}) \delta \dot{Q}^- \quad (3.7)$$

where \dot{Q}^- is the heat exchange rate released from the system at temperature T .

Exergy transfer to the system by mass flow \dot{E}_y^+ can be defined as

$$\dot{E}_{yk}^+ \equiv \dot{M}_k (k_{in} - k_{out}) = \dot{M}_k [(h_{in} - h_{out}) - T_0 (s_{in} - s_{out})] \quad (3.8)$$

Exergy transfer from the system by mass flow \dot{E}_y^- can be defined as

$$\dot{E}_{yk}^- \equiv \dot{M}_k (k_{out} - k_{in}) = \dot{M}_k [(h_{out} - h_{in}) - T_0 (s_{out} - s_{in})] \quad (3.9)$$

where k , h and s are specific exergy of a mass flow and specific enthalpy and entropy, respectively.

In the perfect gas flow,

$$h_{in} - h_{out} = c_p (T_{in} - T_{out}) \quad (3.10)$$

$$s_{in} - s_{out} = c_p \ln \frac{T_{in}}{T_{out}} - r \ln \frac{P_{in}}{P_{out}} \quad (3.11)$$

where r is the specific gas constant.

For liquid flow, neglecting density change ($d\rho \cong 0$),

$$h_{in} - h_{out} = c_p (T_{in} - T_{out}) + \frac{P_{in} - P_{out}}{\tilde{\rho}} \quad (3.12)$$

$$s_{in} - s_{out} = c \ln \frac{T_{in}}{T_{out}} \quad (3.13)$$

where c is the specific heat and $\tilde{\rho}$ is the average density of the liquid.

It is reasonable to neglect the density change of water by pumping in this study, since if the ambient temperature (20°C) of water is isentropically pressurized from 5 MPa to 20 MPa, the volume change of water is about 0.7%.

Fig. 3.6 and Fig. 3.7 show the energy and exergy flow of the novel CAES system. The system is divided into two sub-systems [33], a sub-system A (compressed air part) and a sub-system B (hydraulic part). There is an interaction by boundary work between sub-system A and sub-system B due to charging or discharging of compressed air.

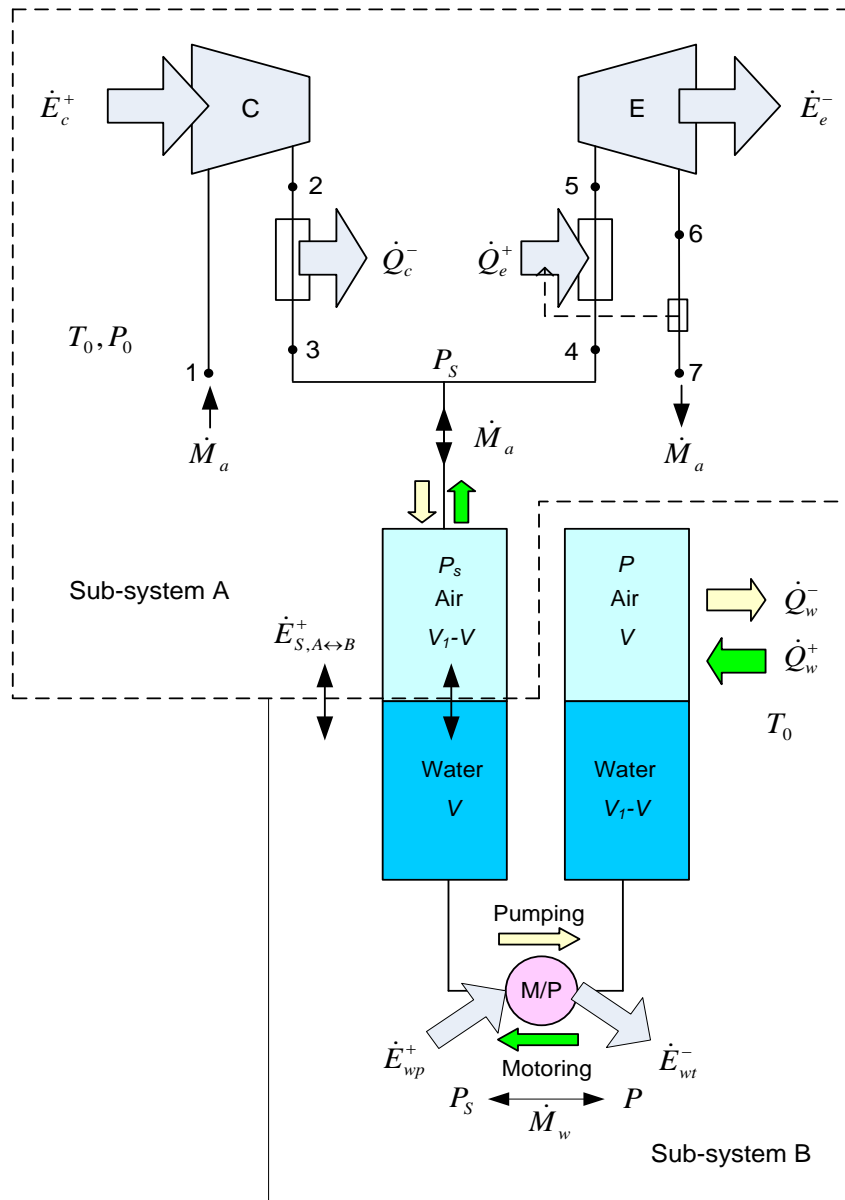


Fig. 3.6: Energy and exergy flow of the novel CAES system.

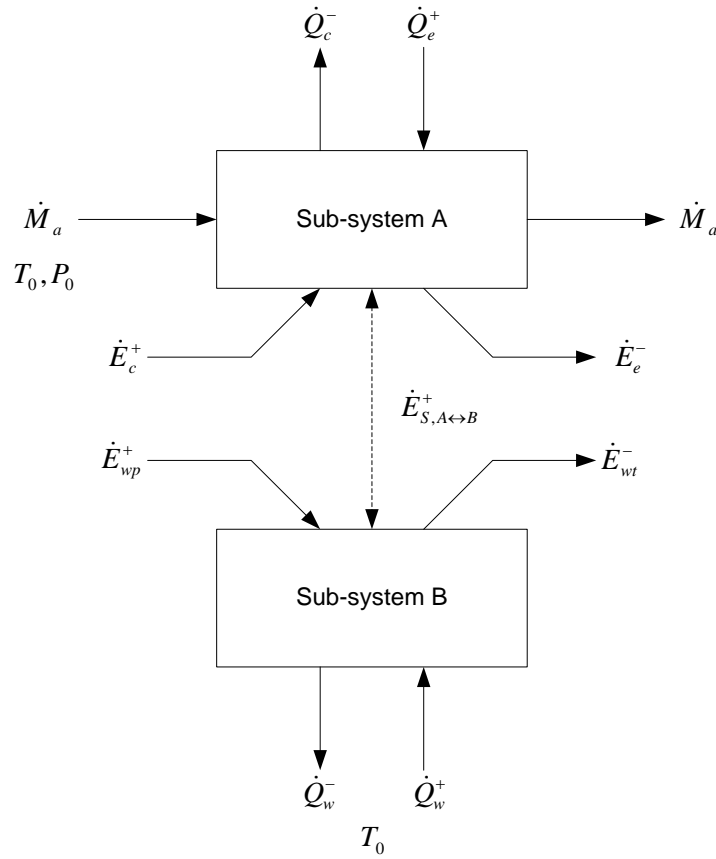


Fig. 3.7: Energy and exergy flow of the simplified sub-systems

For the compression process, the exergy balance is as follows:

$$\dot{L}_c = \dot{E}_c^+ - \dot{E}_{ya}^- \quad (3.14)$$

where \dot{E}_c^+ is the exergy transfer to the system by compression work and \dot{E}_{ya}^- is the exergy transfer from the compressor to the air flow.

Exergy efficiency (second law efficiency) of the compressor can be defined as:

$$\eta_{II,c} \equiv \frac{\dot{E}_{ya}^-}{\dot{E}_c^+} \quad (3.15)$$

The total exergy from the compressor to the air flow for charging process E_{ya}^- can be expressed as

$$E_{ya}^- = \int_1^2 \dot{E}_{ya}^- dt \quad (3.16)$$

In a similar manner, for the water pump in the charging process, the exergy balance is expressed as follows:

$$\dot{L}_{wp} = \dot{E}_{wp}^+ - \dot{E}_{yw}^- \quad (3.17)$$

where \dot{E}_{wp}^+ is the exergy transfer to the system by pumping work and \dot{E}_{yw}^- is the exergy transfer from the water pump to the water flow.

Exergy efficiency (second law efficiency) of the water pump can be defined as

$$\eta_{II,wp} \equiv \frac{\dot{E}_{yw}^-}{\dot{E}_{wp}^+} \quad (3.18)$$

In this study, if the ambient temperature (20°C) of water is isentropically pressurized from 5 MPa (left tank) up to 20 MPa (right tank), the temperature change of the water is about 0.24°C (less than 0.1%). By neglecting the temperature change of water when pumping from the left tank (P_s) to the right tank (P), the exergy transfer from the water pump to the water flow \dot{E}_{yw}^- from Eqs. 3.9, 3.12, and 3.13, can be expressed as

$$\dot{E}_{yw}^- \equiv \dot{M}_w (k_{out} - k_{in}) \cong \dot{M}_w \frac{P - P_s}{\tilde{\rho}} \quad (3.19)$$

The mass flow rate of water can be expressed as

$$\dot{M}_w = -\tilde{\rho} \frac{dV}{dt} \quad (3.20)$$

where V is the volume of sealed air in the right tank, which changes according to the transferred water.

\dot{E}_{yw}^- can then be expressed as

$$\dot{E}_{yw}^- = (P_s - P) \frac{dV}{dt} \quad (3.21)$$

The gas compression or expansion process of sealed air in the right tank can be modeled as a polytropic process ($PV^n = const$). Then, the total exergy from the water pump to the water

flow E_{yw}^- can be expressed as

$$E_{yw}^- = \int_1^2 \dot{E}_{yw}^- dt = \int_1^2 (P_S - P) \frac{dV}{dt} dt = \int_1^2 (P_S - \frac{P_1 V_1^n}{V^n}) dV \quad (3.22a)$$

$$n \neq 1: \quad E_{yw}^- = \frac{P_2 V_2 - P_1 V_1}{n-1} - P_S (V_1 - V_2) \quad (3.22b)$$

$$n = 1: \quad E_{yw}^- = P_1 V_1 \ln \frac{V_1}{V_2} - P_S (V_1 - V_2) \quad (3.22c)$$

For an ideal case without exergy loss due to heat transfer, the compression process of the enclosed air in the right tank was assumed to be a quasi-isothermal process ($PV = const$) that results from sufficient heat transfer with the environment considering that the compression pressure ratio of the sealed air, P_2/P_1 , is low and the charging process in the CAES system is a very slow process with a duration of 10 hr. However, the effect of heat transfer between the two media (air, water) and the cavern on the performance of the system and the exergy loss due to the heat transfer were examined in the later part of this study.

Similarly, for the expansion process of the discharging process, the exergy balance is as follows:

$$\dot{L}_e = \dot{E}_{ya}^+ - \dot{E}_e^- \quad (3.23)$$

where \dot{E}_{ya}^+ is the exergy transfer from the air flow to the expander and \dot{E}_e^- is the resulting exergy transfer from the expander to the generator.

Exergy efficiency (second law efficiency) of the expander can be defined as

$$\eta_{II,e} \equiv \frac{\dot{E}_e^-}{\dot{E}_{ya}^+} \quad (3.24)$$

For the water turbine in the discharging process, the exergy balance is as follows:

$$\dot{L}_{wt} = \dot{E}_{yw}^+ - \dot{E}_{wt}^- \quad (3.25)$$

where \dot{E}_{yw}^+ is the exergy transfer from the water flow to the water turbine and \dot{E}_{wt}^- is the exergy transfer from the water turbine to the generator.

Exergy efficiency (second law efficiency) of the water turbine can be defined as

$$\eta_{II,wt} \equiv \frac{\dot{E}_{wt}^-}{\dot{E}_{yw}^+} \quad (3.26)$$

In this study, the exergy efficiencies of the water pump and water turbine are assumed to be 0.9, and the exergy efficiencies of the compressor and expander are assumed to be 0.85. Although the compression work varies according to various compression processes—e.g., isothermal, adiabatic compression, and two-, three-, and four-stage compression with intercooling—the compressed air is cooled and stored at the same state. The kinetic and potential energies are neglected; in addition, the temperature of the compressed air to or from the storage tank is nearly equal to the ambient temperature, so the difference between the two temperatures is neglected. The final exergy transfer from the system to the air flow, from state 1 with a reference environment (T_0, P_0) to state 3 (T_0, P_S) , before storage, from Eqs. 3.9–3.11 can be expressed as

$${}^3_1\dot{E}_{ya}^- \equiv \dot{M}_a r T_0 \ln \frac{P_S}{P_0} \quad (3.27)$$

The exergy loss rate of air flow due to heat transfer by cooler is as follows:

$$\begin{aligned} \dot{L}_{q,c} &= -{}_2^3\dot{E}_{ya}^- = \dot{M}_a (k_2 - k_3) = \dot{M}_a [(h_2 - h_3) - T_0 (s_2 - s_3)] \\ &= \dot{M}_a \left[c_p (T_2 - T_0) - T_0 c_p \ln \frac{T_2}{T_0} \right] \end{aligned} \quad (3.28)$$

Although the exergy loss of air flow by cooler can be dissipated, the heat exergy can be stored and reused by the thermal storage for generation. In the case of multi-stage compression with intercooling, the total exergy loss rate of air flow due to heat transfer by coolers is the sum of the exergy loss rates in every stage.

The exergy transfer to or from the storage tank by compressed air with a reference environment (T_0, P_0) is defined as

$$\dot{E}_a \equiv \dot{M}_a r T_0 \ln \frac{P_S}{P_0} \quad (3.29)$$

When the air volume inside the right tank decreases from V_1 to V_2 owing to the transferred water, the volume of compressed air charged in the left tank is $V_1 - V_2$, and the total exergy of the compressed air charged in the left tank for one cycle can be defined as

$$E_a \equiv \int_1^2 \dot{E}_a dt = rT_0 \ln \frac{P_s}{P_0} \int_1^2 \dot{M}_a dt \quad (3.30)$$

The total mass of compressed air charged for one cycle, M_a , can be expressed as

$$M_a \equiv \int_1^2 \dot{M}_a dt = \frac{P_s(V_1 - V_2)}{rT_0} \quad (3.31)$$

Eq. 3.30 can then be expressed as

$$\begin{aligned} E_a &\equiv \int_1^2 \dot{E}_a dt = M_a rT_0 \ln \frac{P_s}{P_0} \\ &= P_s(V_1 - V_2) \ln \frac{P_s}{P_0} \end{aligned} \quad (3.32)$$

Exergy rate balance in the sub-system A [27] for the charging process can be expressed as

$$\dot{L}_{ch,A} = \dot{E}_c^+ + \dot{E}_{S,B \rightarrow A}^+ + \dot{M}_a k_1 - \dot{M}_a (u_3 + P_0 v_3 - T_0 s_3) \quad (3.33)$$

where $\dot{L}_{ch,A}$ is the global exergy loss rate of the sub-system A for the charging process and $\dot{E}_{S,B \rightarrow A}^+$ is work-power received by the sub-system B.

$$\dot{E}_{S,B \rightarrow A}^+ = (P_s - P_0) \dot{V} \quad (3.34)$$

If we assume that $T_3 = T_1 = T_0$, we obtain that $k_1 = u_0 + P_0 v_0 - T_0 s_0$ and $P_0 v_0 = P_s v_3$

Then, the Eq. 3.33 is expressed as

$$\dot{L}_{ch,A} = \dot{E}_c^+ - M_a rT_0 \ln \frac{P_s}{P_0} = \dot{E}_c^+ - \dot{E}_a = \dot{L}_c + \dot{L}_{q,c} \quad (3.35)$$

The global exergy loss rate of the sub-system A for the charging process, $\dot{L}_{ch,A}$, is the sum of the exergy loss due to irreversibility of compressor, \dot{L}_c , and the exergy loss due to heat transfer of cooler, $\dot{L}_{q,c}$.

In practice, the work required for the charging process is larger than the exergy stored; in particular, the compression work varies according to the compression process, which can be isothermal, adiabatic, or multi-stage compression with intercooling.

The compression factor can be defined as

$$CF \equiv \frac{\dot{E}_{ya,c}^-}{\dot{E}_a} = \frac{\dot{E}_a + \dot{L}_{q,c}}{\dot{E}_a} \quad (3.36)$$

where $\dot{E}_{ya,c}^-$ is the exergy transfer from the compressor to the air flow before cooling and $\dot{L}_{q,c}$ is the exergy loss of air flow by cooler.

The compression factor is the ratio of the exergy transfer from the compressor to the air flow, depending on the compression process, to the final exergy transfer to the storage tank by air flow and represents the degree of exergy loss by cooling of the compressed air. The compression factor CF is 1, 1.15, 1.21, 1.34, and 1.84 for isothermal, four-stage, three-stage, two-stage, and adiabatic compression, respectively. For multi-stage compression, each stage was assumed to have an adiabatic compression process and the same pressure ratio, and the compressed air was cooled to ambient temperature by intercooling. For the adiabatic compression process, CF is 1.84, which means that 84% of additional work is required for compression and is lost by cooling of the compressed air before storage. However, it is possible to reduce the exergy loss by capturing the heat and reusing it, which is the case for advanced-adiabatic CAES [31].

For an ideal hydraulic energy storage without exergy loss due to heat transfer with the environment, the total exergy of the sealed air stored in the right tank can be defined from Eq. 3.22c with $n=1$ as

$$E_h \equiv \int_1^2 \dot{E}_h dt = P_1 V_1 \ln \frac{V_1}{V_2} - P_S (V_1 - V_2) \quad (3.37)$$

The total power required for the charging process in the novel CAES system can be defined as

$$\dot{E}_{ch}^+ \equiv \dot{E}_c^+ + \dot{E}_{wp}^+ = (\dot{E}_a \times CF) / \eta_c + \dot{E}_h / \eta_{wp} \quad (3.38)$$

The total work required for the charging process of one cycle can be defined as

$$E_{ch}^+ \equiv \int_1^2 \dot{E}_{ch}^+ dt = (E_a \times CF) / \eta_c + E_h / \eta_{wp} \quad (3.39)$$

For the discharging process, the compressed air in the CAES plant is generally heated by the use of fuel or other heat sources, and the generator output is greater than the exergy of the compressed air from the storage cavern. If the compressed air is heated to above 700°C, the power generated is twice the exergy of the compressed air from the storage cavern. For example, in the Huntorf CAES plant, an air mass flow of 417 kg/s and turbine inlet pressure of 46 bar of compressed air produce a generator output of 290 MW [14]; this is 2.16 times more energy than the exergy of the compressed air. Similarly, for the McIntosh plant, an air mass flow of 154 kg/s and turbine inlet pressure of 43 bar of compressed air produce a generator output of 110 MW [15]; this is 2.26 times more energy than the exergy of the compressed air.

The heating factor can be defined as

$$HF \equiv \frac{\dot{E}_{ya,e}^+}{\dot{E}_a} = \frac{\dot{E}_a + \dot{E}_q^+}{\dot{E}_a} \quad (3.40)$$

where $\dot{E}_{ya,e}^+$ is the exergy transfer from the heated air flow to the expander after heating and \dot{E}_q^+ is the heat exergy received from the heat source.

The heating factor is the ratio of the exergy transfer from the heated air flow to the expander, which depends on the heating of compressed air, to the exergy transfer from the storage tank by air flow; it represents the degree of exergy gain by heating of the compressed air. The heating factor HF corresponds to 1 (isothermal), 1.79 (AA-CAES), and 2.66 (McIntosh) assuming that the exergy efficiency of the turbine is 0.85. For advanced-adiabatic CAES, the compressed air was assumed to be heated up to 600°C [31]. For the McIntosh plant with $HF = 2.66$, assuming that the exergy efficiency of the turbine is 0.85, the heating factor means that 2.26 times more work than the exergy of the compressed air from the storage cavern is produced by heating of the compressed air.

The total power produced for the discharging process in the novel CAES system can be defined as

$$\dot{E}_{dc}^- \equiv \dot{E}_e^- + \dot{E}_{wt}^- = (\dot{E}_a \times HF) \times \eta_e + \dot{E}_h \times \eta_{wt} \quad (3.41)$$

The total work produced for the discharging process for one cycle can be defined as

$$E_{dc}^- \equiv \int_2^1 \dot{E}_{dc}^- dt = (E_a \times HF) \times \eta_e + E_h \times \eta_{wt} \quad (3.42)$$

3.2.3 Operating characteristics of the novel CAES system

The air storage pressure of the CAES system is generally optimized by the energy density, efficiency, and cost of the system. The general value of the air-releasing pressure for CAES gas turbine is around 5 MPa [14,15]; therefore, an assumed P_s value of 5 MPa was used for the novel CAES system. Fig. 3.8 shows the total work output E_{dc}^- and maximum hydraulic pressure P_2 of the novel CAES system according to the charge ratio, which is defined as $(V_1 - V_2)/V_1$.

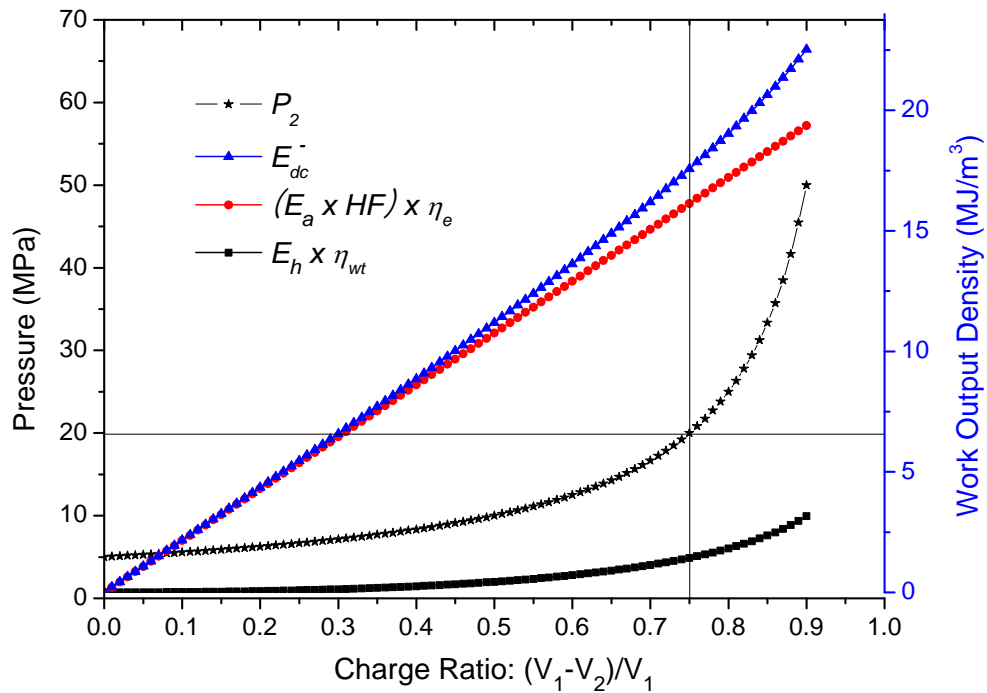


Fig. 3.8: Work outputs and maximum hydraulic pressure of the novel CAES system according to charge ratio (with heating, $HF = 2.6$).

A heating factor of $HF = 2.6$ was assumed; this means that 2.2 times more energy than the exergy of the compressed air from the storage tank is produced by heating of the compressed air as in an existing CAES plant. The work outputs of the compressed air part ($(E_a \times HF) \times \eta_e$), hydraulic part ($E_h \times \eta_{wt}$), and the sum of the two (E_{dc}^-) are presented as work output density; this is defined as the work output per unit volume of total storage ($2V_1 = 1 \text{ m}^3$) since the novel CAES system uses the same volume (V_1) for the two tanks.

If the charge ratio increases, the total work output density (E_{dc}^-) increases almost linearly because the work output by the compressed air part ($(E_a \times HF) \times \eta_e$) is dominant. In this study, the maximum pressure P_2 in the sealed air tank (right) was assumed to be 20 MPa, where the charge ratio is 0.75. Because the maximum pressure P_2 increases very rapidly above the charge ratio 0.75 even though the increase in work output density is not very great, the maximum pressure of 20 MPa was chosen for the novel CAES system in consideration of the maximum pressure for the storage cavern and hydraulic machinery.

Fig. 3.9 shows the total power required for the charging process \dot{E}_{ch}^+ according to various compression processes with $CF = 1$ (isothermal), 1.15 (four-stage), 1.21 (three-stage), 1.34 (two-stage), and 1.84 (adiabatic).

Fig. 3.10 shows the power required for the compressed air part ($(\dot{E}_a \times CF) / \eta_c$), hydraulic part (\dot{E}_h / η_{wp}), and the sum of two (\dot{E}_{ch}^+) during the charging process for three-stage compression with intercooling, which is generally the case in existing CAES plants. Although the power required for the compressed air part is constant owing to the constant mass flow and pressure of the compressed air, the power required for the hydraulic part increases according to the increase in hydraulic pressure. At the end of the charging process, the power required for the hydraulic part accounts for 37% of the total power.

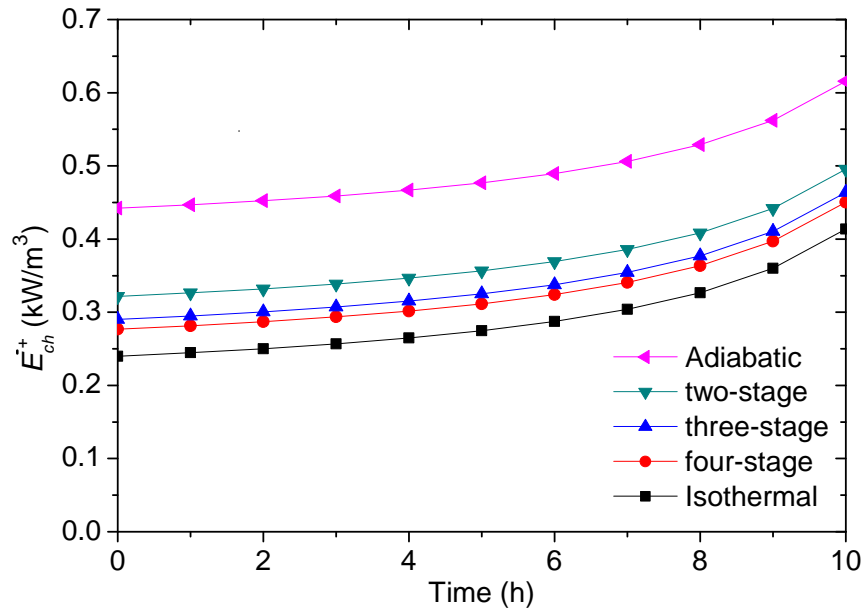


Fig. 3.9: Total power required for charging process according to various compression processes.

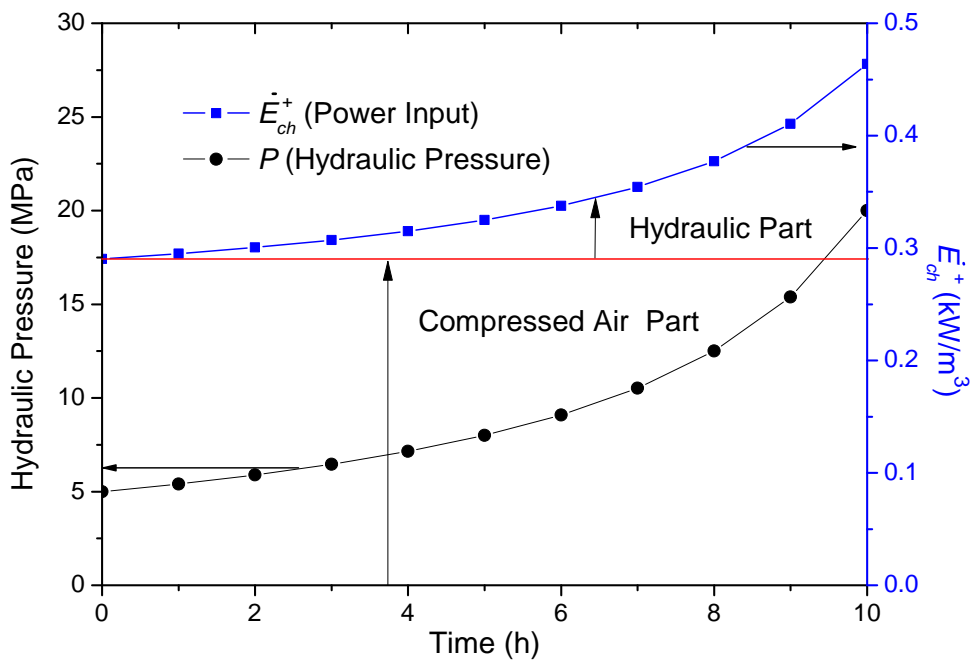


Fig. 3.10: Power required for compressed air part, hydraulic part, and the sum of two during the charging process using three-stage compression with intercooling.

Fig. 3.11 shows the power produced during the discharging process \dot{E}_{dc}^- according to several heating factors: $HF = 1.0$ (isothermal), $HF = 1.79$ (AA-CAES), and $HF = 2.66$ (McIntosh).

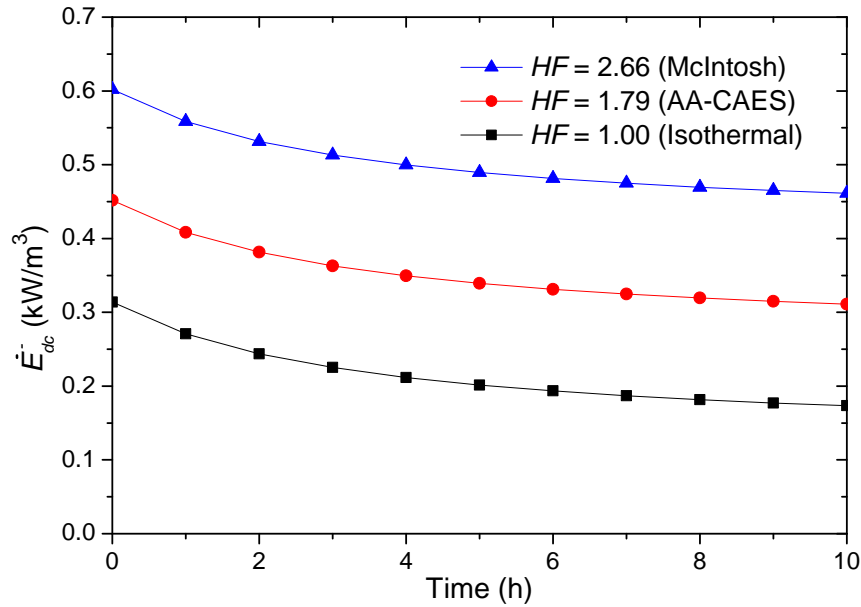


Fig. 3.11: Power produced during discharging process according to several heating factors.

Fig. 3.12 shows the power produced by the compressed air part ($(\dot{E}_a \times HF) \times \eta_e$), hydraulic part ($\dot{E}_h \times \eta_{wr}$), and the sum of two (\dot{E}_{dc}^-) during the discharging process for $HF = 2.66$ (McIntosh). Although the power produced by the compressed air part is constant owing to the constant mass flow and pressure of compressed air, the power produced by the hydraulic part decreases with a decrease in hydraulic pressure. At the start of the discharging process, the power produced by the hydraulic part accounts for 23% of the total power.

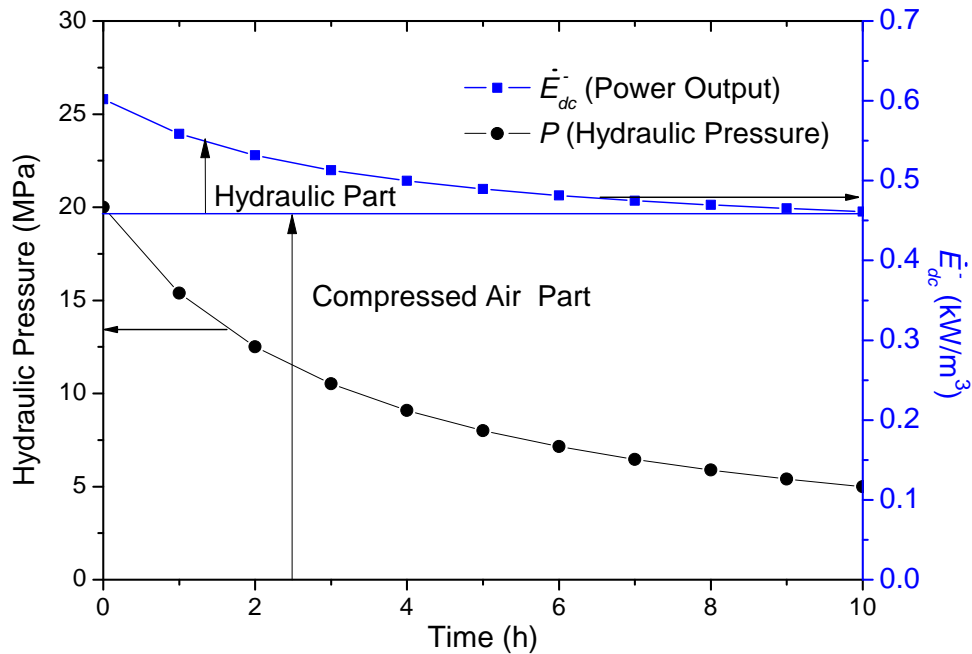


Fig. 3.12: Power produced by the compressed air part, hydraulic part, and sum of the two during the discharging process when $HF=2.66$.

3.2.4 Effect of height of storage cavern on novel CAES system

When applying the novel CAES system to a large scale, it is not easy to neglect the effects of the height of the storage cavern; for example, the height of the salt cavern in the Huntorf CAES plant is 150 m. If the effect of the height of the storage cavern is considered as shown in Fig. 3.13, the initial hydraulic pressure P_1 is slightly higher than $P_s + \rho gH$ (H is the height of the cavern). In the charging process, h_L and h_R are the heights of the water head in the left and right caverns, respectively. The pressure difference across the pump is from $P_s + \rho gh_L$ to $P + \rho gh_R$, and the exergy transfer from the pump to the water flow \dot{E}_{yw}^- in Eq. 3.21 can be revised as

$$\begin{aligned}
 \dot{E}_{yw}^- &= [(P_s + \rho g h_L) - (P + \rho g h_R)] \frac{dV}{dt} \\
 &= [P_s + \rho g (h_L - h_R) - P] \frac{dV}{dt} \\
 &= (P_b - P) \frac{dV}{dt}
 \end{aligned}
 \tag{3.43}$$

where the back pressure P_b , for a similar form as that in Eq. 3.21, is defined as

$$P_b \equiv P_s + \rho g (h_L - h_R)
 \tag{3.44}$$

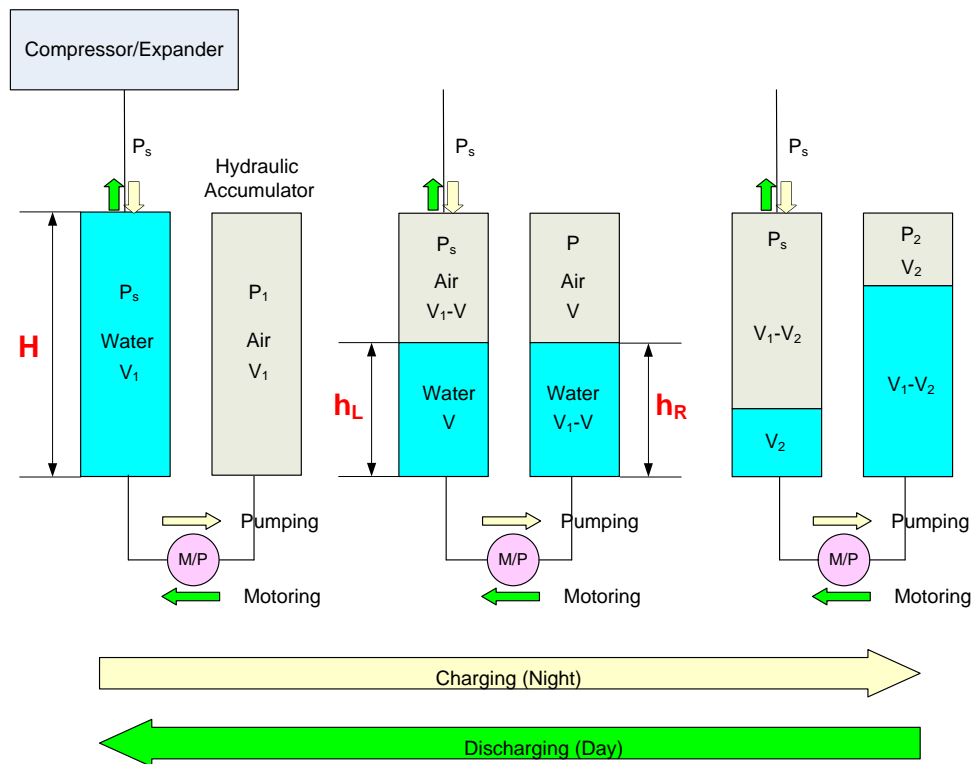


Fig. 3.13: Effect of height of storage cavern on the novel CAES system.

For the charging process, the back pressure assists in pumping water, and the height of the cavern assists in pumping water when $h_L - h_R$ is positive but is a burden when $h_L - h_R$ is negative. The effect of gravity on the overall work reduces the pumping work (exergy transfer from the pump to the water) because the positive work is larger than the negative

work.

To evaluate the effect of gravity on the overall work, the exergy transfer from the pump to the water in Eq. 3.43 can be revised as

$$\begin{aligned}\dot{E}_{yw}^- &= (P_s - P) \frac{dV}{dt} + \rho g (h_L - h_R) \frac{dV}{dt} \\ &= \dot{E}_{yw,a}^- + \dot{E}_{yw,g}^- \end{aligned} \quad (3.45)$$

where $\dot{E}_{yw,a}^-$ and $\dot{E}_{yw,g}^-$ are the exergy transfer from the pump to the water due to compressed air and gravity, respectively.

The total exergy transfer from the pump to the water can be expressed as:

$$\begin{aligned}E_{yw}^- &= \int_1^2 \dot{E}_{yw,a}^- dt + \int_1^2 \dot{E}_{yw,g}^- dt \\ &= E_{yw,a}^- + E_{yw,g}^- \end{aligned} \quad (3.46)$$

where $E_{yw,a}^-$ and $E_{yw,g}^-$ are the total exergy transfer from the pump to the water due to compressed air and gravity, respectively.

Figs. 3.14 and 3.15 show the total power required for the charging process (\dot{E}_{ch}^+), pressure of sealed air (P), and back pressure (P_b) during the charging process for three-stage compression with intercooling when $H = 100$ and 200 m, respectively.

The effect of gravity increases the initial pressure of the sealed air (P_1) and tilts the back pressure slightly. The effect of gravity increases with the height of the cavern. The effects of the height of the cavern on the novel CAES system when $H = 100$ and 200 m are summarized in Table 3.2.

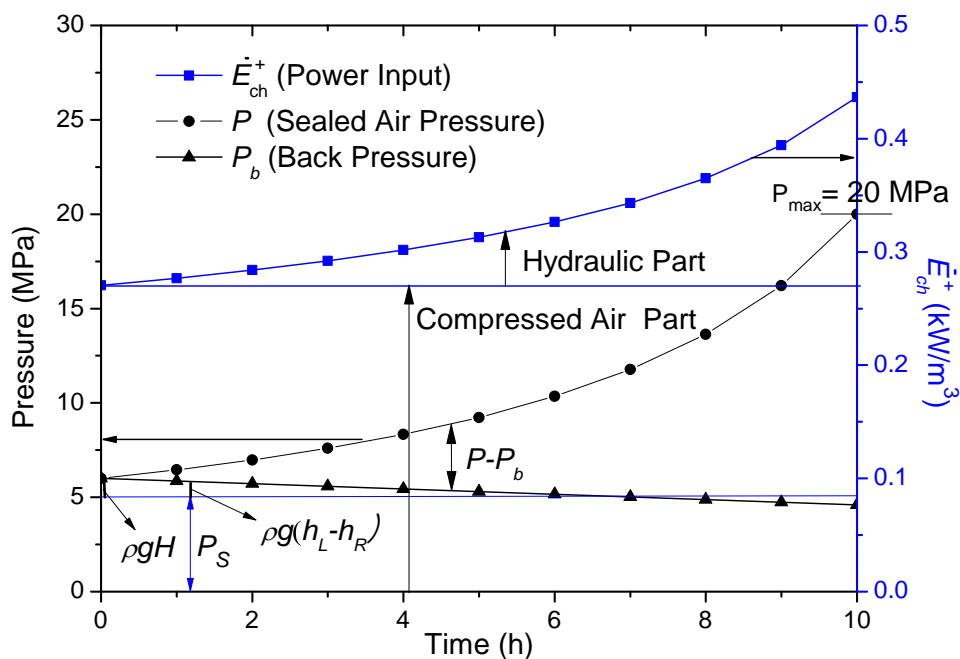


Fig. 3.14: Total power required for charging, pressure of sealed air, and back pressure during the charging process using three-stage compression with intercooling ($H = 100$ m).

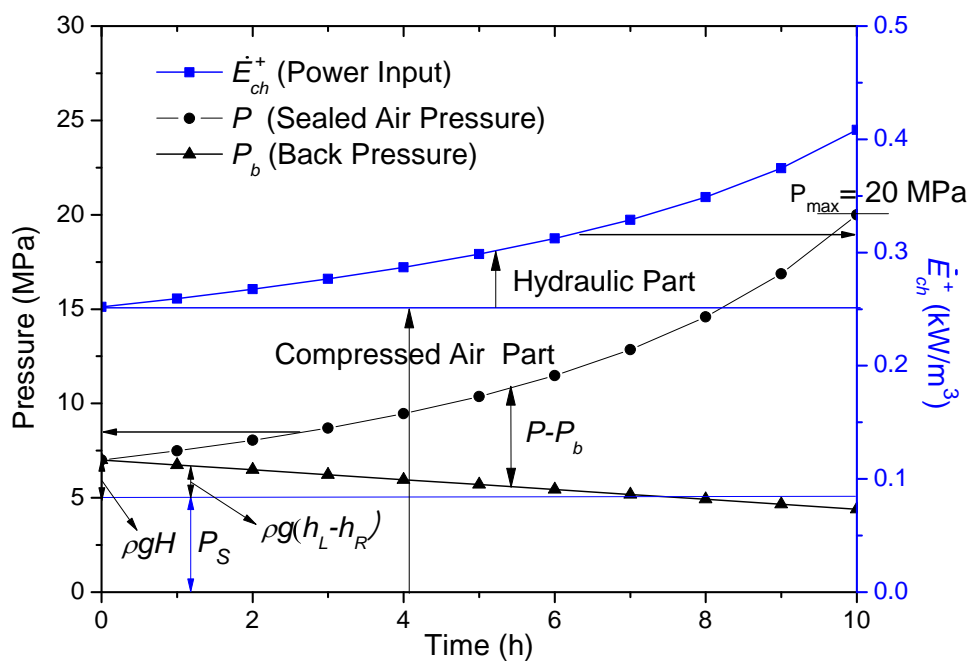


Fig. 3.15: Total power required for charging, pressure of sealed air, and back pressure during the charging process using three-stage compression with intercooling ($H = 200$ m).

Table 3.2: Effect of height of storage cavern on the novel CAES system

Height of cavern			H neglected	$H = 100$ m	$H = 200$ m
P_s (Storage pressure)			5 MPa	5 MPa	5 MPa
P_1 (Initial pressure of sealed air)			5 MPa	6 MPa	7 MPa
P_2 (Final pressure of sealed air)			20 MPa	20 MPa	20 MPa
Charge Ratio ($1 - V_2 / V_1$)			0.75	0.7	0.65
Exergy Transfer (MJ/m ³)	Air	E_a	7.335	6.845	6.358
	Hydraulic	$E_{yw,a}^-$	1.591	1.863	2.05
		$E_{yw,g}^-$	0	-0.105	-0.228
		E_{yw}^-	1.591	1.758	1.822
	Total	$E_a + E_{yw}^-$	8.926	8.603 (3.6% ↓)	8.180 (8.4% ↓)
Charging Work $\eta_c = 0.85$ $CF = 1.21$ $\eta_{wp} = 0.9$	Air	E_c^+	10.442	9.744	9.051
	Hydraulic	E_{wp}^+	1.768	1.953	2.024
	Total	E_{ch}^+	12.209	11.697 (4.2% ↓)	11.075 (9.3% ↓)
Discharging Work $\eta_e = 0.85$ $HF = 2.66$ $\eta_{wt} = 0.9$	Air	E_e^-	16.584	15.477	14.375
	Hydraulic	E_{wt}^-	1.432	1.582	1.640
	Total	E_{dc}^-	18.016	17.059 (5.3% ↓)	16.015 (11.1% ↓)

According to the increase in the height of the cavern, the initial hydraulic pressure P_1 must be increased; inevitably, the charge ratio decreases owing to the limit of the maximum pressure ($P_2 = 20$ MPa). The decrease in charge ratio results in a reduction of the total mass of compressed air being charged, which reduces the exergy stored by the compressed air (E_a). However, the exergy stored by the hydraulic storage (E_{yw}^-) increases owing to the increase in P_1 because the rise in $E_{yw,a}^-$, hydraulic energy due to the compressed air, is much bigger than the small reduction in $E_{yw,g}^-$, pumping work due to gravity. The total exergy $E_a + E_{yw}^-$ stored by the novel CAES system when $H = 100$ and 200 m decreases slightly by 3.6% and 4.9%, respectively, because the reduction in exergy E_a stored by the compressed air part is partly compensated for by the increase in exergy E_{yw}^- stored by the hydraulic part.

For the charging process when $\eta_{wp} = 0.9$, $\eta_c = 0.85$, and $CF = 1.21$ (three-stage with intercooling), the total work required for energy storage E_{ch}^+ decreases by 4.2% and 9.3% when $H = 100$ and 200 m, respectively. For the discharging process when $\eta_{wt} = 0.9$, $\eta_e = 0.85$, and $HF = 2.66$ (McIntosh), the total work produced by energy storage E_{dc}^- decreases by 5.3% and 11.1% when $H = 100$ and 200 m, respectively.

3.2.5 Effect of heat transfer between the two media (air, water) and the cavern

Although the compression process of the sealed air in hydraulic energy storage was assumed to be an isothermal process for an ideal case, further study is needed to consider the heat transfer between the two media (air, water) and the cavern depending on the thermal conductivity, size, and shape of the cavern [34,35]. Some experimental results from the Huntorf plant showed that when the cavern was emptied from 80 bar to 20 bar for 16 hours, the temperature of air in the cavern decreased from 40°C to about 10°C at the saturation point (adiabatically to -62°C) [21].

To consider the heat transfer between the sealed air and the cavern in the novel CAES system, the compression process of the sealed air was simply assumed to be a polytropic process ($PV^n = \text{const}$). If the maximum pressure in the tank is assumed to be 20 MPa and the sealed air is compressed from 5 MPa (P_1) to 20 MPa (P_2), the volume ratio and temperature rise are given by

$$\frac{V_1}{V_2} = \left(\frac{P_2}{P_1}\right)^{1/n} \quad (3.47)$$

$$\frac{T_2}{T_1} = \left(\frac{P_2}{P_1}\right)^{(n-1)/n} = \left(\frac{V_1}{V_2}\right)^{n-1} \quad (3.48)$$

From Eq. 3.22b, the total exergy from the pump to the water flow E_{yw}^- can be given by

$$E_{yw}^- = \frac{P_2 V_2 - P_1 V_1}{n-1} - P_s (V_1 - V_2) \quad (3.49)$$

After the charging process, the compressed hot air at temperature T_2 was assumed to cool down to the ambient temperature $T_2' (=T_0)$ by heat transfer with the environment. When the compressed air at T_2 cools down to T_2' in a constant volume, the pressure P_2 decreases to P_2' as follows:

$$\frac{P_2'}{P_2} = \frac{T_2'}{T_2} \quad (3.50)$$

The final exergy balance in the sub-system B [27] for the total charging process can be expressed as

$$L_{ch,B} = E_{wp}^+ + E_{S,A \rightarrow B}^+ - (\Delta U_w + P_0 \Delta V_w - T_0 \Delta S_w + \Delta U_a + P_0 \Delta V_a - T_0 \Delta S_a) \quad (3.51)$$

where $L_{ch,B}$ is the global exergy loss of the sub-system B for the charging process and $\dot{E}_{S,A \rightarrow B}^+$ is work-power received by sub-system A.

If we neglect the temperature change and volume change of water for charging process and assume that the compressed air is cooled down to the ambient temperature, we obtain the equations as $\Delta U_w = 0$, $\Delta W_w = 0$, $\Delta S_w = 0$, and $\Delta U_a = 0$. And $T_0 \Delta S_a$ is expressed as

$$T_0 \Delta S_a = T_0 m_a \Delta s_a = T_0 \left(\frac{P_1 V_1}{r T_0} \right) \left(-r \ln \frac{P_2'}{P_1} \right) = -P_1 V_1 \ln \frac{P_2'}{P_1} = -P_1 V_1 \ln \frac{V_1}{V_2} \quad (3.52)$$

Then, the Eq. 3.51 is expressed as

$$\begin{aligned} L_{ch,B} &= \left[L_{wp} + \frac{P_2 V_2 - P_1 V_1}{n-1} - P_S (V_1 - V_2) \right] \\ &\quad + (P_S - P_0)(V_1 - V_2) - \left[P_0 (V_2 - V_1) + P_1 V_1 \ln \frac{V_1}{V_2} \right] \\ &= L_{wp} + \frac{P_2 V_2 - P_1 V_1}{n-1} - P_1 V_1 \ln \frac{V_1}{V_2} = L_{wp} + L_{q,w}^{ch} \end{aligned} \quad (3.53)$$

where $L_{q,w}^{ch}$ is the exergy loss due to the heat transfer between the system and the wall for the charging process and can be expressed as

$$L_{q,w}^{ch} = \frac{P_2 V_2 - P_1 V_1}{n-1} - P_1 V_1 \ln \frac{V_1}{V_2} \quad (3.54)$$

For the discharging process, the compressed air at P_2' and $T_2' (= T_0)$ expands to its final state at P_1' and T_1' with the same volume ratio and polytropic index m ($PV^m = const$). After the discharging process, the expanded cool air at temperature T_1' is assumed to be heated up to the ambient temperature T_1 (20°C) owing to heat transfer with the environment.

The pressure P_1' and temperature T_1' after expansion are given by

$$\frac{P_1'}{P_2'} = \left(\frac{V_2}{V_1} \right)^m \quad (3.55)$$

$$\frac{T_1'}{T_2'} = \left(\frac{V_2}{V_1} \right)^{m-1} \quad (3.56)$$

In the discharging process, similar to the charging process, the total exergy from the water flow to the water turbine E_{yw}^+ can be given by

$$E_{yw}^+ = \frac{P_2' V_2 - P_1' V_1}{m-1} - P_S (V_1 - V_2) \quad (3.57)$$

Similarly, the final exergy balance in the sub-system B [27] for the total discharging process can be expressed as

$$L_{dc,B} = -E_{wt}^- + E_{S,A \rightarrow B}^+ - (\Delta U_w + P_0 \Delta V_w - T_0 \Delta S_w + \Delta U_a + P_0 \Delta V_a - T_0 \Delta S_a) \quad (3.58)$$

where $L_{dc,B}$ is the global exergy loss of the sub-system B for the discharging process and $\dot{E}_{S,A \rightarrow B}^+$ is work-power received by sub-system A.

If we neglect the temperature change and volume change of water for the discharging process and assume that the expanded air is heated up to $T_1 (= T_0)$, we obtain the equations as $\Delta U_w = 0$, $\Delta W_w = 0$, $\Delta S_w = 0$, and $\Delta U_a = 0$. And $T_0 \Delta S_a$ is expressed as

$$T_0 \Delta S_a = T_0 m_a \Delta s_a = T_0 \left(\frac{P_1 V_1}{r T_0} \right) (-r \ln \frac{P_1}{P_2}) = -P_1 V_1 \ln \frac{P_1}{P_2} = -P_1 V_1 \ln \frac{V_2}{V_1} \quad (3.59)$$

Then, the Eq. 3.58 is expressed as

$$\begin{aligned} L_{dc,B} &= - \left[\frac{P_2' V_2 - P_1' V_1}{m-1} - P_s (V_1 - V_2) - L_{wt} \right] \\ &\quad - (P_s - P_0)(V_1 - V_2) - \left[P_0 (V_1 - V_2) + P_1 V_1 \ln \frac{V_2}{V_1} \right] \\ &= L_{wt} + P_1 V_1 \ln \frac{V_1}{V_2} - \frac{P_2' V_2 - P_1' V_1}{m-1} = L_{wt} + L_{q,w}^{dc} \end{aligned} \quad (3.60)$$

where $L_{q,w}^{dc}$ is the exergy loss due to the heat transfer between the system and the wall for the discharging process and can be expressed as

$$L_{q,w}^{dc} = P_1 V_1 \ln \frac{V_1}{V_2} - \frac{P_2' V_2 - P_1' V_1}{m-1} \quad (3.61)$$

To show the effect of heat transfer between the two media and the cavern, some performance results are summarized in Table 3.3 according to the polytropic index for the hydraulic part in the novel CAES system. For simplicity, the polytropic index m for the discharging process was assumed to be equal to the polytropic index n for the charging process. If the rise in the final temperature of compressed air is by 20°, 39°, 58°, or 76°C ($n = 1.05, 1.10, 1.15,$ and 1.20) owing to insufficient heat transfer with the environment, the charge ratio ($1 - V_2 / V_1$)

limited by the maximum pressure ($P_2=20$ MPa) is reduced slightly, which in turn reduces the exergy stored by the compressed air, and the total exergy from the pump by water flow is reduced to a lesser extent.

Table 3.3: Effect of heat transfer between the two media (air, water) and the cavern

n	Charging	T_1 (°C)	P_1 (MPa)	T_2 (°C)	P_2 (MPa)	E_{yw}^- (MJ/m ³)	$\frac{E_{yw}^+}{E_{yw}^-}$	$1 - \frac{V_2}{V_1}$
(m)	Discharging	T_1'	P_1'	T_2'	P_2'	E_{yw}^+		
1.0	Charging	20	5	20	20	1.591	1.0	0.750
	Discharging	20	5	20	20	1.591		
1.05	Charging	20	5	40.0	20	1.580	0.862	0.733
	Discharging	1.3	4.68	20	18.72	1.362		
1.1	Charging	20	5	78.1	20	1.567	0.746	0.716
	Discharging	-28.5	4.17	20	16.69	1.169		
1.15	Charging	20	5	78.1	20	1.552	0.648	0.700
	Discharging	-28.5	4.17	20	16.69	1.006		
1.20	Charging	20	5	96.2	20	1.536	0.564	0.685
	Discharging	-40.4	3.97	20	15.87	0.866		

Although the total exergy flow from the pump to the water flow E_{yw}^- for the charging process is reduced slightly, the exergy flow from the water flow to the water turbine E_{yw}^+ for the discharging process is reduced significantly. This means that if the compressed hot air cools down to ambient temperature for the charging process, there is a pressure drop of compressed air, which results in an exergy loss due to the heat transfer and reduction in work produced by the water turbine for the discharging process. When $n = 1.1$ with a rise in the final temperature of the compressed air of 39°C, the ratio of total exergy flow from the pump to the water turbine E_{yw}^+ / E_{yw}^- is 0.746, which means that there is 25.4% of exergy loss due to

the heat transfer.

3.2.6 Quasi-isothermal process of hydraulic storage by spray water

The round trip efficiency of the hydraulic part can be degraded by irreversibility due to insufficient heat transfer between the two media (air, water) and the cavern. For the quasi-isothermal process of hydraulic storage, spraying water to cool the compressed air can be used, as shown in Fig. 3.16. In the charging process, the water from the pump can be sprayed in the cavern. For a simple modeling of the system, the charging process of the hydraulic part for small time steps with index i as the current time step can be divided into two processes, as shown in Fig. 3.17: adiabatic compression by the transferred water by the pump and a thermal equilibrium process of the compressed air with the sprayed water.

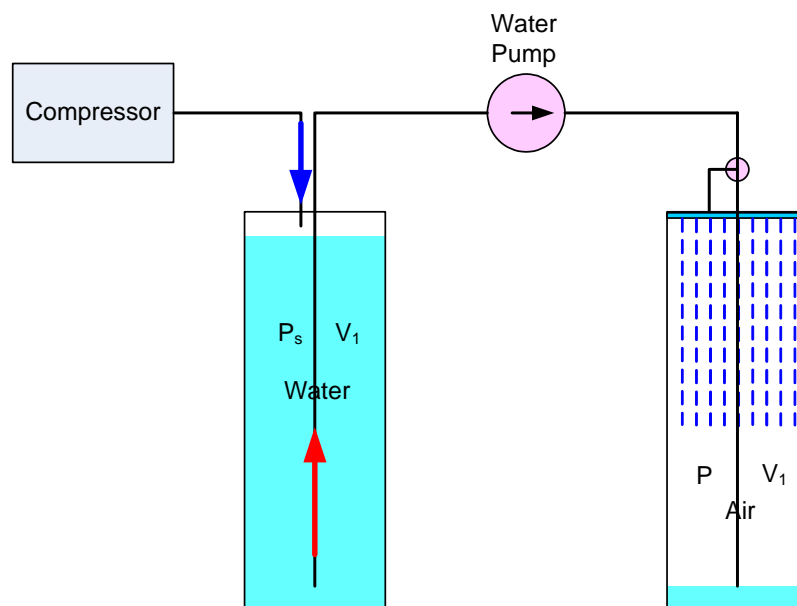


Fig. 3.16: Spraying water in the charging process for a quasi-isothermal process of hydraulic storage.

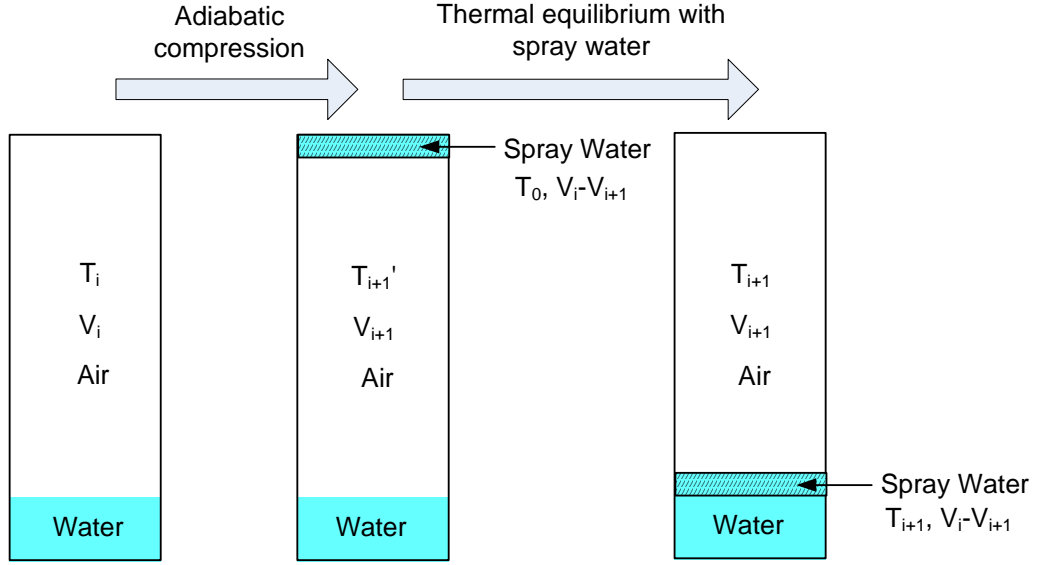


Fig. 3.17: Simple modeling of sprayed water in the charging process for the novel CAES system.

The compressed air at state i (P_i, T_i, V_i) is adiabatically compressed to an intermediate state ($P_{i+1}', T_{i+1}', V_{i+1}'$) and then cooled to a final state $i+1$ ($P_{i+1}, T_{i+1}, V_{i+1}$).

The temperature change due to adiabatic compression can be given by

$$T_{i+1}' = T_i \left(\frac{V_i}{V_{i+1}'} \right)^{\gamma-1} \quad (3.62)$$

The final temperature T_{i+1} by thermal equilibrium of the two media (air, water) is calculated by the following energy balance:

$$m_a \bar{c}_{v,a} (T_{i+1}' - T_{i+1}) = m_w \bar{c}_{v,w} (T_{i+1} - T_0) \quad (3.63)$$

$$T_{i+1} = \frac{m_a \bar{c}_{v,a} T_{i+1}' + m_w \bar{c}_{v,w} T_0}{m_a \bar{c}_{v,a} + m_w \bar{c}_{v,w}} \quad (3.64)$$

where m_a is the mass of compressed air, m_w is the mass of sprayed water from the pump for the time step, T_0 is the initial temperature of the sprayed water, and $\bar{c}_{v,a}$ and $\bar{c}_{v,w}$ are the

average isochoric specific heats of air and water, respectively.

The final pressure P_{i+1} by thermal equilibrium of the two media (air, water) is calculated as follows:

$$\frac{P_i V_i}{T_i} = \frac{P_{i+1} V_{i+1}}{T_{i+1}} = m_a r = \text{const} \quad (3.65)$$

$$\frac{P_{i+1}}{P_i} = \left(\frac{V_i}{V_{i+1}}\right) \left(\frac{T_{i+1}}{T_i}\right) \quad (3.66)$$

Fig. 3.18 shows the temperature and pressure of the sealed air being compressed and cooled by the sprayed water for the charging process. The temperature rise of the sealed air compressed for the total charging process is less than 5°C. This shows that the compression process is very close to an isothermal process when sprayed water is used. Similarly, in the discharging process, some of the water to the water turbine can be sprayed in the cavern by a circulation pump, as shown in Fig. 3.19.

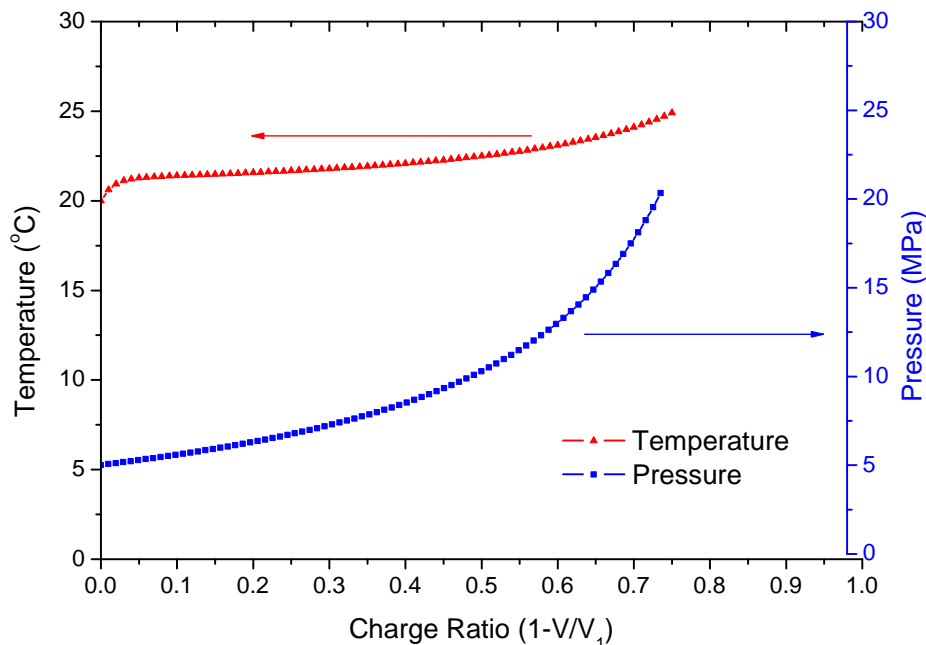


Fig. 3.18: Temperature and pressure of compressed air cooled by sprayed water for the charging process in hydraulic storage.

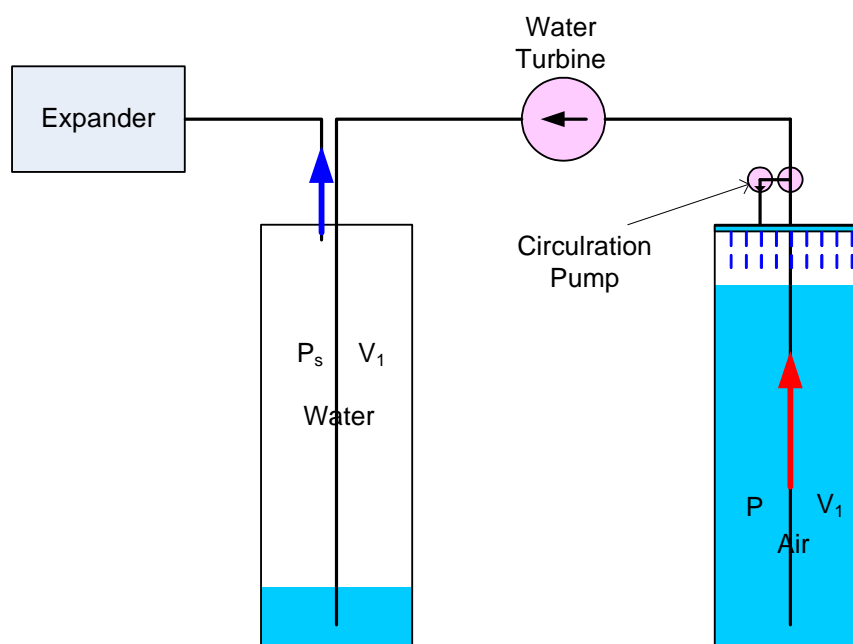


Fig. 3.19: Sprayed water in the discharging process for a quasi-isothermal process of hydraulic storage.

3.3 Applications of novel CP-CAES system combined with PHS

3.3.1 Small-scale CP-CAES system combined with PHS

The novel constant-pressure (CP-) CAES system combined with pumped hydro storage (PHS) can be applied to both small-scale CAES systems using manmade air vessels and large-scale CAES systems using salt caverns or lined rock caverns. In the case of the small-scale CAES systems using manmade air vessels, it is very important to increase the energy density and reduce the volume of the storage tank at a feasible cost, because of the high cost and occupying space of the storage tank. Recently, a CAES system of Electric Power Research Institute Inc., with aboveground air vessels throttles the incoming air to 55 bar (operating between 103 bar and 55 bar), despite the large throttle loss. The constant-pressure CAES system combined pumped hydro storage can be applied in the small-scale CAES systems with man-made air vessels to increase the energy density and efficiency of the

system.

In the case of the small-scale CAES systems, a commercial hydraulic oil motor/pump could be used because these machines display exceptional energy conversion performance and are easily reversible (i.e., they can operate as a motor and as a pump) [24]. However, for ecological reasons water could also be used, with the need for the advances in the current technologies of the components.

3.3.2 Large-scale CP-CAES system combined with PHS

In the case of a large-scale CAES system, it is very important to build storage caverns economically by using natural geological formations such as salt domes or hard rocks. The least expensive method for building caverns is to use salt caverns. These caverns are created by drilling a conventional well that pumps fresh water into a salt dome or bedded salt formation. The salt dissolves until the water is saturated, and the resulting salt water is returned to the surface. This process continues until a cavern of the desired volume and shape is created. The two existing CAES plants, the Huntorf and McIntosh plants, used salt caverns, and many CAES plants that will be built are located in the regions of salt domes. The constant-pressure CAES system combined with pumped hydro storage can be incorporated in salt caverns. Two caverns with the similar volume, as in the case of the Huntorf plant, need to be built, and the saturated brine produced by excavating salt caverns can be reused for the operation of the novel CAES system. The smaller size of the cavern in the novel CAES system and the reuse of brine are beneficial because the high cost of brine disposal may preclude cavern construction and the brine must be disposed of in an environmentally acceptable manner.

In the process of the operation of the novel CAES system, one cavern for compressed air energy storage operates at a constant pressure P_S but the other cavern for hydraulic energy storage operates in a pressure range from P_1 to P_2 , which is much higher than P_S . In general, the pressure of stored gas in salt caverns is in the range from 50 bar to 230 bar. The 200 bar of maximum pressure in this study is reasonable for salt caverns. Although the hydro machinery for seawater pumped storage is more expensive than that for conventional pumped

storage, it is possible to build the pumped storage using brine. Okinawa seawater pumped storage in Japan is one example of this, and the need for seawater pumped storage is increasing.

Unlike the current storage technology, which relies on the existence of salt domes (or thick salt layers), aquifer formations, and depleted oil fields, the lined rock cavern (LRC) concept provides the option of greater flexibility in the management of local and regional gas supplies. The storage of pressurized natural gas in large steel-lined caverns excavated in crystalline rock has been under development in Sweden. One lined rock cavern (LRC) has already been built in Sweden, and commercial operation was begun in 2003. The cavern, which is shaped like a cylinder, is located with its roof at a depth of 115 m and has a diameter of 35 m and a height of 50m. The cavern was designed and tested, and it is capable of operating at a pressure of up to 200 bar. In general, rock caverns are more expensive to mine than salt caverns for CAES purposes. This is because underground rock caverns are created by excavating solid rock formations, whereas salt caverns are created by the solution mining of salt formations. In particular, in the case of the rock cavern for CAES, it is very important to minimize the volume of the cavern as much as possible in order to reduce the cost. The novel CAES system can contribute to the reduction in the volume of rock caverns because of the improved energy density and efficiency of the system.

The constant-pressure CAES system combined with pumped hydro storage can be considered as a combination of CAES and a new type of underground pumped storage. Underground pumped storage has been studied as an alternative to conventional aboveground pumped storage, which requires use of the available topography and consideration of the environmental impacts. Underground pumped storage can be constructed by setting the upper reservoir aboveground and the lower reservoir and powerhouse underground [75,76]. In the case of conventional underground pumped storage, the unit cost of the excavation increases with depth. A deep borehole could be drilled into the rock strata below the mine where the powerhouse would be located. Furthermore, the excavation required for power facilities and installations would add a major cost to the project and thus significantly increase the construction cost [76]. The advantage of the constant-pressure CAES system combined with pumped hydro storage is that it is not dependent on depth; the powerhouse could be installed

aboveground and there would be no need for an upper reservoir aboveground.

For the pumped hydro storage in a large-scale version of the novel CAES system, the equipment could be either a multistage reversible pump-turbine or a separate arrangement consisting of an impulse turbine, usually a Pelton turbine, and a multistage pump. One example of high-head pumped hydro using a multistage reversible (Francis) pump-turbine is the Edolo power station in Italy, with 1290 m, four stages, and 142 MW. One example of high-head pumped hydro with a separate arrangement of a Pelton turbine and a multistage pump is the San Fiorino power station in Italy, with 1440 m and 140 MW. Although the reversible (Francis) pump-turbine is the more cost-attractive solution, one disadvantage is its longer periods of mode changing from turbine to pump. In addition to load leveling, pumped hydro can be of benefit by providing both spinning reserve and stand-by reserves, as well as system frequency control, and it can respond to and correct for low frequency occurrences. The separate arrangement of a Pelton turbine and a multistage pump can be used for a very flexible pumped storage plant and a high-head pumped storage. KOPSWERK II in Austria, which is designed with Pelton turbines and multistage pumps, is a highly flexible pumped storage plant, wherein high outputs can be fed into the network or drawn out of it in a few seconds. The pump and turbine operate simultaneously, and the machines can change over from pump to turbine mode or vice versa extremely quickly.

For the pumped hydro storage in the novel large-scale CAES system, the separate arrangement of a Pelton turbine and a multistage pump is preferred because the Pelton turbine is appropriate for high-head pumped storage and has a high efficiency over a wide range of discharge. However, in the case of the Pelton turbine, the optimal tangential speed of the water turbine is equal to half of the jet velocity v_{jet} , which leaves the nozzle ($v_{jet}/2$) to fully absorb the kinetic energy of water. In the pumped hydro storage in the novel CAES system, the pressure head in the Pelton turbine changes continually, and thus, the jet velocity v_{jet} leaving the nozzle also changes according to the following equation:

$$v_{jet} = \sqrt{\frac{2(P(t) - P_b)}{\rho}} \quad (3.67)$$

where $P(t)$ is the varying hydraulic pressure of the hydro storage, P_b is the back pressure in the compressed air storage, and ρ is the density of water.

To achieve high efficiency of the Pelton turbine over a wide range of pressure head, the runner speed must be matched to the varying pressure head. Because the turbine must operate in free air, there are two possible approaches: (1) The back pressure of the Pelton turbine is maintained at atmospheric pressure, and an additional pump is used to provide the necessary inlet pressure to the compressed air storage. (2) The back pressure of the Pelton turbine is maintained at the high pressure of the compressed air storage, and a transfer pump is used to transfer water for operating the Pelton turbine in the air.

In addition to the water turbine, the multistage water pump must also be designed to accommodate the varying pressure head. Variable speed operation has also been of interest for improving the efficiency and operating range of pumped storage power plants, especially in the case of large variations in the pressure head. In addition, a variable pitch reversible pump turbine has shown that a flat efficiency curve can be obtained over a wide head range. This characteristic of increasing discharge with increasing head can be controlled at the design stage by suitably locating the exit edge of the runner blade.

The separate arrangement of a Pelton turbine and a multistage pump in the novel CAES system can be used for regulation reserves. An example of this would be the primary reserve acting within seconds and the secondary reserve acting within minutes, while still performing the function of maintaining the constant pressure of compressed air storage as the long-term control, as the short-term controls for the regulation reserves do not have much effect on the pressure of compressed air storage.

3.4 Conclusion

In this chapter, for the purpose of reducing the air storage volume while maintaining a high efficiency of CAES system at a design condition, a novel constant-pressure CAES system combined with pumped hydro storage was studied. In addition, the hydraulic energy storage in the system affords advantages over conventional CAES system, including quick start-up,

the ability to provide “spinning reserve,” and voltage and frequency regulation to stabilize the associated power grid [36]. This concept can be applied to both large-scale CAES utilizing lined rock caverns or salt caverns and small-scale CAES using man-made air vessels or ground-level pipelines because it does not depend on the depth of the cavern to produce a pressure difference by means of a water column.

Through an energy and exergy analysis of the novel CAES system, the daily operation characteristics of the system according to several different compression and expansion processes were presented. The air storage pressure of the CAES system was assumed to be 5 MPa as a general value for the air-releasing pressure of CAES gas turbine, and a maximum pressure of 20 MPa was chosen for hydraulic energy storage in the novel CAES system in consideration of the energy density and allowable pressure of the storage cavern and hydraulic machinery.

For the charging process using three-stage compression with intercooling, although the power required for the compressed air part is constant, the power required for the hydraulic part increases according to the rise in hydraulic pressure. At the end of the charging process, the power required for the hydraulic part accounts for 37% of the total power. For the discharging process with heating of the compressed air as in the McIntosh plant, although the power produced by the compressed air part is constant, the power produced by the hydraulic part decreases according to the drop in hydraulic pressure. At the start of the discharging process, the power produced by the hydraulic part accounts for 23% of the total power.

For the novel CAES system at a large scale, the effects of the height of cavern need to be considered. The total exergy stored by the novel CAES system with 100 m and 200 m heights for the storage cavern decreases slightly by 3.6% and 8.4%, respectively.

In addition, the round trip efficiency of the hydraulic part can degrade owing to the irreversibility by insufficient heat transfer between the two media (air, water) and the cavern. For the quasi-isothermal compression process of hydraulic storage, spraying water to cool the compressed air was proposed and shown to be a very effective way of achieving a quasi-isothermal process through the results of a simple modeling.

4. Micro-CAES and air cycle heating and cooling system

Compressed air energy storage (CAES) is a promising method for energy storage, with high reliability and economic feasibility and its low environmental impact. However, large-scale CAES is dependent on the right combination of sites for air storage. Small-scale CAES (called micro-CAES) with man-made air vessels, such as subsurface or aboveground pressure vessels, is a more adaptable solution, especially for distributed generation that could be widely applicable to future power networks [8,9,10].

In the case of the micro-CAES, it is possible to use the dissipated heat of compression for residential heating, which can contribute to improvements in energy efficiencies. In addition, compressed air systems can be used for both power generation and cooling load.

Energy and exergy analyses are performed to investigate performance of several types of micro-CAES systems. In addition, to increase efficiency of the systems, some innovative ideas are introduced.

4.1 Trigeneration micro-CAES systems

Micro-CAES systems can be used as a multipurpose system, as a combination of energy storage and air cycle heating and cooling.

In general, air cycle refrigeration consists of one or more compressors (fan), turbines

(expanders), and heat exchangers; the setup is very similar to the CAES system except for the air storage vessels. Air cycle heating and cooling has many advantages, including high reliability, ease of maintenance, flexibility of temperature, and heating and cooling capacities. In addition, it employs a natural refrigerant, which is environmentally benign [37,38,39,40]. The air cycle approach is one of the long-term alternatives for refrigeration machines, air conditioners, and heat pumps [37]. Air cycle is widely used in industrial freezing with a very low temperature (below -50°C) and transport refrigeration. In the case of conventional refrigeration and air conditioning, the air cycle approach suffers from low energy efficiency and so is not competitive with vapor compression cycles [38]. But, air cycles have been studied for HVAC in office buildings within the framework of European research projects, since they have advantages in applications that require both heating and cooling [37,40] and because of the potential of highly efficient turbo machinery that is used [38,39].

The micro-CAES system combined with air cycle heating and cooling could be a very good solution because it would then be possible to improve the energy efficiency and economics of the system as a multipurpose system. Transportable CAES was proposed as a solution to provide power and energy for desalination of brackish water or seawater for an island by utilizing the superchilled air as a by-product for the freeze-crystallizing process [41]. A new CAES refrigeration system was proposed for electrical power load shifting—one that employs a combination of an air cycle refrigeration cycle and a vapor compression cycle, in which the cooling effect of expanding air is used and the expansion power is used to drive a compressor of the vapor compression cycle [42].

This study focuses on a micro-CAES system for energy storage and air cycle heating and cooling for HVAC of a building. Because the pressure ratio of CAES is much higher than that of conventional air cycle refrigeration to reduce the volume of air storage, multiple-stage compression and expansion is needed to achieve high efficiency for the system; this is effected by matching the temperature of compressed and expanded air to the required temperature of heating and cooling load. Otherwise, quasi-isothermal compression and expansion by liquid injection can be used for a high efficiency micro-CAES and air cycle

heating and cooling system [17].

4.2 Various types of micro-CAES systems

4.2.1 System descriptions

It is possible to build several different types of micro-CAES systems based on compression and expansion processes. In the case of large-scale CAES plants, in order to increase the overall efficiency of the system, it is customary to perform multistage compression with intercooling and multistage expansion with reheating. However, in the case of a micro-CAES system, it is very important to simplify the structure as much as possible while achieving a system with high efficiency. In the following analyses of micro-CAES systems, we assume that pressure ratios of compression and expansion are not changing because of the adoption of the constant-pressure air storage presented in Chapter 3.

In order to increase the efficiency of the system, isothermal compression/expansion (Ericsson cycle) is more desirable than an adiabatic process (Brayton cycle). To achieve quasi-isothermal compression, a large amount of atomized water is injected during the compression stroke to absorb the heat in the Isoengine developed by Linnemann and Coney [43]. Hugenroth et al. [44] proposed a liquid-flooded compressor and expander in an Ericsson cycle cooler. Water (or liquid) is discharged together with compressed air, and is then separated, cooled, and recirculated. The energy of the pressurized water can be recovered through a hydraulic motor to reduce energy consumption.

Compressed air is cooled to ambient temperature by water circulated through a cooler, and it is then stored in vessels. Hot water separated after compression and hot water from the cooler can be used to satisfy the heating load.

Although a heater (or combustor) is often employed in the expansion process of a CAES system, to heat compressed air in order to obtain increased power, it is not indispensable. If

there is no heater in place before the expander, expanding air can be used to supply a cooling load, as in an air-cycle cooling system. In that case, to achieve quasi-isothermal expansion, as with a compression process, liquid can be injected into the expander, separated, used to supply a cooling load, and pressurized by a pump for injection.

In the case of systems with a heater to preheat the expanding air, external heating of the expander or injection of hot liquid, such as thermal oil, can be used to achieve quasi-isothermal expansion, and expanded hot air then transfers its heat to compressed cool air in a recuperator. To achieve quasi-isothermal expansion, a heated scroll expander was proposed by Kim et al. [46] to provide effective heating because of the high area-to-volume ratio of the scroll geometry and its convenient handling of two-phase flow.

Our current study evaluates energetic and exergetic performance of eight types of micro-CAES systems with the compression and expansion processes described above and summarized in Table 4.1.

Table 4.1: Types of micro-CAES systems based on compression and expansion processes
(See also Figs. 4.1- 4.4.)

Type	Compression and Expansion	Number of Stages	Fuel
1	Adiabatic	1	NO
2	Quasi-Isothermal	1	NO
3	Adiabatic	2	NO
4	Quasi-Isothermal	2	NO
5	Adiabatic	1	YES
6	Quasi-Isothermal	1	YES
7	Adiabatic	2	YES
8	Quasi-Isothermal	2	YES

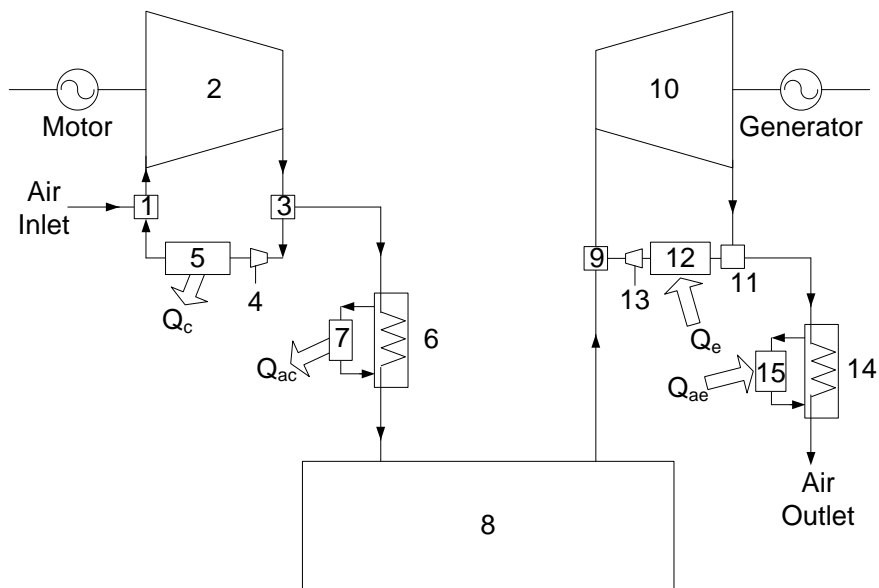


Fig. 4.1: Micro-CAES system (Type 1, 2). (1) mixer; (2) compressor; (3) separator; (4) hydraulic motor; (5), (6), and (7) heat exchanger; (8) high pressure vessel; (9) mixer; (10) expander; (11) separator, (13) pump; and (12), (14) ,and (15) heat exchanger.

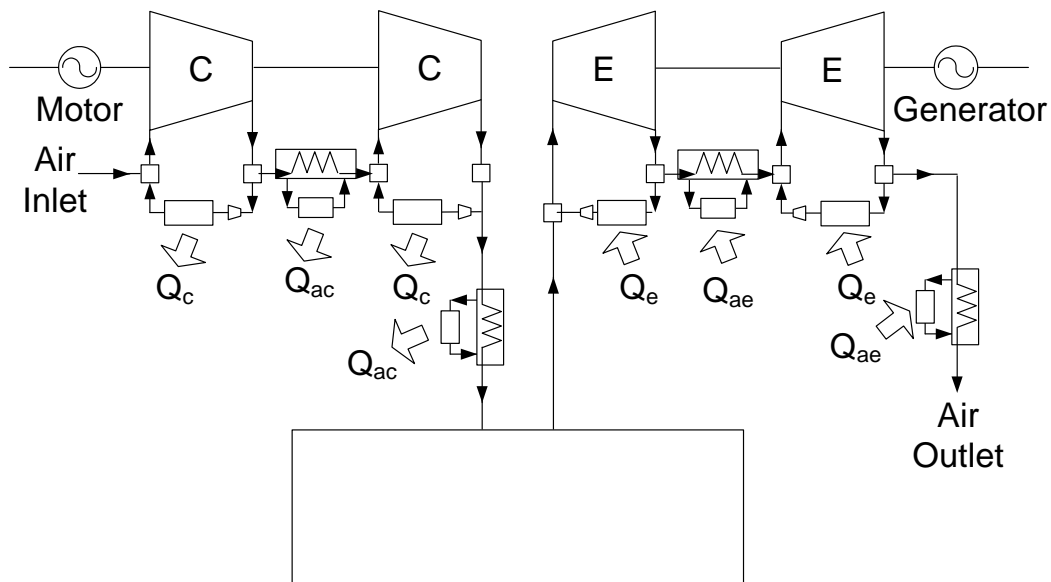


Fig. 4.2: Micro-CAES system (Type 3, 4).

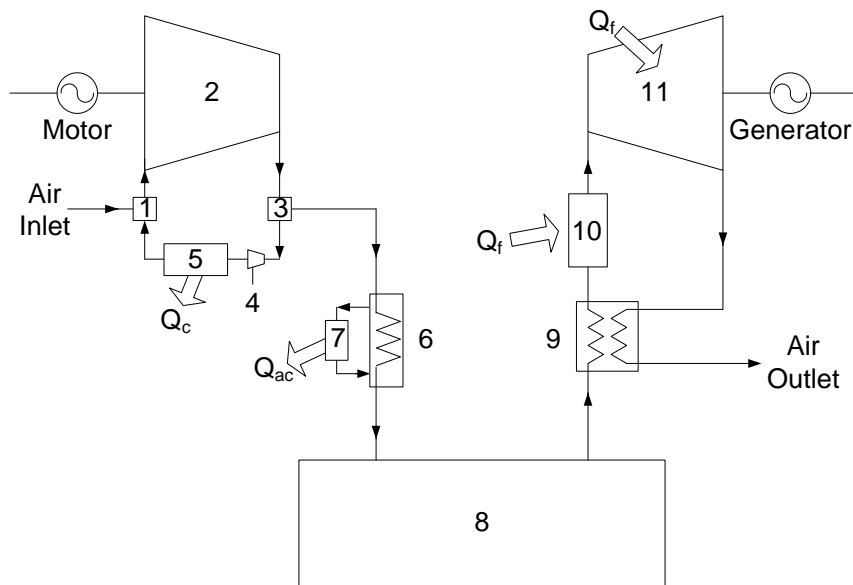


Fig. 4.3: Micro-CAES system (Type 5, 6). (1) Mixer; (2) compressor; (3) separator; (4) hydraulic motor; (5), (6), and (7) heat exchanger; (8) high-pressure vessel; (9) recuperator; (10) heater; and (11) expander.

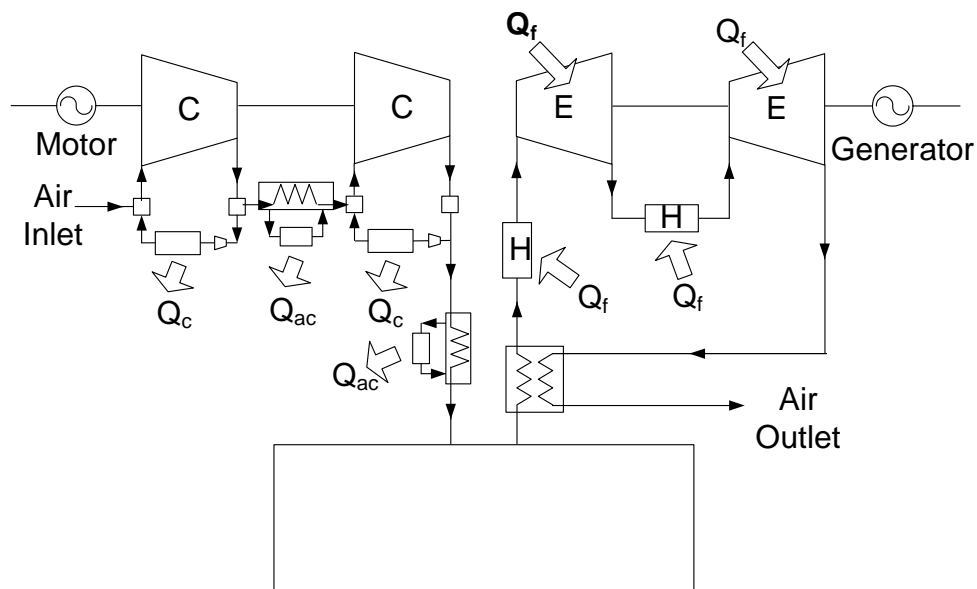


Fig. 4.4: Micro-CAES system (Type 7, 8).

4.2.2 Energy and exergy analyses

In order to study energy and exergy analyses of the eight systems, we have adopted the following assumptions and elements of inlet data:

- (a) Each compression and expansion process is assumed to take place at a steady state with a steady flow, constant-pressure air storage, negligible potential and kinematic energy effects, and no chemical or nuclear reaction.
- (b) For quasi-isothermal compression and expansion processes, it is assumed that methods of liquid injection or external heating using fuel are used, as described above.
- (c) For simplicity, all heat exchangers, except for recuperator ($\varepsilon_R = 0.95$), including cooler and heater, are assumed to be ideally perfect, with $\varepsilon = 1.0$ and no pressure drop (ε denotes temperature effectiveness of heat exchanger).
- (d) Air pressure in the storage vessel is assumed to remain constant at 5 MPa by adoption of constant-pressure air storage. Designed pressure ratios of the compressor and expander are 50, with isentropic efficiencies of 85%. Although the air storage pressure must be optimized by energy density, efficiency, and cost of the system, 5 MPa of air storage pressure, as a general value of air releasing pressure for CAES gas turbine, is adopted.

4.2.2.1 Compressor and expander model

For analyses of compression and expansion of gas-containing liquid, we adopted the liquid-flooded compressor and expander model proposed by Hugenroth et al. [44,45]. The model was developed and used to explore the behavior of the liquid flooded Ericsson cycle, using liquid flooding of compressor and expander to approach isothermal compression and expansion processes. The same concept can be applied for high efficient micro-CAES systems.

An ideal gas with a constant specific heat ratio of k that is undergoing a compression process in thermal equilibrium with an incompressible liquid that has a constant specific heat behaves exactly like an ideal gas that has a constant effective specific heat ratio equal to k^* . The

effective ratio of specific heat of the mixture is given by [44,45]:

$$k^* = \frac{m_g c_{p,g} + m_l c_l}{m_g c_{v,g} + m_l c_l} \quad (4.1)$$

The temperature change for the gas during a reversible flooded compression process is found by substituting k^* for k in the conventional isentropic relationship for ideal gases, thereby resulting in the following expression:

$$\frac{T_{o,ideal}}{T_i} = P_{ratio}^{\frac{k^*-1}{k^*}} \quad (4.2)$$

where $T_{o,ideal}$ is the ideal outlet temperature for a flooded compressor or expander.

The reversible work of the cooled ideal gas is the same as that for adiabatic reversible work of an ideal gas with k^* substituted for k . The result is given by:

$$w_g = \frac{RT_i k^*}{k^* - 1} \left[P_{ratio}^{\frac{k^*-1}{k^*}} - 1 \right] \quad (4.3)$$

where w_g is the specific reversible work required to compress the gas that is in thermal equilibrium with a liquid, and P_{ratio} is the ratio of P_o to P_i .

The reversible work required to pump the incompressible liquid, neglecting the relatively small impact of temperature changes on specific volume of the liquid, is given by the following expression:

$$w_l = v(P_o - P_i) \quad (4.4)$$

The total reversible compressor power is given by:

$$\dot{W}_{ideal} = \dot{m}_g w_g + \dot{m}_l w_l \quad (4.5)$$

Actual compressor and expander powers for the gas and liquid mixture are determined using an isentropic efficiency defined, respectively, as

$$\eta_c \equiv \frac{\dot{W}_{c,ideal}^+}{\dot{W}_c^+} \quad (4.6)$$

$$\eta_e \equiv \frac{\dot{W}_e^-}{\dot{W}_{e,ideal}^-} \quad (4.7)$$

Heat transfer from the gas to the liquid during the compression process and from the liquid to the gas during the expansion process can be obtained as follows:

$$Q_c^- = M_a [w_c^+ - (h_{out} - h_{in})] \quad (4.8)$$

$$Q_e^+ = M_a [w_e^- - (h_{in} - h_{out})] \quad (4.9)$$

4.2.2.2 Energy efficiencies

A CAES system uses inputs in the form of electricity, fuel, or other heat sources to heat compressed air. In the case of a micro-CAES system, it is possible to use dissipated heat of compression for local heating demands and to use the cooling effect of expanding air without any fuel consumption for cooling demands. It is possible to calculate several quantitative efficiencies for a CAES system.

In general, we can calculate the net electrical storage efficiency of a CAES system by subtracting the amount of energy "generated" by natural gas (or other fuels) from the electric output of the CAES system, as follows:

$$\eta_s \equiv \frac{E_{out} - Q\eta_p}{E_{in}} \quad (4.10)$$

where $Q\eta_p$ is the electric energy that would be produced if the corresponding fuel consumed in the CAES is burned in another power station (Q is the lower caloric value of the fuel and η_p is the thermal efficiency of the base-load charging plant).

The thermal efficiency η_p is usually taken as equal to 0.4 which could be considered as the average thermal efficiency of conventional base load power plant

Heating performance of a CAES system with dissipated heat of compression can be defined as:

$$\eta_H \equiv \frac{Q_{hc}}{E_{in}} = \frac{Q_c + Q_{ac}}{E_{in}} \quad (4.11)$$

where Q_{hc} is the total dissipated heat of compression, which is the sum of Q_c during compression and Q_{ac} after compression.

Cooling performance, i.e. heat extraction from ambient air, of a CAES system by expanding air, without any fuel use, can be defined as:

$$\eta_C \equiv \frac{Q_{ce}}{E_{in}} = \frac{Q_e + Q_{ae}}{E_{in}} \quad (4.12)$$

where Q_{ce} is total heat extraction from ambient air, which is the sum of Q_e during expansion and Q_{ae} after expansion.

Although operation of a CAES system with use of fuel is different from that of a conventional gas turbine (or other engines), for comparison purposes, its overall thermal efficiency can be defined as:

$$\eta_{th} \equiv \frac{E_{out} - E_{in}}{Q} \quad (4.13)$$

4.2.2.3 Exergy analyses

General exergy balance can be expressed in the rate form as:

$$\dot{E}^+ - \dot{E}^- = \dot{L} \quad (4.14)$$

where \dot{E}^+ is the rate of exergy transfer to the system by heat, work, and mass; \dot{E}^- is the rate of exergy transfer from the system; and \dot{L} is the rate of exergy destruction.

Exergy transfer to the system by heat, \dot{E}_q^+ , can be defined as:

$$\dot{E}_q^+ \equiv \int \left(1 - \frac{T_0}{T}\right) \delta \dot{Q}^+ \quad (4.15)$$

Exergy transfer to the system by mass flow, \dot{E}_y^+ , can be defined as:

$$\begin{aligned}\dot{E}_{yk}^+ &\equiv \dot{M}_k(k_{in} - k_{out}) \\ &= \dot{M}_k[(h_{in} - h_{out}) - T_0(s_{in} - s_{out})]\end{aligned}\quad (4.16)$$

In the case of perfect gas flow,

$$h_{in} - h_{out} = c_p(T_{in} - T_{out}) \quad (4.17)$$

$$s_{in} - s_{out} = c_p \ln \frac{T_{in}}{T_{out}} - r \ln \frac{P_{in}}{P_{out}} \quad (4.18)$$

where r is the specific gas constant.

In the case of liquid flow, neglecting density change ($d\rho \cong 0$),

$$h_{in} - h_{out} = c(T_{in} - T_{out}) + \frac{P_{in} - P_{out}}{\tilde{\rho}} \quad (4.19)$$

$$s_{in} - s_{out} = c \ln \frac{T_{in}}{T_{out}} \quad (4.20)$$

where c is the specific heat, and $\tilde{\rho}$ is the average density of the liquid.

Exergy transfer from the system by mass flow, \dot{E}_y^- , can be defined as:

$$\begin{aligned}\dot{E}_{yk}^- &\equiv \dot{M}_k(k_{out} - k_{in}) = -\dot{E}_{yk}^+ \\ &= \dot{M}_k[(h_{out} - h_{in}) - T_0(s_{out} - s_{in})]\end{aligned}\quad (4.21)$$

In the case of the compression process of the gas and liquid mixture, the exergy balance is as follows:

$$\dot{L}_c = \dot{E}^+ - \dot{E}^- \quad (4.22)$$

$$\dot{E}^+ = \dot{E}_c^+ \quad (4.23)$$

$$\dot{E}^- = \dot{E}_{ya}^- + \dot{E}_{yl}^- \quad (4.24)$$

where \dot{E}_c^+ is exergy transfer to the system by compression work, \dot{E}_{ya}^- is exergy transfer from the system by air flow, and \dot{E}_{yl}^- is exergy transfer from the system by liquid flow.

Exergy efficiency (second law efficiency) of the compressor can be defined as:

$$\eta_{II,c} \equiv \frac{\dot{E}_{ya}^- + \dot{E}_{yl}^-}{\dot{E}_c^+} \quad (4.25)$$

After compression, the air is cooled to the storage temperature through an after-cooler. Heat balance in the after-cooler is as follows:

$$\dot{Q}_{ac} = \dot{M}_a c_p (T_{in,a} - T_{out,a}) = \dot{M}_l c_l (T_{out,l} - T_{in,l}) \quad (4.26)$$

Once the mass flow rate of air and inlet and outlet temperatures are known, Eq. 4.26 can be used to determine the required mass flow rate of cooling water.

General exergy balance in the after-cooler can be expressed in the rate form as:

$$\dot{L}_{ac} = \dot{E}_{ya}^+ - \dot{E}_{yl}^- \quad (4.27)$$

Exergy efficiency of the after-cooler can be defined as:

$$\eta_{II,ac} \equiv \frac{\dot{E}_{yl}^-}{\dot{E}_{ya}^+} \quad (4.28)$$

In the case of the expansion process of the gas and liquid mixture without any fuel use, the result is as follows:

$$\dot{L}_e = \dot{E}^+ - \dot{E}^- \quad (4.29)$$

$$\dot{E}^+ = \dot{E}_{ya}^+ + \dot{E}_{yl}^+ \quad (4.30)$$

$$\dot{E}^- = \dot{E}_e^- \quad (4.31)$$

where \dot{E}_e^- is exergy transfer from the system by expansion work, \dot{E}_{ya}^+ is exergy transfer to the system by air flow, and \dot{E}_{yl}^+ is exergy transfer to the system by liquid flow.

Exergy efficiency (second law efficiency) of the expander can be defined as:

$$\eta_{II,e} \equiv \frac{\dot{E}_e^-}{\dot{E}_{ya}^+ + \dot{E}_{yl}^+} \quad (4.32)$$

In the case of a CAES system without any fuel use (or other heat source), given only the

input as compression work, it is possible to use the expansion work (\dot{E}_e^-), the hot liquid by cooling the heat of compression during compression ($\dot{E}_{yl.c}^-$) and after compression ($\dot{E}_{yl.ac}^-$), and the cool liquid by the cooling effect of expanding air during expansion ($\dot{E}_{yl.e}^-$) and after expansion ($\dot{E}_{yl.ae}^-$) as outputs. Exergy efficiency of the overall CAES system can be defined as:

$$\eta_{II,CAES} \equiv \frac{\dot{E}_e^- + \dot{E}_{yl.c}^- + \dot{E}_{yl.ac}^- + \dot{E}_{yl.e}^- + \dot{E}_{yl.ae}^-}{\dot{E}_c^+} \quad (4.33)$$

In the case of the expansion process of the gas accompanied by heating with the use of fuel, it is assumed that the compressed air is externally heated. The system includes the regeneration and preheating processes.

Exergy balance in the recuperator can be expressed in the rate form as:

$$\dot{L}_{reg} = \dot{E}_{ya}^+ - \dot{E}_{ya}^- \quad (4.34)$$

where \dot{E}_{ya}^+ is exergy transfer to the recuperator by flow of exhaust hot air, and \dot{E}_{ya}^- is exergy transfer from the recuperator by flow of the compressed air.

Exergy efficiency of the recuperator can be defined as:

$$\eta_{II,reg} \equiv \frac{\dot{E}_{ya}^-}{\dot{E}_{ya}^+} \quad (4.35)$$

After regeneration, air is heated further through a preheater with use of fuel. Heat balance in the preheater is as follows:

$$\dot{Q}_h = \dot{M}_a c_p (T_{out} - T_{in}) \quad (4.36)$$

Exergy balance in the preheater can be expressed in the rate form as:

$$\dot{L}_h = \dot{E}_f^+ - \dot{E}_{ya}^- \quad (4.37)$$

where \dot{E}_f^+ is exergy transfer to the preheater by fuel (exergy value of fuel), and \dot{E}_{ya}^- is exergy transfer from the preheater by flow of compressed air.

Exergy transfer by fuel can be expressed as:

$$\dot{E}_f^+ = \dot{M}_f \underline{\Delta k}^0 \quad (4.38)$$

where \dot{M}_f is mass flow rate of fuel and $\underline{\Delta k}^0$ is maximum specific exergy by complete oxidation of fuel on a mass basis.

Exergy efficiency of the preheater can be defined as:

$$\eta_{II,h} \equiv \frac{\dot{E}^-}{\dot{E}^+} = \frac{\dot{E}_{ya}^-}{\dot{M}_f \underline{\Delta k}^0} \quad (4.39)$$

As discussed above, the expansion process can be accompanied by external heating with the use of fuel in order to achieve a quasi-isothermal expansion process. Exergy balance in the expander can be expressed in the rate form as:

$$\dot{L}_e = \dot{E}_{ya}^+ + \dot{E}_f^+ - \dot{E}_e^- \quad (4.40)$$

where \dot{E}_{ya}^+ is exergy transfer to the expander by flow of hot compressed air, \dot{E}_f^+ is exergy transfer to the expander by fuel, and \dot{E}_e^- is exergy transfer from the system by expansion work.

Exergy efficiency of the expander can be defined as:

$$\eta_{II,e} \equiv \frac{\dot{E}_e^-}{\dot{E}_{ya}^+ + \dot{E}_f^+} \quad (4.41)$$

In the case of a CAES system accompanied by heating with the use of fuel, given inputs as compression work and fuel, it is possible to use the expansion work (\dot{E}_e^-), the hot liquid energy by cooling the heat of compression during compression ($\dot{E}_{yl,c}^-$) and after compression ($\dot{E}_{yl,ac}^-$), and by heat recovery of hot exhaust air after expansion ($\dot{E}_{yl,ae}^-$) as outputs. Exergy efficiency of the overall CAES system can be defined as:

$$\eta_{II,CAES} \equiv \frac{\dot{E}_e^- + \dot{E}_{yl,c}^- + \dot{E}_{yl,ac}^- + \dot{E}_{yl,ae}^-}{\dot{E}_c^+ + \dot{E}_f^+} \quad (4.42)$$

4.2.3 Results and discussion

Results obtained from energy and exergy analyses are summarized in Table 4.2 and Table 4.3, respectively. In the course of the analyses, additional compression work owing to liquid injected for achieving quasi-isothermal compression, $m_l w_l$, was neglected, because the work is only a few percent ($\sim 2\%$) of the gas compression work, $m_g w_g$, and it can be recovered by a hydraulic motor. Furthermore, in the case of expansion, work to pump the liquid injected for achieving quasi-isothermal expansion was neglected, because the work is only a few percent of the gas expansion work, and it can be recovered by the expander. Water was considered as the liquid injected. Latent heats of vaporization and freezing of the liquid were not considered because liquid mass flow rates may be significantly greater than gas flow rates and so the temperature after compression is below saturation point.

Table 4.2: Energy analyses of micro-CAES systems

TYPE	P_c, P_e (P_1 & P_2)	T_c (T_i) (°C)	E_c^+	T_e (T_i) (°C)	E_e^-	η_s (%)	Q_{hc}^-	η_H (%)	Q_{ce}^+ (T_o)	η_C (%)	Q_j^+	η_{th} (%)
1	50	623 (20)	713	-177 (20)	168	23.6	606 (80°C)	85.0	198 (-177°C)	27.8	-	-
2	50	80 (20)	425	-30 (20)	255	60.0	362 (80°C)	85.0	300 (-30°C)	70.6	-	-
3	7.1 & 7.1	239 (20)	519	-106 (20)	214	41.3	441 (80°C)	85.0	252 (-106°C)	48.6	-	-
4	7.1 & 7.1	80 (20)	425	-6 (20)	267	62.8	361 (80°C)	85.0	314 (-6°C)	73.9	-	-
5	50	623 (20)	713	45 (700)	559	41.5	606 (80°C)	85.0	-	-	659	-23.3
6	50	80 (20)	425	535 (700)	847	103.0	362 (80°C)	85.0	-	-	1023	41.2
7	7.1 & 7.1	239 (20)	518	283 (700)	711	71.6	441 (80°C)	85.0	-	-	850	22.7
8	7.1 & 7.1	80 (20)	425	613 (700)	887	107.6	362 (80°C)	85.0	-	-	1073	43.0

Although the temperature after expansion is slightly below freezing point, antifreeze mixture can be used to prevent freezing. In the cases with working liquids other than water, if the flow rate is controlled according to the heat capacity, we can get the same results as with water. We assumed that both compression and expansion efficiencies (η_c and η_e defined in Eqs. 4.6 and 4.7) are equal to 0.85.

From the energy balance, ideally, the total dissipated heat of compression before storage, Q_{hc} , is equal to compression work, regardless of the different types of compression processes. However, if it is assumed that the cooling fluid is heated to 80°C ($T_{o,f} = 80^\circ\text{C}$), in the case of adiabatic compression, especially with one stage, irreversibility during cooling compressed air, L_{ac} , is very large because of the high temperature at the end of the compression process. In the case of quasi-isothermal compression, it is possible to match the temperature after compression to the heating temperature required while minimizing exergy loss by controlling the mass flow rate of injected liquid.

Similarly, total heat extraction from ambient air by expanding air without any fuel use, Q_{ce} , is equal to expansion work, regardless of the different types of expansion processes. However, in the case of adiabatic expansion, especially with one stage, air temperature at the end of the expansion process is very low. If we do not fully utilize the low temperature of exergy, irreversibility is very large. If we consider heat transfer with a secondary fluid, exergy loss is dependent on outlet temperature of cooled secondary fluid ($T_{o,f}$). In the case of Type 1 in Table 4.3, exergy of the fluid cooled to -177°C is 131kJ/kg with no exergy loss, but with cooling to -30°C , it is only 19kJ/kg, with a large exergy loss that is similar to the case of Type 3 with two stages of adiabatic expansion. In the case of quasi-isothermal expansion, it is possible to match the temperature after expansion to the cooling temperature required while minimizing exergy loss by controlling the mass flow rate of injected liquid.

In the case of a CAES system with air heating to 700°C with the use of fuel, it is possible to produce even more power than without any fuel use, although we cannot use the cooling effect of the expanding air. In this study, the temperature of compressed air is limited to 700°C by external heating, but the rise in the temperature can lead to improvements in the

energetic and exergetic performance of the system. Otherwise it is possible to use waste heat from gas engine or gas turbine while minimizing exergy loss.

In the case of adiabatic expansion with air heating, irreversibility during heating compressed air in the preheater, L_h , is very large because of the big temperature drop during expansion and small heat recovery in the recuperator. In the case of quasi-isothermal expansion with air heating, irreversibility during heating compressed air in the preheater, L_h , is small because the temperature drop during expansion is small and it is possible to raise the compressed air temperature sufficiently by heat recovery in the recuperator.

Table 4.3: Exergy analyses of micro-CAES systems

Type	E_c^+	L_c	L_{ac}	L_h	E_e^-	L_e	L_{reg}	$E_{yf,c}^-$ ($T_{o,f}$)	$E_{yf,ac}^-$ ($T_{o,f}$)	$E_{yf,e}^-$ ($T_{o,f}$)	$E_{yf,ae}^-$ ($T_{o,f}$)	E_f^+	$\eta_{II,CAES}$ (%)
1	713	107	222	-	168	30	-	0	55 (80°C)	0	131 (-177°C)	-	49.6
											19 (-30°C)		34.0
2	425	58	0	-	255	51	-	27 (80°C)	5 (80°C)	24 (-30°C)	5 (-30°C)	-	74.4
3	519	78	72	-	214	38	-	0	40 (80°C)	0	77 (-106°C)	-	63.8
											24 (-30°C)		53.7
4	425	85	0	-	267	60	-	22 (80°C)	11 (80°C)	12 (-6°C)	2 (-6°C)	-	74.0
5	713	107	222	330	559	99	0.1	0	55 (80°C)	-	-	659	44.7
6	425	91	0	64	847	424	15	27 (80°C)	5 (80°C)	-	-	1023	60.8
7	518	78	72	426	711	126	6	0	40 (80°C)	-	-	850	54.9
8	425	85	0	97	887	431	18	22 (80°C)	11 (80°C)			1073	61.5

In the micro-CAES system, the pressure ratio is much higher than conventional gas power or refrigeration cycle and so the temperature changes after compression and expansion processes are much bigger. In the case of adiabatic compression and expansion, two stages of compression with intercooling and expansion with reheating are necessary to increase the energetic and exergetic efficiency of the system. But in the case of quasi-isothermal compression and expansion, the increase in the efficiency of the system with two stages of compression and expansion is much smaller than adiabatic case and so two stages of compression and expansion are not necessarily needed. Quasi-isothermal compression and expansion processes are very helpful to minimize exergy loss in heat transfer process and effective for a micro-CAES system to meet a residential heating and cooling load.

Fig. 4.5 shows the energy and exergy flow of the trigeneration micro-CAES system for the production of 1 kWh output. The case of one stage of quasi-isothermal compression ($k_c^* = 1.05$) and expansion ($k_e^* = 1.025$) with liquid injection was considered. It was assumed that the isentropic efficiencies of the compressor and expander are 85%, the efficiencies of the motor and generator are 95%, and we can use 90% of the heat of compression and cooling effect of expanding air. The electrical storage efficiency of the micro-CAES system without any external thermal input is 57%. In addition, hot and cold water accompanied by a significant amount of heat transfer are available, in which the COP of the heat pump ($Q_{\text{hot}}/E_{\text{net}}$) is equivalent to 2.0 and the COP of refrigeration ($Q_{\text{cold}}/E_{\text{net}}$) is equivalent to 1.3. Considering the thermal exergy of the hot and cold water, the second law efficiency of the trigeneration micro-CAES system is 68%.

To obtain increased electric power without use of the cooling effect, a heater (or combustor) can be used to heat the compressed air. Fig. 4.6 shows the energy and exergy flow of the micro-CAES system with fuel, as in the conventional CAES system.

These systems display energy densities feasible for distributed energy storage system and good efficiencies due to the multipurpose systems.

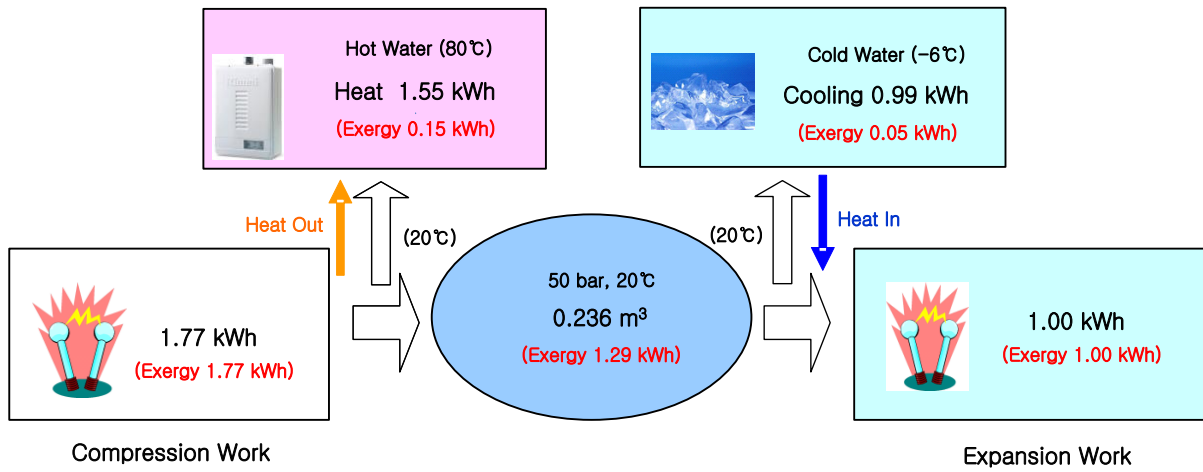


Fig. 4.5: Energy and exergy flow of Trigen micro-CAES system.

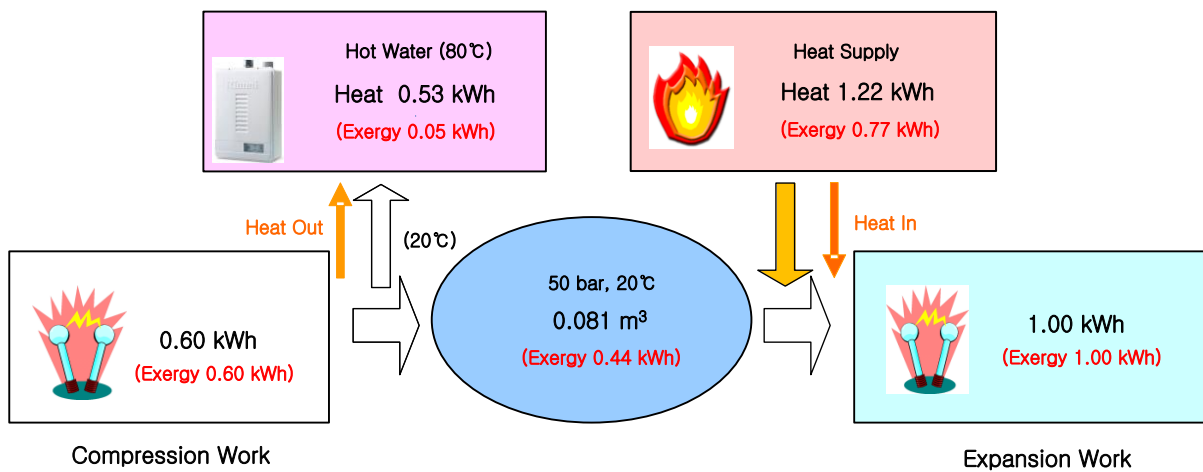


Fig. 4.6: Energy and exergy flow of micro-CAES system with the fuel.

4.3 Conclusion

This study presents results of energy and exergy analyses of different types of micro-CAES systems, as well as some innovative ideas for achieving high efficiency of these systems. In a micro-CAES system, it is possible to use dissipated heat of compression for heating load and to use compressed air for both power generation and cooling load.

For high efficiency of the system, quasi-isothermal compression and expansion processes (Ericsson cycle) are more desirable than adiabatic processes (Brayton cycle), especially because of the high pressure ratio of the micro-CAES system. In the case of systems with adiabatic processes, there are larger exergy losses by heat transfer with bigger temperature differences after compression and expansion processes and so two (or more) stages of compression with intercooling and expansion with reheating are necessary to increase the energetic and exergetic efficiency of the system.

For quasi-isothermal compression and expansion process, it is assumed that methods of liquid injection or external heating are used, where the liquid mass flow rates may be significantly greater than gas flow rates. In the case of systems with quasi-isothermal processes, it is possible to match the temperature after compression to the required temperature of heating load and the temperature after expansion to the temperature of cooling load by controlling the mass flow rate of injected liquid while minimizing exergy loss. And the increase in the energetic and exergetic efficiency of the multistage system is much smaller than adiabatic case and so two stages of compression and expansion is not necessarily needed.

Moreover, a micro-CAES system, especially with quasi-isothermal compression and expansion processes, is a very effective system for distributed power networks, because it is a combination of energy storage, generation, and air-cycle heating and cooling system, with an energy density feasible for distributed energy storage system and a good efficiency due to the multipurpose system.

5. Isothermal thermo-electric energy storage with transcritical CO₂ cycles

Although conventional CAES that uses fuel still depends on the combustion of fuel, adiabatic CAES traps the heat of compression and reuses it for expansion. Hence, it can be considered to be a combination of CAES and thermal energy storage (TES), because a substantial portion of the exergy is stored in the form of thermal energy.

Recently, thermoelectric energy storage (TEES) systems have been proposed as a new method for large-scale energy storage wherein electric power is stored as thermal energy by using a heat pump and retrieved from the TES by using a heat engine. The advantages of TEES systems are their higher energy density and independence from geological formations.

In particular, a TEES system with transcritical CO₂ cycles is considered to be a promising method for large-scale energy storage. This chapter reviews current TEES systems and proposes a novel isothermal TEES system with transcritical CO₂ cycles. It is shown that in the case of TEES systems with transcritical CO₂ cycles, the round-trip efficiency and energy density can be increased by isothermal compression/expansion. Some ideas for its applications are also proposed by considering the characteristics of CO₂ transcritical cycles.

5.1 Thermo-electric energy storage (TEES)

Desrues et al. [47] presented a thermal energy storage process for large-scale electric applications based on a high-temperature heat pump cycle followed by a thermal engine cycle with a closed Brayton cycle. Recently, a new concept for bulk electric energy storage called

thermo-electric energy storage (TEES) was proposed by the ABB Corporate Research Center [48]. The concept is based on heat pump and heat engine technologies using transcritical CO₂ cycles, storage of pumped heat in hot water, and ice formation and melting at the cold end of the cycles. Furthermore, some results of conceptual system design were presented. A maximum round-trip efficiency of approximately 0.60 ~ 0.62 was obtained for the base case TEES configuration by assuming isentropic efficiencies of expansion and compression similar to those of commercially available turbomachinery [49,50].

In this chapter, a novel isothermal TEES system with transcritical CO₂ cycles is proposed for higher round-trip efficiency. During isothermal expansion of CO₂ in the heat engine mode of the system, the CO₂ gas can do more expansion work by absorbing heat directly from the hot storage. The round-trip efficiency of the isothermal TEES system is higher than that of a conventional TEES system because of its lower back work ratio. Isothermal compression and expansion involves slow gas pressure change rates so that sufficient heat exchange occurs between the gas and its hot storage. The use of hydraulic pumps and motors enables variable compression and expansion ratio of supercritical CO₂, heat transfer with its hot storage, and a high level of thermal and overall system efficiency.

5.1.1 Working principle of thermo-electric energy storage

The working principle of a TEES system is that in charging mode, shown in Fig. 5.1, electric power is used to compress a working fluid, and the heat from the compressed working fluid is transferred to a hot storage. Then, the compressed working fluid is expanded, producing power that can be used to reduce compression power, and the cold expanded working fluid is used to remove the heat from a cold storage.

In discharging mode, shown in Fig. 5.2, the process of the TEES system is the reverse of that in the charging mode. The working fluid that was cooled by the cold storage is compressed and heated to ambient temperature. Then, the compressed working fluid is further heated by the hot storage and expanded through an expander producing power, a portion of which is used for compression power, and cooled to ambient temperature. Two datum heat exchangers

maintaining ambient temperature are used to correct the temperature drift caused by the irreversibility of the system in both modes. The working fluid in the TEES system can undergo a phase change as in the Rankine cycle, or it may not undergo a phase change as in the Brayton cycle.

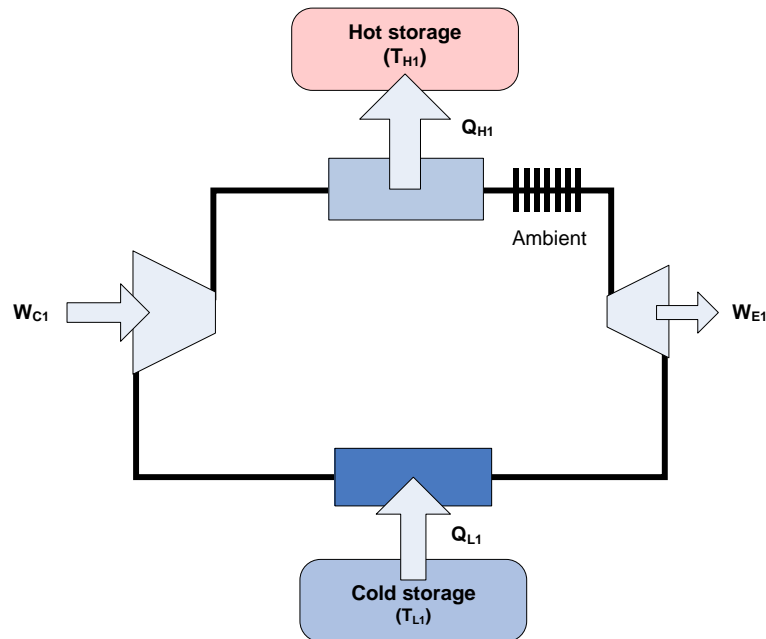


Fig. 5.1: Working principle of a thermo-electric energy storage system (charging mode).

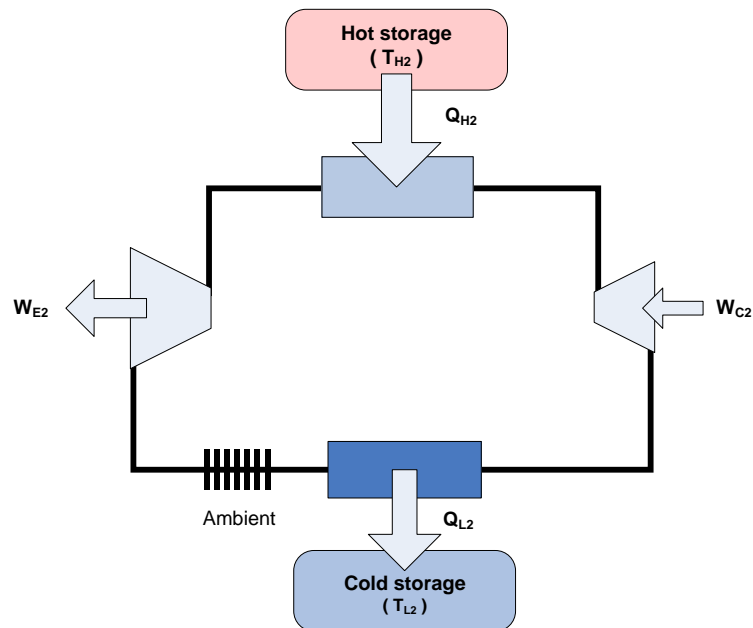


Fig. 5.2: Working principle of a thermo-electric energy storage system (discharging mode).

5.1.2 Round-trip efficiency of thermo-electric energy storage

The round-trip efficiency of the TEES system can be defined as the ratio of electric output power during discharging mode to electric input power during charging mode. In the charging mode, the actual compressor and expander powers for the working fluid are determined using compression and expansion efficiency defined, respectively, as

$$\eta_{C1} = \frac{W_{C1,i}}{W_{C1}} \quad (5.1)$$

$$\eta_{E1} = \frac{W_{E1}}{W_{E1,i}} \quad (5.2)$$

where the subscript i denotes ideal compression/expansion process without the loss of mechanical work by internal dissipation.

Back work ratio for the charging mode r_{bw1} is defined as the ratio of ideal expansion work to ideal compression work as follows:

$$r_{bw1} = \frac{W_{E1,i}}{W_{C1,i}} \quad (5.3)$$

In a similar manner, for the discharging mode, the actual compressor and expander powers for the working fluid are determined using compression and expansion efficiency defined, respectively, as

$$\eta_{C2} = \frac{W_{C2,i}}{W_{C2}} \quad (5.4)$$

$$\eta_{E2} = \frac{W_{E2}}{W_{E2,i}} \quad (5.5)$$

Back work ratio for the discharging mode r_{bw2} is defined as the ratio of ideal compression work to ideal expansion work as follows:

$$r_{bw2} = \frac{W_{C2,i}}{W_{E2,i}} \quad (5.6)$$

The round-trip efficiency of the TEES system can be obtained as

$$\begin{aligned}\eta_{RT} &= \frac{W_{net2}}{W_{net1}} = \frac{W_{E2} - W_{C2}}{W_{C1} - W_{E1}} = \frac{\eta_{E2}W_{E2,i} - (r_{bw2}W_{E2,i})/\eta_{C2}}{W_{C1,i}/\eta_{C1} - \eta_{E1}(r_{bw1}W_{C1,i})} \\ &= \frac{\eta_{C1}}{\eta_{C2}} \frac{\eta_{C2}\eta_{E2} - r_{bw2}}{1 - \eta_{C1}\eta_{E1}r_{bw1}} \frac{W_{E2,i}}{W_{C1,i}}\end{aligned}\quad (5.7)$$

where the subscript *net* denotes net power.

The round-trip efficiency of the TEES system can be degraded because of the exergy losses of the system. Because a minimum temperature difference is required for heat transfer to/from the thermal storages, the temperature difference between the high and low operating temperatures of the heat engine is slightly less than that of the heat pump. This means that the thermodynamic cycle of the TEES is not perfectly reversible ('reversible' refers to thermodynamic cycles that can be operated in both clockwise and counterclockwise direction), and in Eq. 5.7, the ideal expansion work of the heat engine $W_{E2,i}$ is slightly less than the ideal compression work of the heat pump $W_{C1,i}$. The maximum round-trip efficiency of the TEES system limited by the Carnot cycle, assuming that η_{C1} , η_{E1} , η_{C2} , and η_{E2} are equal to 1 and based on the temperature level of the hot and cold reservoirs used in the operation of the cycle, was used to plot the round-trip efficiency of a Carnot TEES as a function of a finite temperature difference for heat transfer and a hot storage temperature for different values of the heat sink temperature [48]. Furthermore, it was shown that regardless of the hot storage temperature and the heat sink temperature, the round-trip efficiency is equal to 1 if the heat transfer takes place over an infinitely small difference [48]. A closer fit of the two thermodynamic cycles of the charging and discharging modes, a better matching of the selected cycle to the heat sources and heat sinks with which the cycle interacts, is necessary to get a higher round-trip efficiency [48].

In TEES systems with good thermal-matching, since the exergy losses occurring in the turbomachinery have a greater impact on round-trip efficiency compared to the exergy losses in the heat exchangers, it is useful to define another maximum round-trip efficiency by assuming an infinitely small temperature difference for heat transfer to optimize the reference thermodynamic cycle of the TEES system. If the exergy losses in the heat exchangers are

neglected in Eq. 5.7, $W_{E2,i}$ is equal to $W_{C1,i}$, and r_{bw2} is equal to r_{bw1} . Then, the maximum round-trip efficiency, neglecting the exergy losses in the heat exchangers, can be obtained as:

$$\eta_{RT,max'} = \frac{\eta_{C1} \eta_{C2} \eta_{E2} - r_{bw}}{\eta_{C2} (1 - \eta_{C1} \eta_{E1} r_{bw})} \quad (5.8)$$

For simplicity, if it is assumed that η_{C1} , η_{E1} , η_{C2} , and η_{E2} are equal to $\eta_{C/E}$, Eq. 5.8 can be revised as:

$$\eta_{RT,max} = \frac{\eta_{C/E}^2 - r_{bw}}{1 - \eta_{C/E}^2 r_{bw}} \quad (5.9)$$

Fig. 5.3 shows the maximum round-trip efficiency as a function of back work ratio r_{bw} and the efficiency of the compressor/expander $\eta_{C/E}$. For a given efficiency of the compressor/expander, the maximum round-trip efficiency decreases rapidly with an increase in the r_{bw} . This means that it is very important to minimize the r_{bw} of the reference thermodynamic cycle to optimize the TEES system.

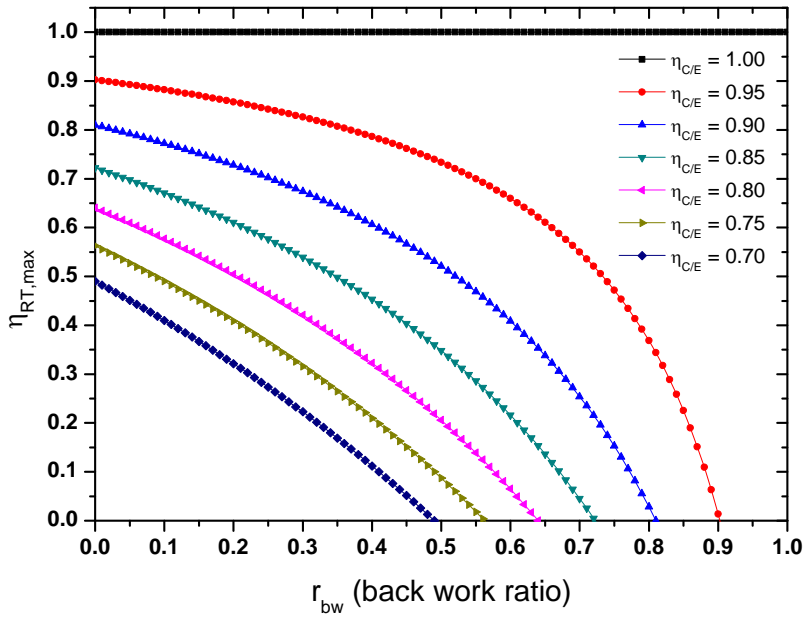


Fig. 5.3: Maximum round-trip efficiency of a TEES system as a function of r_{bw} and $\eta_{C/E}$.

5.1.3 TEES system with Brayton cycles

An UK technology start-up company Isentropic is developing a *pumped heat electricity storage* (PHES) system with a Brayton cycle using argon gas, as shown in Fig. 5.4. The storage comprises two large containers of gravel, one hot (500 °C) and one cold (−160 °C). Electrical power is input to a machine that compresses air to 500 °C on the hot side and expands it to −160 °C on the cold side. Argon is passed through the two piles of gravel where it transfers its heat/cold to the gravel. To regenerate the electricity, the cycle is simply reversed. The temperature difference is used to run the Isentropic machine as a heat engine.

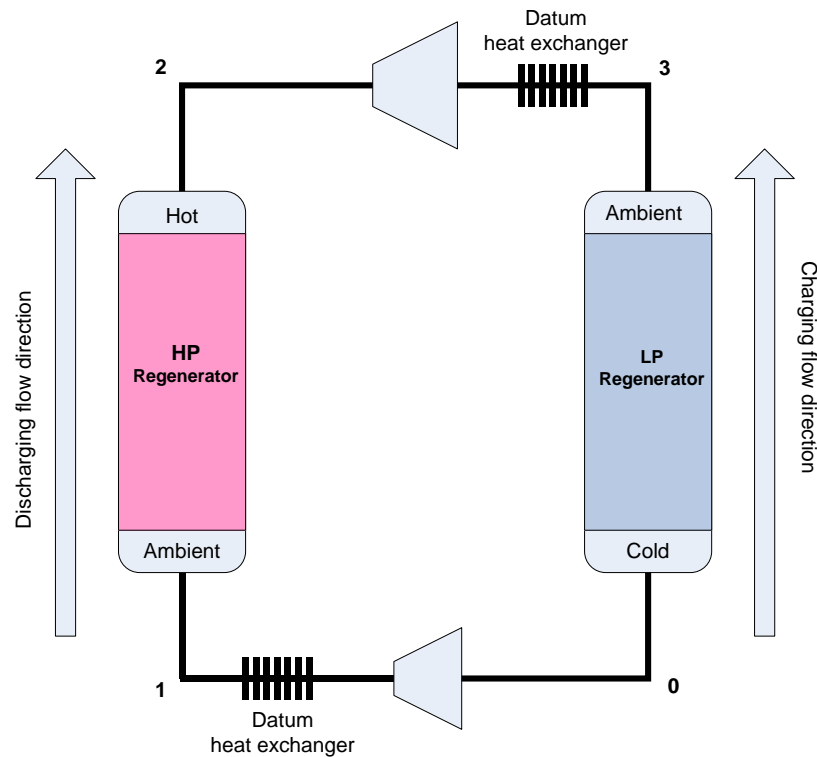


Fig. 5.4: PHES system with a Brayton cycle (Source: Isentropic Energy).

Fig. 5.5 shows the T-s diagram of the reference cycle of the Isentropic system. At the reference condition of the cycle, the back work ratio ($r_{bw} = W_{1,s}/W_{2,s}$) is 0.365, and the maximum round-trip efficiency as a function of the efficiency of the compressor/expander $\eta_{C/E}$ can be obtained as shown in Fig. 5.6.

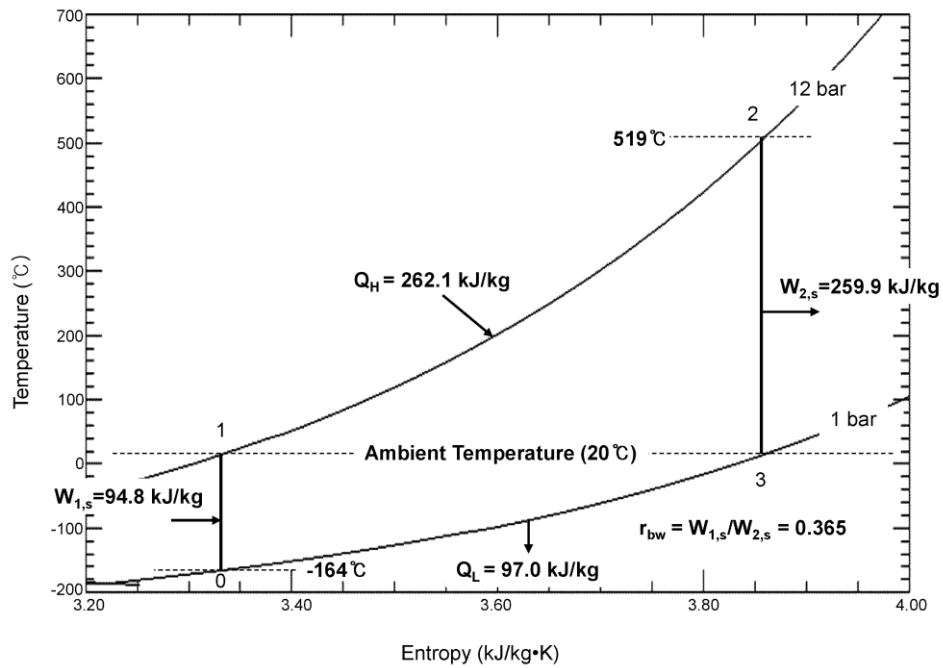


Fig. 5.5: Reference cycle of PHES system with Brayton cycle (Source: Isentropic Energy).

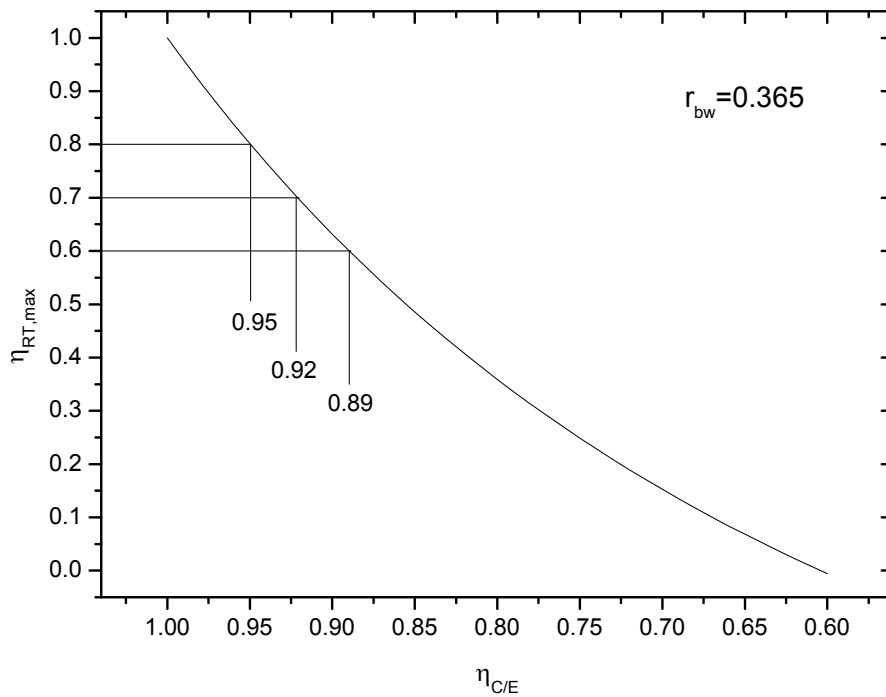


Fig. 5.6: Maximum round-trip efficiency of TEES system with reference cycle in Fig. 5.5.

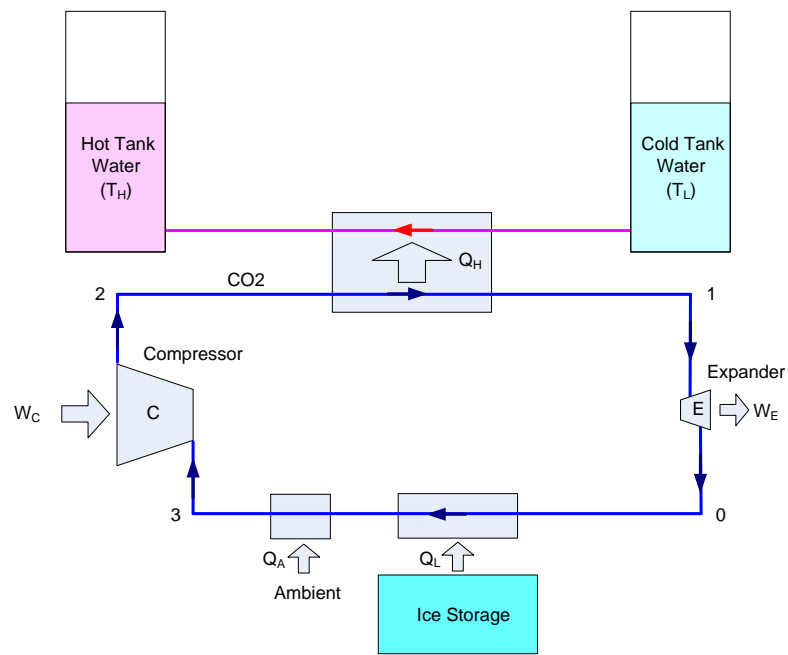
As shown in Fig. 5.6, to reach round-trip efficiencies of 0.6, 0.7, and 0.8, the efficiency of the compressor and expander must be greater than 0.89, 0.92, and 0.95, respectively.

In the case of TEES systems with a Brayton cycle, a very high temperature difference between the hot storage and the cold storage is generally needed to reduce the r_{bw} , and a highly efficient compressor and expander are needed to achieve a reasonable round-trip efficiency. Argon gas is used because it is possible to achieve a higher temperature rise/drop with the same pressure ratio of compression/expansion because its specific heat ratio (c_p / c_v) is higher than that of air.

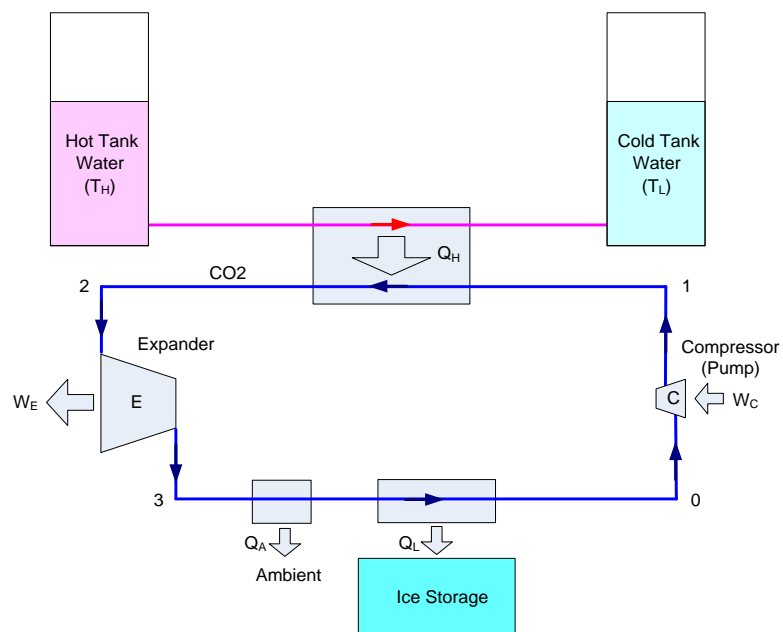
5.1.4 TEES system with transcritical CO₂ cycles

A new type of TEES system with transcritical CO₂ cycles was recently proposed by the ABB Corporate Research Center [48,49,50]. A peculiar drop in the compressibility factor around the critical point can be utilized to reduce compressor work (back work ratio) in a CO₂ power cycles. The system layout is shown in Fig. 5.7, and the T-s diagram of the base reference cycle is shown in Fig. 5.8. The Figs. are based on the preferred realization of the transcritical cycle with CO₂ as the working fluid and hot water and ice as the storage materials. Liquid water has a very high heat capacity, resulting in a high energy storage density in both volume and mass [48]. The potential advantages of using the ice storage include increased site-independence with minimum interaction with the environment, reduction of back work ratio, and increased temperature potential [48]. When the match between the cycle and the temperature curves of the heat source and sink are considered, the transcritical cycle is suitable for operation between a constant-temperature heat bath on the low-pressure side and a gliding-temperature heat bath on the high-pressure side [48].

At the reference condition of the base cycle, the back work ratio ($r_{bw} = W_{1,s} / W_{2,s}$) is 0.202, and the maximum round-trip efficiency as a function of the efficiency of the compressor/expander $\eta_{C/E}$ can be obtained as shown in Fig. 5.9.



(a) Charging mode



(b) Discharging mode

(c)

Fig. 5.7: Schematic of TEES system with transcritical CO₂ cycle, charging (a) and discharging (b) modes.

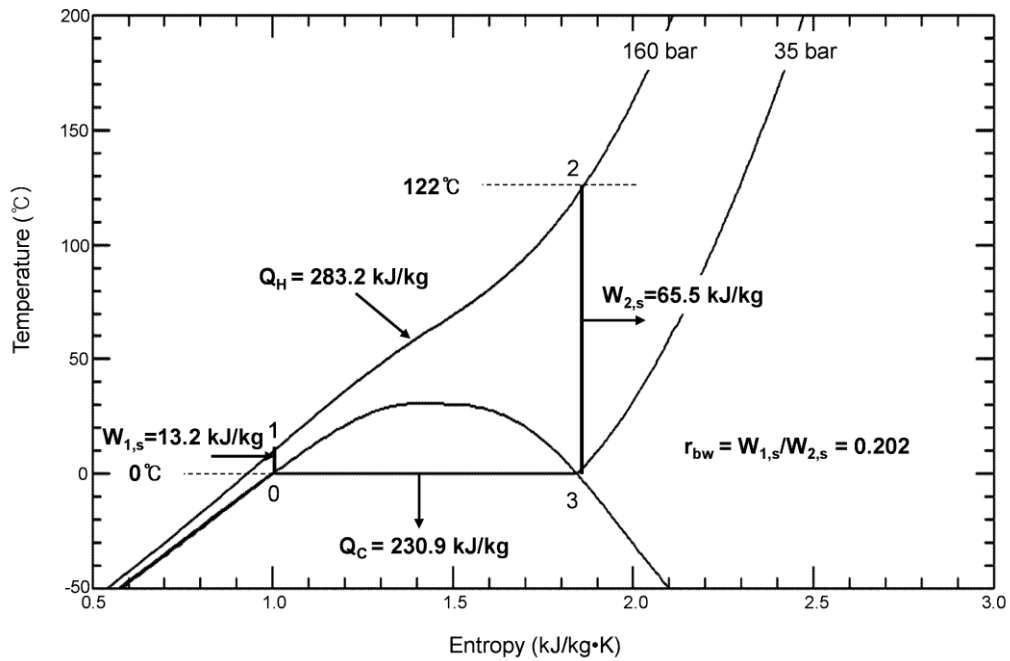


Fig. 5.8: Base reference cycle of TEES system with transcritical CO₂ cycle.

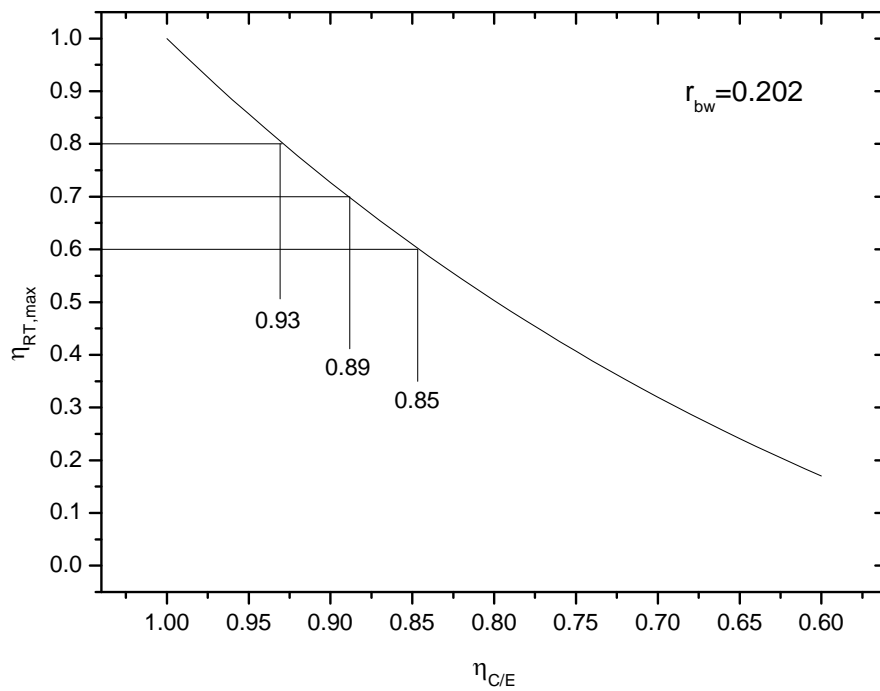


Fig. 5.9: Maximum round-trip efficiency of TEES system with reference cycle in Fig. 5.8.

To achieve round-trip efficiencies of 0.6, 0.7, and 0.8, the efficiency of the compressor and expander must be greater than 0.85, 0.89, and 0.93, respectively. In the case of a TEES system with transcritical CO₂ cycles, even if the temperature difference between the hot storage tank and the cold storage tank is much smaller than with the previous Brayton cycles, its round-trip efficiency is higher than with the previous Brayton cycles with the same compressor/expander efficiency $\eta_{C/E}$ because of the reduced r_{bw} .

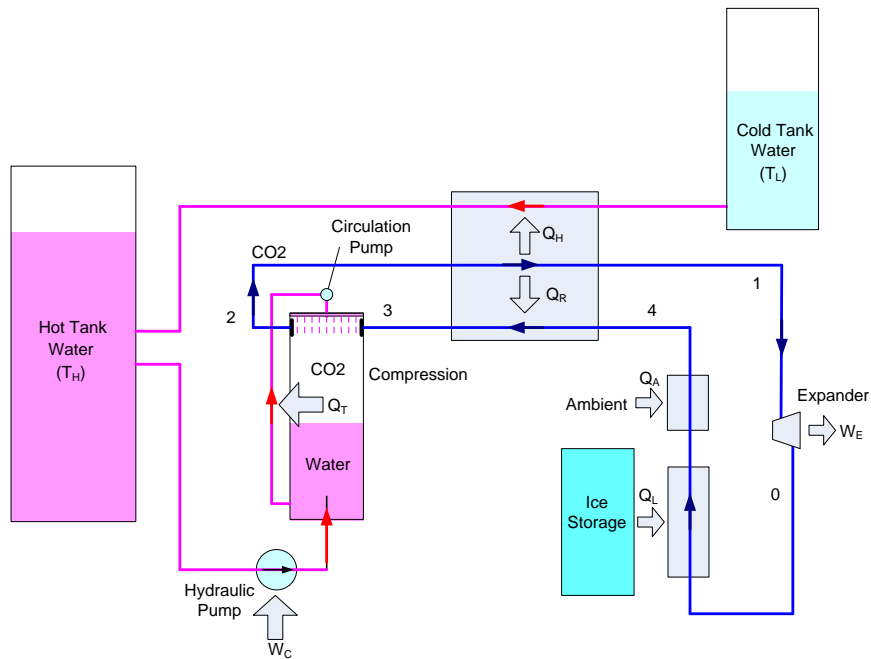
5.2 Isothermal TEES system with transcritical CO₂ cycles

A TEES system with transcritical CO₂ cycles has some advantages such as its higher efficiency and the use of water as an inexpensive thermal storage compared to a TEES system with Brayton cycles. However, according to the results of the first optimization of the system based on pinch analysis, a realistic round-trip efficiency of 0.6 was obtained for the base case TEES configuration by assuming isentropic efficiencies of expansion and compression similar to those of commercially available turbomachinery and by considering a minimum temperature difference for heat transfer [49]. If the same isentropic efficiencies of expansion and compression presented in Reference [49] ($\eta_{C1} = 0.86$, $\eta_{E1} = 0.85$, $\eta_{C2} = 0.85$, and $\eta_{E2} = 0.88$) are assumed, at the reference condition in Fig. 5.8, the maximum round-trip efficiency in Eq. 5.8 is 0.648.

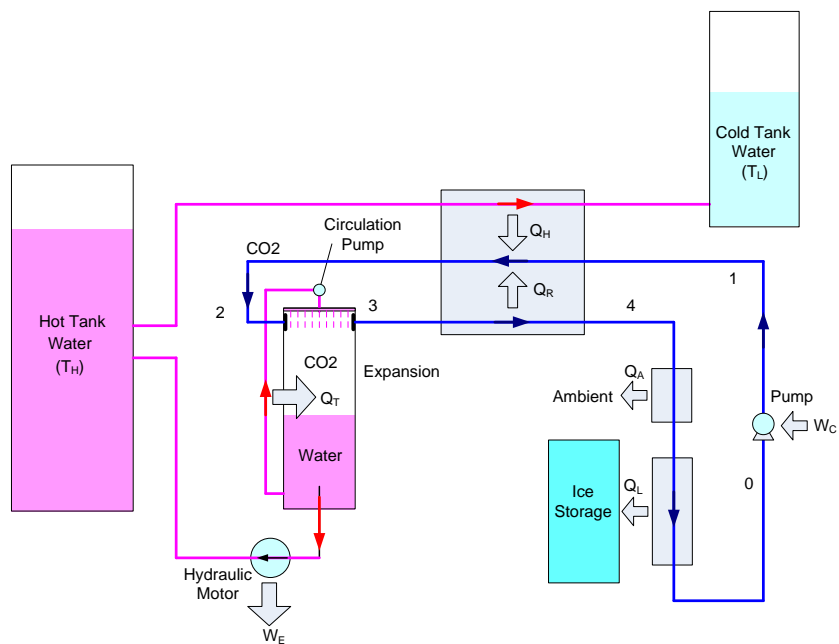
In this chapter, for the purpose of increasing the round-trip efficiency of a TEES system with transcritical CO₂ cycles, a novel type of isothermal TEES system is proposed.

5.2.1 System description

The system layout is shown in Fig. 5.10, and the T-s diagram of the base reference cycle is shown in Fig. 5.11. As shown in Fig. 5.11, the sequences of the charging (HP) mode and the discharging (TE) modes are 4-3-2-1-0 and 0-1-2-3-4, respectively.



(a) Charging mode



(b) Discharging mode

Fig. 5.10: Schematic of isothermal TEES systems with transcritical CO₂ cycles, charging (a) and discharging (b) modes.

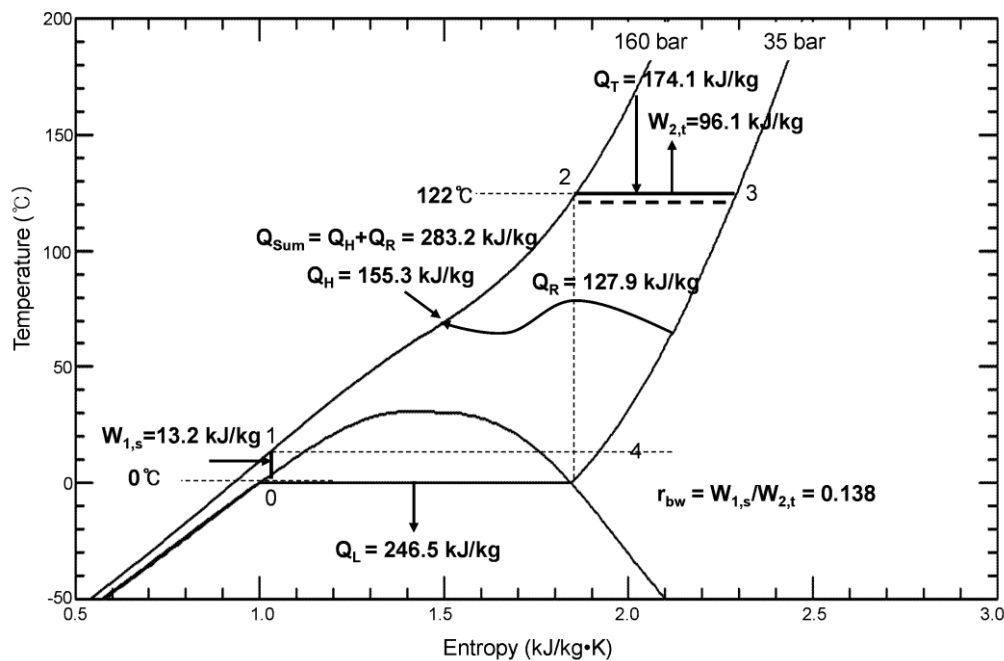


Fig. 5.11: Base reference cycle of isothermal TEES systems with transcritical CO₂ cycles.

During the discharging mode, the process of isothermal TEES can maximize the expansion work by isothermal expansion (2-3) with effective heat transfer directly with the hot storage tank, resulting in a higher round-trip efficiency because of the reduced back work ratio. After the isothermal expansion, the residual heat of the hot expanded CO₂ gas is transferred to the cold compressed supercritical CO₂ (3-4) in the recuperator where the supplementary heat is supplied by the hot water flowing from the hot tank to the cold tank to heat the compressed supercritical CO₂ (1-2). Because approximately half of the heat needed from state 1 to state 2 is supplied by waste heat from the low-pressure side, the heat supplied by the flowing hot water is approximately half of that in the previous isentropic case, and much more heat is supplied directly from the hot tank during isothermal expansion.

The same concept of isothermal compression and expansion was used in the isothermal CAES system. The isothermal CAES system uses a hydraulic pump/motor to compress/expand air isothermally at rates that allow the high-pressure air to exchange heat with its surroundings, and it uses slow gas pressure change rates to allow sufficient heat exchange between the gas and its surroundings [20,24].

In the case of an isothermal TEES system, the hot water heated from the hot storage tank is used by the pump/motor to compress/expand the supercritical CO₂ as the liquid piston, and a portion of the water is sprayed to cool/heat the supercritical CO₂ by a circulation pump. In reality, as shown in Fig. 5.12, the liquid piston type of compressor/expander can be a double-acting type of compressor/expander, and a four-way valve can be used to make the hydraulic pump/motor operate in one direction with both directions of the liquid piston [24].

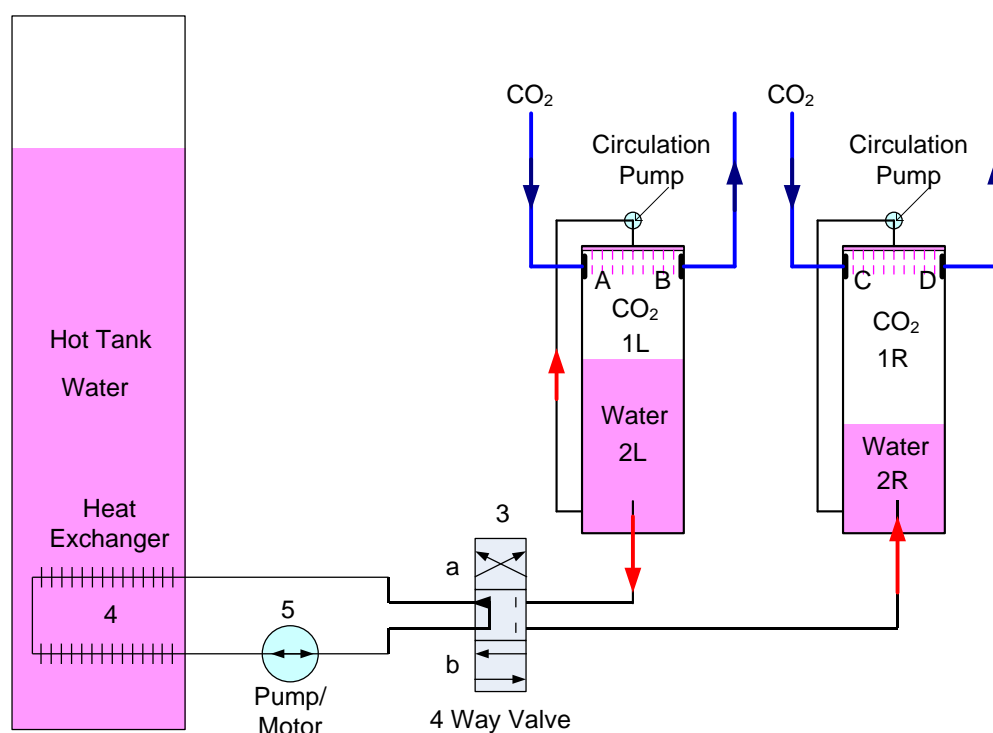


Fig. 5.12: Schematic of a double-acting liquid piston type of isothermal compressor/expander.

During the discharging (expansion) process, the compressed CO₂ enters through the opened valve (A) of the left cylinder, the work-chamber (1L) of the left cylinder comprising the liquid piston (2L); the said valve (A) being controlled so as to admit exactly the quantity of compressed CO₂ which, once expanded, will reach the low pressure of CO₂. The pressure established in the left cylinder is transmitted through the four-way valve (3) in position (b) and the heat exchanger (4) to the hydrostatics (5) and thus activates the motor port. This leads to the expulsion of the expanded CO₂ in the work-chamber (1R) by the return flow of (5),

which enters the recuperator through the opened valve (D). In the left-hand work-chamber (1L), a portion of the water is sprayed to heat the expanding CO₂ by a circulation pump, so any cooling down of the CO₂ is strongly limited (the same would happen during compression, where a temperature rise would be limited). As the stroke ends, four-way valve (3) inverts the flow by switching to the position (a) without changing the rotational direction of the hydraulic motor, the inertia of the liquid pistons being negligible [24].

In the case of an isothermal TEES system, when the water is used by the pump/motor to compress/expand the supercritical CO₂ as a liquid piston, the CO₂ can dissolve into the water, which may cause internal corrosion in the pipelines, water pump/motor, and heat exchanger. In addition, the presence of water in CO₂ flows may also cause internal corrosion in the pipelines, CO₂ pump/motor, and heat exchanger system.

In order to solve the corrosion problem caused by the mixture of CO₂ and water, the refrigeration oil for the CO₂ compressor can be used by the pump/motor to compress/expand the supercritical CO₂ as a liquid piston, and the heat of the refrigeration oil is transferred to/from the water in the hot tank by the heat exchanger. Since the refrigeration oil is not used for thermal energy storage but as a secondary fluid for heat transfer, it is possible to minimize the quantity of refrigeration oil in the system. Some studies have found that PAG is the best lubricant for a CO₂ refrigeration system [77] because of its high chemical stability and good lubricity under high pressure. Newly developed refrigeration lubricants using PAG have been successfully introduced into the market for CO₂ heat pump water heater systems and CO₂ automotive A/C systems.

Although the following description applies mainly to the discharging mode (heat engine mode), the charging mode (heat pump mode) is the reverse of the discharging mode. In Fig. 5.11, the expansion work $w_{2,t}$ ($W_{2,t}/m$) and the heat input q_T (Q_T/m) during the isothermal expansion process (2-3) can be obtained as:

$$w_{2,t} = q_T - (h_3 - h_2) \quad (5.10)$$

$$q_T = T_2(s_3 - s_2) \quad (5.11)$$

At the reference condition of the base cycle, the isothermal expansion work $W_{2,t}$ is approximately 50% greater than the isentropic expansion work $W_{2,s}$, and the r_{bw} ($W_{1,s}/W_{2,t}$) is 0.136. If the same efficiencies of expansion and compression are assumed ($\eta_{C1} = 0.86$, $\eta_{E1} = 0.85$, $\eta_{C2} = 0.85$, and $\eta_{E2} = 0.88$), at the reference condition in Fig. 5.11, the maximum round-trip efficiency in Eq. 5.8 is increased to 0.688 from 0.648 in the previous isentropic case. The use of hydraulic pumps and motors enables a variable ratio of compression and expansion of CO₂, heat transfer with the hot storage tank, and a high level of thermal and overall system efficiency. Although the same efficiencies of the compressor and expander as those presented with turbomachinery are assumed, the efficiencies of the liquid piston type of compressors and the expander with a similarly designed hydraulic pump/turbine are greater than 0.90.

The actual compressor and expander powers for the working fluid are determined using an isothermal efficiency defined, respectively, as

$$\eta_{C1} = \frac{W_{C1,t}}{W_{C1}} \quad (5.12)$$

$$\eta_{E2} = \frac{W_{E2}}{W_{E2,t}} \quad (5.13)$$

where the subscript t denotes an ideal isothermal compression/expansion process.

If higher efficiencies than those in the previous isentropic case are assumed for compression and expansion in the liquid piston part as $\eta_{C1} = \eta_{E2} = 0.90$, the maximum round-trip efficiency in Eq. 5.8 is increased to 0.743 from 0.648 in the previous isentropic case.

5.2.2 Operating characteristics of isothermal TEES systems with transcritical CO₂ cycles

As mentioned before, in the case of an isothermal TEES system with transcritical CO₂ cycles, much heat is supplied directly from the hot tank during the isothermal expansion. Therefore, the temperature of the hot tank decreases slightly with time during the discharging mode, resulting in a varying condition and performance of the system. For a simple model of the system, the discharging process of the system in small time steps, where index i is the current time step, can be expressed as follows. The rate of temperature drop of the hot tank owing to the supply of heat for the isothermal expansion can be obtained as:

$$M_{w(h),i} c_{p,w,i} \dot{T}_{H,i} = \dot{m}_{CO_2} q_{T,i} \quad (5.14)$$

where $M_{w(h),i}$, $c_{p,w,i}$, and $T_{H,i}$ are the mass, specific heat, and temperature of water in the hot tank, respectively; \dot{m}_{CO_2} is the mass flow rate of CO₂ and is assumed to be constant; and $q_{T,i}$ is the heat input per unit mass of CO₂ for the isothermal expansion.

The mass flow rate of water from the hot tank to the cold tank used to heat the supercritical CO₂ from state 1 to state 2 can be obtained as:

$$\dot{m}_{w,i} c_{p,w,i} (T_{H,i} - T_L) = \dot{m}_{CO_2} [(h_{2,i} - h_1) - (h_{3,i} - h_4)] \quad (5.15)$$

where T_L is the temperature of water in the cold tank, $T_4 = T_1$, and T_L and T_1 are constant.

Although in Eq. 5.15, the efficiency of recuperator is assumed to be 1.0 and the actual efficiency is less than 1.0, it is reasonable to consider that the additional heat is due to the irreversibility of the expander and the pump. The efficiency of the recuperator η_R can be defined as:

$$\eta_R = \frac{q_R}{h_3 - h_4} \quad (5.16)$$

where q_R is the heat recovered from the low-pressure side and transferred to the high-pressure side by the recuperator, and $h_3 - h_4$ is the maximum available heat from the low-pressure side.

If the efficiency of the recuperator is assumed to be 0.95, more heat as $(1 - \eta_R)(h_3 - h_4)$ is required from the hot tank to heat the supercritical CO₂ compared with the ideal recuperator ($\eta_R = 1.0$). However, if the efficiencies of the expander and pump are assumed to be 0.9, the additional heat due to the irreversibilities of the expander and pump, i.e., the mechanical energy converted to thermal energy by internal dissipation can sufficiently compensate for the deficiency of the heat recovery from the low-pressure side.

In reality, in Eq. 5.11, the heat input q_T from the hot tank to the supercritical CO₂ for isothermal expansion is less than $T_2(s_3 - s_2)$ by as much as the additional heat due to the irreversibility of isothermal expander. The real cycles will be discussed later in detail by considering the additional heat due to internal dissipation during the compression and expansion processes. At this point, for simplicity, it is reasonable to assume that the waste heat from the low-pressure side is fully recovered by the ideal recuperator by considering the additional heat due to the irreversibilities of the expander and pump.

The mass of the water in the hot tank at the next time step $i + 1$ can be obtained as:

$$M_{w(h),i+1} = M_{w(h),i} - \dot{m}_{w,i} \Delta t \quad (5.17)$$

The mass flow rate of CO₂ is assumed to be 1 kg/s to evaluate the performance of the system per unit mass flow rate of CO₂. The discharging process begins at the reference condition of the base cycle shown in Fig. 5.11, and the discharging period τ_D is assumed to be 5 h. The initial mass of the water in the hot tank $M_{w(h),0}$ is assumed to be 16000 kg by considering the equivalent storage volume of the previous isentropic TEES system.

Fig. 5.13 shows the temperature drop of the hot tank and the expansion and compression power during the discharging period. As the temperature of hot tank drops from 122 °C to 56 °C, the expansion power drops from 86 kW to 56 kW, and the instantaneous maximum round-trip efficiency of the system defined in Eq. 5.9 decreases slightly because of the increase in the r_{bw} , as shown in Fig. 5.14, where the efficiencies of a liquid piston compressor and expander are assumed to be 0.90.

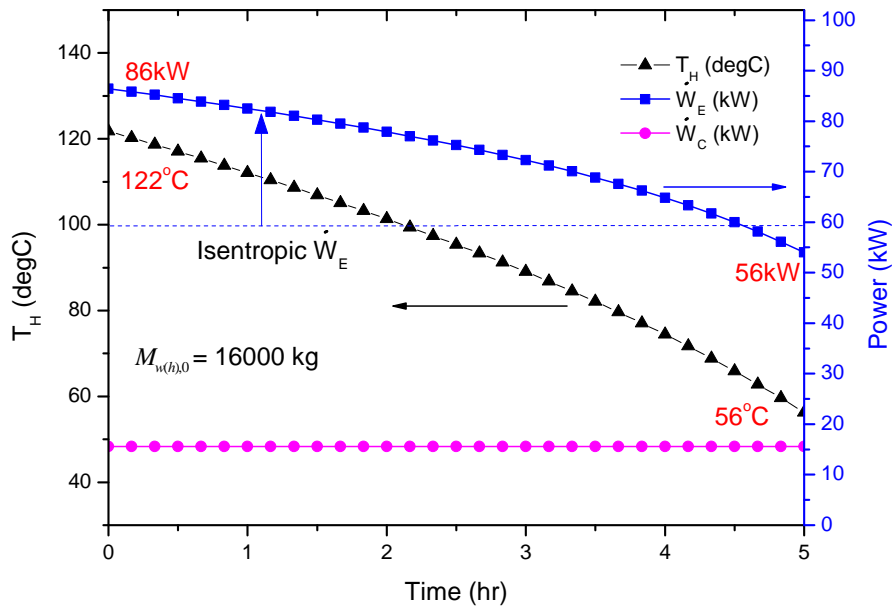


Fig. 5.13: Expansion and compression power and temperature drop of the hot tank during the discharging process in an isothermal TEES system with the reference cycle shown in Fig. 5.11 (Case 1).

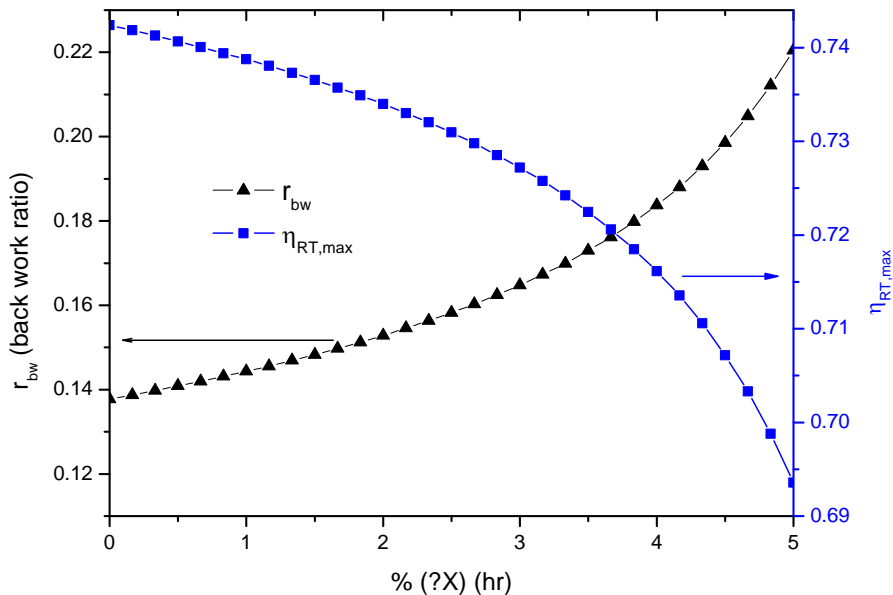


Fig. 5.14: Instantaneous r_{bw} and maximum round-trip efficiency during the discharging process in an isothermal TEES system (Case 1).

Fig. 5.15 shows the varying net power $\dot{W}_{net,ch}$ and $\dot{W}_{net,dc}$ during the charging and discharging periods, respectively, and the overall maximum round-trip efficiency of the system can be calculated as 0.729.

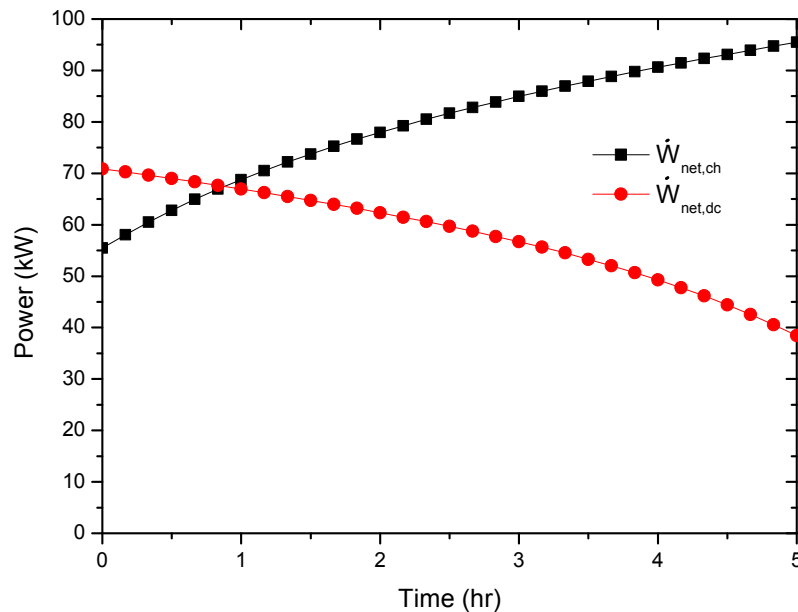


Fig. 5.15: Net power during the charging and discharging processes in an isothermal TEES system (Case 1).

Fig. 5.16 shows the mass of water in the hot tank and the mass flow rate of water flowing from the hot tank to the cold tank during the discharging period. The mass flow rate of water from the hot tank to the cold tank is approximately half of that of the isentropic TEES system because approximately half of the heat required from state 1 to state 2 is supplied by waste heat from the low-pressure side. Moreover, approximately two thirds of the water in the hot tank remains in the hot tank at the end of discharging process. Therefore, the volume of the cold tank V_c is approximately one third of volume of the hot tank V_h .

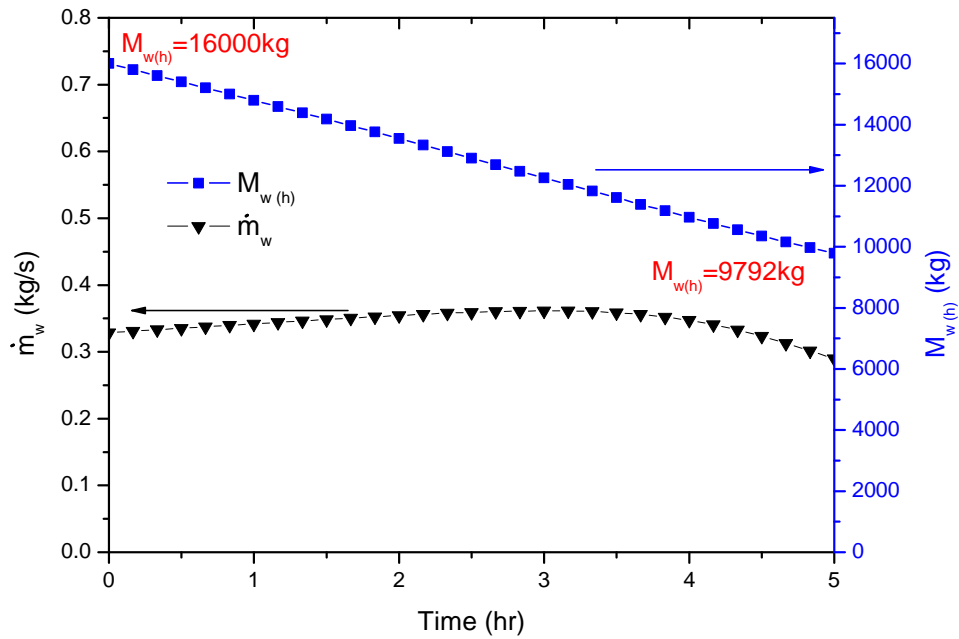


Fig. 5.16: Mass flow rate of water from the hot tank to the cold tank and the mass of the water in the hot tank during the discharging process in an isothermal TEES system (Case 1).

The performance of the isothermal TEES system with the reference cycle shown in Fig. 5.11 and the initial mass of the water in the hot tank ($M_{w(h),0}$) of 16000 kg (Case 1) is compared with that of the isentropic TEES system, as summarized in Table 5.1. The maximum round-trip efficiency and the energy density, defined as the total net power for the discharging period per unit volume of the sum of the hot and cold tanks, of the isothermal TEES system are much higher than those of the isentropic TEES system.

Table 5.1: Performance of isothermal TEES (Case 1) compared with isentropic TEES

C/E	$\dot{W}_{C2,i}$ (kW)	$\dot{W}_{E2,i}$ (kW) (T_H)	r_{bw}	$\eta_{C/E}$	$\eta_{RT,max}$	Energy (kWh)	$V_h + V_c$ (m ³)	Energy/ V_t (kWh/m ³)
Isentropic	13.2	65.5 (122 °C)	0.202	C1: 0.86 E1: 0.85 C2: 0.85 E2: 0.88	0.648	210.5 (42.1 kW × 5h)	21.6 (10.8 + 10.8)	9.75
Isothermal	13.2	96.1~ 60.0 (122 °C ~56 °C)	0.136~ 0.214	C1: 0.86 E1: 0.85 C2: 0.85 E2: 0.88 C1: 0.90 E1: 0.85 C2: 0.85 E2: 0.90	0.672 0.729	280.4 (56.1 kW × 5 h)	22.2 (16.0 + 6.2)	12.63 13.66
Conditions	$P_0 = 35$ bar, $T_0 = 0$ °C $P_2 = 160$ bar, $T_2 = 122$ °C		$\dot{m}_{CO_2} = 1$ kg/s $\tau_D = 5$ h		$M_{w(h)} = 16000$ kg			

If the initial mass of the water in the hot tank at the start of discharging process is increased from 16000 kg to 20000 kg (Case 2), the temperature drop in the hot tank during the discharging process is reduced and the drop of expansion power is also reduced, as shown in Fig. 5.17. Therefore, as shown in Fig. 5.18, the drop in instantaneous maximum round-trip efficiency of the system is less than the previous case because of a smaller increase in the r_{bw} .

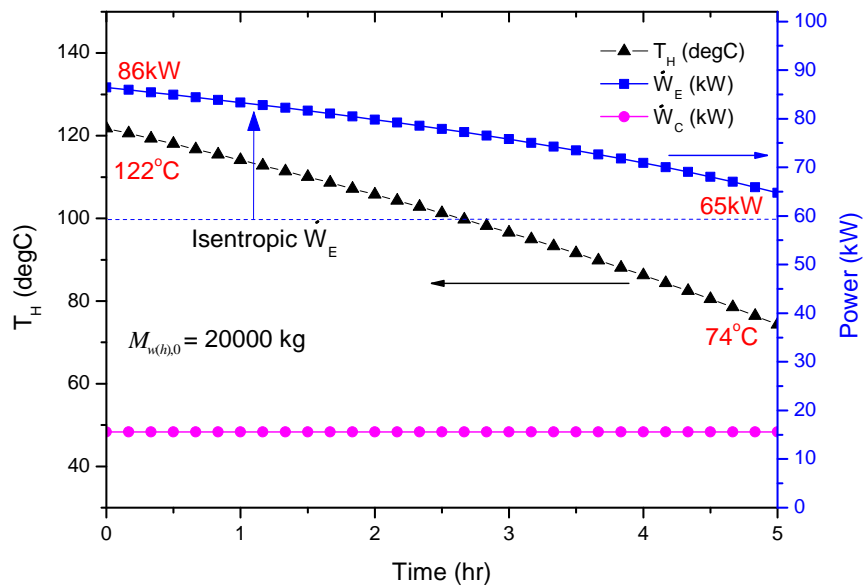


Fig. 5.17: Expansion and compression power and temperature drop of the hot tank during the discharging process in an isothermal TEES system with the reference cycle shown in Fig. 5.11, and $M_{w(h),0} = 20000$ kg (Case 2).

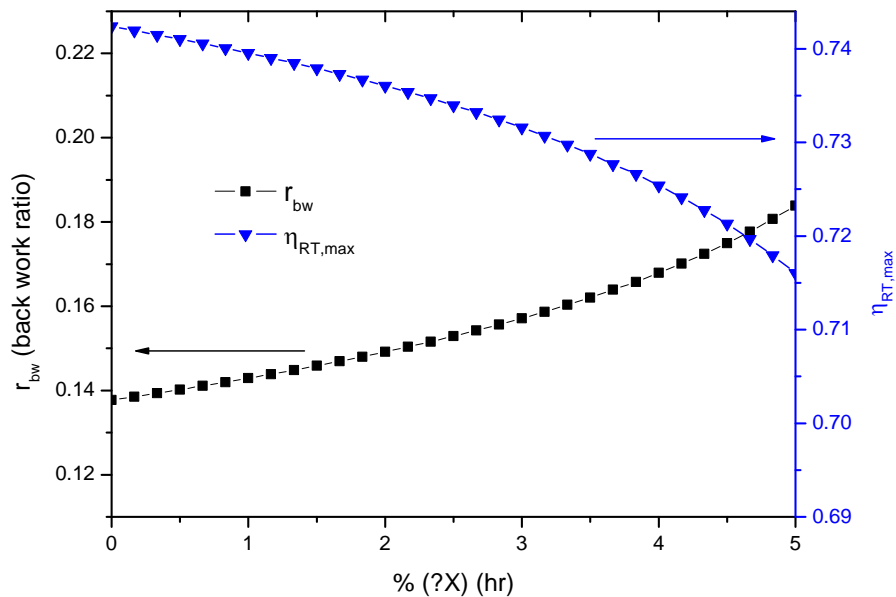


Fig. 5.18: Instantaneous r_{bw} and maximum round-trip efficiency during the discharging process in an isothermal TEES system (Case 2).

Fig. 5.19 shows the variations in net power $\dot{W}_{net,ch}$ and $\dot{W}_{net,dc}$ during the charging and discharging periods, and the overall maximum round-trip efficiency of the system can be calculated as 0.733. With the increase in the initial mass of the water in the hot tank, it is possible to reduce the variation in net power during the charging and discharging periods and obtain a slightly higher round-trip efficiency of the system.

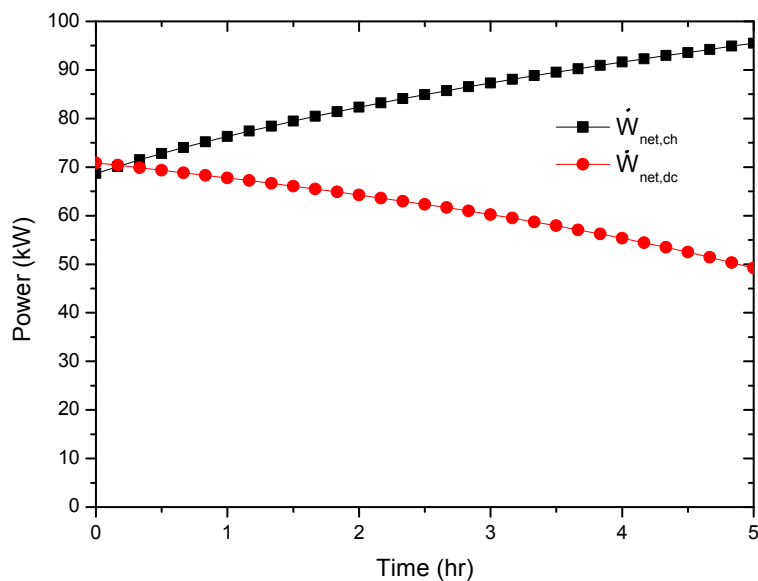


Fig. 5.19: Net power during the charging and discharging processes in an isothermal TEES system (Case 2).

Fig. 5.20 shows the mass of water in the hot tank and the mass flow rate of water flowing from the hot tank to the cold tank during the discharging period. Approximately three fourths of water in the hot tank is retained at the end of the discharging process.

The performance of the isothermal TEES system with an initial $M_{w(h)}$ of 20000 kg and the reference cycle shown in Fig. 5.11 is summarized in Table 5.2.

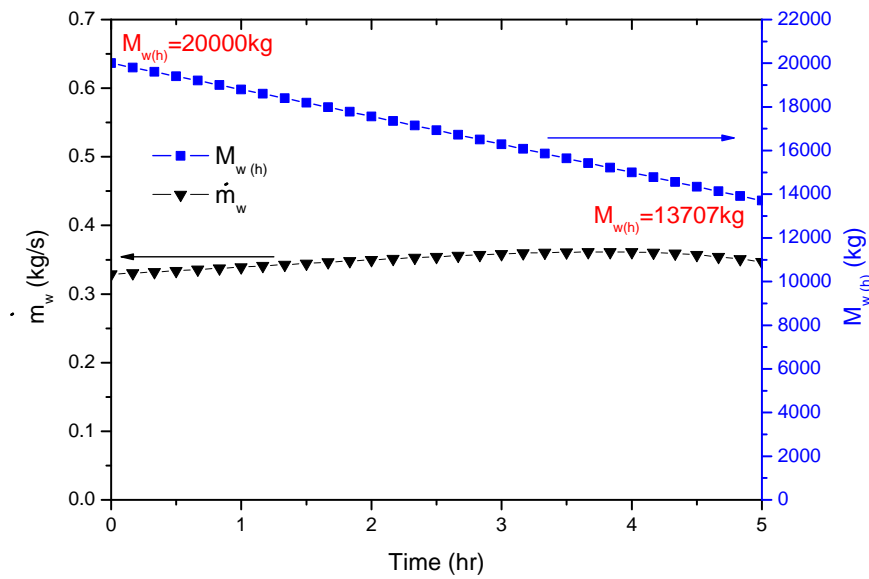


Fig. 5.20: Mass flow rate of water from the hot tank to the cold tank and the mass of the water in the hot tank during the discharging process in an isothermal TEES system (Case 2).

Table 5.2: Performances of isothermal TEES system (Case 2)

C/E	$\dot{W}_{C2,i}$ (kW)	$\dot{W}_{E2,i}$ (kW) (T_H)	r_{bw}	$\eta_{C/E}$	$\eta_{RT,max}$	Energy (kWh)	$V_h + V_c$ (m ³)	Energy/ V_i (kWh/m ³)
Isothermal	13.2	96.1~ 72.7 (122 °C ~74 °C)	0.136~ 0.184	C1: 0.86	0.677	299.6 (59.9 kW × 5 h)	26.3 (20.0 + 6.3)	11.39
				E1: 0.85				
				C2: 0.85				
				E2: 0.88				
				C1: 0.90				
Conditions	$P_0 = 35$ bar, $T_0 = 0$ °C $P_2 = 160$ bar, $T_2 = 122$ °C			$\dot{m}_{CO_2} = 1$ kg/s	0.733	308.0 (61.6 kW × 5 h)	26.3 (20.0 + 6.3)	11.71
				E1: 0.85				
				C2: 0.85				
				E2: 0.90				
				$M_{w(h)} = 20000$ kg				

If the initial temperature of water in the hot tank at the start of the discharging process is increased from 122 °C to 150 °C (Case 3), as shown in Fig. 5.21, the performance of the isothermal TEES system can be improved compared with the previous case.

Fig. 5.22 shows the temperature drop of the hot tank and the expansion and compression power during the discharging period. As the temperature of the hot tank drops from 150 °C to 107 °C, the expansion power drops from 97 kW to 80 kW.

Fig. 5.23 shows the varying net power $\dot{W}_{net,ch}$ and $\dot{W}_{net,dc}$ during the charging and discharging periods, and the overall maximum round-trip efficiency of the system can be calculated as 0.745.

The power and volume flow rate of the hydraulic motor (or turbine) used for the liquid piston type expander during the discharging periods are shown in Fig. 5.24. The volume rate of the hydraulic motor can be calculated as the difference in the CO₂ volume flow rate between the inlet (high pressure) of the expander and the outlet (low pressure) of the expander. The average power and volume flow rate of the hydraulic motor are approximately 90 kW and 17 l/s, respectively.

Table 5.3 summarizes the performance of isothermal TEES system with an initial temperature of 150 °C, initial mass of hot water of 20000 kg, and the reference cycle shown in Fig. 5.21.

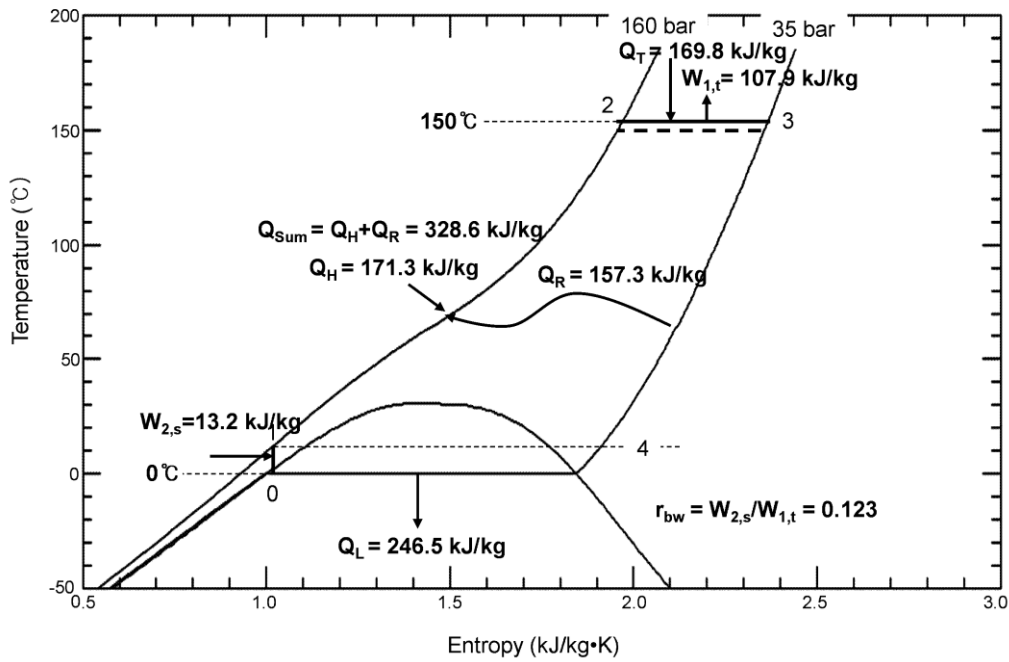


Fig. 5.21: Reference cycle of an isothermal TEES system with T-CO₂ cycles (Case 3).

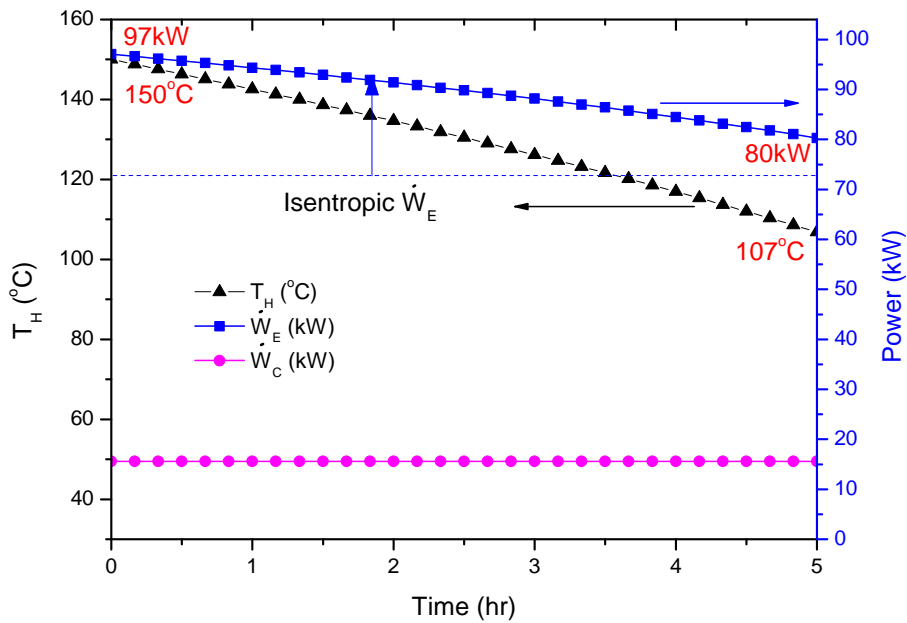


Fig. 5.22: Expansion and compression power and temperature drop of the hot tank during the discharging process in an isothermal TEES system (Case 3).

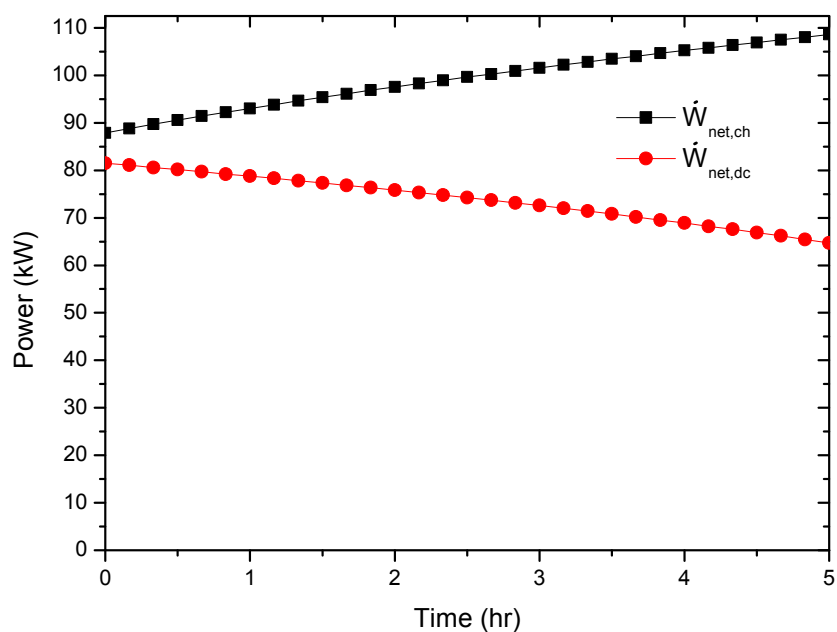


Fig. 5.23: Net power during the charging and discharging processes in an isothermal TEES system (Case3).

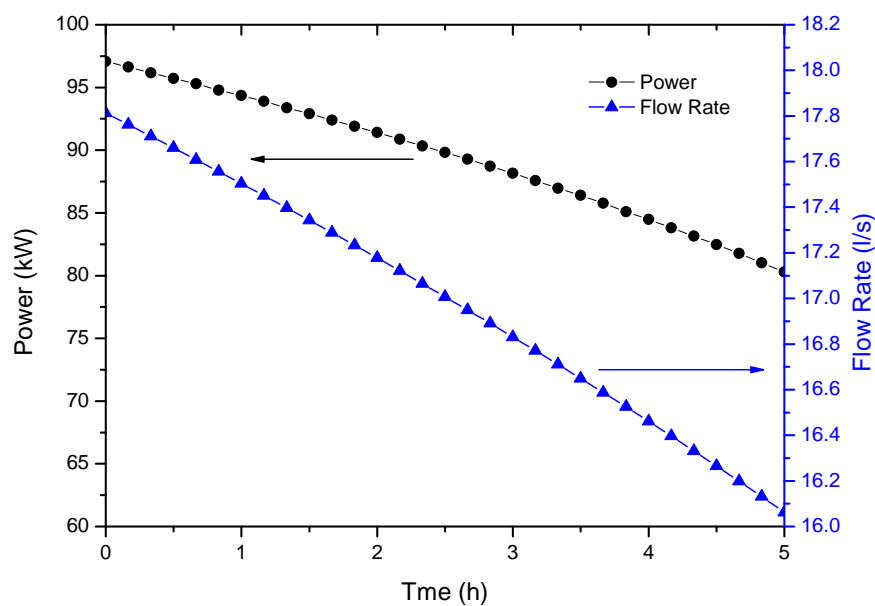


Fig. 5.24: Power and volume flow rate of a hydraulic turbine during the discharging process in an isothermal TEES system (Case 3).

Table 5.3: Performances of isothermal TEES system (Case 3)

C/E	$\dot{W}_{C2,i}$ (kW)	$\dot{W}_{E2,i}$ (kW) (T_H)	r_{bw}	$\eta_{C/E}$	$\eta_{RT,max}$	Energy (kWh)	$V_h + V_c$ (m ³)	Energy/ V_t (kWh/m ³)
Isothermal	13.2	97.1~ 80.3 (150 °C ~107 °C)	0.123~ 0.148	C1: 0.86	0.689	361.3 (72.3 kW × 5 h)	25.7 (20.0 + 5.7)	14.06
				E1: 0.85				
				C2: 0.85				
				E2: 0.88				
				C1: 0.90	0.745	369.4 (73.9 kW × 5 h)	25.7 (20.0 + 5.7)	14.37
				E1: 0.85				
				C2: 0.85				
				E2: 0.90				
Conditions	$P_0 = 35 \text{ bar}, T_0 = 0 \text{ °C}$		$\dot{m}_{CO_2} = 1 \text{ kg/s}$		$M_{w(h)} = 20000 \text{ kg}$			
	$P_2 = 160 \text{ bar}, T_2 = 150 \text{ °C}$		$\tau_D = 5 \text{ h}$					

5.2.3 Higher pressure of isothermal TEES systems with transcritical CO₂ cycles

One of the difficulties in TEES systems with transcritical CO₂ cycles is matching the thermal capacity of water with that of CO₂ to allow the best possible thermal integration. As shown in Fig. 5.25, the isobaric specific heat of CO₂ in the high-pressure side changes significantly in the operating temperature range while that of water is almost constant. Although it is possible to reduce the variation in the isobaric specific heat of CO₂ by increasing the maximum CO₂ pressure, in the case of isentropic TEES systems with transcritical CO₂ cycles, the maximum operating temperature of CO₂ increases because of the high pressure ratio, and therefore, the pressure of the water tank must be greatly increased to prevent boiling of water. So, an array

of 5 or 6 water storage tanks was proposed with the maximum CO₂ pressure below 200 bar [49,50].

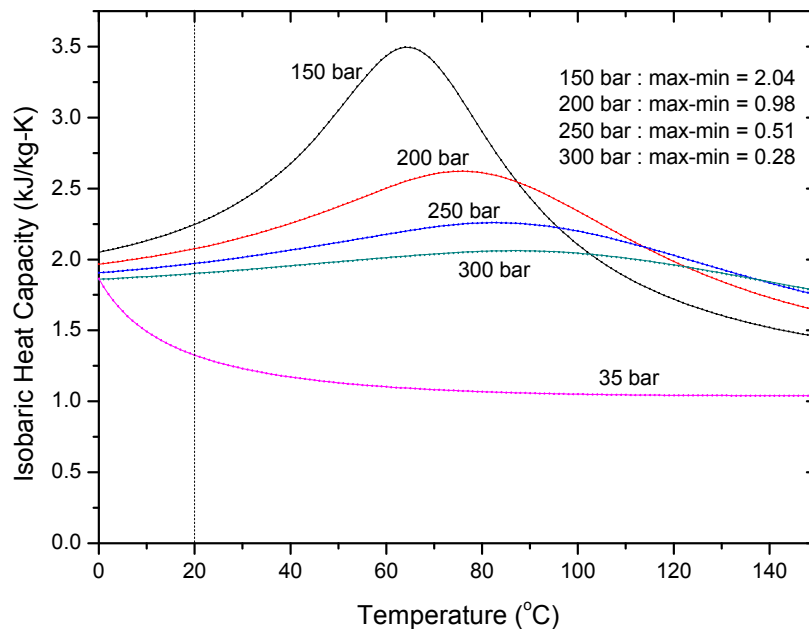


Fig. 5.25: Variation in the isobaric specific heat of CO₂ in the operating temperature range depending on the CO₂ pressure.

However, in the case of isothermal TEES systems with transcritical CO₂ cycles, it is possible to limit the maximum operating temperature freely in spite of the high pressure ratio. Fig. 5.26 shows the required thermal capacity of the water in the high-pressure side of CO₂ in an isothermal TEES system, as the difference in the specific heat between the high-pressure side and the low-pressure side of CO₂.

The reference cycle of the isothermal TEES systems with a maximum temperature of 150 °C and a maximum pressure of 300 bar (Case 4) is shown in Fig. 5.27. The performance of the system is shown in Fig. 5.28, Fig. 5.29, and Table 5.4. Although it is possible to reduce the variation in the required thermal capacity of the water with an increase in the maximum CO₂ pressure, the round-trip efficiency of the system is lower because of the higher r_{bw} . It is necessary to optimize the maximum CO₂ pressure by the efficiency and cost of the system.

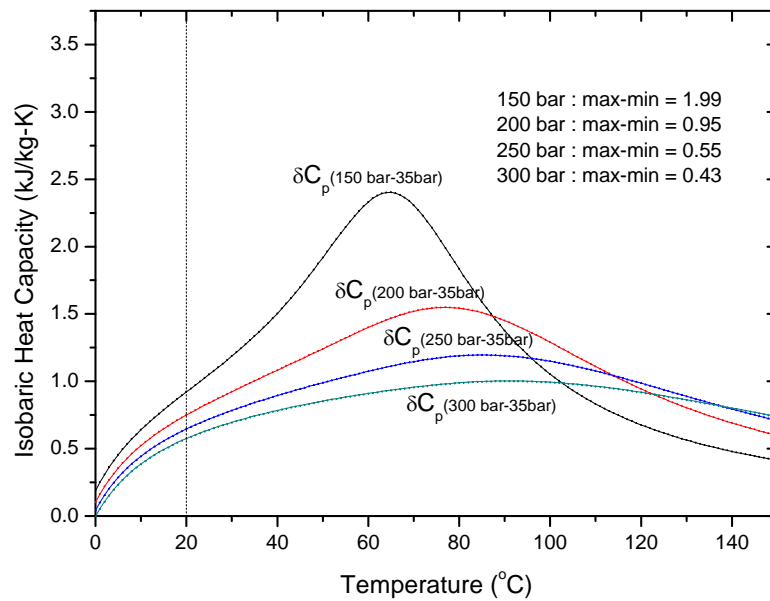


Fig. 5.26: Required thermal capacity of water in the operating temperature range depending on the maximum CO₂ pressure in an isothermal TEES system.

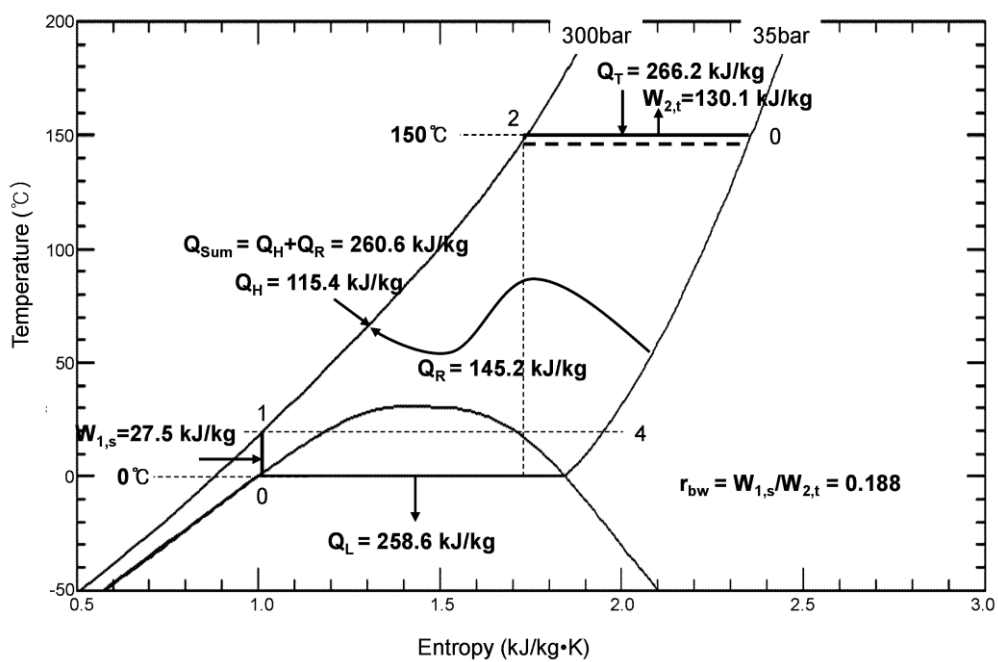


Fig. 5.27: Reference cycle of an isothermal TEES system with T-CO₂ cycle (Case 4).

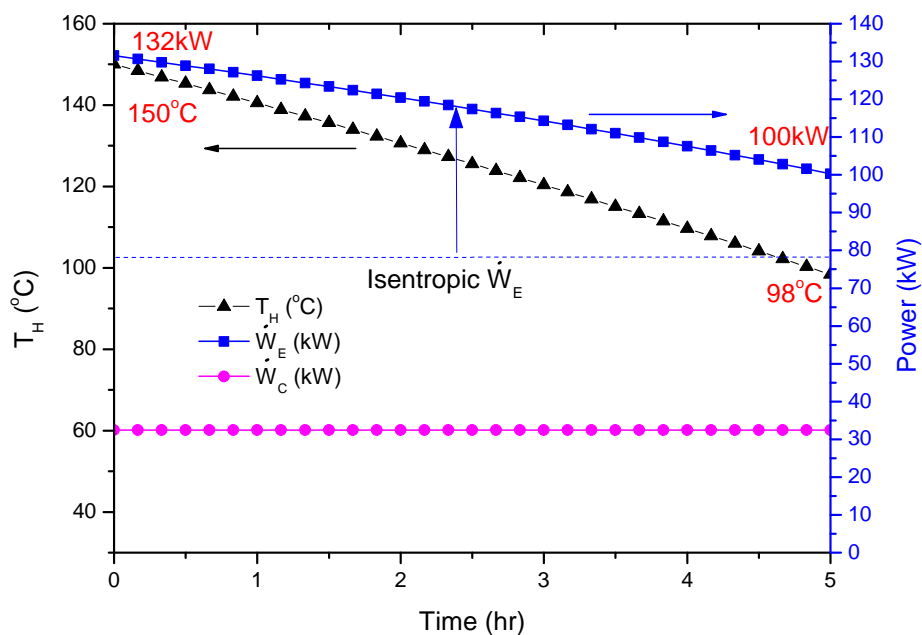


Fig. 5.28: Expansion and compression power and temperature drop of the hot tank during the discharging process in an isothermal TEES system (Case 4).

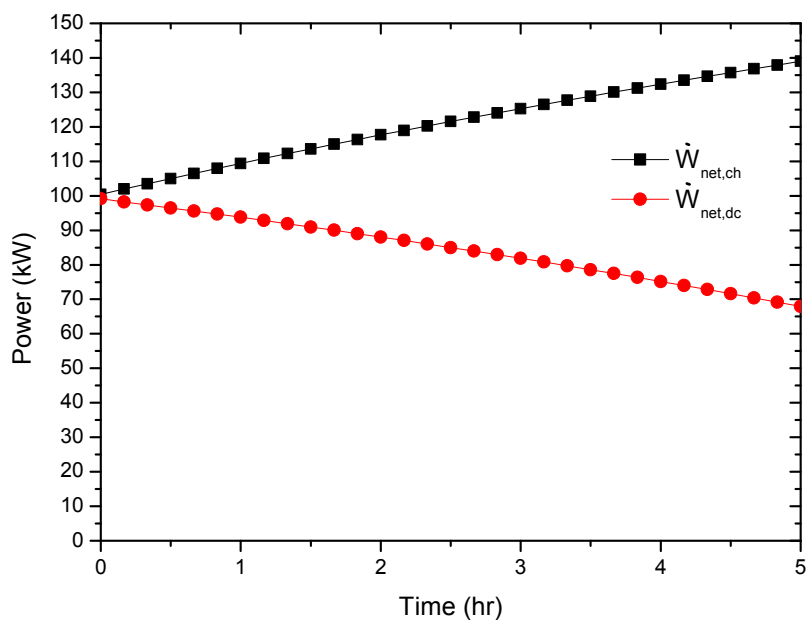


Fig. 5.29: Net power during the charging and discharging processes in an isothermal TEES system (Case 4).

Table 5.4: Performances of isothermal TEES system (Case 4)

C/E	$\dot{W}_{C2,i}$ (kW)	$\dot{W}_{E2,i}$ (kW) (T_H)	r_{bw}	$\eta_{C/E}$	$\eta_{RT,max}$	Energy (kWh)	$V_h + V_c$ (m ³)	Energy/ V_t (kWh/m ³)
Isothermal	27.5	146.2~ 111.4 (150 °C ~98 °C)	0.188~ 0.247	C1: 0.86	0.642	411.9 (82.4 kW × 5 h)	27.7 (24.0 + 3.7)	14.85
				E1: 0.85				
				C2: 0.85				
				E2: 0.88				
Isothermal	27.5	146.2~ 111.4 (150 °C ~98 °C)	0.188~ 0.247	C1: 0.90	0.699	422.6 (84.5 kW × 5 h)	27.7 (24.0 + 3.7)	15.23
				E1: 0.85				
				C2: 0.85				
				E2: 0.90				
Conditions	$P_0 = 35 \text{ bar}, T_0 = 0 \text{ °C}$		$\dot{m}_{CO_2} = 1 \text{ kg/s}$		$M_{w(h)} = 24000 \text{ kg}$			
	$P_2 = 300 \text{ bar}, T_2 = 150 \text{ °C}$		$\tau_D = 5 \text{ h}$					

5.2.4 Real cycles of isothermal TEES system with transcritical CO₂ cycles

In the previous section, the reference thermodynamic cycle of the TEES was considered, assuming a perfect reversible cycle (reversible means exactly same in both clockwise and counterclockwise direction) with zero temperature difference for heat transfer to/from the thermal storages. However, the thermodynamic cycle of the TEES is not perfectly reversible as mentioned before.

An optimized real cycle of an isentropic TEES system with transcritical CO₂ cycles presented by Morandin et al. [50] is shown in Fig. 5.30. On the cold side, while pure water freezes at 0 °C, a mixture of salt-water in various salt concentrations can freeze at lower temperatures.

As shown in Fig. 5.30, the sequences of the charging (HP) mode and the discharging (TE) modes are 0-1-2-3-4 and 5-6-7-8-9, respectively. A round-trip efficiency of 0.623 (by assuming 95% efficiencies for the motor and generator) was found for the following values of the HP and TE intensive parameters: [50]

- HP parameters: $P_1 = 17.9$ bar ; $T_2 = 9.7$ °C ; $P_2 = 122.1$ bar ; $T_4 = 5.6$ °C.
- TE parameters: $P_5 = 20.7$ bar ; $P_6 = 143.9$ bar ; $T_7 = 175.8$ °C.

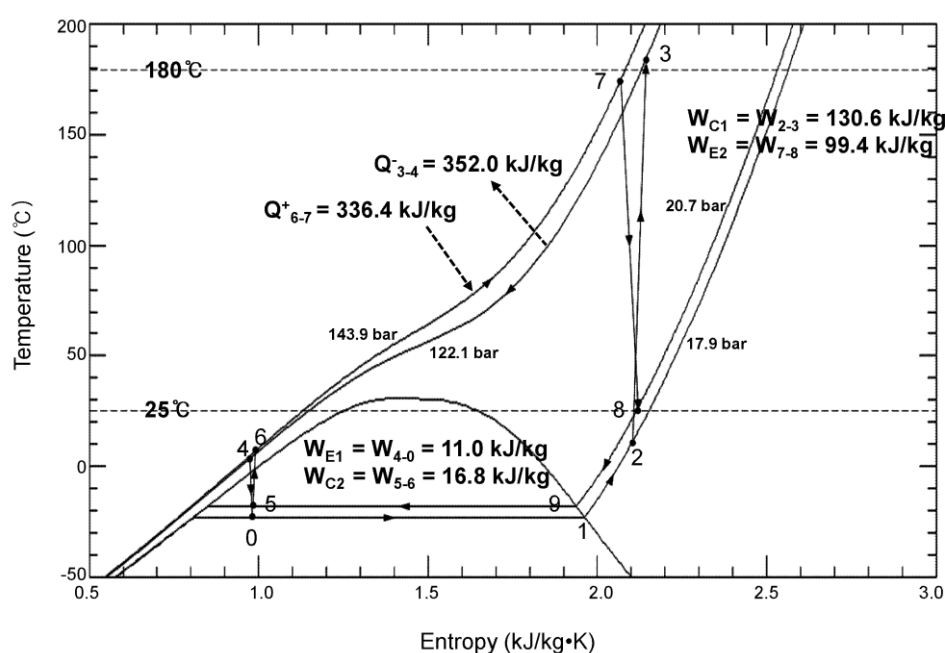


Fig. 5.30: An optimized real cycle of an isentropic TEES system with T-CO₂ cycles.

For a comparison between the isothermal TEES system and the isentropic TEES system with transcritical CO₂ cycles, Fig. 5.31 shows an optimized real cycle of the isothermal TEES system with the same efficiencies for all components ($\eta_{C1} = 0.86$, $\eta_{E1} = 0.85$, $\eta_{C2} = 0.85$, and $\eta_{E2} = 0.88$) and similar conditions to the previous isentropic TEES system. As shown in Fig. 31, the sequences of the charging (HP) and discharging (TE) modes are 0-1-2-3-4 and 5-6-7b-7c-8-9, respectively. Because the processes of compression and expansion are not perfectly isothermal, the temperature rise during the compression process and the temperature drop during the expansion process were assumed to be 5 °C.

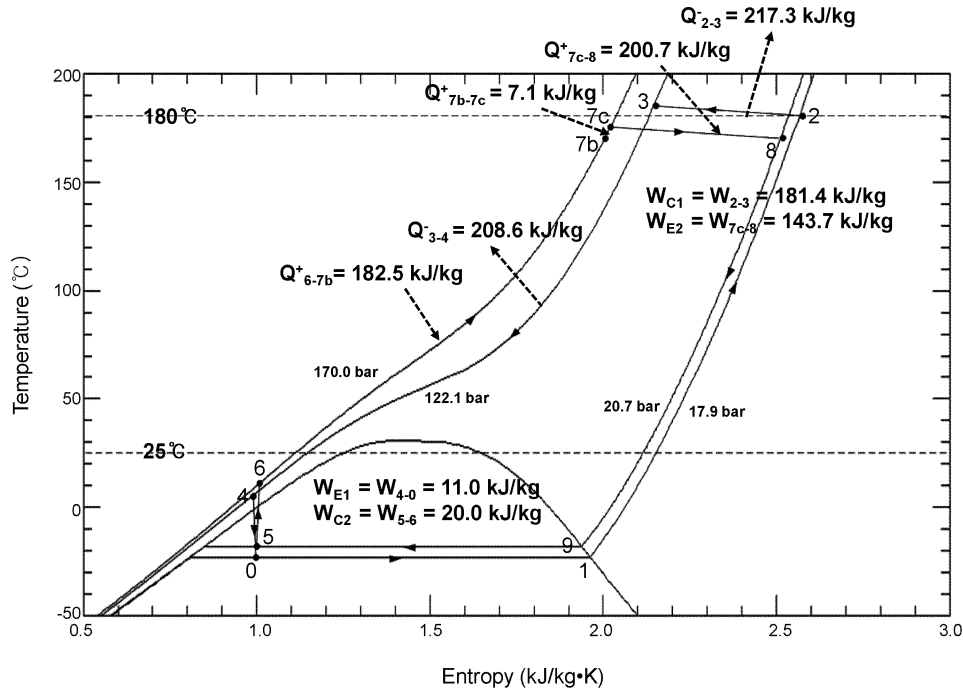


Fig. 5.31: An optimized real cycle of an isothermal TEES system with T-CO₂ cycles.

The detailed compression process is shown in Fig. 5.32. The temperature difference between the compressed CO₂ and the hot water was assumed to be 5 °C. The heat of the compressed CO₂ is transferred to the water flow and the low-pressure side of the CO₂ flow. If there is no loss of mechanical work converted to thermal energy by internal dissipation, i.e., frictional phenomena internal to the system, the compression work $w_{2-3,i}^+$ and the heat output $q_{2-3,i}^-$ during the ideal compression process (2-3) can be obtained as:

$$w_{2-3,i}^+ = q_{2-3,i}^- - (h_2 - h_3) \quad (5.18)$$

$$q_{2-3,i}^- = -\int_2^3 T ds \cong \frac{T_2 + T_3}{2} (s_2 - s_3) \quad (5.19)$$

The real compression work w_{2-3}^+ , considering the loss of mechanical work by internal dissipation, can be obtained by the efficiency of the compressor defined below as:

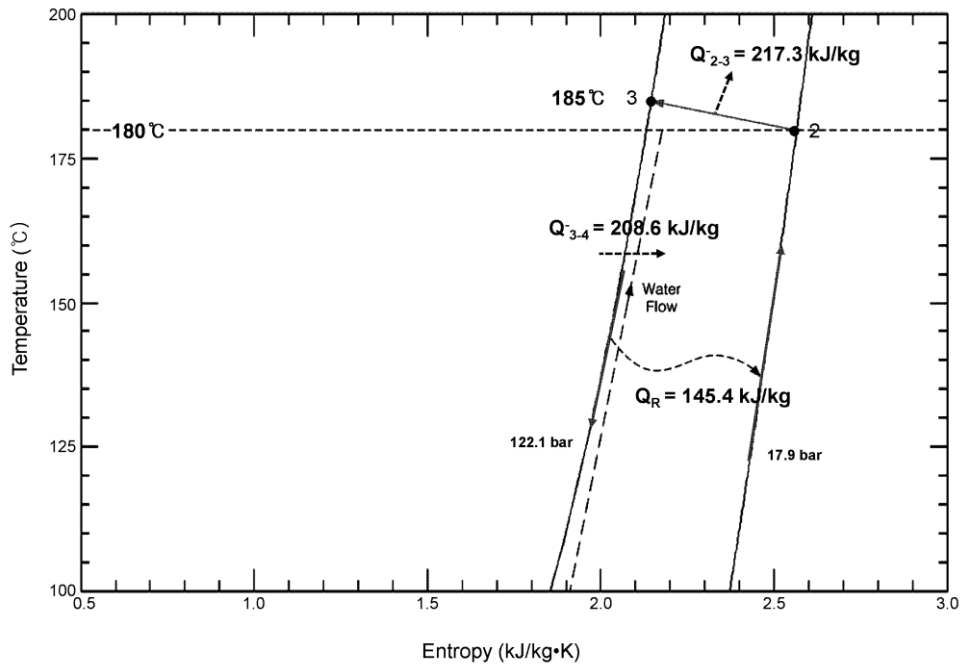


Fig. 5.32: Isothermal compression process in an isothermal TEES system with T-CO₂ cycles.

$$\eta_{C1} = \frac{w_{2-3,i}^+}{w_{2-3}^+} \quad (5.20)$$

The mechanical energy converted to thermal energy by internal dissipation r_{2-3} is defined as:

$$r_{2-3} = w_{2-3}^+ - w_{2-3,i}^+ \quad (5.21)$$

The real heat output during the compression process can be obtained as:

$$\begin{aligned} q_{2-3}^- &= w_{2-3}^+ + (h_2 - h_3) \\ &= q_{2-3,i}^- + r_{2-3} \end{aligned} \quad (5.22)$$

The real heat output q_{2-3}^- (217.3 kJ/kg) is larger than the ideal heat output $q_{2-3,i}^-$ (191.9 kJ/kg) by the internal dissipation r_{2-3} (25.4 kJ/kg) in Fig. 5.32.

The detailed expansion process is shown in Fig. 5.33. The temperature difference between the compressed CO₂ and the hot water was assumed to be 5 °C. The heat of the hot water flow

and the heat of the low-pressure side of the CO₂ flow are together transferred to the high-pressure side of the CO₂ flow. In Fig. 5.33, the temperature of CO₂ at point 7a indicates the temperature of CO₂ heated by the low-pressure side of the CO₂ flow and the temperature of CO₂ at point 7c indicates the temperature of CO₂ heated by the hot water flow. The midpoint 7b between 7a and 7c indicates the real temperature of CO₂ heated by both heat sources.

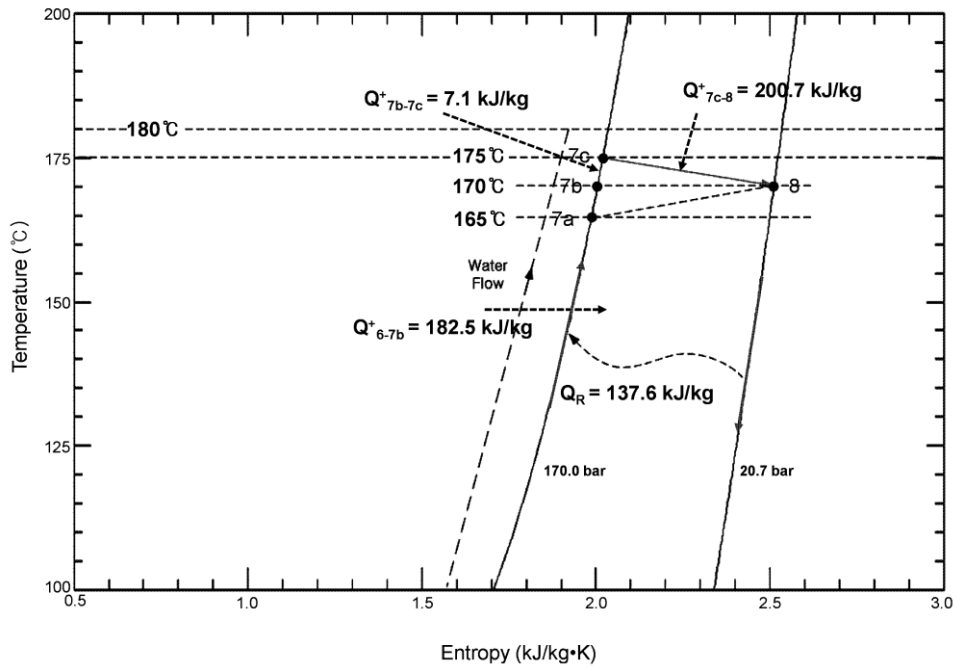


Fig. 5.33: Isothermal expansion process in an isothermal TEES system with T-CO₂ cycles.

Although the temperature at point 7b is slightly lower than the temperature at point 7c, CO₂ can be heated from 7b to 7c using a small heater that is directly heated by the hot storage tank. The additional heat input q_{7b-7c}^+ (7.1 kJ/kg) from 7b to 7c is shown in Fig. 5.33. In a manner similar to that of the previous compression process, if there is no loss of mechanical work converted to thermal energy by internal dissipation, the expansion work $w_{7c-8,i}^-$ and the heat input $q_{7c-8,i}^+$ during the ideal expansion process (7c–8) can be obtained as:

$$w_{7c-8,i}^- = q_{7c-8,i}^+ - (h_8 - h_{7c}) \quad (5.23)$$

$$q_{7c-8,i}^+ = \int_{7c}^8 T ds \cong \frac{T_{7c} + T_8}{2} (s_8 - s_{7c}) \quad (5.24)$$

The real expansion work w_{7c-8}^- , considering the loss of mechanical work by internal dissipation, can be obtained by the efficiency of the expander defined below as:

$$\eta_{E2} = \frac{w_{7c-8}^-}{w_{7c-8,i}^-} \quad (5.25)$$

The mechanical energy converted to thermal energy by internal dissipation r_{7c-8} is defined as:

$$r_{7c-8} = w_{7c-8,i}^- - w_{7c-8}^- \quad (5.26)$$

The real heat input during the expansion process can be obtained as:

$$\begin{aligned} q_{7c-8}^+ &= w_{7c-8}^- + (h_3 - h_2) \\ &= q_{7c-8,i}^+ - r_{7c-8} \end{aligned} \quad (5.27)$$

The real heat input q_{7c-8}^+ (200.7 kJ/kg) is smaller than the ideal heat input $q_{7c-8,i}^+$ (220.3 kJ/kg) by the internal dissipation r_{7c-8} (19.6 kJ/kg) in Fig. 5.33.

The thermal matching of the hot storage tank between the charging mode and the discharging mode can be obtained as:

$$q_{2-3}^- = q_{7b-7c}^+ + q_{7c-8}^+ \quad (5.28)$$

$$q_{2-3,i}^- + r_{2-3} = q_{7b-7c}^+ + q_{7c-8,i}^+ - r_{7c-8} \quad (5.29)$$

$$q_{7c-8,i}^+ = q_{2-3,i}^- + r_{2-3} + r_{7c-8} - q_{7b-7c}^+ \quad (5.30)$$

From Eq. 5.30, it is known that $q_{7c-8,i}^+$ ($= \int_{7c}^8 T ds$) is much larger than $q_{2-3,i}^-$ ($= - \int_2^3 T ds$) by the amount of thermal energy from internal dissipation. The thermal energy by internal dissipation, i.e., the sum of r_{2-3} (25.4 kJ/kg) and r_{7c-8} (19.6 kJ/kg), can contribute to provide the heat input q_{7b-7c}^+ (7.1 kJ/kg) required from 7b to 7c and the additional heat input during the isothermal expansion process. Therefore, it is possible to increase the pressure ratio of isothermal expansion (P_{7c}/P_8) sufficiently during the discharging mode from the pressure

ratio of isothermal compression (P_3/P_2) during charging mode to increase power recovery. This means that the isothermal compression and expansion processes have the advantage that the thermal energy due to internal dissipation can be stored and used at the maximum cycle temperature, and the exergy loss due to internal dissipation is lower than in the isentropic TEES system.

A round-trip efficiency of 0.656 (by assuming 95% efficiencies for the motor and generator) was found for the following values of the HP and TE intensive parameters, as shown in Fig. 5.31:

- HP parameters: $P_1 = 17.9$ bar ; $T_2 = 180.0$ °C ; $P_2 = 122.1$ bar ; $T_4 = 5.6$ °C.

- TE parameters: $P_5 = 20.7$ bar ; $P_6 = 170.0$ bar ; $T_{7c} = 175.0$ °C.

The round-trip efficiency of the isothermal TEES system is 3.3 percentage points higher in absolute efficiency than in the previous isentropic TEES system with the same efficiencies of all components and under similar conditions. If higher efficiencies of compression and expansion than those in the previous isentropic case are assumed in the hydraulic part as $\eta_{C1} = \eta_{E2} = 0.90$, the round-trip efficiency in Eq. 5.7 is increased to 0.706 from 0.623 in the previous isentropic case.

In the case of the isothermal TEES system, the temperature of the hot storage tank decreases during the discharging mode and increases during the charging mode. The instant round-trip efficiencies of the isothermal TEES system (with $\eta_{C1} = 0.86$, $\eta_{E1} = 0.85$, $\eta_{C2} = 0.85$, and $\eta_{E2} = 0.88$) with the varying temperature of the hot storage tank are shown in Fig. 5.34. Since the instant round-trip efficiencies of the isothermal TEES system decreases with the decrease in the temperature of the hot storage tank, it is desirable to use a larger hot storage tank with a greater initial mass of water to achieve higher round-trip efficiency because of a smaller temperature drop in the hot storage tank.

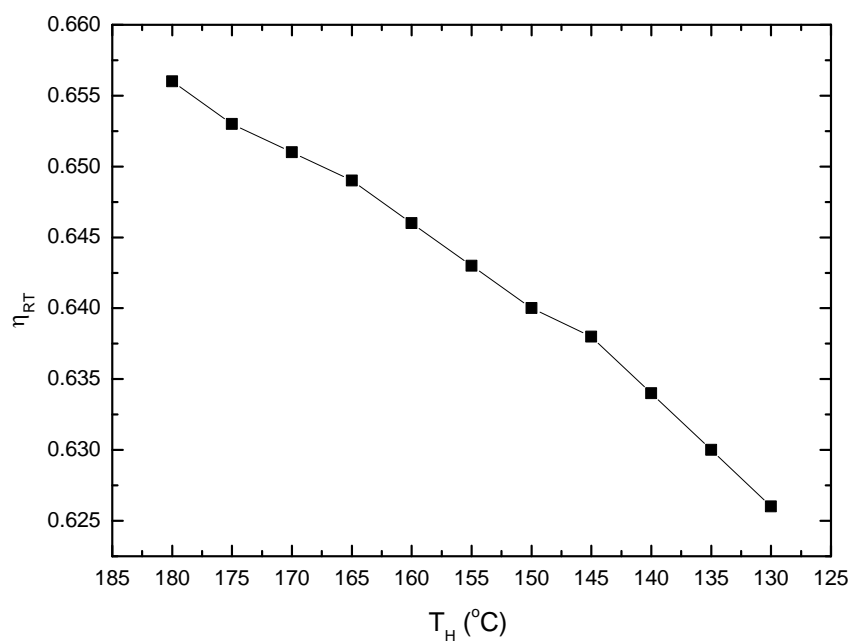


Fig. 5.34: Maximum round-trip efficiency of an isothermal TEES system with varying temperature of the hot storage tank.

5.3 Conclusion

Recently, thermo-electric energy storage (TEES) systems, using heat pumps and heat engines with thermal energy storage, have been proposed as a new method for large-scale energy storage. This chapter reviews the current TEES systems and proposes a novel isothermal TEES system with transcritical CO₂ cycles.

Since the exergy losses occurring in turbomachinery have a greater impact on the round-trip efficiency, the maximum round-trip efficiency is very useful to optimize the reference thermodynamic cycle of the TEES system by assuming very little temperature difference for heat transfer. For optimization of the reference thermodynamic cycle of the TEES system at a given efficiency of the compressor/expander, it is very important to minimize the back work ratio since the maximum round-trip efficiency decreases rapidly with an increasing back work ratio. In the case of TEES systems with Brayton cycles using argon gas, a very high temperature difference between the hot storage and the cold storage is needed to reduce the back work ratio; further, highly efficient compressors and expanders are needed to reach a reasonable round-trip efficiency. However, in the case of TEES systems with transcritical CO₂ cycles, even if the temperature difference between the hot storage and the cold storage is much lower than in previous systems with Brayton cycles, its round-trip efficiency is higher than in previous systems with Brayton cycles because of the reduced back work ratio, assuming the same efficiency of the compressor/expander. Moreover, the TEES system with transcritical CO₂ cycles has the advantage of using water for inexpensive thermal storage.

The novel isothermal TEES system with transcritical CO₂ cycles proposed in this chapter can maximize the expansion work by isothermal expansion with effective heat transfer directly with the hot storage tank, resulting in higher round-trip efficiency because of a lower back work ratio than in the previous isentropic case. Hot water from the hot storage tank is used by the water pump/turbine to compress/expand the supercritical CO₂ with the liquid piston, and a portion of the water is sprayed to cool/heat the supercritical CO₂ with a circulation pump. Therefore, the temperature of the hot tank slightly increases/decreases with time during the charging/discharging mode. Through a simple model of the isothermal TEES system, it was shown that a greater mass and higher temperature of the water in the hot tank can result

in a higher round-trip efficiency of the isothermal TEES system. Moreover, although it is possible to reduce the variation in the required thermal capacity of flowing water between the hot tank and the cold tank by increasing the maximum CO₂ pressure, the round-trip efficiency of the system becomes lower because of the higher back work ratio.

In addition, the real cycles of the isothermal TEES system with transcritical CO₂ cycles were studied in comparison with the isentropic case by considering a small temperature rise/drop during the isothermal compression/expansion and thermal energy by the internal dissipation of the compressor/expander. In the case of the isothermal TEES system, it is possible to increase the pressure ratio of isothermal expansion sufficiently during the discharging mode from the pressure ratio of isothermal compression during charging mode to obtain greater power recovery since the thermal energy due to internal dissipation during the isothermal compression/expansion can be stored and used at the maximum cycle temperature, and the exergy loss due to internal dissipation is lower than in the isentropic case.

6. Transcritical or supercritical CO₂ cycles using both low- and high-temperature heat sources

In CO₂ cycles with high-temperature heat sources that are used in applications such as nuclear power, concentrated solar power, and combustion, partial condensation transcritical CO₂ (T-CO₂) cycles or recompression supercritical CO₂ (S-CO₂) cycles are considered to be promising cycles; this is because these cycles cause a reduction in the large internal irreversibility in the recuperator owing to the higher specific heat of the high-pressure side than that of the low-pressure side. However, if heat is available in the low-temperature range, the T-CO₂ Rankine cycles (or fully cooled S-CO₂ cycles) will be more effective than the T-CO₂ Brayton cycles (or less-cooled S-CO₂ cycles) and even than the partial condensation T-CO₂ cycles (or recompression S-CO₂ cycles). This is because the compression work is reduced while achieving the same temperature rise by heat recovery through the recuperator before the high-temperature heater.

This chapter proposes a novel T-CO₂ Rankine cycles or fully-cooled S-CO₂ cycles using both the low- and high-temperature heat sources ('low-temperature' means an intermediate temperature between the highest temperature of heat sources and the lowest temperature of heat sink) to maximize the power output of the CO₂ power cycle with the given high-temperature heat sources. Moreover, the proposed CO₂ cycles combined with the thermal energy storage of the low-temperature waste heat by itself offer the advantage of load leveling over other CO₂ cycles, with the given high-temperature heat sources.

6.1 Transcritical or supercritical CO₂ (T-CO₂ or S-CO₂)

power cycles

Recently, interest in a supercritical CO₂ power cycle has increased in conjunction with its application in nuclear reactors owing to its simplicity, compactness, sustainability, enhanced safety, and superior economy [51-55]. The supercritical CO₂ cycle is expected to benefit fossil, renewable, and advanced nuclear power plants because CO₂ is an extremely effective working fluid in its supercritical state.

In the case of CO₂ cycles with high-temperature (HT) heat sources such as nuclear power, concentrated solar power, and combustion, the working fluid goes through both subcritical and supercritical states (transcritical cycle), or is used entirely above its critical pressure (supercritical cycle). Further, the CO₂ cycles can be gas cycles (Brayton cycles) or condensation cycles (Rankine cycles). Feher [56] proposed a supercritical CO₂ (S-CO₂) power cycle that operates entirely above the critical pressure of CO₂, is regenerative, and ensures the pressurization in the liquid phase to minimize pump work [51]. Angelino [57] conducted one of the most detailed investigations on transcritical CO₂ (T-CO₂) cycles and primarily focused on condensation cycles [51]. However, it was found that the T-CO₂ Rankine cycles exhibited a large internal irreversibility in the recuperator owing to heat transfer from the turbine exhaust stream with a low specific heat to the pump exit stream with a high specific heat [51].

Feher [56] first revealed the same problem associated with irreversibility in the recuperator used in the S-CO₂ cycles. A recompression cycle was proposed to avoid the problem; the recuperator was divided into low- and high-temperature parts, each having different flow rates to cope with a large variation in the heat capacity of the fluid. Thus, only a fraction of the CO₂ fluid flow is bypassed to the recompressing compressor before pre-cooling and is merged with the rest of the fluid flow, heated through the low temperature (LT) recuperator, from the main pump (or compressor) before it enters the HT recuperator. The recompression cycle can be applied to both the S-CO₂ and the T-CO₂ cycles, and it has been studied as the most promising CO₂ cycle for HT heat conversion [51-59]. Sarkar et al. [60] studied the

effects of various operating conditions and performance of components on the optimization of the S-CO₂ recompression cycle.

Meanwhile, the T-CO₂ Rankine cycles (full condensation cycles) have been mostly studied for low-grade heat conversion such as geothermal energy, waste heat, and LT solar collectors [61-69]. In the case of the T-CO₂ Rankine cycle for HT heat conversion, although the compression work is significantly reduced, the outlet temperature of CO₂ heated through the recuperator is much lower than that in the T-CO₂ Brayton cycle. This is because at temperatures below 150°C, especially below 120°C, the isobaric specific heat of CO₂ in the high-pressure side is considerably higher than that in the low-pressure side. The operation of the T-CO₂ Brayton cycle can escape from this temperature range, and therefore, the outlet temperature of CO₂ heated through the recuperator in this cycle is much higher than that in the T-CO₂ Rankine cycle.

6.1.1 Energy and exergy analyses

The configurations and T-s diagrams of the basic T-CO₂ Rankine and Brayton cycles studied here are shown in Figs. 6.1 and 6.2 and in Figs. 6.3 and 6.4, respectively. The following general assumptions are used in this analysis: the kinetic and potential energies as well as the heat and friction losses are negligible, isentropic efficiencies of the pump or compressor and the turbine are both 90%, temperature effectiveness of the recuperator is 0.95, condensation temperature for CO₂ is 20°C, and saturated liquid exits the condenser. For the power range of 300~500MWe considered in this study, the assumed isentropic efficiencies of 90% are reasonable and are based on the values of conservative turbomachinery design [52]. In the case of the T-CO₂ Brayton cycle, saturated vapor, which is about to condense, exits the cooler. The properties of CO₂ are obtained from REFPROP-NIST [71]. The equations for the different components of the cycle are as follows.

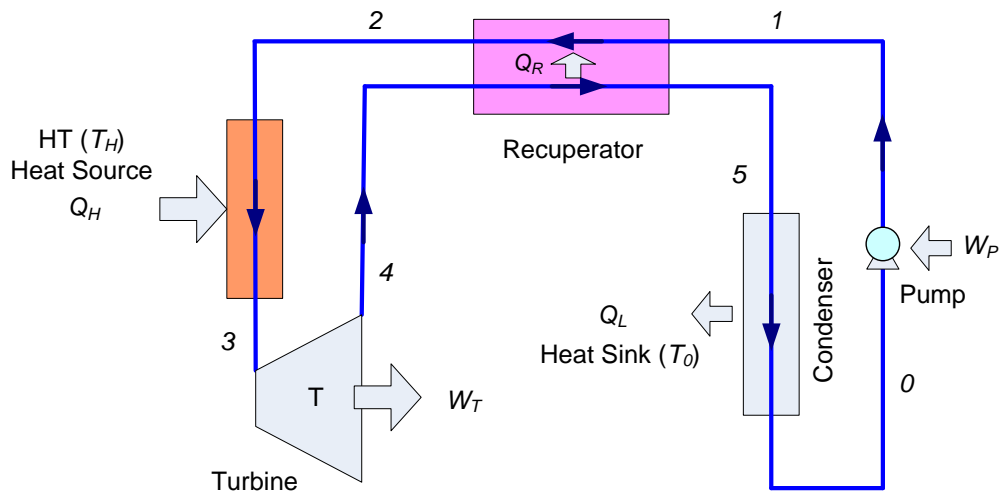


Fig. 6.1: Schematic of T-CO₂ Rankine cycle with HT heat source.

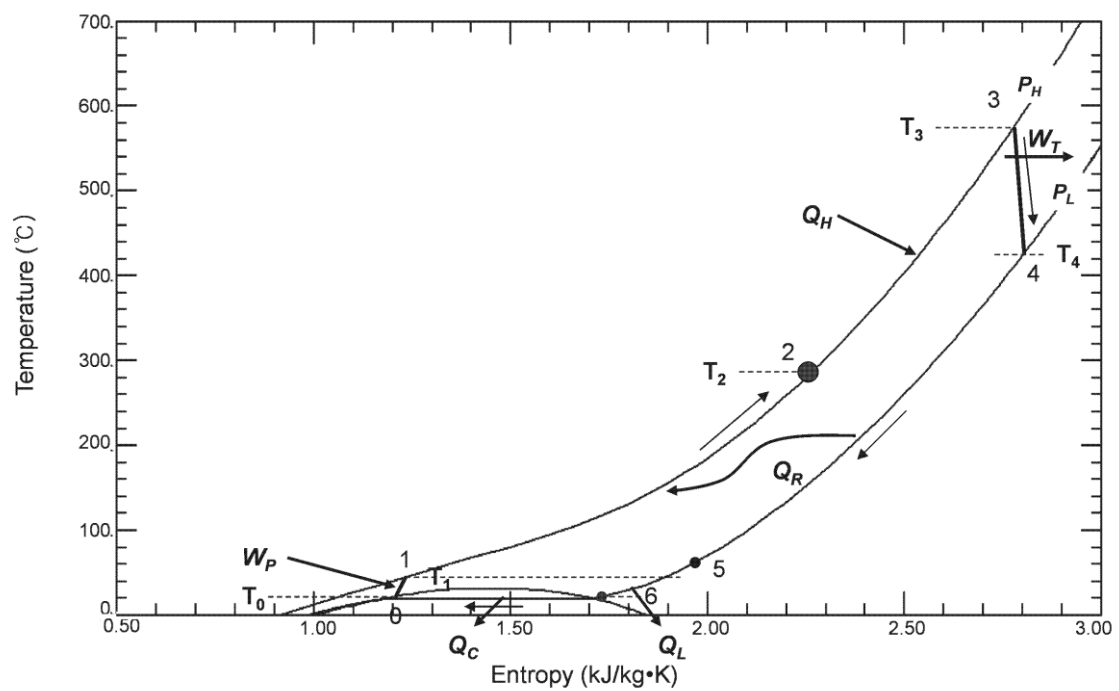


Fig. 6.2: T-s diagram of T-CO₂ Rankine cycle with HT heat source.

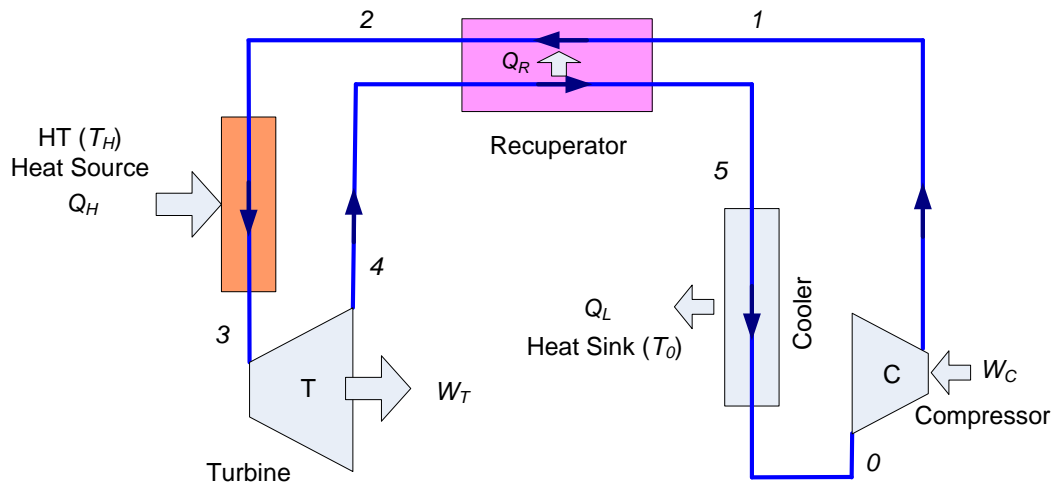


Fig. 6.3: Schematic of T-CO₂ Brayton cycle with HT heat source.

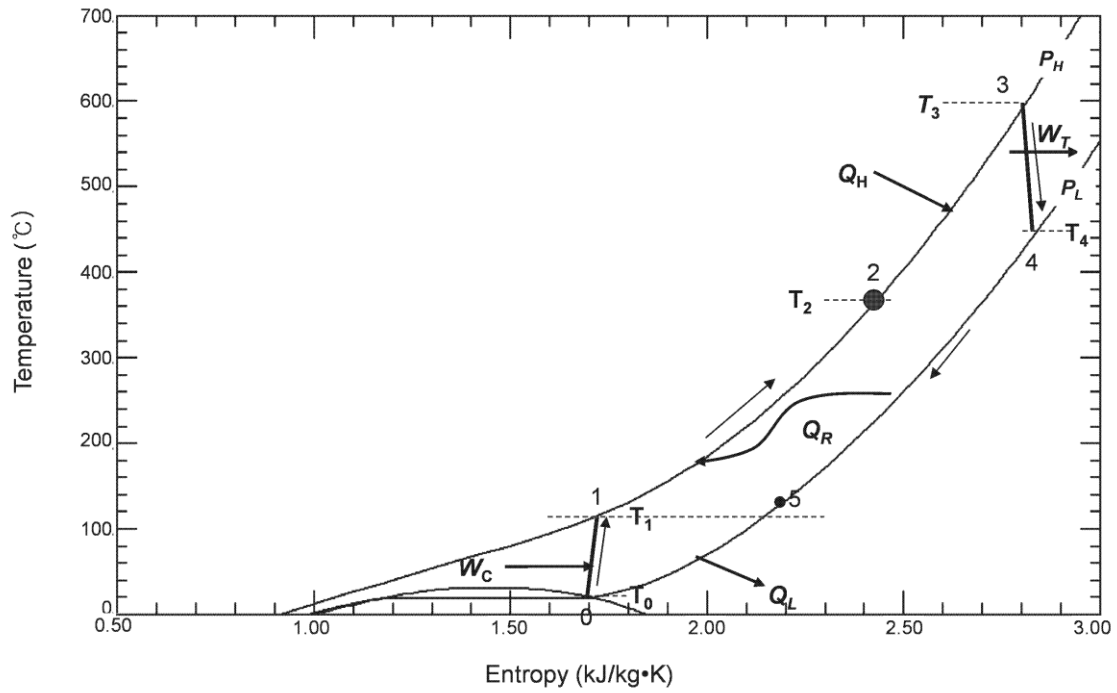


Fig. 6.4: T-s diagram of T-CO₂ Brayton cycle with HT heat source.

For the pump or compressor,

$$\eta_{P(C)} = \frac{h_{1,s} - h_o}{h_1 - h_o} \quad (6.1)$$

$$\dot{W}_{P(C)} = \dot{m}_{CO_2}(h_1 - h_o) \quad (6.2)$$

For the turbine,

$$\eta_T = \frac{h_3 - h_4}{h_{3,s} - h_4} \quad (6.3)$$

$$\dot{W}_T = \dot{m}_{CO_2}(h_3 - h_4) \quad (6.4)$$

The efficiency of the recuperator, ε_R , is expressed as

$$\varepsilon_R = \frac{\dot{m}_{CO_2}(h_4 - h_5)}{\dot{Q}_{\max}} = \frac{\dot{m}_{CO_2}(h_2 - h_1)}{\dot{Q}_{\max}} \quad (6.5)$$

The rate of maximum heat exchange, \dot{Q}_{\max} , is given as follows:

$$\dot{Q}_{\max} = \dot{m}_{CO_2}(h_4 - h_5) \text{ assuming } T_5 = T_1 \quad (6.6)$$

For the heater,

$$\dot{Q}_H = \dot{m}_{CO_2}(h_3 - h_2) \quad (6.7)$$

For the condenser or cooler,

$$\dot{Q}_W = \dot{m}_{CO_2}(h_5 - h_o). \quad (6.8)$$

The rate of heat wasted to the heat sink, \dot{Q}_W , can be split into the rate of heat to cool down, \dot{Q}_L , and the rate of heat to condense, \dot{Q}_C , as follows:

$$\dot{Q}_L = \dot{m}_{CO_2}(h_5 - h_6) \quad (6.9)$$

$$\dot{Q}_C = \dot{m}_{CO_2}(h_6 - h_o) \quad (6.10)$$

where state 6 is the saturated vapor state.

For the thermal efficiency of the cycle,

$$\eta_{th} = \frac{\dot{W}_T - \dot{W}_{P(C)}}{\dot{Q}_H}. \quad (6.11)$$

The purpose of the idea proposed in this chapter is to find a novel CO₂ cycle that maximizes the power output of the CO₂ cycle with the given HT heat sources by using available LT heat sources. Exergy analysis is very helpful in understanding the advantages of the novel CO₂ cycle over other CO₂ cycles. Although increasing the maximum cycle temperature can increase the cycle efficiency, the maximum cycle temperature is assumed to be 600°C considering the cost and lifetime of materials under the high-pressure conditions of CO₂ cycles. In this study, the ideal cycle is assumed to be a Carnot cycle operating between a HT ($T_H = 600^\circ\text{C}$) heat source and an LT ($T_C = 15^\circ\text{C}$) heat sink with water cooling. Therefore, the maximum work by the Carnot engine can be written as

$$E_H = W_{\max} = \left(1 - \frac{T_C}{T_H}\right) Q_H$$

(6.12)

This work can be assumed to be the exergy input from the HT heat source, E_H^+ , and then the exergy losses in the following components are investigated.

The exergy of a CO₂ stream can be expressed as

$$\dot{E}_{CO_2} = \dot{m}_{CO_2} k = \dot{m}_{CO_2} [h - h_a - T_a (s - s_a)] \quad (6.13)$$

where k , h , and s are the specific exergy, enthalpy, and entropy, respectively, and the subscript a indicates that the properties are taken at ambient temperature and pressure (T_a, P_a). The ambient temperature T_a is assumed to be the temperature of the heat sink, T_C , and the ambient pressure P_a is assumed to be the atmospheric pressure.

The general exergy balance can be expressed as a rate equation [27]:

$$\dot{E}^+ - \dot{E}^- = \dot{L} \quad (6.14)$$

where \dot{E}^+ is the rate of exergy transfer to the system by heat, work, and mass; \dot{E}^- is the rate of exergy transfer from the system; and \dot{L} is the rate of exergy loss.

The exergy loss of compression (pumping) is given by

$$\dot{L}_{C(P)} = \dot{E}_{C(P)}^+ - \dot{m}_{CO_2}(k_1 - k_0) \quad (6.15)$$

The exergy loss of the turbine is given by

$$\dot{L}_T = \dot{m}_{CO_2}(k_3 - k_4) - \dot{E}_T^- \quad (6.16)$$

The exergy loss of the recuperator is given by

$$\dot{L}_R = \dot{m}_{CO_2}(k_4 - k_5) - \dot{m}_{CO_2}(k_2 - k_1). \quad (6.17)$$

The exergy loss of the heater is given by

$$\dot{L}_H = \dot{E}_H^+ - \dot{m}_{CO_2}(k_3 - k_2). \quad (6.18)$$

The exergy loss of waste heat to the condenser or cooler is given as

$$\dot{L}_W = \dot{m}_{CO_2}(k_5 - k_0). \quad (6.19)$$

The second law (exergy) efficiency of the overall system with transcritical or supercritical cycles can be defined as

$$\eta_{II} = \frac{\dot{E}_T^- - \dot{E}_{C(P)}^+}{\dot{E}_H^+}. \quad (6.20)$$

6.1.2 Comparison between T-CO₂ Rankine cycle and T-CO₂ Brayton cycle

To compare the basic two cycles (i.e., the T-CO₂ Rankine and Brayton cycles), we assume the following conditions: high pressure of 200 bar, low pressure of 57.3 bar (condensation temperature 20°C), and turbine inlet temperature of 600°C. These conditions are similar to those in other literatures that discuss the use of S-CO₂ cycles for next-generation nuclear reactors [51-63]. Figs. 6.5 and 6.6 show the energy flow per unit mass of the working fluid on temperature versus entropy (T-s) diagrams of the T-CO₂ Rankine and Brayton cycles, respectively.

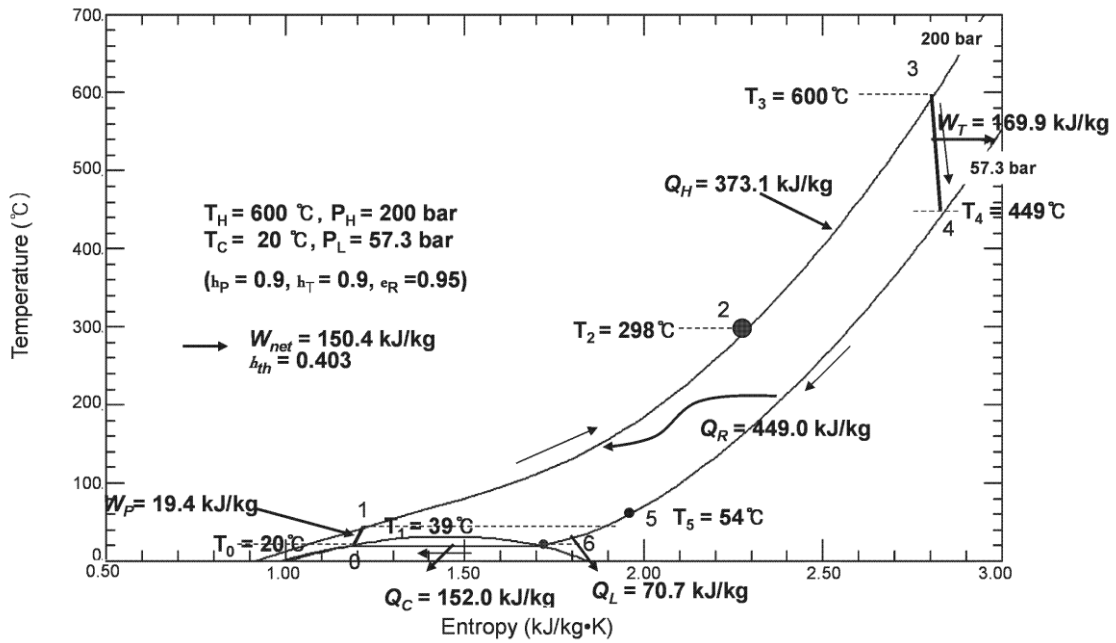


Fig. 6.5: Reference cycle of T-CO₂ Rankine cycle with HT heat source.

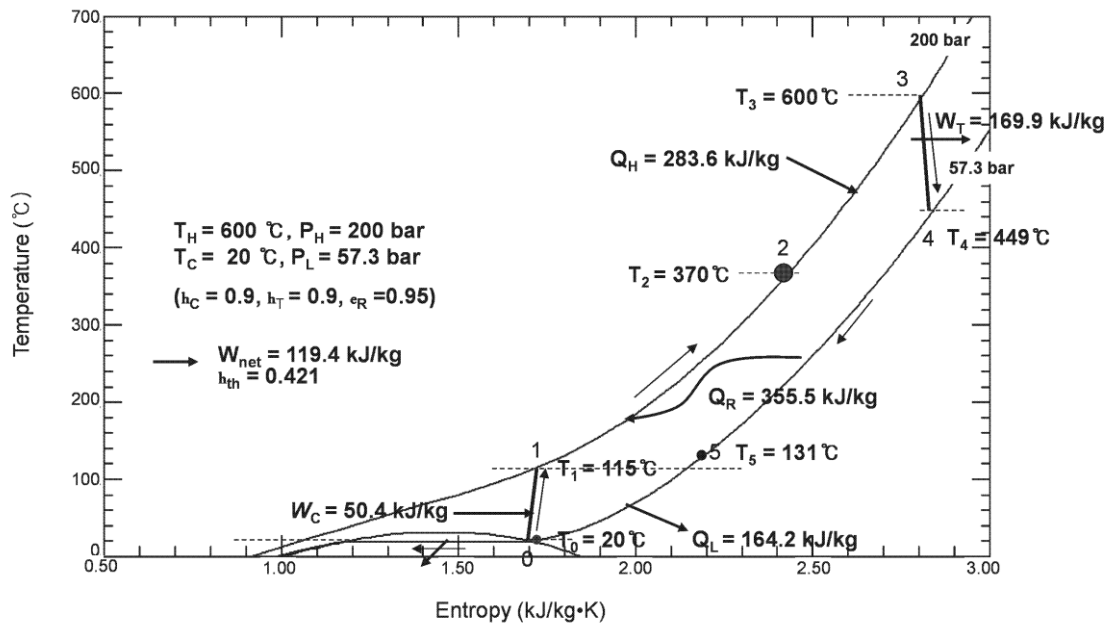


Fig. 6.6: Reference cycle of T-CO₂ Brayton cycle with HT heat source.

The exergy analyses of the T-CO₂ Rankine and Brayton cycles, expressed on a unit mass basis, are summarized in Tables 6.1 and 6.2, respectively.

Table 6.1: Exergy analysis of transcritical CO₂ Rankine cycle with HT heat source

State (i)	T (°C)	P (bar)	$k_i - k_0$ (kJ/kg)	$Q(E), W(E)$ (kJ/kg)	L (kJ/kg)
0	20.0	57.3	0.0	$Q_W^- = 222.7$ ($E_W^- = 7.0$)	$L_W = 7.0$ (7.0%)
1	39.2	200.0	17.6	$W_P^+ = 19.4$ ($E_P^+ = 19.4$)	$L_P = 1.8$ (1.8%)
2	297.5	200.0	180.7	$Q_R^+ = 449.0$ ($E_R^+ = 163.1$)	$L_R = 25.2$ (25.3%)
3	600.0	200.0	372.8	$Q_H^+ = 373.1$ ($E_H^+ = 245.0$)	$L_H = 57.9$ (58.2%)
4	449.0	57.3	195.3	$W_T^- = 169.9$ ($E_T^- = 169.9$)	$L_T = 7.6$ (7.6%)
5	54.3	57.3	7.0	$Q_R^- = 449.0$ ($E_R^- = 188.3$)	($L_R = 25.2$)
$\eta_{II} = \frac{E_T^- - E_P^+}{E_H^+} = 0.614$				$E_H^+ = 245.0$	$L_{tot} = 99.5$ (100%)

Table 6.2: Exergy analysis of transcritical CO₂ Brayton cycle with HT heat source

State (i)	T (°C)	P (bar)	$k_i - k_0$ (kJ/kg)	$Q(E), W(E)$ (kJ/kg)	L (kJ/kg)
0	20.0	57.3	0.0	$Q_W^- = 164.2$ ($E_W^- = 23.6$)	$L_W = 23.6$ (33.4%)
1	114.6	200.0	46.7	$W_C^+ = 50.4$ ($E_C^+ = 50.4$)	$L_C = 3.8$ (5.4%)
2	370.0	200.0	195.2	$Q_R^+ = 355.5$ ($E_R^+ = 148.5$)	$L_R = 20.6$ (29.2%)
3	600.0	200.0	370.2	$Q_H^+ = 283.6$ ($E_H^+ = 190.0$)	$L_H = 15.0$ (21.2%)
4	449.0	57.3	192.7	$W_T^- = 169.9$ ($E_T^- = 169.9$)	$L_T = 7.6$ (10.8%)
5	131.1	57.3	23.6	$Q_R^- = 355.5$ ($E_R^- = 169.1$)	($L_R = 20.6$)
$\eta_{II} = \frac{E_T^- - E_C^+}{E_H^+} = 0.629$				$E_H^+ = 190.0$	$L_{tot} = 70.6$ (100%)

The efficiency of the T-CO₂ Rankine cycle is lower than that of the T-CO₂ Brayton cycle. Although the compression work of the T-CO₂ Rankine cycle is significantly reduced, the outlet temperature of CO₂ heated through the recuperator in this cycle is much lower than that of the T-CO₂ Brayton cycle. This is because below 150°C and especially below 120°C, the isobaric specific heat, c_p , of CO₂ in the high-pressure side is much higher than that in the low-pressure side, as shown in Fig. 6.7.

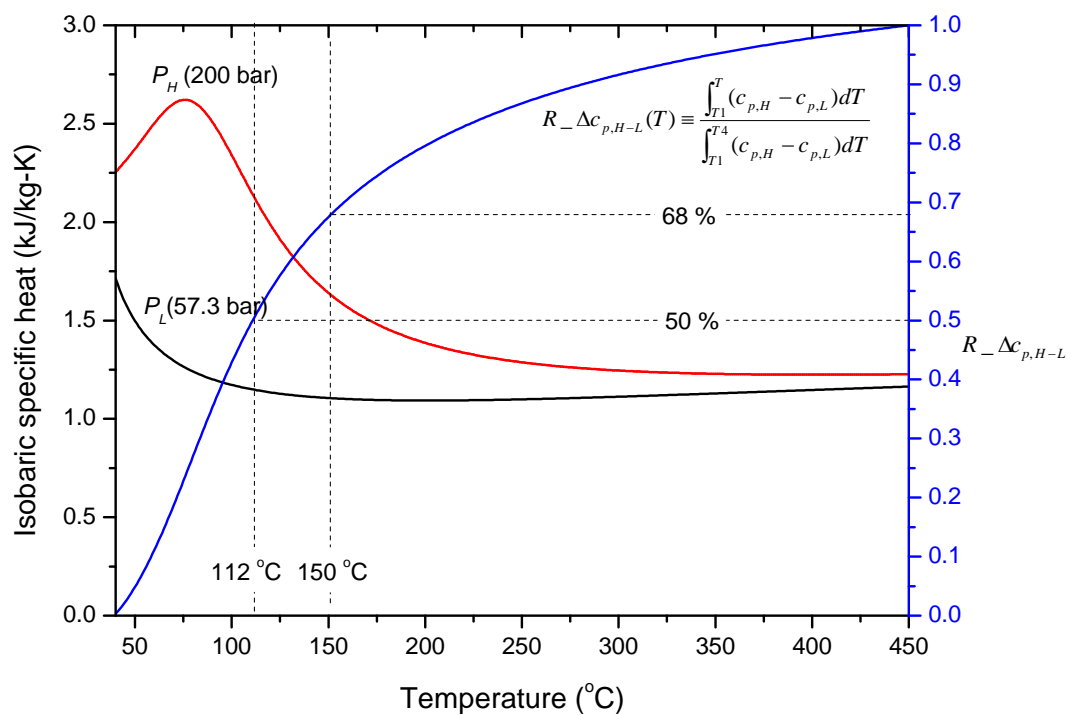


Fig. 6.7: Isobaric specific heats of CO₂ in high- and low-pressure sides over temperature range of heat recovery.

The operation of T-CO₂ Brayton cycle can escape from this temperature range, and therefore, the outlet temperature of CO₂ heated through the recuperator is much higher in the T-CO₂ Brayton cycle than in the T-CO₂ Rankine cycle. The accumulated difference in the isobaric specific heat between the high-pressure side ($c_{p,H}$) and the low-pressure side ($c_{p,L}$) below a temperature T that is over the temperature range for heat recovery in the T-CO₂ Rankine

cycle (from T_1 to T_4) can be defined as

$$R_{-\Delta c_{p,H-L}}(T) \equiv \frac{\int_{T_1}^T (c_{p,H} - c_{p,L}) dT}{\int_{T_1}^{T_4} (c_{p,H} - c_{p,L}) dT} \quad (6.21)$$

As shown in Fig. 6.7, $R_{-\Delta c_{p,H-L}}(T)$ is approximately 0.5 at 112°C and approximately 0.68 at 150°C. This indicates that the outlet temperature of CO₂ heated through the recuperator is low owing to the large difference in the specific heat between the high- and low-pressure sides in this LT range.

6.2 Transcritical CO₂ cycles using both low- and high-temperature heat sources (LH T-CO₂ cycle)

As mentioned before, in the case of the T-CO₂ Rankine cycle with HT heat sources, although the compression work and exergy loss of waste heat are significantly reduced, the outlet temperature of CO₂ heated through the recuperator is much lower than that of the T-CO₂ Brayton cycle owing to the large difference in the isobaric specific heat of CO₂ between the high- and low-pressure sides in the LT range. Therefore, the thermal efficiency of the T-CO₂ Rankine cycle is lower than that of the T-CO₂ Brayton cycle.

However, if heat is available from other heat sources in this LT range, it is possible to make up for the difference in the isobaric specific heat of CO₂ between the high- and low-pressure sides and rectify this imbalance in specific heats. Therefore, a T-CO₂ cycle using both the LT and the HT heat sources (named an LH T-CO₂ cycle) is proposed. The configuration of the LH T-CO₂ cycle system is shown in Fig. 6.8. The recuperator is divided into two parts: a low-temperature (LT) recuperator and a high-temperature (HT) recuperator. In the LT recuperator, the supplemental heat is supplied by an LT (T_{H1}) heat source.

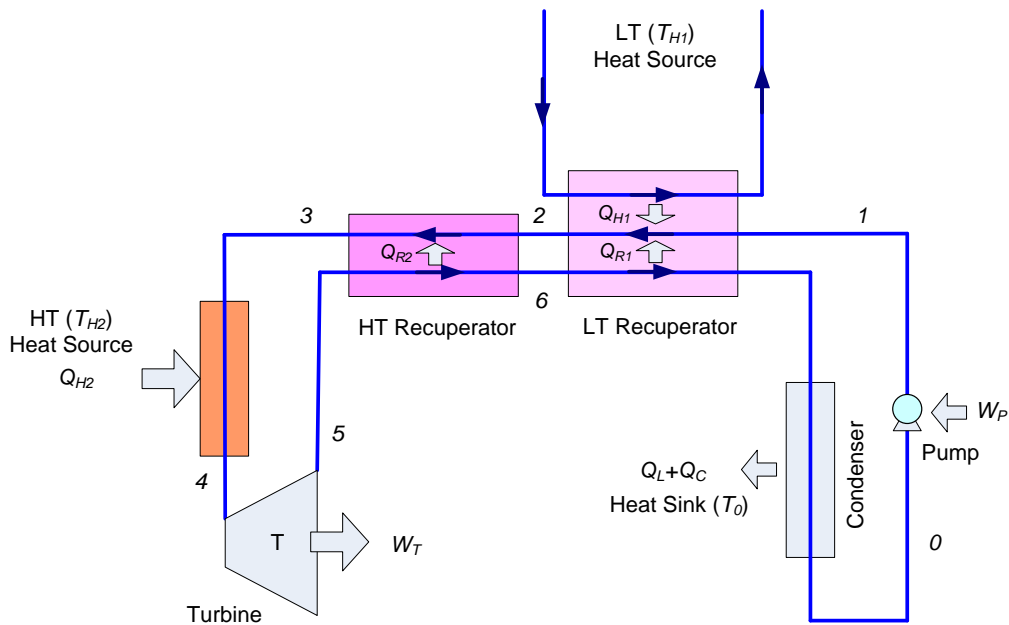


Fig. 6.8: Schematic of LH T-CO₂ cycle using both LT and HT heat sources.

Fig. 6.9 shows the energy flow per unit mass of the working fluid on the T-s diagram of the system for the previous T-CO₂ Rankine cycle with an additional LT heat source to heat CO₂ up to 112°C.

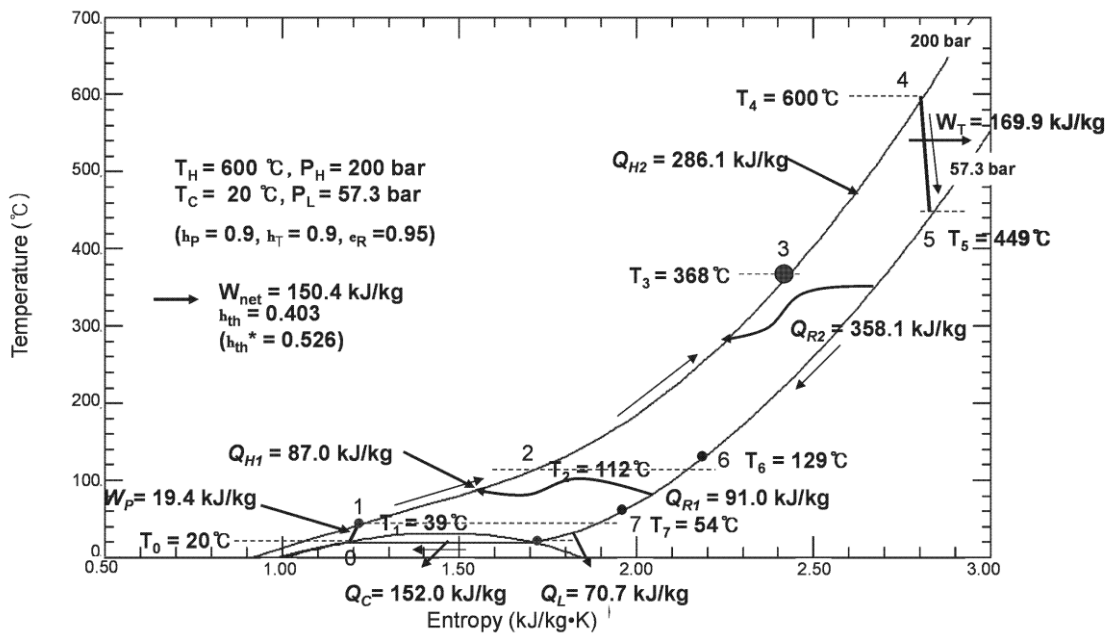


Fig. 6.9: Reference cycle of LH T-CO₂ cycle using both LT and HT heat sources.

Table 6.3 compares the performances, expressed on a unit mass basis, of different CO₂ cycles.

Table 6.3: Comparison of performances of different T-CO₂ cycles (H: High temperature of T_{H2} , L: Low temperature of T_{H1} , R: Rankine, B: Brayton)

Cycle	T_{H1} (°C)	Q_{H1} (kJ/kg)	T_{H2} (°C)	Q_{H2} (kJ/kg)	T_R (°C)	$W_{P(C)}$ (kJ/kg)	W_T (kJ/kg)	W_{net} (kJ/kg)	η_{th}	η_{th}^*
H-R (1)	-	-	600	373.1	298	19.4	169.9	150.4	0.403	-
H-B (2)	-	-	600	283.6	370	50.4	169.9	119.4	0.421	-
L-R (3)	112	178.0	-	-	-	19.4	40.9	21.4	0.120	-
LH-R (4)	112	87.0	600	286.1	368	19.4	169.9	150.4	0.403	0.526
L-R (3) + H-B (2)	112	87.0	600	286.1	370	9.5 + 50.9	20.0 + 171.3	10.5 + 120.5	0.351	-

Hot water is used as an example of an LT heat source, and the mass flow rate and inlet/outlet temperature of the hot water are shown in Fig. 6.10. The mass flow rate and inlet/outlet temperature of hot water required in the LT recuperator can be calculated from the thermal match of three flows as follows. As shown in Fig. 6.11, $\Delta c_p(T)$ is the isobaric specific heat of an LT heat source required to make up for the difference in the isobaric specific heats between the high-pressure (P_H) side and the low-pressure (P_L) side. Considering the temperature difference, ΔT , for the heat transfer from the low-pressure side to the high-pressure side, $\Delta c_p(T)$ can be defined as

$$\Delta c_p(T) \equiv c_p(P_H, T) - c_p(P_L, T + \Delta T) \quad (6.22)$$

Because the isobaric specific heat of water as an LT heat source is almost constant, the average isobaric specific heat, $\Delta \bar{c}_p(T)$, to make up for $\Delta c_p(T)$ over the temperature range of

the LT recuperator can be obtained as shown in Fig. 6.11, where the area marked S+ is equal to the area marked S-.

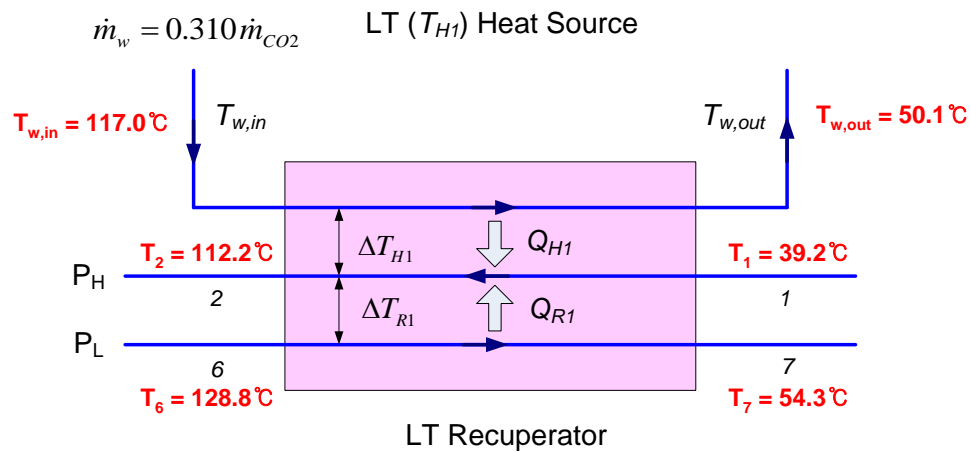


Fig. 6.10: Mass flow rate and inlet/outlet temperature of hot water required in LT recuperator.

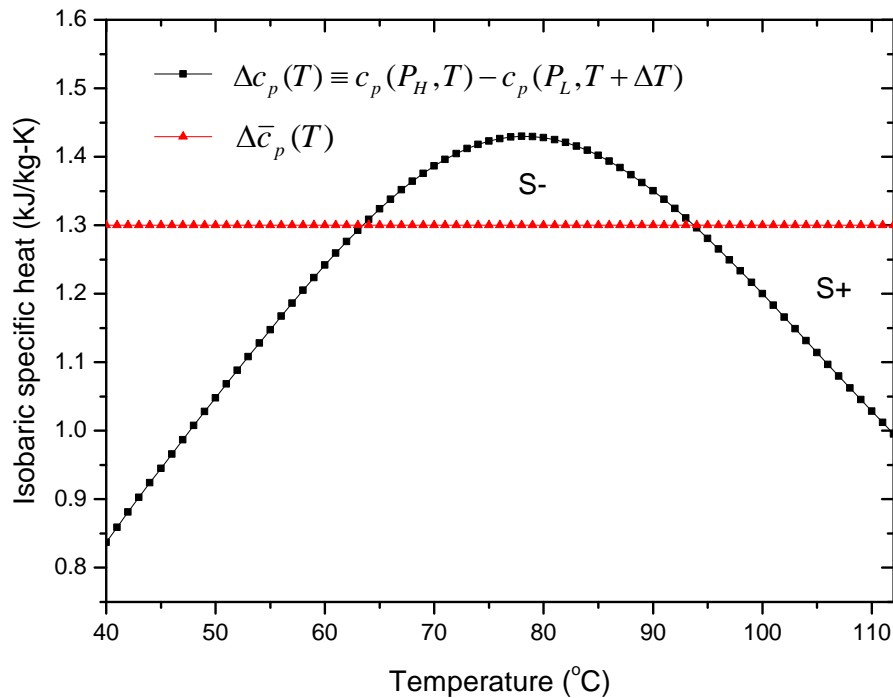


Fig. 6.11: Isobaric specific heat of LT heat source required to make up for difference in isobaric specific heats between two CO₂ streams.

The mass flow rate of hot water can be calculated from the obtained $\Delta\bar{c}_p(T)$ as

$$\dot{m}_w \tilde{c}_w = \dot{m}_{CO_2} \Delta\bar{c}_p \quad (6.23)$$

where \dot{m}_w and \tilde{c}_w are the mass flow rate and average specific heat of water flowing through the LT recuperator, respectively.

If the minimum temperature difference for heat transfer from the hot water to the side with CO₂ at high pressure is assumed to 5°C, the outlet temperature of water can be calculated from a heat balance equation as

$$\dot{Q}_{H1} = \dot{m}_w \tilde{c}_w (T_{w,in} - T_{w,out}) \quad (6.24)$$

where $T_{w,in}$ and $T_{w,out}$ are the inlet and outlet temperatures of water flowing through the LT recuperator, respectively.

With additional heat, $Q_{H1} = 87.0$ kJ/kg, provided by the LT heat source, the temperature after the HT recuperator, T_R , can be increased significantly, and therefore, it is possible to reduce the heat input, Q_{H2} , from the HT (T_{H2}) heat source in the T-CO₂ Rankine cycle. As compared to the previous T-CO₂ Rankine cycle, the LH T-CO₂ cycle can achieve the same thermal efficiency using 23.3% of the total heat input from the LT heat source, not from the HT heat source.

In order to compare the LH T-CO₂ cycle with other CO₂ cycles, two different thermal efficiencies are defined:

$$\eta_{th} = \frac{\dot{W}_T - \dot{W}_P}{\dot{Q}_{H1} + \dot{Q}_{H2}} \quad (6.25)$$

$$\eta_{th}^* = \frac{\dot{W}_T - \dot{W}_P}{\dot{Q}_{H2}} \quad (6.26)$$

η_{th} represents general thermal efficiency; however, η_{th}^* represents the increased thermal efficiency with the given heat input from the HT heat source by using the heat available from the LT heat source.

As compared to the previous T-CO₂ Brayton cycle with the same heat input Q_{H2} from the

HT heat source, the LH T-CO₂ cycle can produce approximately 25% more power by reducing the compression work and achieve an increased thermal efficiency of $\eta_{th}^* = 0.526$.

Fig. 6.12 shows the temperature after the HT recuperator, T_R , and the increased efficiency, η_{th}^* , as functions of the temperature (T_{H1}) of the LT heat source. It can be seen that the LT heat source below 150°C aids in increasing T_R and η_{th}^* of the T-CO₂ Rankine cycle with the given heat input Q_{H2} from the HT heat source, despite the low grade of the heat source.

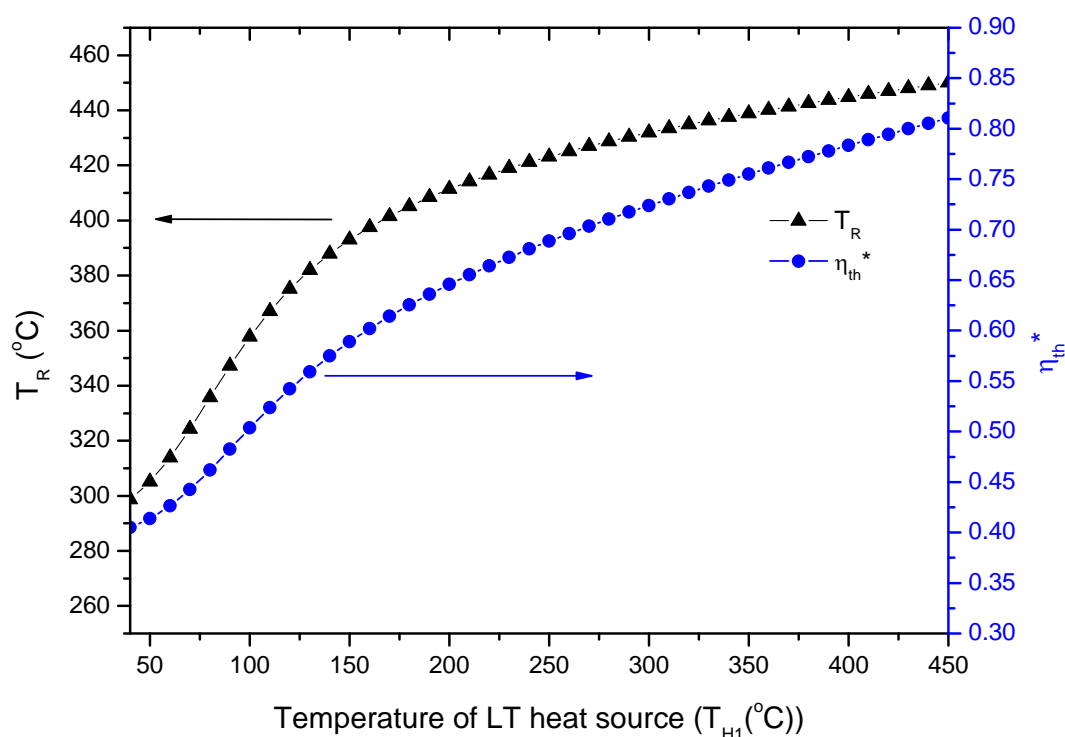


Fig. 6.12: Temperature T_R and thermal efficiency η_{th}^* according to temperature of LT heat source (T_{H1}).

The LH T-CO₂ cycle operates synergistically with the sum of the two separate cycles (i.e., a T-CO₂ Rankine cycle with the LT (T_{H1}) heat source, as shown in Fig. 6.13, and a T-CO₂ Brayton cycle with the HT (T_{H2}) heat source, as shown in Fig. 6.6). The LH T-CO₂ cycle can eliminate both exergy losses from the turbine in the LT cycle and the compressor in the HT

cycle by combining them; moreover, the LH T-CO₂ cycle can utilize the waste heat from the HT cycle for the LT cycle.

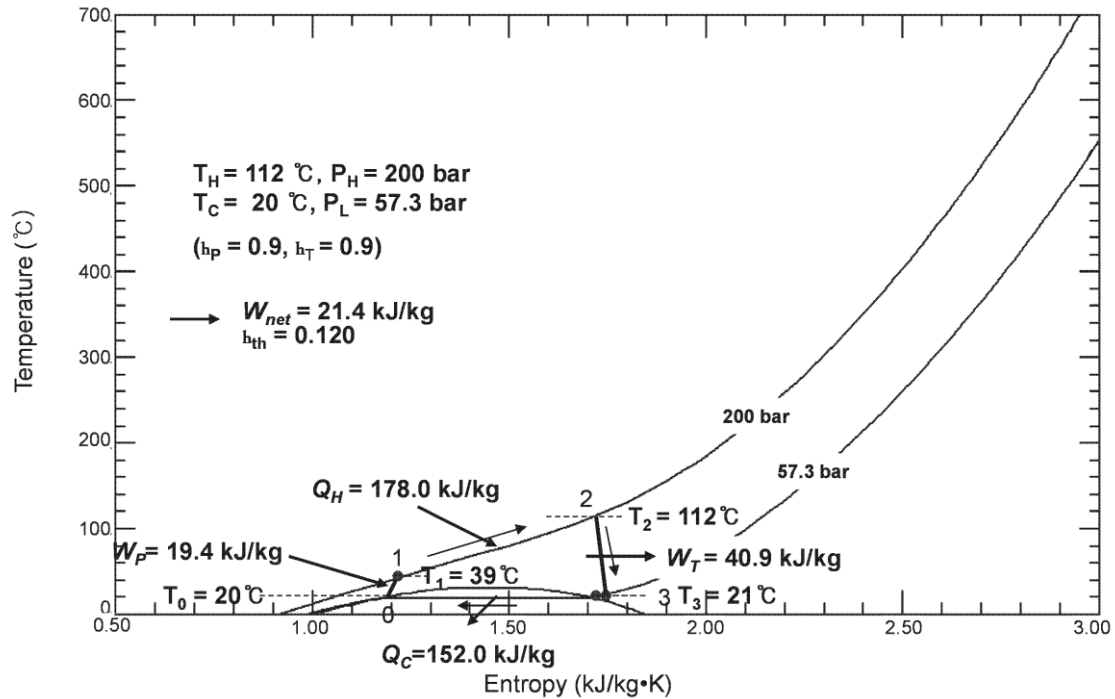


Fig. 6.13: Reference cycle of T-CO₂ cycle with LT heat source.

As shown in Table 6.3, the LH T-CO₂ cycle can produce approximately 15% more power than the sum of the separate two cycles with the same heat inputs by these synergistic effects. The exergy analysis of the LH T-CO₂ cycle, expressed on unit mass basis, is summarized in Table 6.4. The exergy loss of the heater, which is the main exergy loss in the previous T-CO₂ Rankine cycle, is reduced in the LH T-CO₂ cycle and the exergy loss of the waste heat, which is the main exergy loss in the previous T-CO₂ Brayton cycle, is also reduced in the LH T-CO₂ cycle. The LH T-CO₂ cycle has an exergy efficiency of 72%, approximately over 10% higher than those of the T-CO₂ Rankine and Brayton cycles.

Table 6.4: Exergy analysis of transcritical CO₂ cycle using both LT and HT heat sources

State (i)	T (°C)	P (bar)	$k_i - k_0$ (kJ/kg)	$Q(E), W(E)$ (kJ/kg)	L (kJ/kg)
0	20.0	57.3	0.0	$Q_W^- = 222.7 (E_W^- = 7.0)$	$L_W = 7.0 (12.1\%)$
1	39.2	200.0	17.6	$W_P^+ = 19.4 (E_P^+ = 19.4)$	$L_P = 1.8 (3.1\%)$
2	112.2	200.0	48.0	$Q_{R1}^+ = 91.0 (E_{R1}^+ = 18.6)$ $Q_{H1}^+ = 87.0 (E_{H1}^+ = 16.6)$	$L_{R1+H1} = 4.8 (8.3\%)$
3	368.0	200.0	196.4	$Q_{R2}^+ = 358.1 (E_R^+ = 148.4)$	$L_{R2} = 21.4 (37.0\%)$
4	600.0	200.0	372.8	$Q_{H2}^+ = 286.1 (E_{H2}^+ = 191.7)$	$L_{H2} = 15.3 (26.4\%)$
5	449.0	57.3	195.3	$W_T^- = 169.9 (E_T^- = 169.9)$	$L_T = 7.6 (13.1\%)$
6	128.8	57.3	25.5	$Q_{R2}^- = 358.1 (E_R^- = 169.8)$	$(L_{R2} = 21.4)$
7	54.3	57.3	7.0	$Q_{R1}^- = 91.0 (E_R^- = 18.6)$	$(L_{R1} = 3.5)$
$\eta_{II} = \frac{E_T^- - E_P^+}{E_{H1}^+ + E_{H2}^+} = 0.723$				$E_{H1}^+ = 16.6$ $E_{H2}^+ = 191.7$	$L_{tot} = 57.9 (100\%)$

Chen et al. studied transcritical Rankine cycles using CO₂ and R32 as the working fluids for converting low-grade heat to power [61] and found that the exergy efficiencies of these cycles are in the range of 50%~60% at the cycle high temperature of 160°C. In their analysis, the isentropic efficiencies of the compressor and turbine were fixed at 85% and the condensation temperature for the working fluids was fixed at 24°C. Zhao et al. [72] investigated the multiple reheat helium Brayton cycles for sodium-cooled fast reactors. In their analysis, the isentropic efficiencies of the compressor and turbine were fixed at 88% and 93%, respectively, and the temperature effectiveness of the recuperator was fixed at 0.95. At turbine inlet temperature of 600°C and compressor inlet temperature of 20°C, the thermal efficiency of the cycle with three expansion stages and six compression stages was approximately 47%, which is equivalent to an exergy efficiency of 71% in this study. The exergy efficiency of 72% of the proposed LH T-CO₂ cycle in this study is a significant achievement considering the simplicity of the cycle.

6.3 Applications of LH T-CO₂ cycle

6.3.1 Nuclear power plant

As mentioned previously, interest in the S-CO₂ cycle has recently been revived in conjunction with its application to Generation IV nuclear reactors at the Massachusetts Institute of Technology (MIT) and the Tokyo Institute of Technology (TIT) [51-55]. At the TIT, a partial pre-cooling (or a partial condensation) T-CO₂ cycle was studied to eliminate the temperature mismatch in the CO₂ cycles between the high- and low-pressure sides. As shown in Fig. 6.14 [51-55], if the CO₂ flow is bypassed to the compressor before pre-cooling, this temperature mismatch will be avoided. However, the bypassed flow reduces the heat rejected to the cooling water through the pre-cooler and increases the required compressor work.

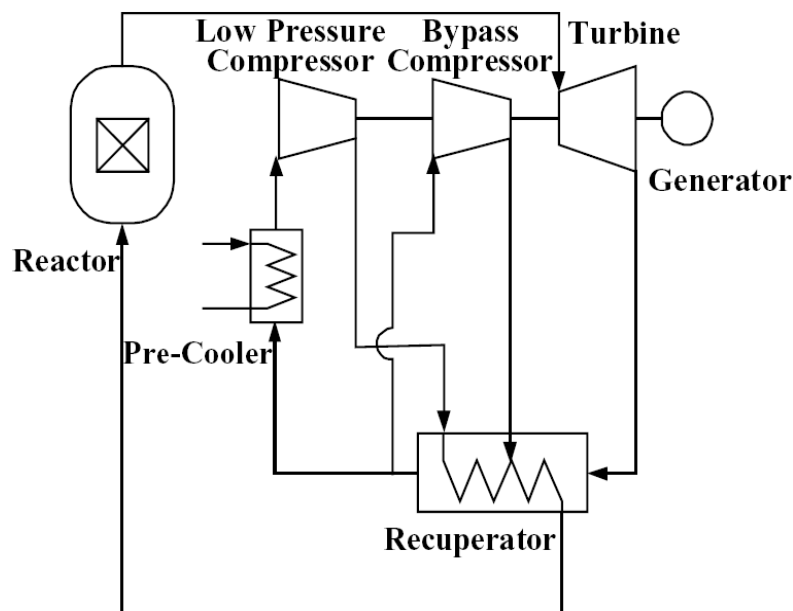


Fig. 6.14: Schematic of partial pre-cooling S-CO₂ cycle.

Despite the opposing effect on the cycle efficiency owing to the bypassed flow of CO₂, the cycle efficiency is enhanced by approximately 4% at 800°C [51]. The MIT is developing the recompression S-CO₂ cycle recommended by Feher [56]. However, the condensation of CO₂ was eliminated, and the pump was replaced by a compressor because condensing CO₂ cycles require year-round supply of very cold cooling water (10~15°C), which is not available in all regions worldwide [51].

The LH T-CO₂ cycle can also be used to avoid the temperature mismatch in the CO₂ cycles and improve the cycle efficiency with the given heat input from the nuclear reactor. If heat is available from the LT heat source below 120°C, then our results, which were discussed previously, suggest that the cycle efficiency can be enhanced by slightly over 10% at 600°C from the basic T-CO₂ Rankine and Brayton cycles. However, if no heat is available from the LT heat source, the LH T-CO₂ cycle combined with the T-CO₂ Brayton cycle and an LT thermal energy storage (TES) can be used. A schematic of the cycle is shown in Fig. 6.15 (night) and Fig. 6.16 (day).

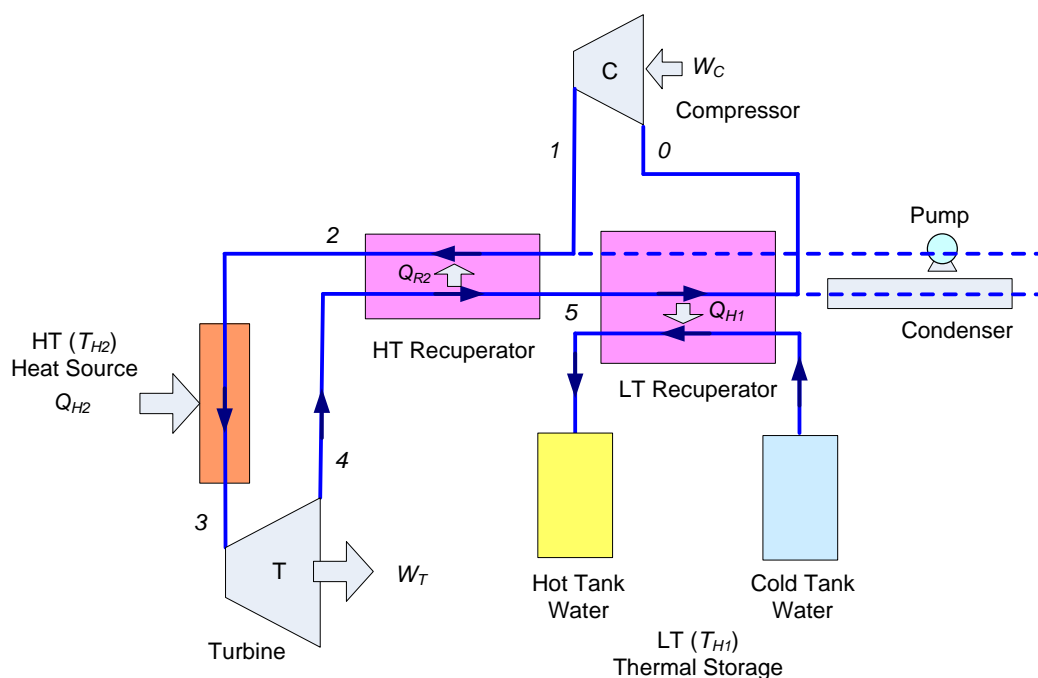


Fig. 6.15: Schematic of LH T-CO₂ cycle combined with T-CO₂ Brayton cycle and TES, T-CO₂ Brayton mode (night).

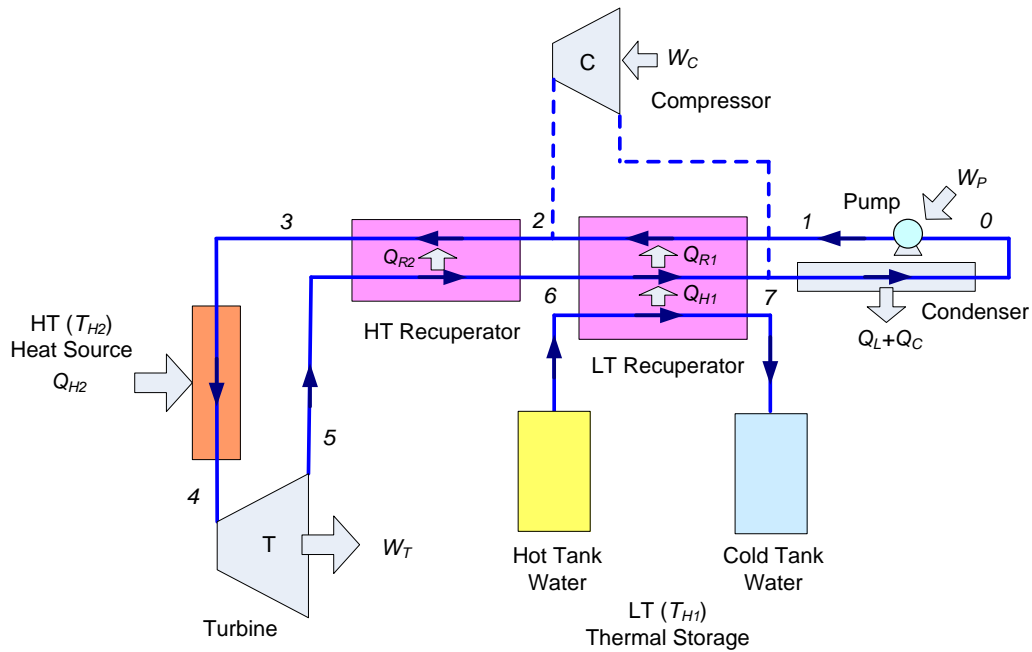


Fig. 6.16. Schematic of LH T-CO₂ cycle combined with T-CO₂ Brayton cycle and TES, LH T-CO₂ mode (day).

During the night, when the demand for electricity is low, the system is operated as the T-CO₂ Brayton cycle (Fig. 6.6) and the waste heat (Q_L) is stored in the LT TES using the water flowing from the cold tank to the hot tank. During the day, when the demand for electricity is high, the system is operated as the LH T-CO₂ cycle (Fig. 6.9) and the supplemental heat needed in the LT range (Q_{H1}) is supplied by the LT TES using the water flowing from the hot tank to the cold tank. The amount of waste heat (Q_L) from the T-CO₂ Brayton cycle is larger than the supplemental heat needed in the LT range (Q_{H1}) for the LH T-CO₂ cycle. Moreover, as shown in Fig. 6.17, twice (current + stored) the isobaric specific heat of CO₂ in the low-pressure side is well matched to that in the high-pressure, and given the unused waste heat from the HT recuperator, it is possible to supply Q_{H1} for the LH T-CO₂ cycle by using Q_L stored from the previous T-CO₂ Brayton cycle.

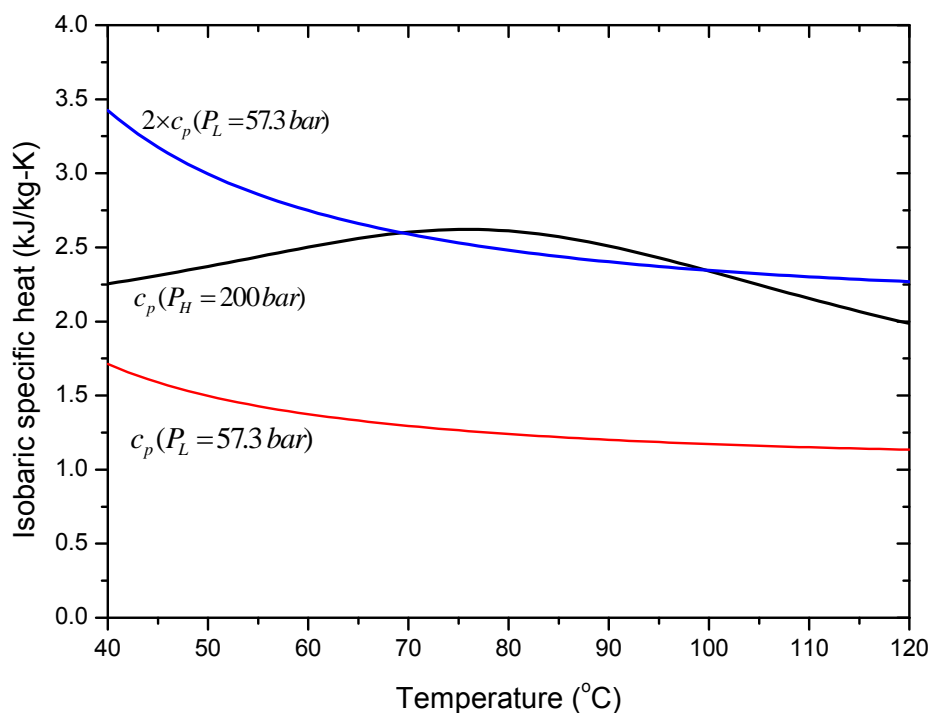


Fig. 6.17: Thermal match over low-temperature range in LH T-CO₂ cycle combined with T-CO₂ Brayton cycle and TES.

As shown in our previous results, during the day with high demand for electricity, the LH T-CO₂ cycle can produce approximately 25% more power than during the night by reducing the compression work and by enhancing the cycle efficiency from 42.1% to 52.6% at 600°C with the same heat input from the nuclear reactor. The thermal energy storage used is very similar to that of a new type of thermo-electric energy storage (TEES) system with transcritical CO₂ cycles using hot water storage, recently proposed by the ABB Corporate Research Center. Water tanks (289MWt, thermal energy storage) similar to that of the 50 MWe TEES system are needed for the nuclear power plant operating from 400 MWe (night) to 500 MWe (day) using the proposed LH T-CO₂ cycle.

As shown in Fig. 6.18, the partial condensation T-CO₂ cycle in a study at the TIT is similar to a compound cycle of the T-CO₂ Rankine and Brayton cycles in this study. The configuration of the system is similar to that of the previously combined LH T-CO₂ cycle as shown in Fig. 6.15 and Fig. 6.16; however, no thermal energy is stored, and half a fraction of the fluid flow is bypassed to the compressor before it enters the condenser. If the mass flow in the high-pressure side is half of that in the low-pressure side in the LT recuperator, the temperature mismatch problem in the LT recuperator can be avoided in the same way as shown in Fig. 6.17.

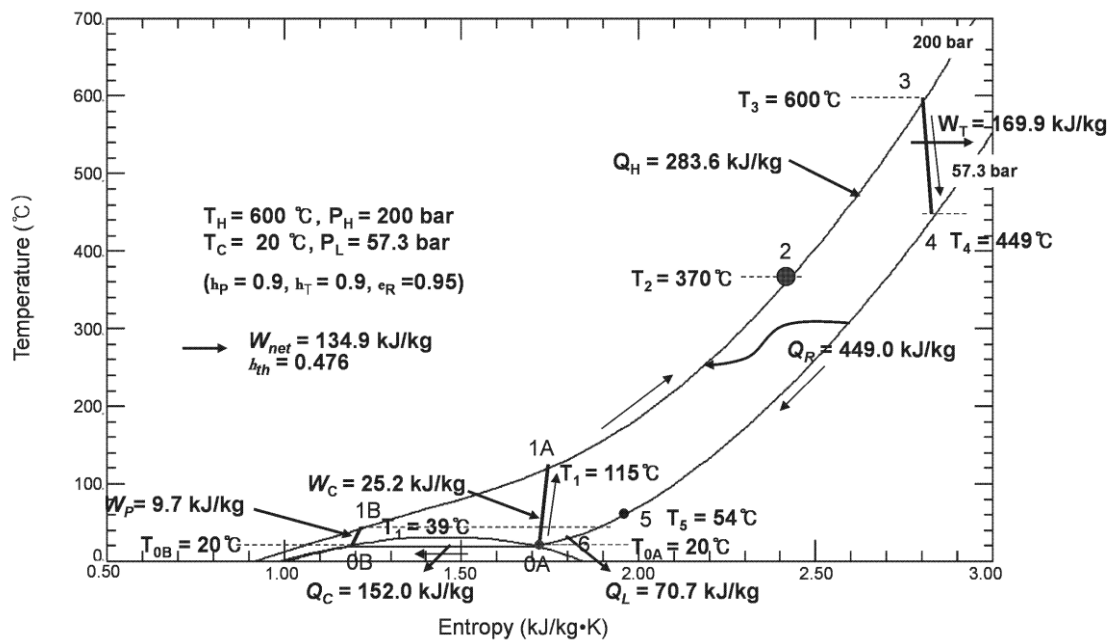


Fig. 6.18: Reference cycle of partial condensation T-CO₂ cycle.

As shown in Fig. 6.18, the compression work and the power output of the partial condensation T-CO₂ cycle are the mean values of those in the T-CO₂ Brayton cycle (night) and the LH T-CO₂ cycle with LT TES (day), indicating a nuclear power plant with a constant power output of 450 MWe. However, the proposed LH T-CO₂ cycle combined with the T-CO₂ Brayton cycle and the LT TES offers the advantage of load leveling from 400 MWe to 500 MWe by regulating the split ratio for the bypass CO₂ flow and the direction and the quantity of water flow of the LT TES. Traditionally, reactor power control has been used in

base-load operating conditions. With the increasing share of power plant, it seems that the load-follow operating of nuclear reactors will be inevitable in the future. But, it is hard to get the satisfying performance with classic control strategy to control nuclear reactor power [73,74].

The concept of the LH T-CO₂ cycle can also be applied to the S-CO₂ cycle. The turbine inlet temperature and pressure in the S-CO₂ cycle are maintained constant (600°C and 200 bar); however, the compressor inlet temperature and pressure are slightly higher than those in the T-CO₂ cycle (32°C and 77 bar), which is very close to the optimal recompression S-CO₂ cycle in other literatures [51-53]. Similar to the previous LH T-CO₂ cycle, two S-CO₂ cycles—fully-cooled and less-cooled S-CO₂ cycles—can be considered as shown in Fig. 6.19 and Fig. 6.20, respectively.

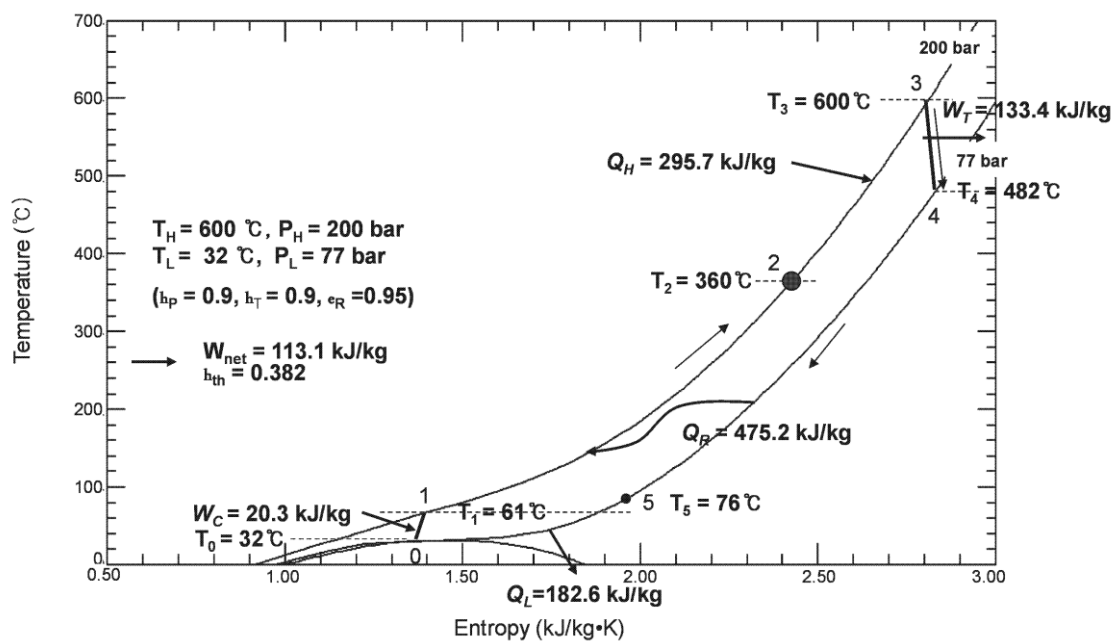


Fig. 6.19: Reference cycle of fully-cooled S-CO₂ cycle.

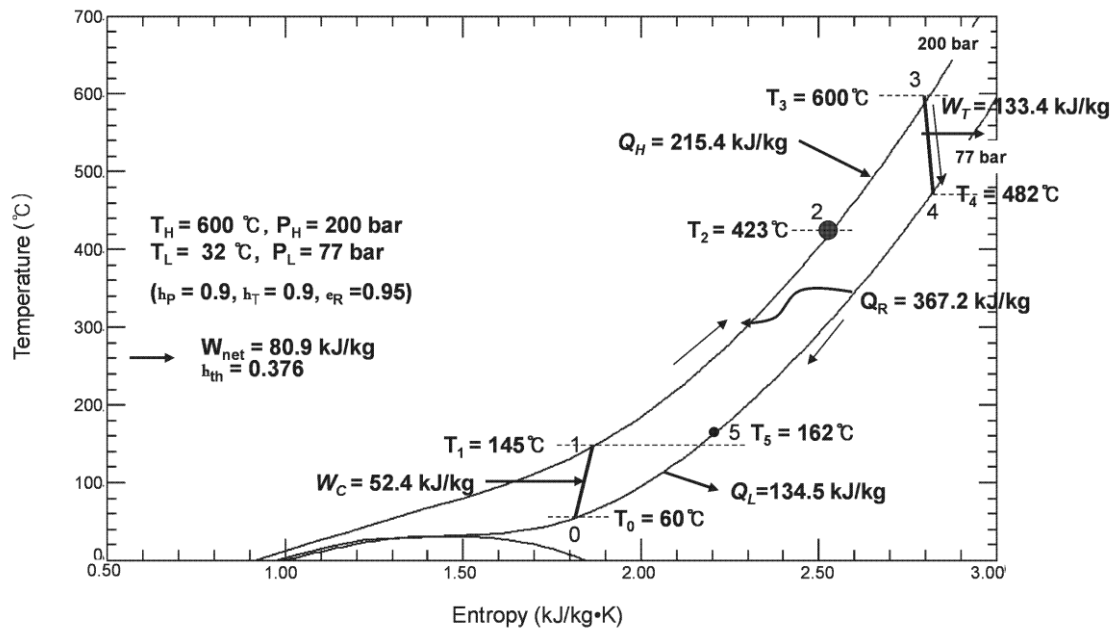


Fig. 6.20: Reference cycle of less-cooled S-CO₂ cycle.

The recompression S-CO₂ cycle is similar to a compound cycle of the two S-CO₂ cycles, as shown in Fig. 6.21.

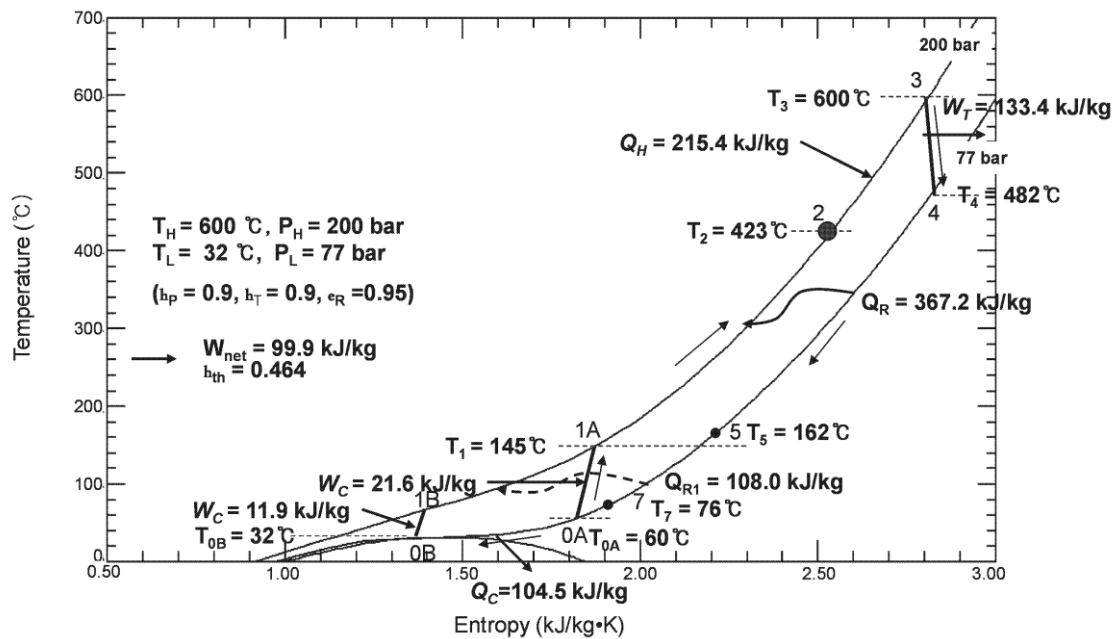


Fig. 6.21: Reference cycle of recompression S-CO₂ cycle.

If 41% of the fluid flow at point 0A is bypassed to the compressor before the final cooler (0A-0B), temperature mismatch in the LT recuperator can be avoided in the same way, as that shown in Fig. 6.22, and the cycle efficiency can be increased up to 46.4% from the two basic S-CO₂ cycles.

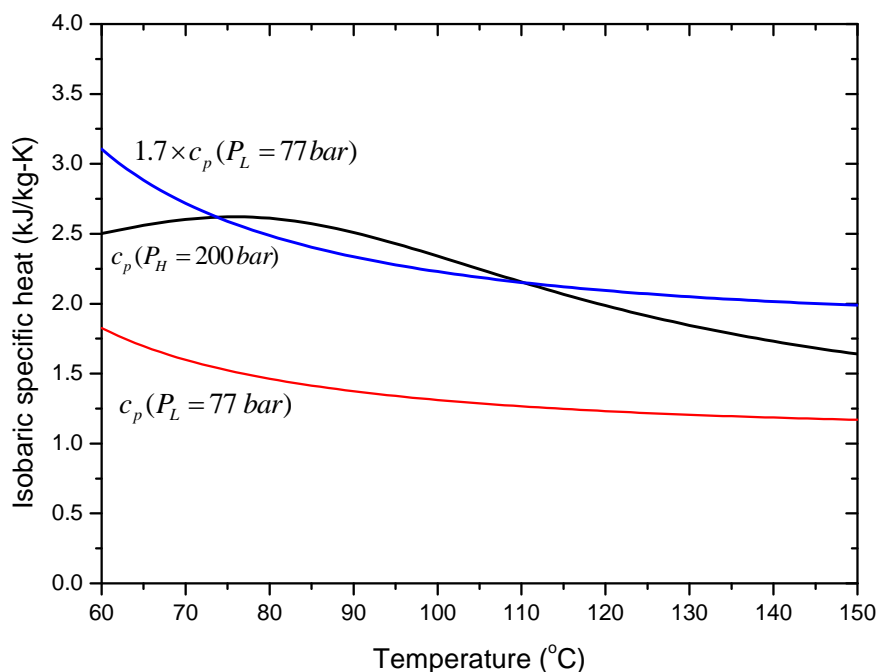


Fig. 6.22: Thermal match over low-temperature range in recompression S-CO₂ cycle.

The present numerical model was verified using the same data and operating conditions as those used by Dostal [52]; these conditions are as follows: maximum cycle temperature of 550°C, maximum cycle pressure of 200 bar, pressure ratio of 2.6, recompressed mass flow ratio of 0.41, ε_R of 96.3%, and turbine and compressor isentropic efficiencies of 90% and 89%, respectively. The calculated cycle efficiency (45.8%) is slightly higher than that of the reference case (45.3%), considering the assumption of zero pressure drop in the primary system in this study.

On the other way, the LH S-CO₂ cycle combined with the LT TES can be used. During the

night, the system is operated as a less-cooled S-CO₂ cycle (Fig. 6.20), and the waste heat (Q_L) is stored in the LT TES using the water flowing from the cold tank to the hot tank. During the day, when the demand for electricity is high, the system is operated as an LH S-CO₂ cycle (Fig. 6.23) and the supplemental heat needed in the LT range (Q_{H1}) is supplied by the LT TES using the water flowing from the hot tank to the cold tank.

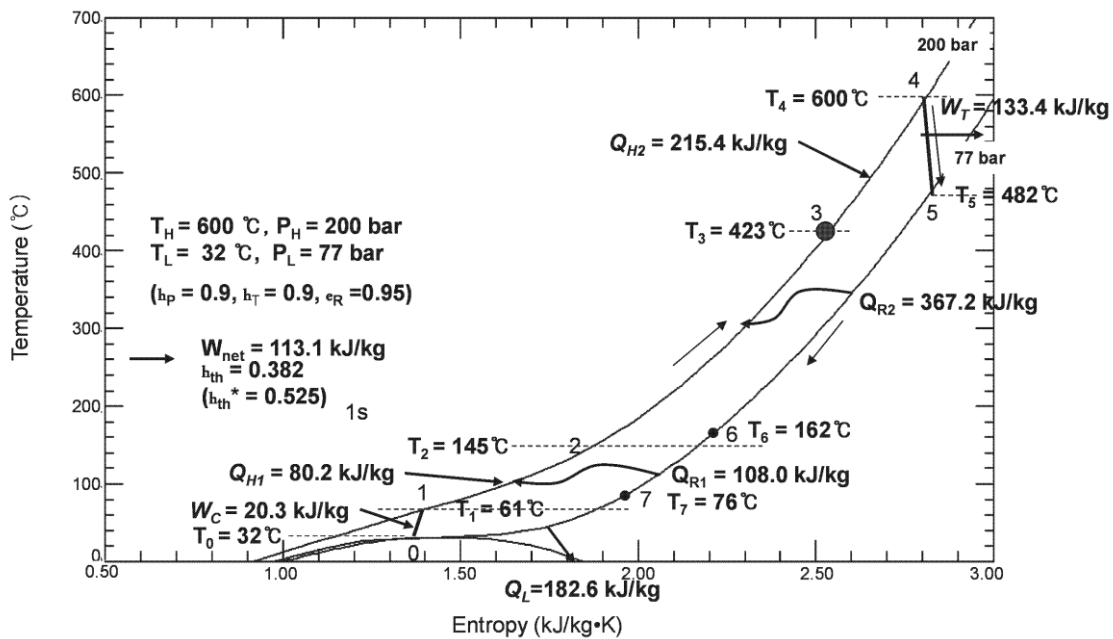


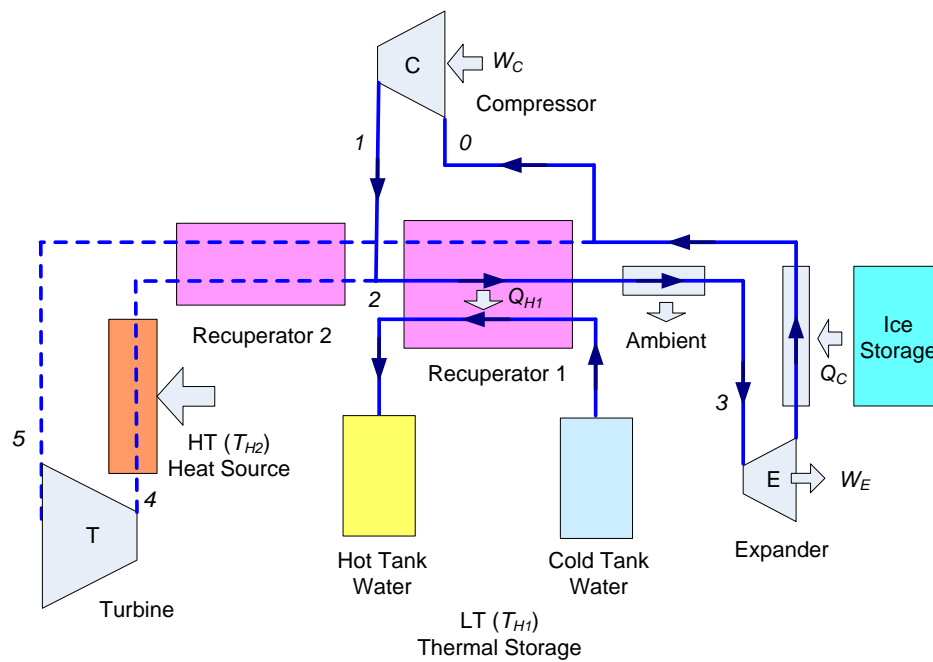
Fig. 6.23: Reference cycle of LH S-CO₂ cycle using both LT and HT heat sources.

As shown in Fig. 6.22, 1.7 times (current + stored) the isobaric specific heat of CO₂ in the low-pressure side is well matched to that in the high-pressure side. For thermal matching, the system is operated as a less-cooled S-CO₂ cycle (Fig. 6.20) for 10 hours and an LH S-CO₂ cycle (Fig. 6.23) for 14 hours. During the day, when there is a high demand for electricity, the LH S-CO₂ cycle can produce approximately 40% more power than during the night by reducing the compression work and enhancing the cycle efficiency from 37.6% to 52.5% at 600°C with the same heat input from the nuclear reactor. The proposed LH S-CO₂ cycle combined with the LT TES offers the advantages of load leveling from 358 MWe to 500 MWe with the constant nuclear reactor by regulating the split ratio for the bypass CO₂ flow and the direction and the quantity of water flow of the LT TES.

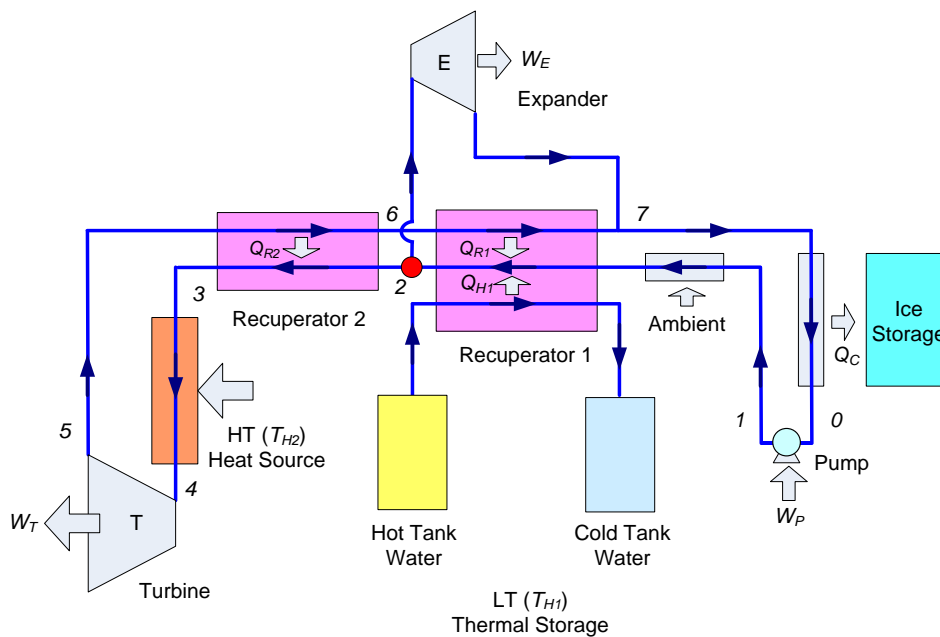
6.3.2 Hybrid system of LH transcritical CO₂ cycle combined with TEES

As mentioned before, a new type of TEES system with reversible T-CO₂ cycles was recently proposed by the ABB Corporate Research Center [69]. The system layout is shown in Fig. 5.7, and the energy flow per unit mass of working fluid on T-s diagram of the base reference (reversible) cycle is shown in Fig. 5.8. The concept is based on heat pump and heat engine (reverse cycle) technologies utilizing T-CO₂ cycles, storage of pumped heat in hot water, and ice generation and melting at the cold end of the cycles. The TEES systems with transcritical CO₂ cycles can be used as a hybrid system combined with an LH T-CO₂ cycle (we refer to this as an LH T-CO₂ cycle with TEES). The schematic and reference cycle of this system are shown in Figs. 6.24 and 6.25, respectively.

The charging mode of the system is the same as the TEES system. However, in the discharging mode of the system, the high-pressure CO₂ gas heated by the LT source (thermal energy storage) is divided by two parts by a split ratio y , which is controlled according to the demand for electricity. One portion, y , of the CO₂ gas is sent to the HT heater and the other portion, $1 - y$, is sent to the LT expander. The expanded hot CO₂ gas from the HT turbine transfers its heat to the compressed CO₂ gas through the HT recuperator, where it is cooled down and combined with the expanded CO₂ gas from the LT expander. The combined, expanded CO₂ gas transfers its heat to the compressed CO₂ gas through the LT recuperator.



(a) Charging mode



(b) Discharging mode

Fig. 6.24: Schematic of TEES LH T-CO₂ cycles, charging mode (a) and discharging and generation mode (b).

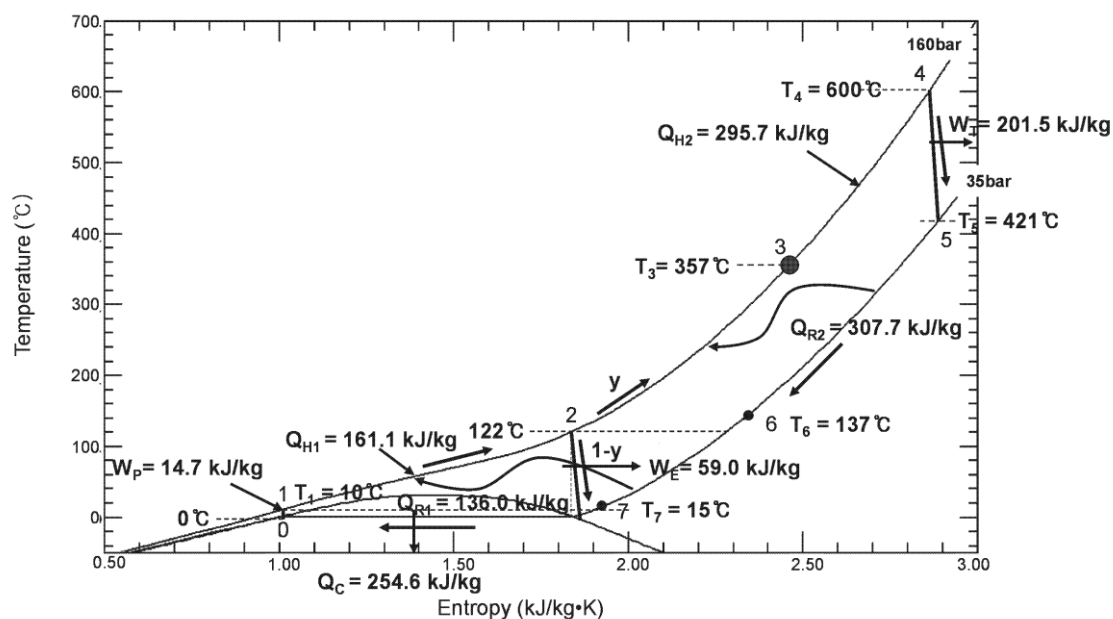


Fig. 6.25: Reference cycle of TEES LH T-CO₂ cycle, discharging and generation mode.

Fig. 6.26 shows the heat input and the work input/output according to the split ratio, expressed on a unit mass basis. Table 6.5 compares the performances, expressed on unit mass basis, of different CO₂ cycles based on the reference cycle in Fig. 6.25 to show the synergistic effects of the hybrid system that combines the TEES system with the LH T-CO₂ cycle. During the day with high demand for electricity, in comparison with the T-CO₂ Brayton cycle, the LH T-CO₂ cycle can produce approximately 45% more power by reducing the compression work and improve the cycle efficiency, η_{th}^* , by approximately 19% at 600°C with the same heat input from the HT heat source.

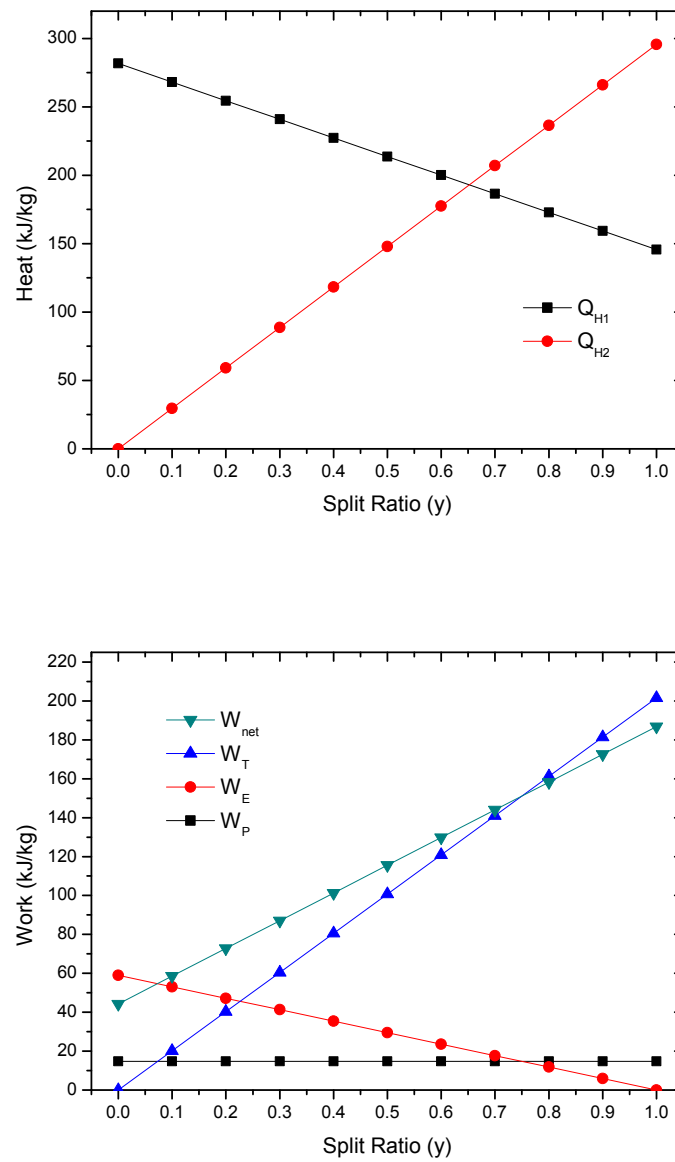


Fig. 6.26: Heat input (top) and work input/output (bottom) as a function of split ratio y in TEES LH T-CO₂ cycle.

Table 6.5: Comparison of performances of different T-CO₂ cycles with TEES (H: High temperature of T_{H2} , L: Low temperature of T_{H1} , R: Rankine, B: Brayton)

Cycle	T_{H1} (°C)	Q_{H1} (kJ/kg)	T_{H2} (°C)	Q_{H2} (kJ/kg)	T_R (°C)	$W_{P(C)}$ (kJ/kg)	W_T (kJ/kg)	W_{net} (kJ/kg)	η_{th}	η_{th}^*
H-R (1)	-	-	600	456.8	225	14.7	201.5	186.8	0.409	-
H-B (2)	-	-	600	292.6	360	72.8	201.5	128.7	0.440	-
L-R (3)	122	281.7	-	-	-	14.7	59.0	44.3	0.157	-
LH-R (4)	122	161.1	600	295.7	357	14.7	201.5	186.8	0.409	0.632
L-R (3) + H-B (2)	122	161.1	600	295.7	360	8.4 + 73.6	33.7 + 203.7	25.3 + 130.1	0.340	-

6.4 Conclusion

In this chapter, a novel transcritical CO₂ Rankine cycle using both the LT and the HT heat sources (LH T-CO₂ cycle) ('low-temperature' means an intermediate temperature between the highest temperature of heat sources and the lowest temperature of heat sink) is proposed to maximize the power output of the CO₂ power cycle with the given HT heat sources for use in applications such as nuclear power, concentrated solar power, and combustion.

Although the compression work and exergy loss of waste heat are significantly reduced in the T-CO₂ Rankine cycle with HT heat sources as compared to the T-CO₂ Brayton cycle, the outlet temperature of CO₂ heated through the recuperator is considerably lower than that in the T-CO₂ Brayton cycle. Therefore, the thermal efficiency of the T-CO₂ Rankine cycle is lower than that of the T-CO₂ Brayton cycle. This is because below 150°C, particularly below 120°C, the isobaric specific heat of CO₂ in the high-pressure side is considerably higher than that in the low-pressure side.

However, if heat is available in this LT range to compensate for the difference in the specific heat of CO₂ between the high- and the low-pressure sides, the T-CO₂ Rankine cycle will be more effective than the T-CO₂ Brayton cycle. Further, the T-CO₂ is more effective than the partial condensation T-CO₂ cycle, which is a compound cycle of the T-CO₂ Rankine and Brayton cycles, because low compression work is required while obtaining the same outlet temperature of CO₂ heated through the recuperator before it enters the HT heater.

As compared to the T-CO₂ Brayton cycle with a HT heat source, the proposed LH T-CO₂ cycle can produce approximately 25% more power by reducing the compression work and enhancing the cycle efficiency by approximately 10% at 600°C with the same heat input from the HT heat source by utilizing an LT heat source. The exergy efficiency of the LH T-CO₂ cycle using both the LT and the HT heat sources is approximately 10% higher than that of the T-CO₂ Brayton cycle with a HT heat source.

For the application of this novel concept to nuclear power plants, during the night, when the demand for electricity is low, the system is operated as a T-CO₂ Brayton cycle, and the waste heat is stored in an LT TES. Further, during the day, when the demand for electricity is high, the system is operated as an LH T-CO₂ cycle using the LT TES. During the day, the LH T-CO₂ cycle can produce approximately 25% more power than during the night by reducing the compression work and enhancing the cycle efficiency from 42.1% to 52.6% at 600°C with the same heat input from the nuclear reactor. The proposed LH T-CO₂ cycle combined with the T-CO₂ Brayton cycle and LT TES offers the advantage of load leveling from 400 MWe to 500 MWe over the partial condensation T-CO₂ cycle with a constant power output of 450 MWe. The concept of the LH T-CO₂ cycle can also be applied to the S-CO₂ cycle, and the LH S-CO₂ cycle combined with the LT TES offers the advantage of load leveling from 358 MWe for 10 hours to 500 MWe for 14 hours over the recompression S-CO₂ cycle with a constant power output of 442 MWe.

Moreover, a new type of thermo-electric energy storage (TEES) system with reversible transcritical CO₂ cycles can be used as a hybrid system combined with the LH T-CO₂ cycle.

7. General conclusions

7.1 Conclusions

The interest in energy storage is currently increasing, especially for matching intermittent sources of renewable energy with customer demand, as well as for storing excess nuclear or thermal power during the daily cycle. Although pumped hydro is a well-known and widely used method of energy storage, its dependence on specific geographic features and environmental concerns make new developments of this technology difficult. Compressed air energy storage (CAES) and thermo-electric energy storage (TEES) are promising methods of electrical energy storage for load leveling. Both are based on energy conversion processes characterized by well-known thermodynamic cycles. However, since they are different from conventional power cycles, it is very important to precisely understand each system and the key parameters for achieving high efficiency of the system.

Analyses of energy and exergy of CAES systems were used to provide an understanding of the drawbacks of currently used CAES methods and the advantages of innovative CAES concepts such as adiabatic CAES, isothermal CAES, micro-CAES combined with air-cycle heating and cooling, and constant-pressure CAES combined with pumped hydro storage. Although existing CAES plants use natural gas as fuel, waste heat and renewable energies such as solar, biomass, and biogas can be used as heat sources for CAES systems. Adiabatic CAES traps the heat of compression and reuses it for expansion, and hence, it can be considered a combination of CAES and thermal energy storage (TES), because a substantial portion of the exergy is stored in the form of thermal energy. Isothermal CAES can minimize the compression work and maximize the expansion work done through isothermal compression/expansion by effectively transferring heat to/from the system's surroundings and without the use of fuel or high temperature thermal storage.

Conventional CAES systems are most commonly operated under constant volume conditions with a fixed, rigid reservoir and compressors and turbines that can run over an appropriate pressure range. These varying pressure ratios can degrade the efficiencies of compression and power generation owing to deviation from design points. Although it is possible to increase the storage volume to reduce the operating pressure range, doing so results in low energy density and high construction costs. Therefore, in order to resolve such problems, a novel constant-pressure CAES system combined with pumped hydro storage is proposed. The novel CAES system can reduce the throttling loss during expansion in existing CAES plants; this method requires a small cavern (or vessel) with a storage volume only half of that required for existing CAES plants. The hydraulic part of the system is used to maintain a constant pressure in the air storage vessel of the CAES system and also serves as hydraulic energy storage, which is one of the most efficient methods for storing energy. Moreover, the hydraulic energy storage component in the system has many advantages over a conventional CAES system, including quick start-up, the ability to provide “spinning reserve,” and voltage and frequency regulation to stabilize the associated power grid. This concept can be applied to both large-scale CAES using salt caverns or lined rock caverns and small-scale CAES using man-made air vessels.

A micro-CAES system with man-made air vessels is a more adaptable solution for decentralized energy systems. In a micro-CAES system, it is possible to use dissipated heat of compression for heating load and to use compressed air for both power generation and cooling load. Moreover, a micro-CAES system, especially with quasi-isothermal compression and expansion processes, could be a very effective system with a energy density feasible for distributed energy storage system and a good efficiency and economics due to the multipurpose system, because it can provides energy storage, generates electric power using various heat sources, and incorporates an air cycle heating and cooling system. For the quasi-isothermal compression and expansion processes, a method of liquid injection can be used, where the liquid mass flow rates may be significantly greater than gas flow rates. In the case of systems with the quasi-isothermal processes by liquid injection, it is possible to match the temperature after compression to the heating load or the temperature after expansion to the cooling load by controlling the mass flow rate of injected liquid.

The existing CAES systems have a few drawbacks, but these can be addressed by employing some innovative CAES concepts. Compressed air energy storage can be combined with power generation using various heat sources, thermal energy storage, air cycle heating and cooling, and pumped hydro storage; such combinations have great synergistic effects.

Recently, another type of mechanical storage, thermo-electric energy storage (TEES) systems, which use heat pumps and heat engines with thermal energy storage, have been proposed as a new method for large-scale energy storage. For optimization of the reference thermodynamic cycle of a TEES system with a given efficiency of the compressor/expander, it is very important to minimize the back work ratio since the maximum round-trip efficiency decreases rapidly with an increasing back work ratio. In the case of TEES systems with Brayton cycles using argon gas, a very high temperature difference between the hot storage and the cold storage is needed to reduce the back work ratio. Furthermore, highly efficient compressors and expanders are needed to achieve a reasonable round-trip efficiency. However, in the case of TEES systems with transcritical CO₂ cycles, even if the temperature difference between the hot storage and the cold storage is much smaller than in systems with Brayton cycles, the round-trip efficiency of the TEES systems is higher because of the reduced back work ratio, assuming the same efficiency of the compressor/expander. Moreover, TEES systems with transcritical CO₂ cycles have the advantage of using water for inexpensive thermal storage.

The novel isothermal TEES system with transcritical CO₂ cycles proposed in this thesis can maximize the expansion work by isothermal expansion with effective heat transfer directly with the hot storage tank, resulting in higher round-trip efficiency because of a lower back work ratio than in the isentropic case. Hot water from the hot storage tank is used by the water pump/turbine to compress/expand the supercritical CO₂ as the liquid piston, and a portion of the water is sprayed with a circulation pump to cool/heat the supercritical CO₂. Through a simple model of the isothermal TEES system, it was shown that a greater mass and higher temperature of the water in the hot tank can result in a higher round-trip efficiency for the isothermal TEES system. Furthermore, the pressure ratio of isothermal expansion during the discharging mode can be sufficiently increased relative to the pressure ratio of isothermal compression during the charging mode to obtain greater power recovery because

the thermal energy resulting from internal heat dissipation during the isothermal compression/expansion can be stored and used at the maximum cycle temperature, and the exergy loss due to internal dissipation is lower than in the isentropic case.

In addition, novel transcritical (T-) or supercritical (S-) CO₂ cycles using both the low temperature (LT) and high temperature (HT) heat sources (LH T- or S-CO₂ cycle) ('low-temperature' means an intermediate temperature between the highest temperature of heat sources and the lowest temperature of heat sink) are proposed to maximize the power output of the CO₂ power cycle with the given HT heat sources for use in applications such as nuclear power, concentrated solar power, and combustion. For the application of this novel concept to nuclear power plants, the LH S-CO₂ cycle combined with low-temperature thermal energy storage offers the advantage of load leveling over the recompression S-CO₂ cycle with a constant power output. Moreover, a TEES system with transcritical CO₂ cycles can be combined with the LH T-CO₂ cycle.

7.2 Future work

With respect to the thermodynamics involved, the advantages of the proposed novel concepts of compressed air energy storage (CAES) and thermo-electric energy storage (TEES) are shown from the results of the energy and exergy analyses of the systems. In order to apply these novel concepts to a real site, however, the following further work would bring additional informations.

- Thermo-economic optimization of the novel systems

Thermo-economic modeling and optimization of the novel systems, considering both energy efficiency and economic and environmental (environomic) factors, would bring new highlight for the best integration of the energy systems. This could be done using a hybrid multi-objective optimization procedure that combines a linear programming problem and a multi-objective optimizer (MOO).

- Dynamic simulation of the novel systems

Although each compression and expansion is assumed to take place at a steady state with a steady flow in this study, the energy storage systems actually operate alternately in the charging mode and the discharging mode. Therefore, a dynamic simulation of the novel systems, considering the thermal inertia of all components and kinematic energy effects, should be developed. And the performance characteristics of the components at the transient and part load conditions must be considered. The developed dynamical model may enable a control system designer or a system operator to carry out accurate computer simulations for the systems under a wide range of operational modes of the system.

In addition, although it is assumed that the temperatures of the thermal energy storage and the working fluid are uniform at a given time and state, in the case of the large-scale system, the non-uniformity of the temperatures must be considered. And in the case of thermal energy storage, although the loss of heat transfer of the system with the environment is neglected, it must be considered for a more accurate model of the system. Since the thermal insulation losses are related to the surface to volume ratio (S/V), a larger system results in a more accurate adiabatic assumption.

Bibliography

- [1] I. E. Agency, “Energy technology perspectives 2010”, tech. rep., International Energy Agency, www.iea.org, 2010.
- [2] P. Morico, G. Maislin, R. Faries, “The role of energy storage in intelligent energy system”, Raytheon Technology Today, 2011 issue 1, pp. 26-29, Raytheon, 2011.
- [3] C. Dotsch, “Energy storage”, Technology Guide, pp. 361- 367, Springer, 2009.
- [4] Lund H, Salgi G, Elmegaard B, Andersen A.N. Optimal operation strategies of compressed air energy storage (CAES) on electricity spot markets with fluctuating prices. *Applied Thermal Engineering* 2009; 29: 893-904.
- [5] Cavallo A. Controllable and affordable utility-scale electricity from intermittent wind resources and compressed air energy storage (CAES). *Energy* 2009; 32: 120-127.
- [6] Lund H, Salgi G. The role of compressed air energy storage (CAES) in future sustainable energy systems. *Energy Conversion and Management* 2009; 50: 1172-1179.
- [7] Swanbarton Limited. 2004. Status of Electrical Energy Storage Systems, *DTI Report No. 04/1878*, UK.
- [8] Denholm P, Kulcinski GL. Life cycle energy requirements and greenhouse gas emissions from large-scale energy storage systems. *Energy Conversion and Management* 2004; 45: 2153-2172.
- [9] TENI Services Limited. An appraisal of new and renewable generation technologies as transmission upgrade alternatives. *NZ Electricity Commission Report P5NZ01*, 2005.
- [10] UCC Sustainable Energy Research Group. Study of Electricity Storage Technologies and Their Potential to Address Wind Energy Intermittency in Ireland. University College Cork Final Report RE/HC/103/001, 2004.
- [11] Mercangoez M, Hemrle J, Kaufmann L, Buchter F, and Ohler C. Thermoelectric energy storage with transcritical CO₂ cycles. In: ECOS 2011: Proceedings of the 23rd International Conference on Efficiency, Cost, Optimization, Simulation, and Environmental Impact of Energy Systems; 2011 Jul 4–7; Novi Sad, Serbia.

-
- [12] Desrues T, Ruer J, Marty P, and Fourmigue JF. A thermal energy storage process for large-scale electric applications. *Applied Thermal Engineering* 2010; 30: 425–432.
- [13] Kim YM, Shin DG, and Kim CG. Potential and evolution of compressed air energy storage for future power networks. World Engineers' Convention, Geneva, 2011.
- [14] Ter-Gazarian A. Energy storage for power systems. UK: The Institution of Engineering and Technology, 2008.
- [15] Succar S, Williams RH. Compressed air energy storage: theory, resources, and applications for wind power. Princeton Environmental Institute Report, 8 April 2008. Available online at <http://www.princeton.edu/~ssuccar/caesReport.html>.
- [16] Kim YM, Shin DG, and Favrat D. Operating characteristics of constant-pressure compressed air energy storage (CAES) system combined with pumped hydro storage based on energy and exergy analysis. *Energy* 2011; 36: 6220–6233.
- [17] Kim YM, Favrat D. Energy and exergy analysis of a micro compressed air energy storage and air cycle heating and cooling system. *Energy* 2010; 35: 213–20.
- [18] US Patent 7,663,255. Compressed-air-storing electricity generating system and electricity generating method using the same.
- [19] C. Dotsch, “Hybrid energy storage system for urban use”, Fraunhofer-Gesellschaft-Research News, Press Release 10. May 2011, Fraunhofer-Gesellschaft, 2011.
- [20] Eckard, R. CAES compressed air energy storage worldwide, SBI Energy: Rockville, Maryland, 2010.
- [21] Crotagino F, Mohmeyer KU, Scharf R. Huntorf CAES: More than 20 years of successful operation, KBB GmbH and E.ON Kraftwerke Bremen, Spring 2001 Meeting, Orlando, Florida, USA, 15–18 April, 2001.
- [22] Grazzini G, Milazzo A. Thermodynamic analysis of CAES/TES systems for renewable energy plants. *Renew Energy* 2008; 33(9): 1998–2006.
- [23] Hartmann N, Vohringer O, Kruck C, Eltrop L. Simulation and analysis of different adiabatic compressed air energy storage plant configurations. *Appl Energy* 2012; 93: 541–8.
- [24] Lemofouet S. Investigation and optimization of hybrid electricity storage systems based on compressed air and supercapacitors, PhD Thesis in EPFL, Lausanne, Switzerland, 2006.

-
- [25] Inage S-I, 2009, Prospects for large-scale energy storage in decarbonized power grids. International energy agency working paper series, OECD/IEA, 2009.
- [26] Tsatsaronis G. Definition and nomenclature in exergy analysis and exergoeconomics. *Energy* 2007; 32: 249–53.
- [27] Borel L, Favrat D. Thermodynamics and energy systems analysis. Lausanne: EPFL Press; 2010, pp. 399–490.
- [28] Elmegaard B, Brix W. Efficiency of compressed air energy storage. International Conference on Efficiency, Cost, Optimization, Simulation and Environmental Impact of Energy Systems; 2011 July 4–7; Novi Sad, Serbia.
- [29] Kondoh J, Ishii I, Yamaguchi H, Murata A, Ontai K, Sakuta K et al. Electrical energy storage systems for energy networks. *Energ Convers Manage* 2000; 41: 1863–74.
- [30] Nakhamkin M, Chiruvolu M. Available compressed air energy storage (CAES) plant concepts. Power-Gen Conference-MIN, December 2007.
- [31] Bullough C, Gatzen C, Jakiel C, Koller M, Nowi A, Zunft S. Advanced adiabatic compressed air energy storage for the integration of wind energy. European Wind Energy, Conference EWEC 2004, London, UK, 2004.
- [32] Zaugg P. Air-storage power generating plants. *Brown Boveri Review* 1975; 62: 338-347.
- [33] E. P. Gyftopoulos. Thermodynamics: Generalized Available Energy and Availability or Exergy, Chapter 1 in "Thermodynamics and the destruction of resources", The Cambridge University Press, Cambridge, 2011, pp. 15-44.
- [34] Nielsen L, Leithner. Dynamic simulation of an innovative compressed air energy storage plant – detailed modeling of the storage cavern. *WSEAS Transactions on Power Systems* 2009; Issue 8; 4: 253-263.
- [35] Salgi G. CAES Future Scenarios; An Investment Analysis for Denmark, MSc. Thesis in Energy Planning in Aalborg University, January 2006.
- [36] Cole S, Van Hertem D, Meeus L, Belmans R. SWOT analysis of utility side energy storage technologies. 5th WSEAS/IASME International conference on Electric Power Systems, High Voltages, Electric Machines; 2005. Available online at http://www.esat.kuleuven.be/electa/publications/fulltexts/pub_1514.pdf.

-
- [37] Verschoor MJE, editor. Guidelines for the application and design of air cycle systems for heating, ventilating and air conditioning in buildings. Apeldoorn, The Netherlands: TNOMEP; 2001.
- [38] Shengjun L, Zhenying Z, Lili T. Thermodynamics analysis of the actual air cycle refrigeration system. *Syst Eng Proc* 2011; 1: 112–116.
- [39] Foster AM, Brown T, Gigiel AJ, Alford A, Evans JA. Air cycle combined heating and cooling for the food industry. *Int J Refrig* 2011; 34: 1296–1304.
- [40] Spence SWT, Doran WJ, Artt DW, McCullough G. Performance analysis of a feasible air-cycle refrigeration system for road transport. *Int J Refrig* 2005; 28: 381–388.
- [41] Enis B, Lieberman P, Rubin I, Linden S. Wind turbine generator and compressed air energy storage system for production of electric power and co-generation for chilled air for desalination. In: *International Conference on Efficiency, Cost, Optimization, Simulation and Environmental Impact of Energy Systems*. 2007; pp. 43–51.
- [42] Wang S, Chen G, Fang M, Wang Q. A new compressed air energy storage refrigeration system. *Energy Convers Manage* 2006; 47: 3408–16.
- [43] Linnemann C, Coney MW. The isoengine: Realization of a high-efficiency power cycle based on isothermal compression, *Int J Energy Tech Pol* 2005; 3(1/2).
- [44] Hugenothe J, Braun J, Groll E, King G. Liquid-flooded Ericsson cycle cooler: Part 1—thermodynamic analysis. In: *International Refrigeration and Air Conditioning Conference at Purdue*; 2006, p. R168.
- [45] Hugenothe J, Braun J, Groll E, King G. Thermodynamic analysis of a liquid-flooded Ericsson cycle cooler. *Int J Refrig* 2007; 30: 1176–1186.
- [46] Kim YM, Shin DK, Lee JH. 2005. Heated scroll expander and its application for distributed power source. In: *International Conference on Conference on Compressors and their Systems*, pp. 133-142.
- [47] Desrues T, Ruer J, Marty P, and Fourmigue JF. A thermal energy storage process for large-scale electric applications. *Applied Thermal Engineering* 2010; 30: 425–432.
- [48] Mercangoez M, Hemrle J, Kaufmann L, Buchter F, and Ohler C. Thermoelectric energy storage with transcritical CO₂ cycles. In: *ECOS 2011: Proceedings of the 23rd International Conference on Efficiency, Cost, Optimization, Simulation, and Environmental Impact of Energy Systems*; 2011 Jul 4–7; Novi Sad, Serbia.

-
- [49] Morandin M, Marechal F, Buchter F, and Mercangoez M. Conceptual design of a thermoelectric energy storage system based on heat integration of thermodynamic cycles – Part A: methodology and base case system configuration. In: ECOS 2011: Proceedings of the 23rd International Conference on Efficiency, Cost, Optimization, Simulation, and Environmental Impact of Energy Systems; 2011 Jul 4–7; Novi Sad, Serbia.
- [50] Morandin M, Marechal F, Buchter F, and Mercangoez M. Conceptual design of a thermoelectric energy storage system based on heat integration of thermodynamic cycles – Part B: studying alternative system configurations. In: ECOS 2011: Proceedings of the 23rd International Conference on Efficiency, Cost, Optimization, Simulation, and Environmental Impact of Energy Systems; 2011 Jul 4–7; Novi Sad, Serbia.
- [51] Hejzlar P, Dostal V, Driscoll MJ, Dumaz P, Poullennec G, and Alpy N. Assessment of gas cooled fast reactor with indirect supercritical CO₂ cycle. *Nuclear Engineering and Technology* 2006; 38: 109-118.
- [52] Dostal V. A supercritical carbon dioxide cycle for next-generation nuclear reactors. Ph.D. thesis, Department of Nuclear Engineering, MIT, USA; 2004.
- [53] Dostal V, Hejzlar P, and Driscoll MJ. The supercritical carbon dioxide power cycle: comparison to other advanced power cycles. *Nuclear Technology* 2006; 154: 283-301.
- [54] Sarkar J. Second law analysis of supercritical CO₂ recompression Brayton cycle. *Energy* 2009; 34: 1172-1178.
- [55] Kato Y, Nitawaki T, and Muto Y. Medium temperature carbon dioxide gas turbine reactor. *Nuclear Engineering and Design* 2004; 230: 195-207.
- [56] Feher EG. The supercritical thermodynamic power cycle. *Energy Convers* 1968; 8: 85-90.
- [57] Angelino G. Carbon dioxide condensation cycles for power production; 1968 [ASME paper no. 68-CT-23].
- [58] Jeong WS, Lee JI, and Jeong YH. Potential improvements of supercritical recompression CO₂ Brayton cycle by mixing other gases for power conversion system of a SFR. *Nuclear Engineering and Design* 2011; 241: 2128-2137.

-
- [59] Kulhanek M, Dostal V. Supercritical carbon dioxide cycles thermodynamic analysis and comparison. In: Student's Conference 2009 at Faculty of Mechanical Engineering of Czech Technical University; Prague, Czech.
- [60] Sarkar J, Bhattacharyya. Optimization of recompression S-CO₂ power cycle with reheating. *Energy Convers Manage* 2009; 50: 1939–1945.
- [61] Chen H, Goswami DY, Rahman MM, Stefanakos EK. Energetic and exergetic analysis of CO₂- and R32-based transcritical Rankine cycles for low-grade heat conversion. *Applied Energy* 2011; 88: 2802-2808.
- [62] Li X and Zhang X. Component exergy analysis of solar powered transcritical CO₂ Rankine cycle system. *Journal of Thermal Science* 2011; 20: 195-200.
- [63] Galanis N, Cayer E, Roy P, Denis ES, and Desilets M. Electricity generation from low temperature sources. *Journal of Applied Fluid Mechanics* 2009; 2: 55-67.
- [64] Cayer E, Galanis N, Desilets M, Nesreddine H, and Roy P. Analysis of a carbon dioxide transcritical power cycle using a low temperature source. *Applied Energy* 2009; 86: 1055-1063.
- [65] Yamaguchi H, Zhang XR, Fujima K, Sawada N. Solar energy powered Rankine cycle using supercritical CO₂. *Appl Therm Eng* 2006; 26: 2345-2354.
- [66] Chen Y. Novel cycles using carbon dioxide as working fluid. Licentiate thesis, School of Industrial Engineering and Management, KTH, Sweden; 2006.
- [67] Chen Y, Lundqvist P, Johansson A, and Platell P. A comparative study of the carbon dioxide transcritical power cycle compared with an organic Rankine cycle with R123 as working fluid in waste heat recovery. *Applied Thermal Engineering* 2006; 26: 2142-2147.
- [68] Zhang S, Wang H, and Guo T. Performance comparison and parametric optimization of subcritical Organic Rankine Cycle (ORC) and transcritical power cycle system for low-temperature geothermal power generation. *Applied Energy* 2011; 88: 2740-2754.
- [69] Mercangoez M, Hemrle J, Kaufmann L, Z'Graggen A, and Ohler C. Electrothermal energy storage with transcritical CO₂ cycles. *Energy* 2012; 45: 407-415.
- [70] Baghernejad A, Yaghoubi M. Exergy analysis of an integrated solar combined cycle system. *Renewable Energy* 2010; 35: 2157-2164.

-
- [71] Lemmon EW, McLinden MO, and Huber ML. Reference fluid thermodynamic and transport properties (REFPROP). NIST Standard Reference Database 23, Version 7.0; 2002.
- [72] Zhao H, Peterson PF. Multiple reheat helium Brayton cycles for sodium cooled fast reactors. *Nuclear Engineering and Design* 2008; 238: 1535-1546.
- [73] Liu C, Peng JF, Zhao FY, and Li C. Design and optimization of fuzzy-PID controller for the nuclear reactor power control. *Nuclear Engineering and Design* 2009; 239: 2311-2316.
- [74] Sohn SW, Lee KJ. Development of a boron concentration prediction model using multi-cell simulation of the automatic load follow operation. *Annals of Nuclear Energy* 2011; 38: 463-473.
- [75] Wong, I.H. An underground pumped storage scheme in the Bukit Timah granite of Singapore. *Tunnelling and Underground Space Technology* 1996; 11: 485–489.
- [76] Uddin, N.; Asce, M. Preliminary design of an underground reservoir for pumped storage. *Geotechnical and Geological Engineering* 2003; 21: 331–355.
- [77] Ikeda H, Yagi J, and Kawaguchi Y. The development of PAG refrigeration lubricants for hermetic compressors with CO₂. In: *International Refrigeration and Air Conditioning Conference at Purdue*; 2004, p. R080.

Nomenclature

Acronyms

B	Brayton
CAES	Compressed air energy storage
HT	High temperature
LT	Low temperature
max	maximum
PHS	Pumped hydro storage
R	Rankine
S-	Supercritical
T-	Transcritical
TES	Thermal Energy Storage
TEES	Thermo-electric energy storage
TES	Thermal Energy Storage

Symbols

c	specific heat [kJ/(kg.K)]
c_p	constant pressure specific heat [kJ/(kgK)]
c_v	constant volume specific heat [kJ/(kgK)]
CF	compression factor (dimensionless)
e	specific exergy (kJ/kg)
E	exergy (kJ)

\dot{E}	rate of exergy (kW)
\dot{E}^+	rate of exergy to the system (kW)
\dot{E}^-	rate of exergy from the system (kW)
g	acceleration of gravity (m/s ²)
HF	heating factor of compressed air (dimensionless)
H	height of cavern (m)
h	height of water head (m)
h	specific enthalpy (kJ/kg)
k	specific heat ratio
k^*	effective ratio of specific heat
k	specific flow exergy (kJ/kg)
L	exergy loss (kJ)
\dot{L}	rate of exergy loss (kW)
n, m	polytropic exponent
m, M	mass (kg)
\dot{M}	mass flow rate (kg/s)
$M_{w(h)}$	mass of water in hot tank (kg)
\dot{m}_w	mass flow rate of flowing water between hot tank and cold tank (kg/s)
\dot{m}_{CO_2}	mass flow rate of working fluid CO ₂ (kg/s)
P	pressure (kPa)
Q	heat transfer (kJ)
\dot{Q}	rate of heat (kW)
q	specific heat (kJ/kg)
r	specific gas constant (kJ/kgK)
r_{bw1}	back work ratio for charging mode
r_{bw2}	back work ratio for discharging mode
r	specific internal dissipation (kJ/kg)
$R_{-\Delta c_{p,H-L}}(T)$	ratio of specific heat difference at T
s	specific entropy (kJ/kgK)
t	time (s)

T	temperature (K)
V	volume (m ³)
v	specific volume (m ³ /kg)
w	specific work (kJ/kg)
W	work (kJ)
\dot{W}	rate of total work (kW)
y	split ratio

Greek symbols

η	efficiency (dimensionless)
$\eta_{C/E}$	compression/expansion efficiency
η_{RT}	round-trip efficiency
η_R	recuperator efficiency
η_{th}	thermal efficiency
η_{th}^*	increased thermal efficiency
η_{II}	second law efficiency
τ_D	discharging period
ρ	density (kg/m ³)
ε	heat exchanger temperature effectiveness

Indices

A	ambient temperature
a	air
a	atmospheric (environmental) state
ac	after compression or after-cooler
ae	after expansion
b	back
C	cooling performance
c	compression

<i>C</i>	compressor, condenser
<i>ce</i>	cooling by expanding air
<i>ch</i>	charging
<i>CO2</i>	carbon dioxide
<i>C1</i>	compression during charging mode
<i>C2</i>	compression during discharging mode
<i>dc</i>	discharging
<i>e</i>	expansion
<i>E</i>	expander
<i>ee</i>	energy efficiency
<i>E1</i>	expansion during charging mode
<i>E2</i>	expansion during discharging mode
<i>f</i>	fuel or secondary fluid
<i>g</i>	gas
<i>g</i>	generator
<i>g</i>	gravity
<i>H</i>	heating performance
<i>h, H</i>	heater
<i>hc</i>	heat of compression
<i>h</i>	hydraulic
<i>h, c</i>	hot, cold water tank
<i>H, C</i>	heat source, cooling water (heat sink)
<i>H, L</i>	hot, low temperature
<i>H, L</i>	high pressure, low pressure
<i>H1, H2</i>	LT heat source, HT heat source
<i>i</i>	inlet
<i>i(deal)</i>	ideal process
<i>i</i>	current time step
<i>i</i>	state point
<i>l</i>	liquid
<i>L, R</i>	left, right

<i>L</i>	cool down to lowest temperature
<i>m</i>	motor
<i>M</i>	mechanical
max	maximum
<i>net</i>	net power
o	outlet
<i>P</i>	pump
q	heat exergy
reg	regeneration
<i>rev</i>	reversible process
<i>R</i>	recuperator
<i>R1, R2</i>	LT recuperator, HT recuperator
s, S	storage
<i>s</i>	isentropic
<i>se</i>	electrical storage efficiency
<i>T</i>	thermal
<i>T, t</i>	isothermal process
<i>T</i>	turbine
<i>t</i>	total
<i>w</i>	water
<i>wp</i>	water pump
<i>wt</i>	water turbine
<i>W</i>	waste heat
y	transformation exergy
0	dead state
1	state at the start of charging of air storage tank
2	state at the end of charging of air storage tank
1	charging mode
2	discharging mode
II	exergy (Second Law)

Superscripts

+	input
-	output

List of Figures

1.1	Comparison of various energy storage technologies in terms of power capacity and discharge time (Source: Raytheon Company)	2
2.1	Conventional CAES system: Schematic of the McIntosh plant in Alabama, USA.....	10
2.2	Energy and exergy flow of simplified CAES system.....	12
2.3	Energy and exergy flow of the conventional CAES system.....	14
2.4	Configuration of CAES system as a bottoming cycle... ..	15
2.5	Diagram of an adiabatic CAES system in single-stage configuration.....	17
2.6	Energy and exergy flow of the adiabatic CAES system in single-stage configuration...17	
2.7	Diagram of an adiabatic CAES system in two-stage configuration... ..	19
2.8	Energy and exergy flow of the adiabatic CAES system in two-stage configuration.....	19
2.10	Energy and exergy flow of the isothermal CAES system.....	21
3.1	Pressure variation in the storage cavern and throttling loss rate for discharging process in the case of Huntorf CAES plant.... ..	26
3.2	Constant-pressure CAES system with compensating water column.... ..	27
3.3	Constant-pressure CAES system with water pump..... ..	27
3.4	Constant-pressure CAES combined with pumped hydro storage.....	28
3.5	Operation process of constant-pressure CAES combined with pumped hydro storage.....	29
3.6	Energy and exergy flow of the novel CAES system.....	27
3.7	Energy and exergy flow of the simplified sub-systems.... ..	33
3.8	Work outputs and maximum pressure of the novel CAES system according to charge ratio (with heating, $HF = 2.6$)..... ..	40

3.9	Total power required for charging process according to various compression processes.....	42
3.10	Power required for compressed air part, hydraulic part, and the sum of two during the charging process using three-stage compression with intercooling.....	43
3.11	Power produced during discharging process according to several heating factors.....	43
3.12	Power produced by the compressed air part, hydraulic part, and sum of the two during the discharging process when $HF = 2.66$	44
3.13	Effect of height of storage cavern on the novel CAES system.....	45
3.14	Total power required for charging, pressure of sealed air, and back pressure during the charging process using three-stage compression with intercooling ($H = 100$ m).....	47
3.15	Total power required for charging, pressure of sealed air, and back pressure during the charging process using three-stage compression with intercooling ($H = 200$ m).....	47
3.16	Spraying water in the charging process for a quasi-isothermal process of hydraulic storage.....	50
3.17	Simple modeling of sprayed water in the charging process for the novel CAES system	50
3.18	Temperature and pressure of compressed air cooled by sprayed water for the charging process in hydraulic storage.....	52
3.19	Sprayed water in the discharging process for a quasi-isothermal process of hydraulic storage.....	52
4.1	Micro-CAES system (Type 1, 2).....	59
4.2	Micro-CAES system (Type 3, 4).....	59
4.3	Micro-CAES system (Type 5, 6).....	60
4.4	Micro-CAES system (Type 7, 8).....	60
4.5	Energy and exergy flow of Trigen micro-CAES system.....	73
4.6	Energy and exergy flow of micro-CAES system with the fuel.....	73
5.1	Working principle of a thermoelectric energy storage system (charging mode).....	77
5.2	Working principle of a thermoelectric energy storage system (discharging mode).....	77

5.3	Maximum round-trip efficiency of a TEES system as a function of r_{bw} and $\eta_{C/E}$	80
5.4	PHES system with a Brayton cycle (Source: Isentropic Energy).....	81
5.5	Reference cycle of PHES system with Brayton cycle (Source: Isentropic Energy).....	82
5.6	Maximum round-trip efficiency of TEES system with reference cycle in Fig. 5.5	82
5.7	Schematic of TEES system with transcritical CO ₂ cycle, charging (a) and discharging (b) modes..	84
5.8	Base reference cycle of TEES system with transcritical CO ₂ cycle.	85
5.9	Maximum round-trip efficiency of TEES system with reference cycle in Fig. 5.8.....	85
5.10	Schematic of isothermal TEES systems with a transcritical CO ₂ cycle, charging (a) and discharging (b) modes.....	87
5.11	Base reference cycle of isothermal TEES systems with a transcritical CO ₂ cycle.....	88
5.12	Schematic of a double-acting liquid piston type of isothermal compressor/expander... ..	89
5.13	Expansion and compression power and temperature drop of the hot tank during the discharging process in an isothermal TEES system with the reference cycle shown in Fig. 5.11 (Case 1).....	93
5.14	Instantaneous r_{bw} and round-trip efficiency during the discharging process in an isothermal TEES system (Case 1).....	93
5.15	Net power during the charging and discharging processes in an isothermal TEES system (Case 1).....	94
5.16	Mass flow rate of water from the hot tank to the cold tank and the mass of the water in the hot tank during the discharging process in an isothermal TEES system (Case 1)... ..	95
5.17	Expansion and compression power and temperature drop of the hot tank during the discharging process in an isothermal TEES system with the reference cycle shown in Fig. 5.11, and $M_{w(h)} = 20000$ kg (Case 2).....	97
5.18	Instantaneous r_{bw} and round-trip efficiency during the discharging process in an isothermal TEES system (Case 2).....	97

5.19	Net power during the charging and discharging processes in an isothermal TEES system (Case 2).....	98
5.20	Mass flow rate of water from the hot tank to the cold tank and the mass of the water in the hot tank during the discharging process in an isothermal TEES system (Case 2)...	99
5.21	Reference cycle of an isothermal TEES system with T-CO ₂ cycles (Case 3).....	101
5.22	Expansion and compression power and temperature drop of the hot tank during the discharging process in an isothermal TEES system (Case 3).....	101
5.23	Net power during the charging and discharging processes in an isothermal TEES system (Case3).....	102
5.24	Power and volume flow rate of a hydraulic turbine during the discharging process in an isothermal TEES system (Case 3).....	102
5.25	Variation in the isobaric specific heat of CO ₂ in the operating temperature range depending on the CO ₂ pressure.....	104
5.26	Required thermal capacity of water in the operating temperature range depending on the maximum CO ₂ pressure in an isothermal TEES system.....	105
5.27	Reference cycle of an isothermal TEES system with T-CO ₂ cycle (Case 4).....	105
5.28	Expansion and compression power and temperature drop of the hot tank during the discharging process in an isothermal TEES system (Case 4).....	106
5.29	Net power during the charging and discharging processes in an isothermal TEES system (Case 4).....	106
5.30	An optimized real cycle of an isentropic TEES system with T-CO ₂ cycles.....	108
5.31	An optimized real cycle of an isothermal TEES system with T-CO ₂ cycles.....	109
5.32	Isothermal compression process in an isothermal TEES system with T-CO ₂ cycles..	110
5.33	Isothermal expansion process in an isothermal TEES system with T-CO ₂ cycles.....	111
5.34	Maximum round-trip efficiency of an isothermal TEES system with varying temperature of the hot storage tank.....	114
6.1	Schematic of T-CO ₂ Rankine cycle with HT heat source.....	120
6.2	T-s diagram of T-CO ₂ Rankine cycle with HT heat source.....	120

6.3	Schematic of T-CO ₂ Brayton cycle with HT heat source	121
6.4	T-s diagram of T-CO ₂ Brayton cycle with HT heat source	121
6.5	Reference cycle of T-CO ₂ Rankine cycle with HT heat source.....	125
6.6	Reference cycle of T-CO ₂ Brayton cycle with HT heat source.....	125
6.7	Isobaric specific heats of CO ₂ in high- and low-pressure sides over temperature range of heat recovery.....	127
6.8	Schematic of LH T-CO ₂ cycle using both LT and HT heat sources.....	129
6.9	Reference cycle of LH T-CO ₂ cycle using both LT and HT heat sources.....	129
6.10	Mass flow rate and inlet/outlet temperature of hot water required in LT recuperator.	131
6.11	Isobaric specific heat of LT heat source required to make up for difference in isobaric specific heats between two CO ₂ streams... ..	131
6.12	Temperature T_R and thermal efficiency η_{th}^* according to temperature of LT heat source (T_{H1})	133
6.13	Reference cycle of T-CO ₂ cycle with LT heat source.... ..	134
6.14	Schematic of partial pre-cooling S-CO ₂ cycle.	136
6.15	Schematic of LH T-CO ₂ cycle combined with T-CO ₂ Brayton cycle and TES, T-CO ₂ Brayton mode (night).....	137
6.16	Schematic of LH T-CO ₂ cycle combined with T-CO ₂ Brayton cycle and TES, LH T-CO ₂ mode (day)	138
6.17	Thermal match over low-temperature range in LH T-CO ₂ cycle combined with T-CO ₂ Brayton cycle and TES	139
6.18	Reference cycle of partial condensation T-CO ₂ cycle	140
6.19	Reference cycle of fully-cooled S-CO ₂ cycle	141
6.20	Reference cycle of less-cooled S-CO ₂ cycle.....	142
6.21	Reference cycle of recompression S-CO ₂ cycle	142
6.22	Thermal match over low-temperature range in recompression S-CO ₂ cycle	143
6.23	Reference cycle of LH S-CO ₂ cycle using both LT and HT heat sources	144

6.24	Schematic of TEES LH T-CO ₂ cycles, charging mode (a) and discharging and generation mode (b)	146
6.25	Reference cycle of TEES LH T-CO ₂ cycle, discharging and generation mode	147
6.26	Heat input (top) and work input/output (bottom) as a function of split ratio y in TEES LH T-CO ₂ cycle	148

List of Tables

3.1	Characteristics of some existing CAES plants with varying pressure of air storage.....	24
3.2	Effect of height of storage cavern on the novel CAES system.....	10
3.3	Effect of heat transfer between the two media (air, water) and the cavern	10
4.1	Energy and exergy flow of simplified CAES system.....	58
4.2	Energy analyses of micro-CAES systems.....	69
4.3	Exergy analyses of micro-CAES systems.....	71
5.1	Performance of isothermal TEES (Case 1) compared with isentropic TEES.....	96
5.2	Performances of isothermal TEES system (Case 2).....	99
5.3	Performances of isothermal TEES system (Case 3).....	103
5.4	Performances of isothermal TEES system (Case 4).....	107
6.1	Exergy analysis of transcritical CO ₂ Rankine cycle with HT heat source.....	126
6.2	Exergy analysis of transcritical CO ₂ Brayton cycle with HT heat source	126
6.3	Comparison of performances of different T-CO ₂ cycles (H: High temperature of T_{H2} , L: Low temperature of T_{H1} , R: Rankine, B: Brayton)	130
6.4	Exergy analysis of transcritical CO ₂ cycle using both LT and HT heat sources	27
6.5	Comparison of performances of different T-CO ₂ cycles with TEES (H: High temperature of T_{H2} , L: Low temperature of T_{H1} , R: Rankine, B: Brayton).....	149

Curriculum Vitae

Young Min KIM

Born on the 3rd of May 1972 in Daegu (South Korea)

Korean citizen

Married, three children

Education:

2008 to 2012: **PhD Student**

Laboratory for Industrial Energy Systems (LENI)

Swiss Federal Institute of Technology Lausanne (EPFL)

1994 – 1996: **M.S.**

Mechanical Engineering

Korea Advanced Institute of Science and Technology (KAIST)

1990 – 1994: **B.S.**

Mechanical Engineering

Korea Advanced Institute of Science and Technology (KAIST)

Experience:

2001 to date: **Senior Researcher**

Laboratory for Green Power Systems

Korea Institute of Machinery and Materials (KIMM)

1996 – 2000: **Researcher**

Laboratory for Green Power Systems

Korea Institute of Machinery and Materials (KIMM)

Publications:**Journal:**

- Y.M. Kim, D. Favrat, Energy and exergy analysis of a micro-compressed air energy storage and air cycle heating and cooling system. *Energy* 35 (2010) 213-220.
- Y.M. Kim, D.G. Shin, S.T. Lee, D. Favrat, Thermodynamic analysis of a closed Brayton/Ericsson cycle engine with scroll machines. *International Journal of Air-Conditioning and Refrigeration*. Vol. 18, No. 4 (2010) 279-287.
- Y.M. Kim, D.G. Shin, D. Favrat, Operating characteristics of constant-pressure compressed air energy storage (CAES) system combined with pumped hydro storage based on energy and exergy analysis. *Energy* 36 (2011) 6220-6233.
- Y.M. Kim, C.G. Kim, D. Favrat, Transcritical or supercritical CO₂ cycle using both low- and high-temperature heat sources. *Energy* 43 (2012) 402-415.
- Y.M. Kim, S.J. Kim, D. Favrat, Potential and evolution of compressed air energy storage: energy and exergy analyses. *Entropy* 14 (2012) 1501-1521.
- Y.M. Kim, D.G. Shin, D. Favrat, Isothermal transcritical CO₂ cycles with thermal energy storage for electrical storage. *Energy*, Submitted.

Conference:

- Y.M. Kim, D. Favrat, Energy and exergy analysis of a micro-compressed air energy storage and air cycle heating and cooling system. *International Refrigeration and Air Conditioning Conference at Purdue*, 2008. R1249.
- Y.M. Kim, D.G. Shin, C.G. Kim, Potential and evolution of compressed air energy storage for future power networks. *World Engineers' Convention*, Geneva, 2011.

Patent:

- Y.M. Kim, D. Favrat, D.G. Shin, K.B. Cho, Compressed-air-storing electricity generating system and electricity generating method using the same, US Patent 7,663,255, Issued on Feb. 16, 2010.
- Y.M. Kim, C.G. Kim, D.G. Shin, S.Y. Lee, D. Favrat, Heat engine based on transcritical

Rankine cycle with improved exergy efficiency and method thereof, KR Patent 2011-0138429.